CCS2022-2024 WP1: The Havnsø structure

Seismic data and interpretation to mature potential geological storage of CO_2

Ulrik Gregersen, Henrik Vosgerau, Florian W.H. Smit, Bodil W. Lauridsen, Anders Mathiesen, Finn Mørk, Lars Henrik Nielsen, Rasmus Rasmussen, Thomas Funck, Karen Dybkjær, Emma Sheldon, Gunver K. Pedersen, Carsten Møller Nielsen, Kenneth Bredesen, Shahjahan Laghari, Maiken L. Olsen & Lasse M. Rasmussen

GEOLOGICAL SURVEY OF DENMARK AND GREENLAND
DANISH MINISTRY OF CLIMATE, ENERGY AND UTILITIES

G E U S

DANMARKS OG GRØNLANDS GEOLOGISKE UNDERSØGELSE **RAPPORT 2023/38**

CCS2022-2024 WP1: The Havnsø structure

Seismic data and interpretation to mature potential geological storage of CO_2

Ulrik Gregersen, Henrik Vosgerau, Florian W.H. Smit, Bodil W. Lauridsen, Anders Mathiesen, Finn Mørk, Lars Henrik Nielsen, Rasmus Rasmussen, Thomas Funck, Karen Dybkjær, Emma Sheldon, Gunver K. Pedersen, Carsten Møller Nielsen, Kenneth Bredesen, Shahjahan Laghari, Maiken L. Olsen & Lasse M. Rasmussen

GEOLOGICAL SURVEY OF DENMARK AND GREENLAND
DANISH MINISTRY OF CLIMATE, ENERGY AND UTILITIES

G E U S

Preface

A new Danish Climate Act was decided by the Danish Government and a large majority of the Danish Parliament on June 26th, 2020. It includes the aim of reducing the Danish greenhouse gas emissions with 70 % by 2030 compared to the level of emissions in 1990. The first part of a new Danish CCS-Strategy of June 30th, 2021 includes a decision to continue the initial investigations of sites for potential geological storage of CO_2 in Denmark. GEUS has therefore from 2022 commenced seismic acquisition and investigations of potential sites for geological storage of CO_2 in Denmark.

The structures decided for maturation by the authorities, are some of the largest structures onshore Zealand, Jutland and Lolland and in the eastern North Sea (Fig. 1.1). The onshore structures include the Havnsø, Gassum, Thorning, and Rødby structures, and in addition the small Stenlille structure as a demonstration (pilot) site. The offshore structures include the Inez, Lisa and Jammerbugt structures. A GEUS Report is produced for each of the structures to mature the structure as part of the CCS2022–2024 project towards potential geological storage of CO_2.

The intension with the project reporting for each structure is to provide a knowledge-based maturation with improved database and solid basic descriptions to improve the understanding of the formation, composition, and geometry of the structure. Each report includes a description overview and mapping of the reservoir and seal formations, the largest faults, the lowermost closure (spill-point) and structural top point of the reservoir, estimations of the overall closure area and gross-rock volume. In addition, the database will be updated, where needed with rescanning of some of the old seismic data, and acquisition of new seismic data in a grid over the structures, except for the Inez and Lisa structures, which have sufficient seismic data for this initial maturation.

The reports will provide an updated overview of the database, geology, and seismic interpretation for all with interests in the structures and will become public available. Each reporting is a first step toward geological maturation and site characterization of the structures. A full technical evaluation of the structures to cover all site characterization aspects related to CO_2 storage including risk assessment is recommended for the further process.

Content

Dansk sammendrag

Regeringen og et bredt flertal i Folketinget vedtog i juni 2021 en køreplan for lagring af CO_2, der inkluderer undersøgelser af potentielle lagringslokaliteter i den danske undergrund. Der er derfor udvalgt fire store strukturer på land med dataindsamling og kortlægning til videre modning: Havnsø, Gassum, Rødby og Thorning, samt den mindre Stenlille struktur til demonstrationslagring (Fig. 1.1–1.3). Derudover indsamles nye data til kortlægning og modning for den kystnære Jammerbugt struktur, mens de to Inez og Lisa strukturer, længere mod vest i Nordsøen, kortlægges og modnes baseret på eksisterende data.

Havnsø strukturen er en stor og dyb struktur, der ligger kystnært i Vestsjælland, nær Havnsø. Tidligere og nye seismiske data viser strukturens form og opbygning. Korrelation med de seismiske data til det nærliggende Stenlille område med 20 boringer giver en vigtig viden om regionens geologiske opbygning, som også kan tolkes op til Havnsø området, hvor der ikke er dybe boringer.

Dette sammendrag opsummerer kort forundersøgelsen og den initiale vurdering af lagringsmuligheden i Havnsø strukturen. Vurderingen bygger på tolkning af eksisterende samt nye geologiske og geofysiske data og viden (Kapitel 3−4), og belyser undergrundens geologiske opbygning i og omkring Havnsø strukturen (Kapitel 5–7). Vurderingen har fokus på strukturens form, størrelse, overordnede opdeling inklusive reservoir- og seglforhold, geologiske risikofaktorer, især større forkastninger og segl, og der foretages en vurdering af statisk lagringskapacitet for det primære reservoir (Kapitel 8). Desuden opsummeres anbefalinger til yderligere modning af strukturen hen imod en mulig CO_2 lagring (Kapitel 9, 10).

Datagrundlag

Havnsø strukturen er dækket af et net af refleksionsseismiske data (Fig. 4.1.1) med 2D profiler af varierende tæthed og kvalitet indsamlet i 1960'erne, 1970'erne, 1980'erne, 1990'erne, samt i 2022 for dette projekt. De ældre datasæt er generelt af dårlig kvalitet med meget støj. Derfor blev der i august til oktober 2022 indsamlet ni nye 2D refleksionsseismiske profiler (i alt c. 130 km) ved hjælp af 2 vibrator trucks (kilde), tilkoblet en land-streamer med geofoner, samt trådløse geofoner i vejsiden. Disse data har forbedret dækning og kvaliteten af data samt tolkningsmulighederne over strukturen og flankerne (Fig. 4.2.1–4.2.7). Uppsala Universitet gennemførte indsamlingen og processeringen på vegne af GEUS, med seismiske kilder (2 vibrator-lastbiler) fra polske Geopartner Sp. zo.o og med feltassistance fra universitetsstuderende fra Københavns- og Uppsala universiteter. COWI varetog ansøgninger om tilladelser, logistik, kommunikation og borgerkontakt. Der blev forud for indsamlingen informeret på tre borgermøder i juni 2022, via webside information hhv. af GEUS og COWI, via informationsbreve og flyers, samt på to besøgsdage under indsamlingen. Det nye 2D seismiske survey (GEUS2022-HAVNSOE) har forbedret data grundlaget over toppen og flankerne af Havnsø strukturen og muliggør en forbedret kortlægning. Surveyet er udført så det også indeholder en lang linje (P1: Fig. 4.1.1), der forbinder og forbedrer korrelationsmulighederne fra den meget store database (boringer og 3D survey) i Stenlille strukturen med Havnsø strukturen. P1 linjen blev indsamlet med startpunkt indenfor 3D surveyet (Fig. 4.1.1) nær Stenlille-19 boringen og fortsætter mod nordvest helt op til kysten, hvor den forbindes med marine data og slutter ude på Nekselø. Derfor forbinder denne linje Stenlille området og de eksisterende data med Havnsø området og marine data. P1 linjen fra den originale processering ved Uppsala Universitet og reprocesseringen ved Realtime Seismic viser begge, at 3D surveyet fra 1997 i Stenlille området skal korrigeres c. 40 millisekunder ned.

Tolkning

Havnsø strukturen er en geologisk 4-vejs lukning med forkastninger, som er dannet fra Jura til Tidlig Kridt tid over en dyb salt pude med Zechstein salt (Fig. 1.2). De primære reservoir-segl-par i Havnsø strukturen forventes at have mange lighedspunkter med det boringspåviste geologiske lagringskompleks i Stenlille, som er vist i Figur 1.3: Det primære reservoir-segl-par er Gassum−Fjerritslev formationerne; De to dybere, sekundære reservoir-segl-par er hhv. Intra Oddesund sandstenslag med overliggende mudderstenssegl (Oddesund Formation), og Bunter Sandstone Formation med overliggende mudderstenssegl (Ørslev Fm) – se også den generelle lithostratigrafi for det Danske Bassin i Figur 3.3.

Strukturen lukker på flere stratigrafiske niveauer fra Trias til Jura. Særligt vigtigt er lukningen på toppen af Gassum Formation (Sen Trias alder) med det primære reservoir, som har fokus i denne vurdering (Kapitel 6). Formationen blev i boringerne i Stenlille området opdelt i 6 zoner (Zone 1–6), som indeholder reservoir sandsten af forskellig tykkelse med de tykkeste sandsten i de to nederste zoner (5 og 6). Reservoirzonerne indeholder primært sandsten men lersten og siltsten indgår i zonerne med varierende tykkelse og er defineret i Stenlille boringerne. Da der ikke er boringer i Havnsø strukturen er disse zoner ikke påvist i strukturen. Der er dog tolket enkelte profiler fra de nye seismiske data med korrelation fra Stenlille boringer og 3D seismik, der illustrerer en mulig opbygning af sekvenser i formationen ud mod Havnsø strukturen (Kapitel 7). Derved gives en tolkning af formationens opbygning og mulige indhold af sandstensdominerede reservoir zoner.

Beskrivelsen af Gassum Formationen er baseret på Stenlille boringerne understøttet af mere regional viden. Gassum Fm er c. 140–160 meter tyk i både Havnsø og Stenlille strukturen baseret på tykkelseskort fra den seismiske tolkning med korrelation til boringer i Stenlille området. Den består i Stenlille strukturen og sandsynligvis også i Havnsø strukturen primært af sandsten med lerstenslag, dog muligvis med færre sandsten og mere lersten i Havnsø strukturen. Formationen har varierende reservoir-egenskaber, som er beregnet i Stenlille boringer både fra logs og kernemålinger, hvorfra data sammen med den seismiske tolkning indgår i vurderingen af Havnsø strukturen (se også Afsnit 7.1).

Et reservoir i Gassum Formationen defineres som en sandsten, der har et ler-indhold <0.5% og porøsitet >10%. Gassum Formationens reservoirsandsten og potentielle reservoiregenskaber i Havnsø strukturen (uden boringer) er vurderet som prognose i tre forskellige scenarier: (1) Som i Stenlille strukturen; (2) Et regionalt gennemsnit fra Stenlille brønde (ST-1 og ST-19) og nærmeste omkringliggende boringer; (3) Ud fra en sekvensstratigrafisk tolkning, der bygger både på seismiske data og korrelation med brønddata (Kapitel 7). Tolkningen viser, at ud mod Havnsø strukturen indeholder Gassum Formationen primært lavstandssandsten fra sekvens 4, 5 og 6, der i Stenlille har gode reservoiregenskaber.

For scenarie 1 gælder det, at der kan forventes reservoirsandsten i sekvenserne 3–7 (i hele formationen) med en samlet reservoirsandstenstykkelse på 111 m, en gennemsnits porøsitet på 21,9% og en permeabilitet på omkring 800 mD. Til scenarie 2 bruges ud over brønde fra Stenlille også andre omkringliggende brønde, som bidrager til en statistisk estimering af reservoirparametrene, som giver anledning til en samlet tykkelse af reservoirsandsten på 69 m, en gennemsnits porøsitet på 23,3% og en permeabilitet på ca. 1100 mD. Scenarie 3 bygger mere på en geologisk aflejringsmodel, som er understøttet af tolkningen af de seismiske data, hvor lavstandssandstenene fra sekvenserne 4 – 6 også forventes aflejret i Havnsø strukturen. Ved dette scenarie belyses reservoiregenskaberne ved en samlet

reservoirsandsten på 47,6 m, en gennemsnits porøsitet på 27,3% og en permeabilitet på ca. 1500 mD. Det bemærkes, at uanset hvilket af disse tre scenarier, der anvendes til at forudsige reservoiregenskaberne i Havnsø strukturen, så ses det, at der er gode reservoiregenskaber.

De nye data med ny kortlægning bekræfter, at Havnsø strukturen lukker på top reservoir niveau ved Top Gassum Fm og ved toppen af de sekundære reservoirholdige formationer i Oddesund Fm (Intra Oddesund sst. lag) og Bunter Sandstone Fm (Fig. 6.3.3). Lukningens størrelse på Top Gassum dybde-struktur kortet (Fig. 6.3.3C, 8.1.1) er c. 70 km^2 ved den lukkende kontur på c. 1710 m dybde under havniveau (below mean sea level - b.msl). Toppen af strukturen ved Top Gassum Fm er c. 1550 m (b.msl) og højden (relief) af strukturen fra spill-point er derfor c. 160 m.

Beregningerne i denne undersøgelse viser en væsentlig potentiel lagringskapacitet (storage capacity) af CO_2 i Gassum Formationen i Havnsø strukturen (Kapitel 8). Lagringskapaciteten er her estimeret for tre scenarier (se beskrivelse ovenfor) ud af mange mulige i en 4-vejs lukning. Den gennemsnitlige (mean) lagringskapacitet (buoyant storage capacity) i Gassum Formationen for Havnsø strukturen er for 4-vejs lukningen af strukturen estimeret for hvert scenarie til hhv.: (1) 65 megaton (MT) CO_2; (2) 58 MT CO_2 og (3) 35 MT CO_2. I scenarie 3 er tolkningen, at Havnsø strukturen primært indeholder reservoir sandsten fra sekvens 4–6, dog kan andre tyndere enheder forekomme. Lagringskapaciteten og de mulige lagringsscenarier bør undersøges nærmere, f.eks. med mere konkrete data (herunder placering af injektionsboringer) og reservoir simuleringsmodeller.

Der kan desuden være lagringspotentiale af CO_2 i dybereliggende sandsten i Oddesund og Bunter Sandsten Formationerne (se Kapitel 7 og 8 for flere detaljer om reservoiregenskaber og lagringskapacitet). Sandsten i Oddesund og Bunter Sandsten Formationerne er i Stenlille området dokumenteret i ST-19 boringen, som er den eneste boring, der boret til dette stratigrafiske niveau, men det må forventes, at der er variationer igennem området til Havnsø.

Sandsten i Oddesund Formationen er også påvist i både Slagelse-1 og Ullerslev-1 boringerne, hvor de dog er tynde. Derfor kan det forventes, at sandsten kan være tynde eller fraværende i Havnsø strukturen. Det vurderes derfor ikke sandsynligt i denne rapport, at Oddesund Formationen har et reservoirpotentiale i Havnsø strukturen.

På samme måde som for Gassum Formationen, er Bunter Sandsten Formationen vurdereret som prognoser i to scenarier, hvor første scenarie baserer sig på data fra Stenlille-19 og Slagelse-1 boringerne, imens scenarie 2 bygger på en mere regional og statistisk tilgang til reservoirkarakteriseringen baseret på data fra flere boringer. I scenarie 1 for Bunter Sandsten Formationen vurderes reservoiregenskaberne i Havnsø strukturen at have en samlet reservoirsandstenstykkelse på 118 m, med en gennemsnitsporøsitet på 19,1% og en permeabilitet på 129 mD. Scenarie 2 inddrager flere brønde (se kap. 7 for flere detaljer), som er mere fordelt over bassinet. Her vurderes den samlede reservoirsandstenstykkelse til at være 90 m med en gennemsnits porøsitet på 18,6% og med en permeabilitet på 204 mD. Derfor forventes det, at Bunter Sandsten Formationen kan betragtes som et rimeligt godt sekundært reservoir i Havnsø strukturen.

Det primære segl for Gassum Fm er Fjerritslev Fm, som er en flere hundrede meter tyk succession af lersten af seneste Trias til Tidlig Jura alder. Den nederste del af formationen (under TS11 sekvensfladen) indeholder i Stenlille boringerne nogle tynde lag af silt- og sandsten, der muligvis kan reducere seglkapaciteten, mens den øverste og tykkeste del af formationen vurderes at have de bedste seglegenskaber. I lighed med Stenlille strukturen,

vurderes det for Havnsø strukturen, at der over Fjerritslev Fm forekommer sekundære segl med lersten fra Vedsted Fm, mergel og kalk fra Rødby Fm (begge Nedre Kridt) og derover en kilometer-tyk enhed (Chalk Group) af primært skrivekridt og kalk af Øvre Kridt til tidlig Paleocæn (Danien) alder, og som er dækket af yngre aflejringer. Fjerritslev Formationen, der er vidt udbredt i Danmark, forventes også at være til stede i Havnsø strukturen med en lignende sammensætning og tykkelse som den kendes fra Stenlille boringerne. Sikker naturgas lagring i Gassum Formationen i Stenlille strukturen er foregået gennem mere end 30 år og har vist, at seglene er effektive.

Overalt i regionen overlejres Bunter Sandsten Formation af den finkornede Ørslev Formation, som formentlig har gode forseglende egenskaber. Både de seismiske data og en mere regional sammensætning taler for, at denne formation sandsynligvis også er til stede i Havnsø strukturen og vil kunne agere som segl for eventuel lagring i Bunter Sandsten Formationen.

Der er identificeret nogle små forkastninger (mest kun i størrelsesordenen 10–15 ms TWT), især med NV-SØ og SV–NØ retninger med små forsætninger i Gassum og Fjerritslev Formationerne i toppen af strukturen (Kapitel 6). Der er også nogle mindre forkastninger oppe i Kalk gruppen. Det er formentlig ældre, inaktive forkastninger og der er i området kun registreret få og meget svage jordskælv. Eventuel CO_2 injektion bør ske væk fra forkastninger og ikke nær saddelpunkter.

De nye 2D seismiske data fra Havnsø strukturen har forbedret datagrundlaget betydeligt med større linjedækning, datakvalitet og tolkningsmuligheder af bl.a. strukturens størrelse, lukning på top reservoir niveau, volumen, detaljer i reservoir- og segl enheder, samt forkastninger til denne initiale modning af strukturen.

De nye seismiske data og grids (to-vejs tid; TWT) af de vigtigste tolkede horisonter fra denne rapport er publiceret og tilgængelige via GEUS projektlinket: https://www.geus.dk/produkter-ydelser-og-faciliteter/data-og-kort/ccs-data-2022-2024

Strukturen bør dog undersøges yderligere forud for en eventuel beslutning om injektion og lagring af CO_2 og det anbefales at supplerende 3D seismiske data indsamles over de områder, der vurderes egnet til lagring, da der på nuværende tidspunkt stadig er noget afstand mellem linjerne med data. Dette ville kunne øge den foreliggende viden om reservoir, segl og forkastninger, og derved forbedre mulighederne for modellering af CO_2 migration, risiko analyser og detail planlægning før injektion (Kapitel 10).

Under en eventuel injektion kan gentagne indsamlinger af seismiske data de samme steder, sammen med anden monitering og målinger (f.eks. via forskellige målinger i observationsboringer og i overfladeære lag, seismometre, sensorkabler, satellit, osv.), desuden bidrage væsentligt til monitering af CO_2 udbredelse.

Viden fra forundersøgelsen af Havnsø strukturen vil indgå i myndighedernes videre arbejde med at afdække muligheder og behov, samt eventuelle krav til flere data og undersøgelser for yderligere modning af et potentielt lager.

1. Summary

The subsurface in Denmark has a large number of deep structures offshore and onshore, and some of these are suited for CO_2 storage and some are also located near emission sources (Fig. 1.1). The named structures are selected for initial investigation and maturation through seismic acquisition, geological analyses, and renewed mapping from 2022 to 2024 by GEUS, and with cooperating partners on acquisition and processing (see database chapter below).

This report provides basic descriptions of the Havnsø structure (Fig. 1.1–1.3) based on a seismic database including newly acquired seismic data over the structures and with ties to wells in the Stenlille structure to improve the understanding of the structure in terms of its geological development, size, relief, composition, and geometry of the structure. It includes a description overview and new mapping of the reservoir and seal formations, the largest faults, the lowermost closure (spill-point) and top point at the top of the reservoir, estimations of the overall closure area and potential storage capacity.

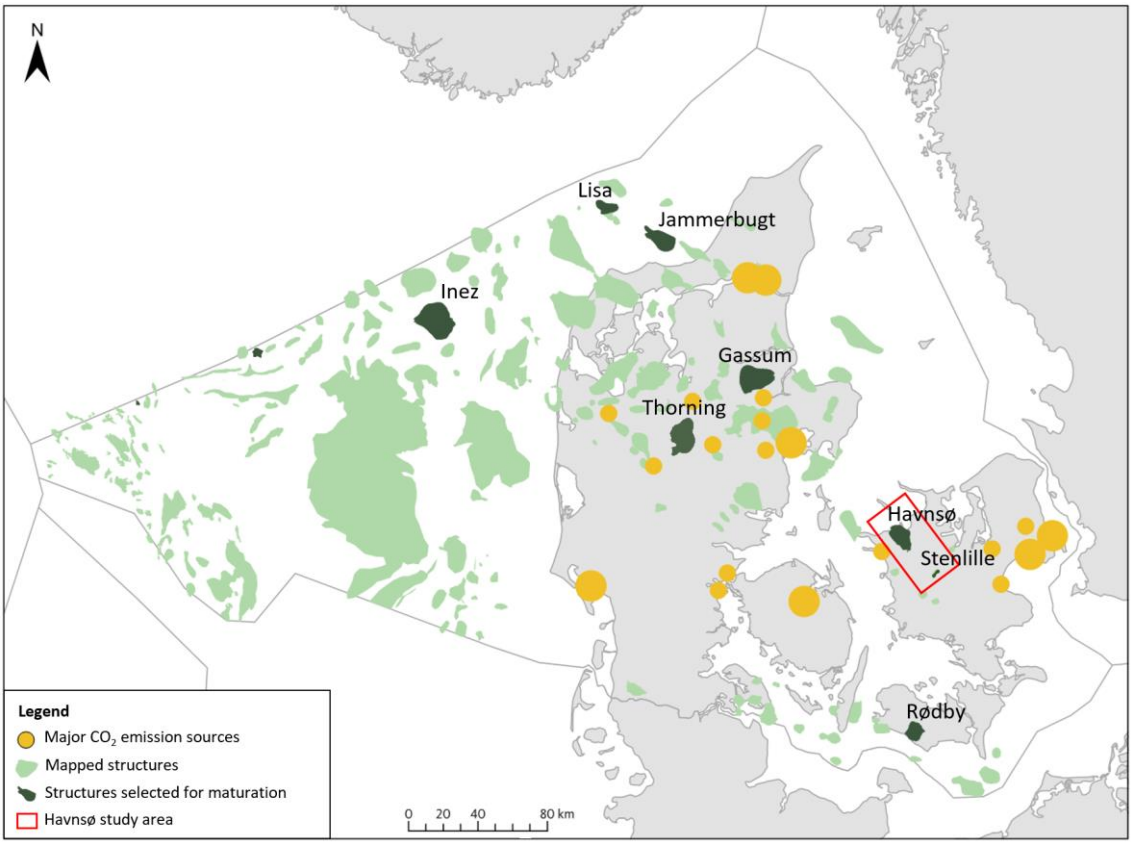

Figure 1.1. *Map of Danish structures with potential for geological storage of CO_2. The named dark green structures (Stenlille, Havnsø, Rødby, Gassum, Thorning, Jammerbugt, Lisa and Inez) are currently investigated with acquisition of new data and updated mapping in GEUS' CCS project during 2022–2024. This reporting is for the Havnsø structure, and the study area is marked with a red rectangle. From Hjelm et al. (2022).*

The new 2D seismic survey (GEUS2022-HAVNSOE survey) included in the present reporting was acquired in the autumn 2022 to enable improved mapping of the Havnsø structure and consists of c. 130 km seismic lines over the structure (Chapter 4). The survey includes

also a long 2D line (P1) that was acquired with the scope of enabling the correlation of the dense high-quality database from the Stenlille structure in the mapping and analyses of the Havnsø structure. This regional line was collected within the 3D survey area near to the Stenlille-19 well to the east and continues to the west coast of Zealand at Havnsø and ends with marine data and data on the island of Nekselø. Thereby a new direct seismic line from the Stenlille area to the sea is acquired and both the original processing by Uppsala University and a reprocessing in 2023 of the line and of the 3D survey by Realtime Seismic (RTS) show that the original 3D seismic dataset from 1997 in the Stenlille area is offset ca. 40 milliseconds (ms TWT) too shallow. Consequently, vintage seismic 2D lines were time-shifted down to fit the new data.

The Havnsø structure is a geological 4-way dip structure with faults probably formed during mainly late Early to Late Jurassic time over a deep Zechstein salt pillow (Fig. 1.2, 6.1.5).

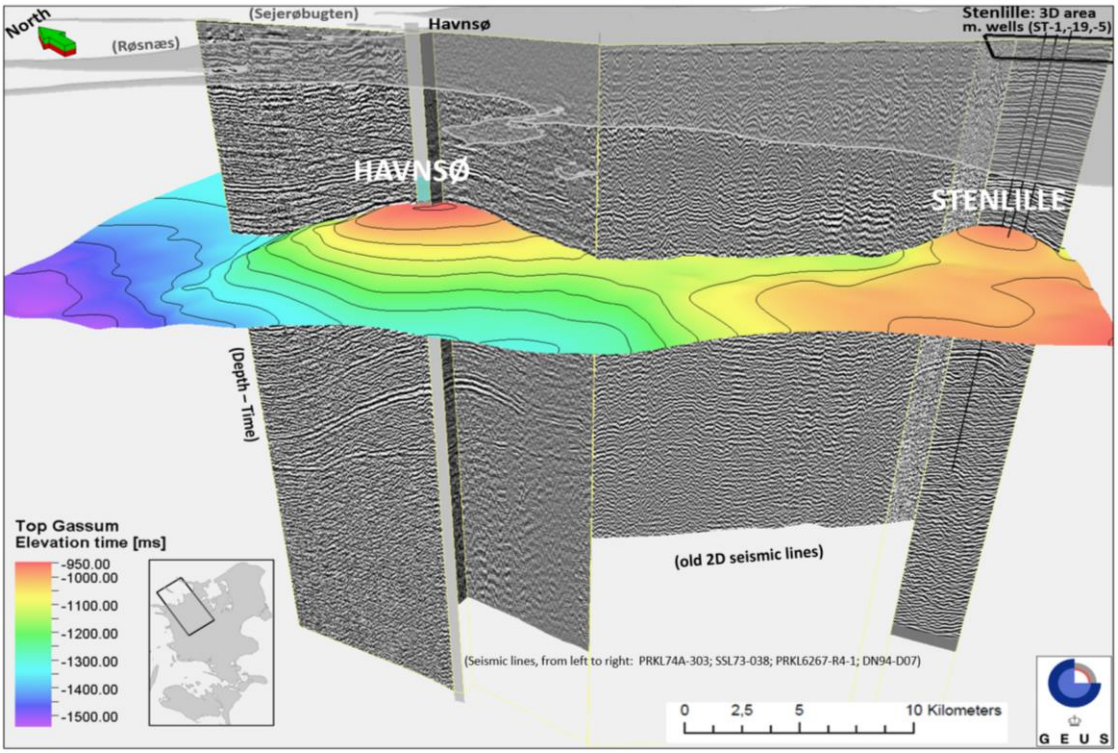

Figure 1.2. *Simplified map of the Top Gassum surface in time (ms TWT) with seismic sections (PRKL74A-303; SSL73-038; PRKL6267-R4-1_part1&2; DN94-D07), showing the Stenlille and the Havnsø structures and the mapped connection with their common saddle-point (near spill-point). The Havnsø structure is much larger than the Stenlille structure. From the reporting of the Stenlille structure (Gregersen et al. 2023).*

The main reservoir-seal couples of the Havnsø structure may be similar to the Stenlille structure storage complex, which is shown in Figure 1.3.

The Gassum Formation is c. 140−160 m thick (Fig. 6.3.4C) in the structure with large lateral continuity based on mapping with seismic correlation from the Stenlille wells (Section 6.3). The Gassum Formation consists in the Stenlille wells of sandstones with interbedded claystones, known from the Stenlille wells. The Gassum Formation is in the Stenlille wells divided into 6 reservoir zones (Zone 1–6) with various thicknesses, variable reservoir properties and variable content of mudstones and siltstones. The quality of the reservoir zones is in the Stenlille wells calculated from both logs and measured in cores and used together with the seismic interpretation and mapping in a prognosis for the Havnsø structure (see Section 7.1).

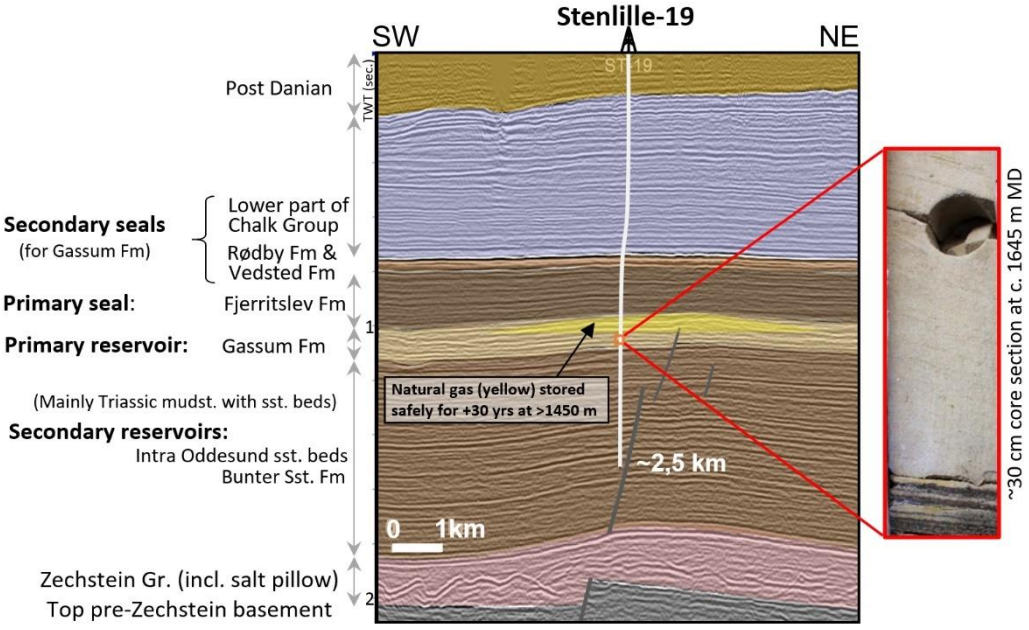

Figure 1.3. *The geological storage complex, here in the Stenlille structure, is expected to be similar in the Havnsø structure. See Fig. 6.1.1 for more detailed lithostratigraphy, seismic stratigraphy and well-tie. See Fig. 6.1.5 and 6.1.8 for similar interpretation of Top and Base Gassum Fm and overlaying Fjerritslev Fm, Top Intra Oddesund sst. beds and Top Bunter Sandstone Fm successions in the Havnsø structure correlated from Stenlille: The Havnsø geological storage complex consists of: The primary reservoir–seal couple of the Gassum Fm–Fjerritslev Fm and its overlying secondary seal successions of the Vedsted Fm, Rødby Fm and Chalk Group. The deeper Triassic secondary reservoir–seal couples with potential reservoirs include the Bunter Sandstone Fm and the Intra Oddesund sandstone (sst.) beds, and their respectively interbedded and overlying mudstone dominated seals. The larger structural and stratigraphic context are outlined in Fig. 3.1–3.4. From Gregersen et al. (2023).*

A reservoir is defined as a sandstone containing a volume of shale <0.5% and with porosities >10%. The Gassum Formation reservoir sandstones and properties in the Havnsø structure (without wells) are evaluated as prognoses in three different scenarios (Chapter 7): (1) As in the Stenlille structure; (2) As a regional average from selected Stenlille wells (ST-1, ST-19) and surrounding wells; (3) From a sequence stratigraphic interpretation of the new seismic data as well as log data from Stenlille showing that mainly lowstand sandstones of sequences 4, 5 and 6 are preserved.

In scenario 1 it is expected that the sequences 3–7 (i.e. throughout the formation) have a combined thickness of reservoir sandstones of 111 m, an average porosity of 21.9% and permeability of c. 800 mD. For scenario 2, two representative wells from the Stenlille area are complemented with regionally distributed wells that all contribute to a statistical evaluation of the Havnsø structure. This gives an estimated thickness of reservoir sandstone of 69 m, with an average porosity of 23.3% and a permeability of c. 1100 mD. Scenario 3 applies a more geological driven depositional model that is supported by the interpretation of the seismic data and log data, where only the sandstones deposited during relative low sea level of sequences 4 – 6 reach the Havnsø area. In this scenario, the combined thickness of the reservoir sandstones adds up to 47.6 m, with an average porosity of 27.3% and a permeability of c. 1500 mD. It is important to note that in all three scenarios, the reservoir parameters used to characterize the Havnsø structure are very good.

The new data and mapping confirm that the Havnsø structure has closures at the Top Gassum Fm and also at deeper levels including the top of the deeper secondary reservoirs of the Intra Oddesund sandstone beds (Oddesund Fm) and the Bunter Sandstone Fm (Fig. 6.3.3). However, the sandstone contents of the formations below the closures towards Havnsø are uncertain. Only in the Gassum Fm and Bunter Sandstone Fm intervals minor progradational reflections (and channels in Gassum) on the seismic data indicate possible sand-prone depositional systems.

The area of lowermost closure on the Top Gassum depth-structure map is c. 70 km^2 at the closing contour of c. 1710 m depth b.msl (Fig. 6.3.3C, 8.1.1). The top of the structure at the Top Gassum map is at c. 1550 m (b.msl), and the relief of the structure at Top Gassum is thus c. 160 m (Fig. 6.3.3C, Appendix A).

The calculations in this study show a significant storage capacity of the Gassum Formation (Chapter 8). The storage capacity of is estimated for three (see description above) out of several possible scenarios in the Gassum Formation of a 4way closure. The mean (buoyant) storage capacity of CO_2 in the Gassum Formation in the structure is estimated for each of the scenarios within the 4way closure to: (1) 65 MT CO_2; (2) 58 MT CO_2 and (3) 35 MT CO_2.

There may also be potential for CO_2 storage in deeper sandstones of the Oddesund and Bunter Sandstone Formations, but their storage capacities have not been assessed here. Sandstone-dominated units in the Oddesund Formation and Bunter Sandstone Formations are documented in the deep Stenlille-19 well with TD in the Bunter Sandstone Formation. Variations of thicknesses and reservoir properties are expected across the region at these two stratigraphic levels. See Chapters 7 and 8 for more details on the reservoirs.

The primary seal for the Gassum Fm is the Fjerritslev Fm, which is several hundred-meter-thick mudstone successions of a latest Triassic to Early Jurassic age, and it includes generally good to very good sealing mudstones. The lowermost part of the formation (F-Ia Mb) includes a number of thin siltstone and sandstone beds, which probably to some extent reduce the seal quality, whereas the upper and thickest part of the formation (F-Ib to F-IV Mb) is a good quality seal. Above this formation are the secondary seals, which includes the Vedsted Fm mudstones and Rødby Fm marl and chalk of Early Cretaceous ages. Above these follows the km-thick Upper Cretaceous Chalk Group, which is overlain by thinner younger deposits. Safe storage in the Gassum Fm of natural gas and monitoring for potential leakage through many years has proven that the F-Ia member of the primary Fjerritslev Formation seal is efficient in the Stenlille structure. The same stratigraphic seal unit is also expected in the Havnsø structure. See also Section 7.2 for more details on the seals.

There are on the seismic sections only identified a few, small faults with minor throws in the Gassum and Fjerritslev Formations and with mainly NW–SE and SW–NE trends parallel or semi parallel, and perpendicular to the outline of the structure, which is elongated NW–SE (Fig. 3.1, 6.3.3). The faults from the present database appears to be old with mostly minor throws, and only few, minor natural earthquakes have been detected in the study area. Possible CO_2 injection should consider risks including the presence of faults.

New 2D seismic data has been acquired across the structure, which has significantly improved the database with more dense, good quality seismic data. This improved database is used in this report for providing the updated interpretation of the size, spill-point, volume, details of reservoir- and seal successions, and faults of the Havnsø structure for this initial maturation. The new seismic data and grids in two-way time of key seismic horizons are available in the GEUS project link: https://www.geus.dk/produkter-ydelser-og-faciliteter/data-og-kort/ccs-data-2022-2024

New seismic acquisition, in particular of 3D data, over the structure and the potential injection- and storage areas is recommended, for more detailed interpretation prior to CO_2 injection, as there is still some distance between the line data coverage. This can improve site-specific knowledge with more details on reservoir, seal, and faults, and can improve modelling of CO_2 migration and risk analyses. Repeated 3D surveys in same place can contribute to monitor the extent of the CO_2 migration, together with other monitoring (e.g., via wells, sampling, seismometers, sensor cables, satellite, etc).

New necessary data acquisition and sampling, analyses and evaluations should be carried out for further maturation, including risk analyses, to cover geological and other technical uncertainties and risks. The knowledge from the investigated structures will be included in the further work of the authorities to reveal opportunities and requirements towards further maturation, site selection and possible licensing of geological CO_2 storage.

2. Introduction

Carbon capture and storage (CCS) is an important instrument for considerably lowering atmospheric CO_2 emissions (IPCC 2022). Geological storage of CO_2 is known from more than 30 sites situated in many countries, including Norway (Sleipner), Canada (Weyburn) and Germany (Ketzin), since the first started more than 25 years ago (e.g., Chadwick et al. 2004) and more than 190 facilities are in the project pipeline (Global CCS Institute 2022).

The Danish subsurface is highly suited for CO_2 storage, and screening studies document an enormous geological storage potential that is widely distributed below the country and adjacent sea areas (Larsen et al. 2003; Anthonsen et al. 2014; Hjelm et al. 2022; Mathiesen et al. 2022). The significant Danish storage potential is based on the favorable geology that includes excellent and regionally distributed reservoirs, tight seals, large structures, and a relatively quiescent tectonic environment. The largest storage potential is contained within saline aquifers and the Danish onshore and nearshore areas contain a number of these structures with a potentially significant CO_2 storage potential (Fig. 1.1; Hjelm et al. 2022).

The Havnsø structure is one of these structures and is a relatively large structure geographically located in the western part of Zealand (Fig. 1.1), and geologically in the south-eastern part of the Danish Basin (Fig. 3.1). The structure was only covered by a limited number of old, poor 2D seismic lines, mainly acquired in the 1960s and early to mid-1970s. However, in 2022 new seismic data for this project was acquired (see Chapter 4). Seismic lines can be tied to the nearby located Stenlille structure with a comprehensive database including 20 wells, which document the geology. Natural gas is here stored in reservoir zones with sandstones interbedded by mudstones of the Gassum Formation below the thick sealing mudstones of the Fjerritslev Formation. The Havnsø structure is also expected to have storage potential for resources such as CO_2, and this structure with the Gassum Formation is the focus of this study, but also deeper reservoir-seals of the structure are described.

Earlier screening projects by GEUS for structures relevant for CCS have also evaluated the Havnsø structure for potential CO_2 storage. The GESTCO project reported in 2003 that the Havnsø structure may be a relevant CO_2 storage site in the closed structure of the Gassum Formation (Fm) sealed by Fjerritslev Fm mudstones (Larsen et al. 2003). The large CCUS2020 project was carried out by GEUS during 2020 and included comprehensive studies of particularly the Stenlille structure, but also with limited work on the Havnsø structure (e.g. Gregersen et al. 2020). A comprehensive summary with an evaluation of the CO_2 storage potential in Denmark was provided by Hjelm et al. (2022). GEUS reports of the CCUS2020 project are available from www.geus.dk web-site (link to the pdf files: CCUS-projekt 2020 (geus.dk)). In 2023 an updated interpretation of the Stenlille structure with new data of this project was published (Gregersen et al. 2023). Thus, there is a comprehensive knowledge available, in particular from the Stenlille structure, which is correlated to the Havnsø structure in the present study using both the existing and the new seismic data.

In this study, the Havnsø structure is investigated further based on evaluation of the integrated database of old and new seismic data, with correlation to wells in the Stenlille area, to characterize its tectonic and depositional evolution, composition with reservoir-seal couples, faults and geometry towards maturation for potentially geological storage of CO_2.

3. Geological setting

The central to western Zealand area, including the Havnsø structure, is located in the eastern part of the Norwegian–Danish Basin (Vejbæk 1997), which is also termed the Danish Basin (Nielsen 2003). The Danish Basin trends WNW−ESE between the Ringkøbing–Fyn High and the North German Basin to the south and the Sorgenfrei–Tornquist Zone at the southern boundary of the Skagerrak–Kattegat Platform to the north (Fig. 3.1, 3.2).

The Danish Basin is an eastern part of the larger Norwegian–Danish Basin with connections to the North Sea region and an intracratonic structure formed since the Late Palaeozoic (Vejbæk 1997) as a major basin caused by Late Carboniferous–Early Permian stretching and faulting, followed by thermal subsidence. The top pre-Zechstein surface or the base of the Zechstein forms the basis of the basin, as shown in Figure 3.2. The deep structures of the crystalline basement and the Cambrian to Lower Permian sedimentary successions constitute the rock sequence below the Danish Basin.

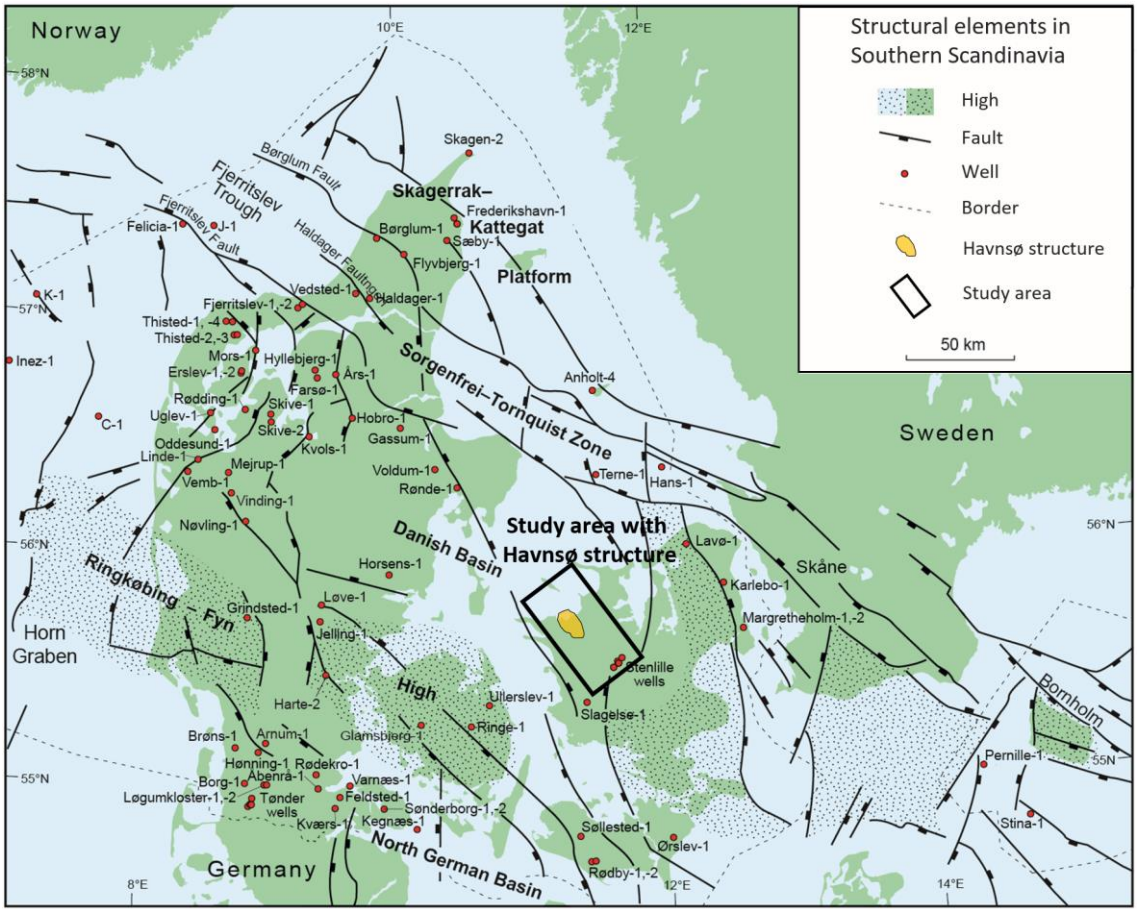

Figure 3.1. *Map of the main structural elements including highs, basins, and main faults onshore and offshore Denmark. The study area is mostly within the black square from the Havnsø structure (orange polygon) to the Stenlille area with wells. The structural elements include the Danish Basin (SE part of the Norwegian–Danish Basin), the Sorgenfrei–Tornquist Zone, the Skagerrak–Kattegat Platform, the Ringkøbing–Fyn High and the northern part of the North German Basin. Positions of deep wells are also marked. Modified from Nielsen (2003).*

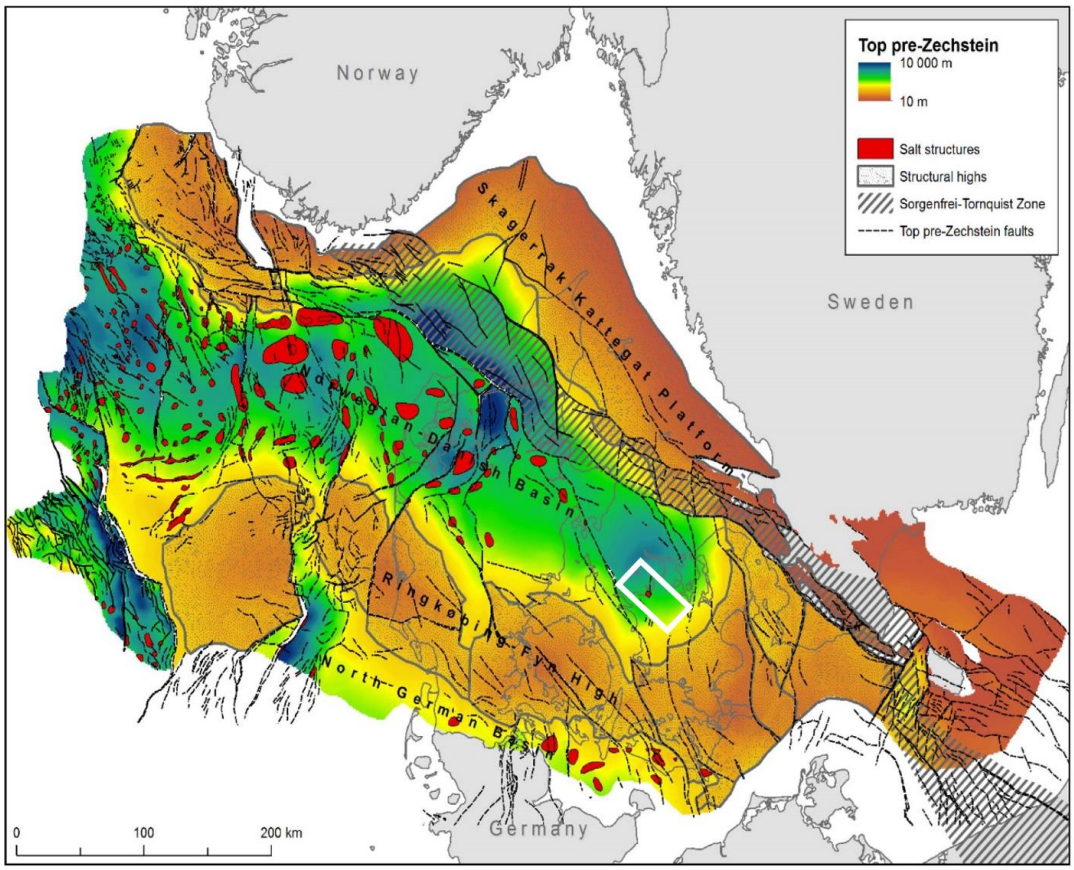

Figure 3.2. *Map to the Top pre-Zechstein surface showing the deep main structural elements onshore and offshore Denmark, including highs, basins, and main faults. The location of the Havnsø to Stenlille study area is marked with a white rectangle. The elements include the Norwegian–Danish Basin (eastern part in Denmark is the Danish Basin), the Sorgenfrei–Tornquist Zone, the Skagerrak–Kattegat Platform, the Ringkøbing–Fyn High and the northern part of the North German Basin. Modified from Vejbæk & Britze (1984).*

Stretching of the lithosphere below the Danish–Norwegian Basin caused Carboniferous−Permian rifting with extension, normal faulting followed by basin subsidence, and the Ringkøbing–Fyn High probably formed at same time due to less stretch than basin areas (Vejbæk 1997). The tectonism led to formation of large, rotated fault blocks, intrusive volcanism, extensive erosion, and mostly coarse siliciclastic deposition (Rotliegende) affecting large parts of the basin (Vejbæk 1997; Michelsen & Nielsen 1991, 1993; Nielsen 2003). After mainly evaporites (Zechstein Group) developed in shallow basin areas during late Permian time, the region subsided and thick Triassic clay and mud-dominated successions formed with a few sandstones, carbonates and halites (Bunter Shale, Bunter Sandstone, Ørslev, Falster, Tønder, Oddesund, Vinding Formations; Fig. 3.3, 3.4, 3.5A,B).Sandstones are in particular known from the Bunter Sandstone Formation (Bertelsen 1978, 1980). During the Late Triassic−Early Jurassic time, sand-rich continental–fluvial, coastal near and shallow marine sand-rich systems interbedded by more clay-rich intervals formed and now constitute the widely distributed Gassum Formation (Fig. 1.3, 3.4, 3.5C). During the latest Triassic (Rhaetian) and into the earliest Jurassic (Hettangian – early Sinemurian) times the coastal to continental areas were repeatedly overstepped by the sea (Fig. 3.6). The relative sea-level rise resulted in the deposition during the Early Jurassic of thick clay-dominated successions with some silty and sandy layers (Fjerritslev Formation), which have been correlated basin wide in several depositional sequences and members (Nielsen 2003; Michelsen et al. 2003).

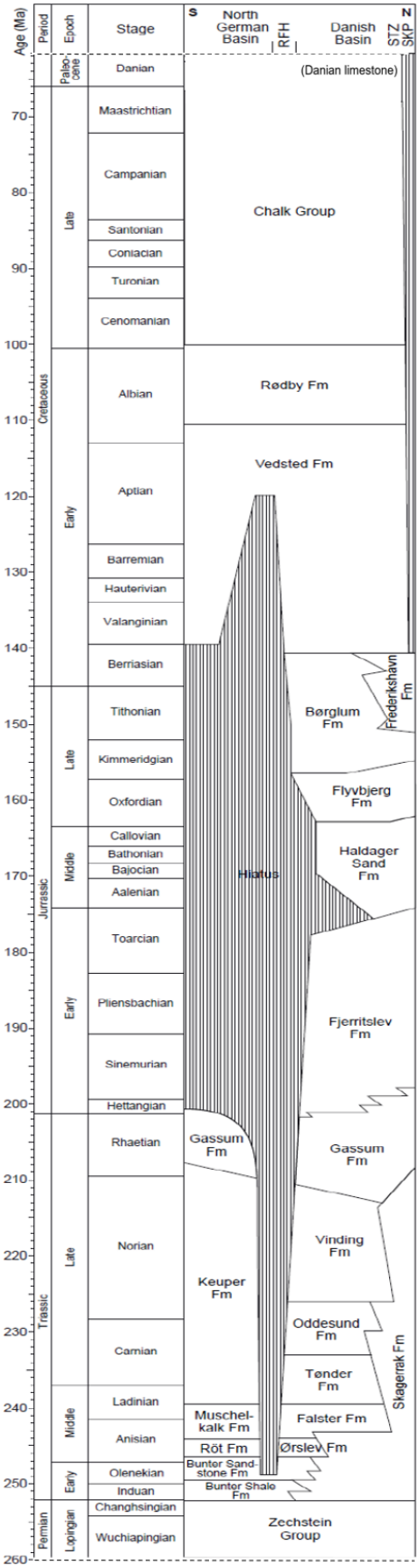

Figure 3.3. *Generalized stratigraphy in the Danish Basin from north to south, mostly representative of the Jutland part of the basin. The Havnsø to Stenlille area is located in the eastern part of the Danish Basin (Fig. 3.2), just north of Ringkøbing-Fyn High (RFH), equivalent to the central figure part, without M-L Jurassic formations. Dashed horizontal lines at the top and base of the scheme indicate omitted Selandian + Quaternary and pre-Zechstein successions, respectively, due to space limitation. Based on Bertelsen (1980) and Nielsen (2003).*

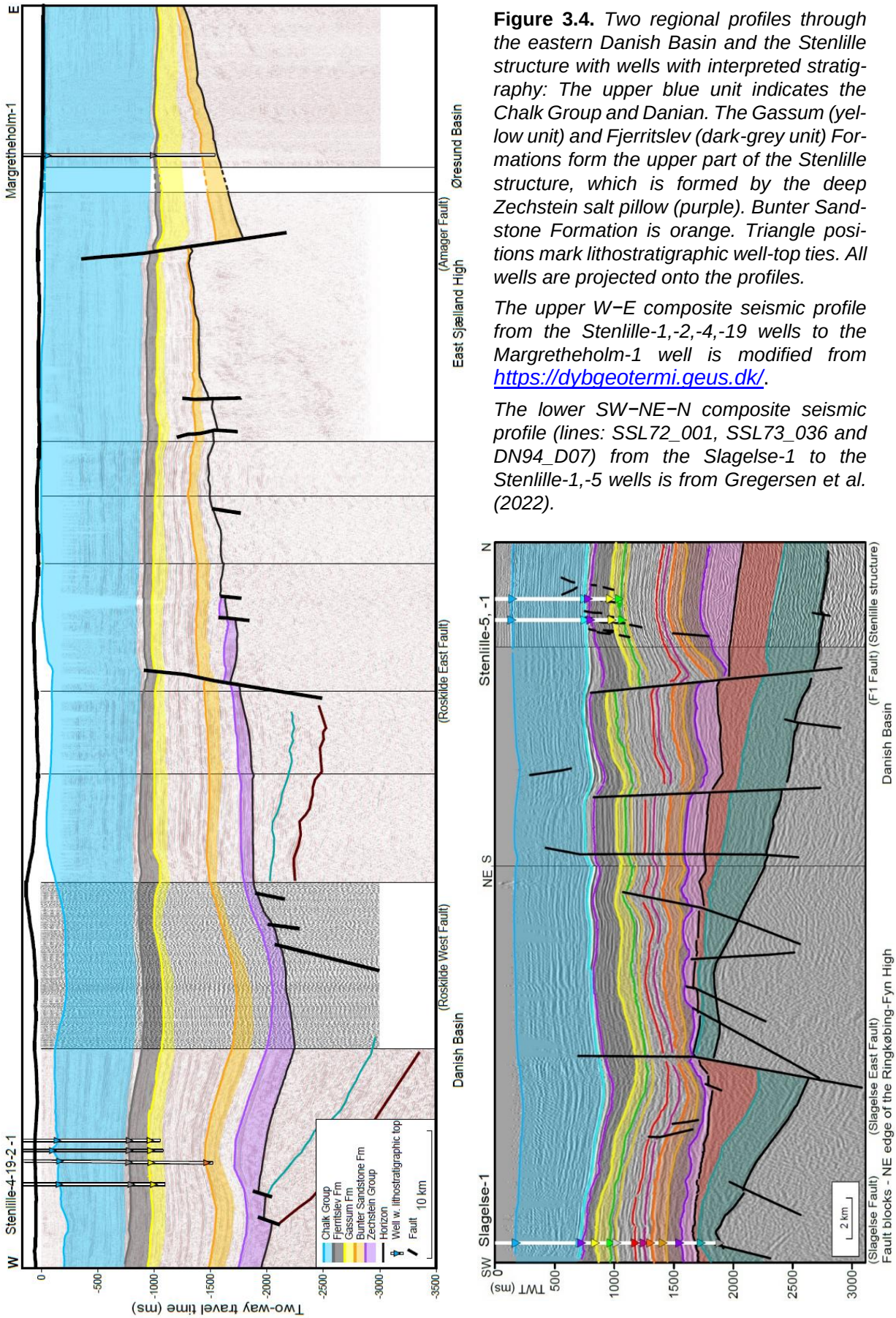

Figure 3.4. *Two regional profiles through the eastern Danish Basin and the Stenlille structure with wells with interpreted stratigraphy: The upper blue unit indicates the Chalk Group and Danian. The Gassum (yellow unit) and Fjerritslev (dark-grey unit) Formations form the upper part of the Stenlille structure, which is formed by the deep Zechstein salt pillow (purple). Bunter Sandstone Formation is orange. Triangle positions mark lithostratigraphic well-top ties. All wells are projected onto the profiles.*

The upper W−E composite seismic profile from the Stenlille-1,-2,-4,-19 wells to the Margretheholm-1 well is modified from https://dybgeotermi.geus.dk/.

The lower SW−NE−N composite seismic profile (lines: SSL72_001, SSL73_036 and DN94_D07) from the Slagelse-1 to the Stenlille-1,-5 wells is from Gregersen et al. (2022).

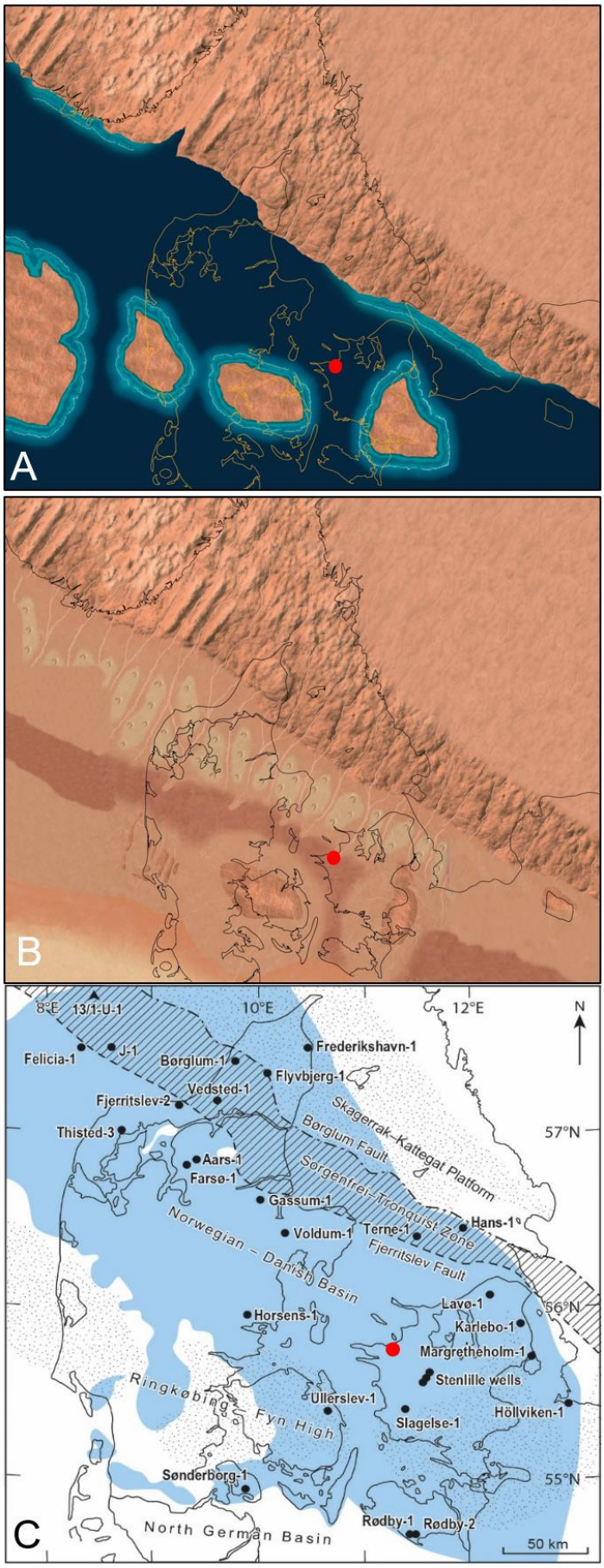

Figure 3.5. *Paleogeographic maps of Denmark and southern Scandinavia illustrating the possible distribution of general depositional environments. The central part of the Havnsø structure area is located at a small red circle.*

A. Late Permian (Zechstein) sea (dark blue), coastal near areas (light blue) and onshore areas (orange red). From Rasmussen & Nielsen (2020).

B. Early–Middle Triassic (incl. the Bunter Sandstone Fm) dominated by desert with local sand dunes, lakes and sabkhas. From Rasmussen & Nielsen (2020).

C. Late Triassic (Rhaetian) to earliest Jurassic (Hettangian – early Sinemurian) Gassum Fm distribution in Denmark. (Olivarius et al. 2022).

Earlier work (e.g. Nielsen 2003; Vosgerau et al. 2020; see also Section 7.1) show, that the Gassum Fm is composed of several depositional sequences with regressions–transgression cycles and deposition in onshore, nearshore, and shallow marine environments.

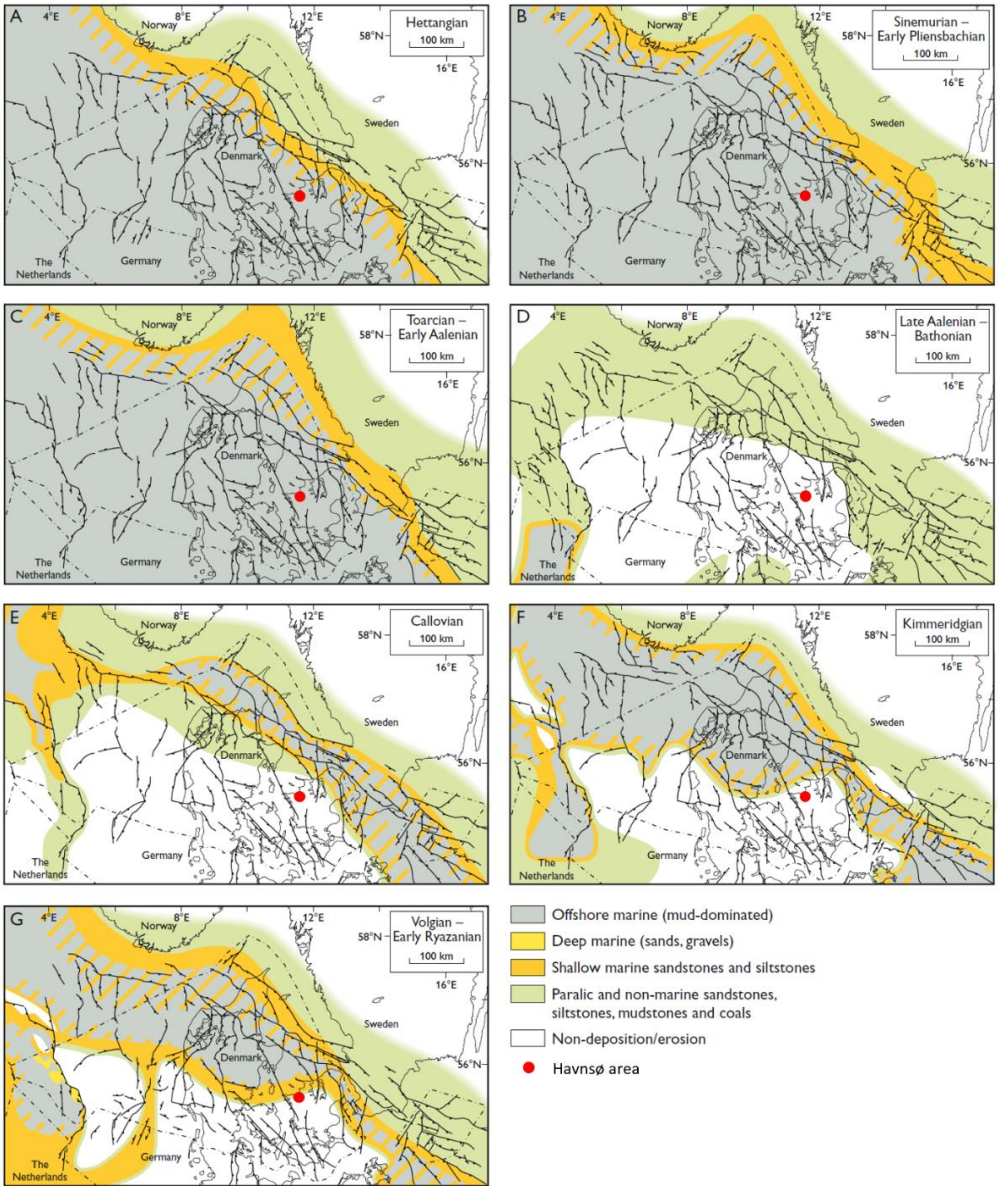

Figure 3.6. *Paleogeographic maps of Denmark showing the inferred distribution of general depositional environments during the Jurassic time, when the primary seal of the Fjerritslev Formation was deposited. The central to western Zealand, incl. the central part of the Havnsø structure area (red circle), is dominated by deposition of marine clays with some layers and beds of siltstone and sandstone, from Hettangian to Toarcian or Aalenian (A–C), whereas sedimentary successions are not shown (removed or not deposited?) during the Middle- and Late Jurassic times. From Petersen et al. (2008) modified from Michelsen et al. (2003).*

Mainly Middle−Late Jurassic regional uplift and salt mobilization led to formation of structures, associated faults, and major erosion in large parts of the eastern Danish Basin, with a hiatus expanding towards the Ringkøbing–Fyn High (Fig. 3.3) (Nielsen 2003). Renewed subsidence in the Early Cretaceous resulted in mudstones dominated successions with local sandstones, which became gradually more calcareous during the Albian (Rødby Formation). Chalk (Chalk Group) was formed throughout the Danish Basin in the Late Cretaceous, and structures were elevated due to regional inversion. Finally, Cenozoic incl. Quaternary successions were deposited in the Danish Basin, with episodic uplift (Japsen & Bidstrup 1999; Japsen et al. 2007).

4. Database

4.1 Seismic data

The geophysical database on the Havnsø structure is limited with mostly old (1960s to 1970s), poor seismic lines, but also with new 2D seismic data (GEUS2022-HAVNSOE survey) from 2022 acquired for this project (Fig. 4.1.1). In contrast, the Stenlille area SE of the Havnsø structure includes a comprehensive database with 20 wells, a 3D seismic survey from 1997 (reprocessed for GEUS in 2023), relatively recent 2D seismic surveys (1980s to 1990s) and a small new (GEUS2022-STENLILLE) survey of this project (see Gregersen et al. 2023).

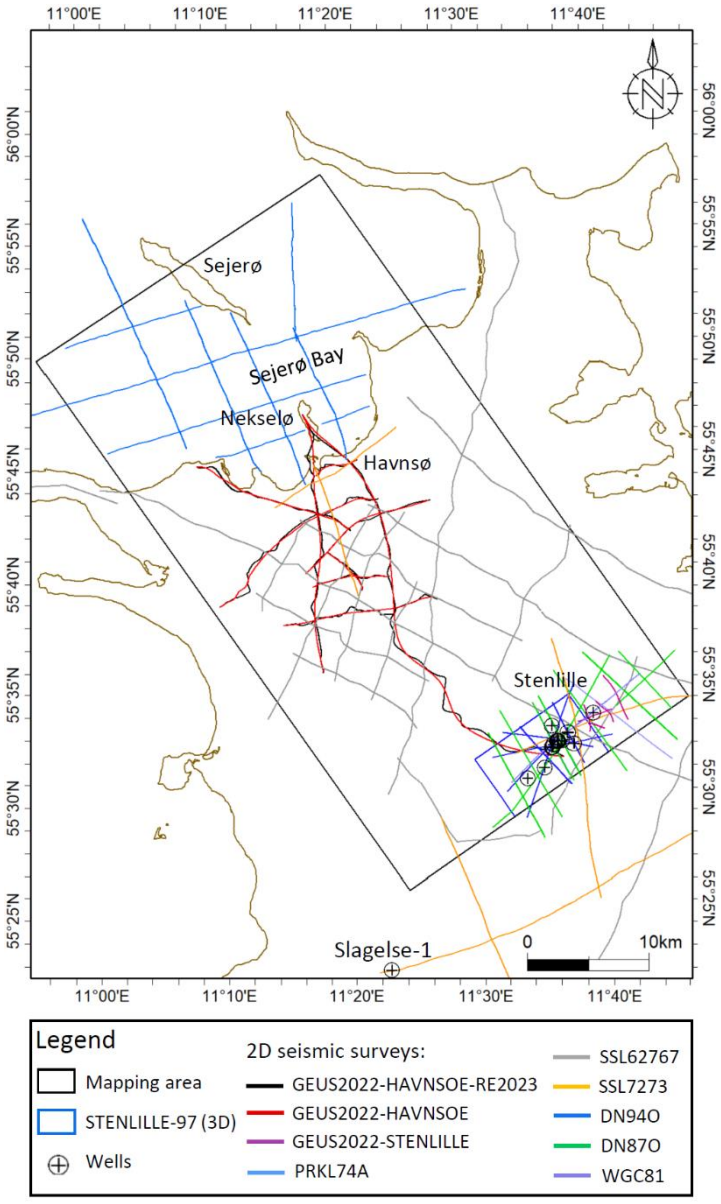

Figure 4.1.1. *Project database at the greater Havnsø area with the new 2022 Havnsø 2D seismic survey (GEUS2022-HAVNSOE) and older onshore and offshore data and wells. The project area also includes comprehensive datasets of the Stenlille area SE of the Havnsø area, with a 3D survey, older 2D surveys and a new from 2022 with five lines, and 20 wells used for ties with the Havnsø data into the Havnsø area. See also positions of the new Havnsø lines in Fig. 4.2.1.*

This chapter will focus on the new data of the GEUS2022-HAVNSOE survey integrated with the old data and used here for description and interpretation of the Havnsø structure. The used seismic data are described below. The database used is shown in Figures 4.1.1,–2 and Table 4.1.1.

The 2D seismic survey GEUS2022-STENLILLE is a new survey acquired February 2022, organized by GEUS as part of the ongoing maturation efforts regarding application of CCS. The survey was acquired and processed by Uppsala University (Malehmir & Papadopoulou 2022). The survey is located at the NE flank of the structure, near the NE boundary of the 3D seismic survey (Fig. 4.1.1). The purpose of the survey was to add quality data and coverage to this data poor part of the structure flank, where only few and old seismic lines exist, for a better definition of the structure geometry and closure, reservoir–seal successions, and faults. In addition, it was a test of equipment, settings and lay-out for possible further site investigations. Five seismic lines, in total c. 12.5 km, were acquired (see more details in Section 4.2). Data and report are available via GEUS: Processing summary sheet (geus.dk)

The 3D seismic survey STENLILLE-97 (Fig. 4.1.2) was carried out in 1997 by THOR Geophysikalische Prospektion GmbH on behalf of Dansk Olie og Naturgas A/S (DONG) and it covers totally 56.4 km^2 and was acquired as vibroseis with 1−3 vibrators conducting minimum 4 sweeps in 20 seconds with a frequency range of 10–120 Hz (THOR, 1997). The survey was processed by CGG, and the survey datum plane elevation is at the mean seal level, the data is in zero phase with reverse SEG polarity, the nominal bin size is 20 m x 20 m, and the nominal stacking fold is 16 (CGG 1998). The 3D survey is reprocessed in 2023 by Realtime Seismic for GEUS and this reprocessed survey: STENLILLE-97-GEUS-RE2023 is also available from GEUS (link to CCS-data).

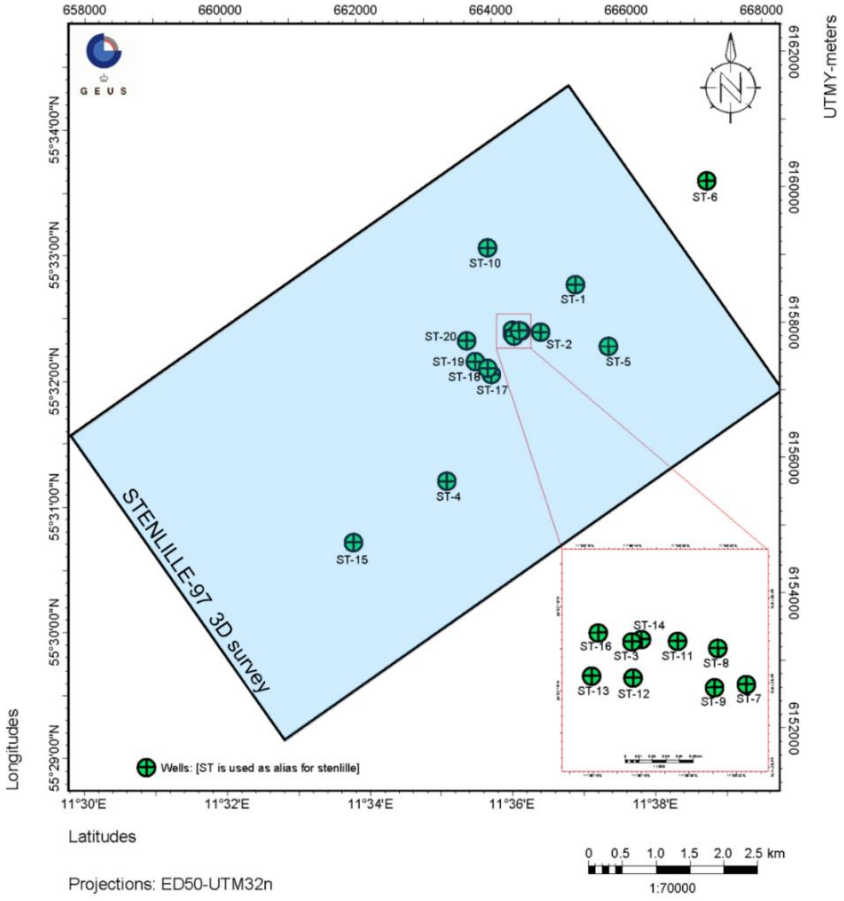

Figure 4.1.2. *Database at the Stenlille structure with positions of wells and the 3D seismic survey (STENLILLE-97). See Fig. 4.1.1 for position of seismic 2D lines and surveys.*

The 2D seismic survey DN94O was acquired in 1994 by Compagnie Générale de Géophysique (CGG) for Dansk Olie og Naturgas A/S (DONG). The eight survey lines are located across the Stenlille structure in the area of the later 3D survey; more details are available in the acquisition report.

The 2D seismic survey DN87 (DN87O and DN87I) was acquired in 1987 by Prakla-Seismos AG for Dansk Operatørselskab i.s. (Danop) and nine lines of the survey were used in the study area. The seismic lines are located across the Stenlille structure in the area of the later 3D survey with a few lines further to the SW and NE; more details are available in the acquisition report.

The more recent vintage data (1987 to 1997) were acquired mainly to develop gas storage in the Stenlille structure. Older data were mainly acquired more regionally to map for structures relevant for petroleum exploration.

The 2D seismic survey WGC81 was carried out in 1981 by Western Geophysical Co. for DONG, and here only two of the lines were used, as some of the lines were approximately acquired again by better quality data of the DN94O survey.

The 2D seismic survey SSL7273 was carried out in 1972 and 1973 by Gulf Oil Co. Denmark for Dansk Undergrunds Consortium (DUC) and six lines were used, although mostly of poor quality.

The oldest seismic dataset is the 2D seismic survey SSL6267, which was acquired in 1962–67 by Gulf Oil Co. Denmark and Shell for DUC, and four lines were used in area where other lines are missing, although they mostly are of very poor quality (Table 4.1.1).

Released seismic surveys, and acquisition and processing reports are available through the data web portal at GEUS: Danish Deep Subsurface Data (geus.dk) or by requests to the GEUS Subsurface Archive: info-data@geus.dk.

The quality of the seismic data in the study area is highly variable from very good to very poor (Table 4.1.1, Fig. 4.1.3, 4.1.4). Most of the oldest 2D seismic surveys from the 1960s and 1970s are generally very poor to poor in quality, whereas the more recent 2D and 3D seismic data are generally of good quality and in digital format.

In the Stenlille area variable data quality and data mis-ties may be related to different parameters and different amounts of gas storage at the difference acquisition times, which affects the seismic signals differently. In some of the data, especially in the old surveys, there are significant noise, however also in the new 2D surveys.

In the new Havnsø data noise especially occur at end and at bendings of the lines. Different processing approaches on the data and line positions, such as the binning, lateral smoothing, and where lines are crocked have affected the final line positions and thus the ties. Preserving much original positions (and crookedness) can more accurately keep the original recording positions and ties to existing seismic and well data but can also give significant noise at the crooked bends, whereas strongest noise can be reduced on more smoothed lines. This has not been studied further in this project, but a good example is at the southernmost end of P1 and the northern part of P2, where the line has been smoothed in the original processing (GEUS2022-HAVNSOE), whereas the reprocessing (GEUS2022-HAVNSOE-RE2023) preserved more crookedness, but also shows the noise zones more clearly at line turnings (Fig. 4.3.3, 4.3.4).

Table 4.1.1. *The seismic surveys and lines used in, and slightly out of the mapped area from Stenlille to Havnsø and the data quality.*

Seismic survey	Seismic lines	Data quality
GEUS2022-HAVNSOE	GEUS22-HVN-P1, P2, P2.5, P3, P4, P6, P7, P8	Good
GEUS2022-HAVNSOE-RE2023	GEUS22-HVN-P1, P2, P2.5, P3, P4, P6, P7, P8	Very good
GEUS2022-STENLILLE	GEUS22-STL-P1, P1.5, P2, P3, P4	Moderate and good
STENLILLE-97-GEUS-RE2023	3D data	Very good
DN94O	01, 02, 03, 04, 05, 06, 07, 08	Good
DN87O	001, 003, 004, 005, 006, 007, 008, 009, 010	Good
SSL6267 (R-lines)	R4-37117, R9-37126, R9-1-37126, R13-37131	Very poor
WGC81	8110, 8113	Moderate and good
SSL7273	72-001, 73-025, -036, -037, -038, -039	Poor and moderate
PRKL74A	All	Moderate

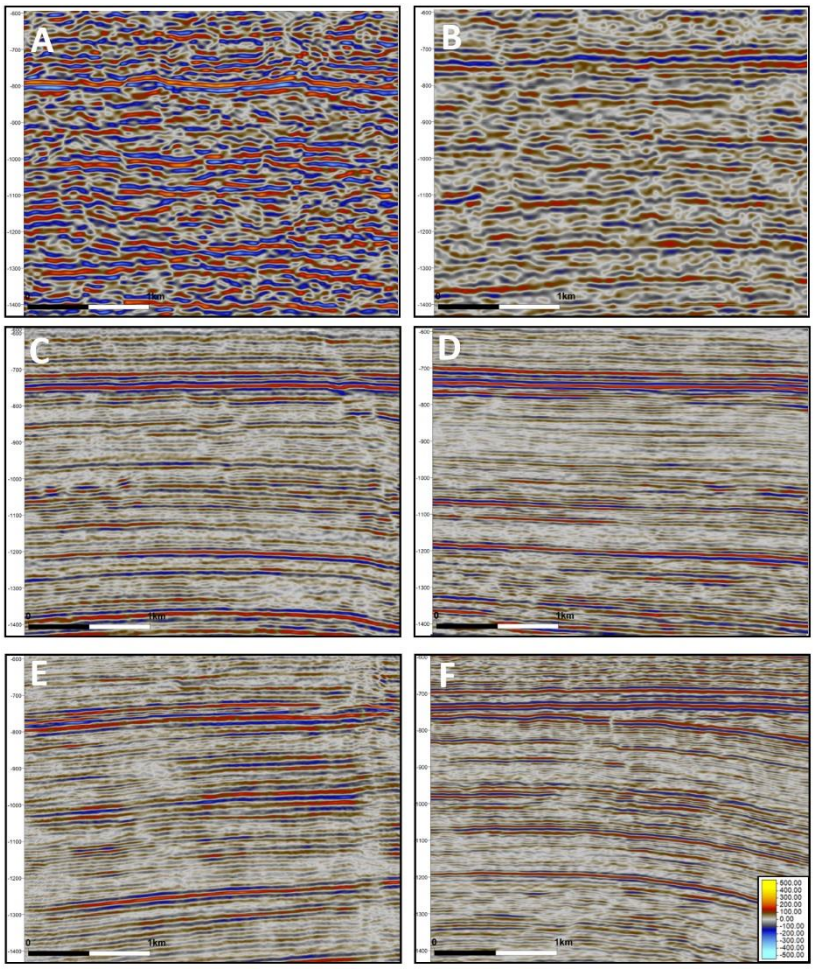

Figure 4.1.3. *Examples of seismic data quality (two-way time sections). A. Very poor data quality of 1960s data (SSL6267_R4). B. Poor to moderate quality of 1973s data (73-036). C. Good quality of the 1987 data (DN87-007), (D) 1994 data (DN94-D01), and (E) 2022 data ('P3'). F. Very good quality of the 1997 3D data (Xline495). All the surveys are represented in the study area (Fig. 3.1). All lines except the 3D Xline are time shifted. Compare these vintage data to the new original and reprocessed data (Fig. 4.1.4, 6.1.3, 6.1.4).*

Seismic data mis-ties

The 2D seismic profiles in the study area (Fig. 4.1.1) have different datum elevations, mostly related to different static corrections, topography, etc. In this context and in relation to the data acquired, also the level of the water saturated zone (groundwater) plays a role and will be slightly different depending on the season of the year and wet or dry periods. The topography from Stenlille to Havnsø is variable, with up to more than 80 m above msl within the new 2D survey area.

In order to compensate for many differences in the datum elevation between seismic profiles, it was decided to use processing to mean sea level (msl) as the seismic reference datum, and for mapping purpose in this project to conduct static vertical time shifts (a constant and non-data stretched shift) of each 2D seismic profile.

The new onshore 2D seismic survey GEUS2022-HAVNSOE was acquired by Uppsala University for GEUS in 2022 across the Havnsø structure (Fig. 4.1.1). The southernmost profile (P1) starts with a tie within the 3D seismic survey near at the Stenlille-19 well to connect with the Stenlille data and interpretation in order to facilitate the tie to the Havnsø structure. This is also important in order to contribute to sort out the mis-fit of the older data and optimize correlation of formations and sequence surfaces.

The Stenlille 3D seismic survey from 1997 is reprocessed by Real Time Seismic for GEUS (STENLILLE-97-GEUS-RE2023) and ties with a line (P1 with a small timeshift) of the new reprocessed version of the 2022 Havnsø 2D seismic survey by Real Time Seismic for GEUS (GEUS2022-HAVNSOE-RE2023). The key-tie line P1 line connects directly all the way from the Stenlille 3D survey area (near wells) and to Havnsø and Nekselø (Fig. 4.1.1). This line is available in a version merged with the marine data (OBS and streamer) recorded in the narrow strait between Havnsø and Nekselø.

The reprocessed 3D survey is also used for tying the seismic data with wells using synthetic seismic data. The reported datum plane elevation of the 3D seismic survey (STENLILLE-97) is the mean sea level, and the final data are with reverse SEG polarity convention (white trough representing an increase of acoustic impedance), in zero phase (CGG, 1998: Final report of seismic data processing. Survey: STENLILLE-97 3D survey). Most 2D data in this project area is also in SEG reverse polarity.

Mis-ties were investigated visually and also digitally with the Petrel SRD Manager to constrain the time-shifts. The visual mis-tie screening and the Petrel mis-tie analysis show that there are data mis-ties between different seismic surveys, but also between lines of the same surveys in the order of mostly approx. 10−40 ms TWT, but up to 48 ms TWT. Some of the mis-ties requires a dynamic shift (gradual time shifts stretching/squeezing the data) on the same line to make a full fit at crossing seismic sections. To preserve sections we use here constant shifts focused on the interval from c. 700 to 1500 ms TWT.

It was decided to first conduct constant digital time-shifts via Petrel manager, and then manual constant time-shift for each seismic line. The adjusted and used time-shifts are shown in Table 4.1.2 below. The new 2D survey, both originally processed and reprocessed fit near to the marine data, and also approximately (only 7 ms difference) the reprocessed 3D data (with msl datum). The original 3D survey (STENLILLE-97) is 40 ms too shallow (not in the table). In this study the reprocessed version was used.

Table 4.1.2. *Seismic surveys & lines used in the mapped Stenlille–Havnsø area with time-shift.*

Survey	**Line and survey: Vertical, constant time-shift (millisecond TWT) - to fit the reprocessed Stenlille 3D survey (STENLILLE-97-GEUS-RE2023)**
GEUS2022-HAVNSOE	GEUS22_HVN_P1: -7ms; P2, P3, P5: 0ms; P2.5, P4: -16ms; P6: -48ms; P7: -30ms; P8: -18ms
GEUS2022-HAVNSOE-RE2023	GEUS22_HVN_P1, P3: -7ms; P2: -21ms; P2.5: -5ms; P4, P5, P6: -26ms; P7: -16ms; P8: -36ms
GEUS2022-STENLILLE	GEUS22_STL_P1, P1.5, P2: 20ms; P3: 40ms; P4: 30ms
STENLILLE-97-GEUS-RE2023 (3D survey)	0ms (datum plane elevation: mean seal level)
DN94O	D01, D02, D03, D05, D07: -16ms; D04, D06, D08: -11ms
DN87O	001, 003, 004, 007: -19ms; 005, 008: 1ms; 006, 009, 010: 6ms
SSL6267	R2, R7, R16: 0ms; Other lines: 21ms
WGC81	8110: 0ms; 8113: 21ms
SSL7273	72-001, 73-025: 30ms; 73-036: 15ms; 73-037, -038, -039: 10ms
PRKL74A (offshore)	0 ms (at mean sea level)

First, the 2D seismic profile GEUS22_HVN_P1 ('P1') is shifted -7 ms (down) to fit the reprocessed 3D seismic survey (e.g., Inline1164 close to the ST-19 well). The P1 line is located c. 700 m South of the ST-17, -18, -19 wells. Then other lines of same survey crossing P1 are adjusted to this line, then the other lines are adjusted internally in this survey, and finally all the other, older 2D lines are adjusted to this survey.

Figure 4.1.4 shows an example, where the new 'P1' line acquired and processed by Uppsala University is shifted -7 ms to fit the 3D survey (inline 1171), reprocessed by Realtime Seismic. Mis-tie corrections for the surveys were only applied in this Petrel project for mapping purposes. It was not possible within the frame of this study to sort out all mis-ties, but mis-ties are described here for the present mapping and for future consideration. It is important to be aware of the mis-ties and adjust data, to avoid bad ties and errors in interpretation and mapping.

It can be suggested for further studies to perform more detailed analyses to set the elevation plane of each seismic line and survey compensating e.g., statics, topography, groundwater level, etc. more accurately and to fit all the seismic profiles. However, this may be rather resource demanding.

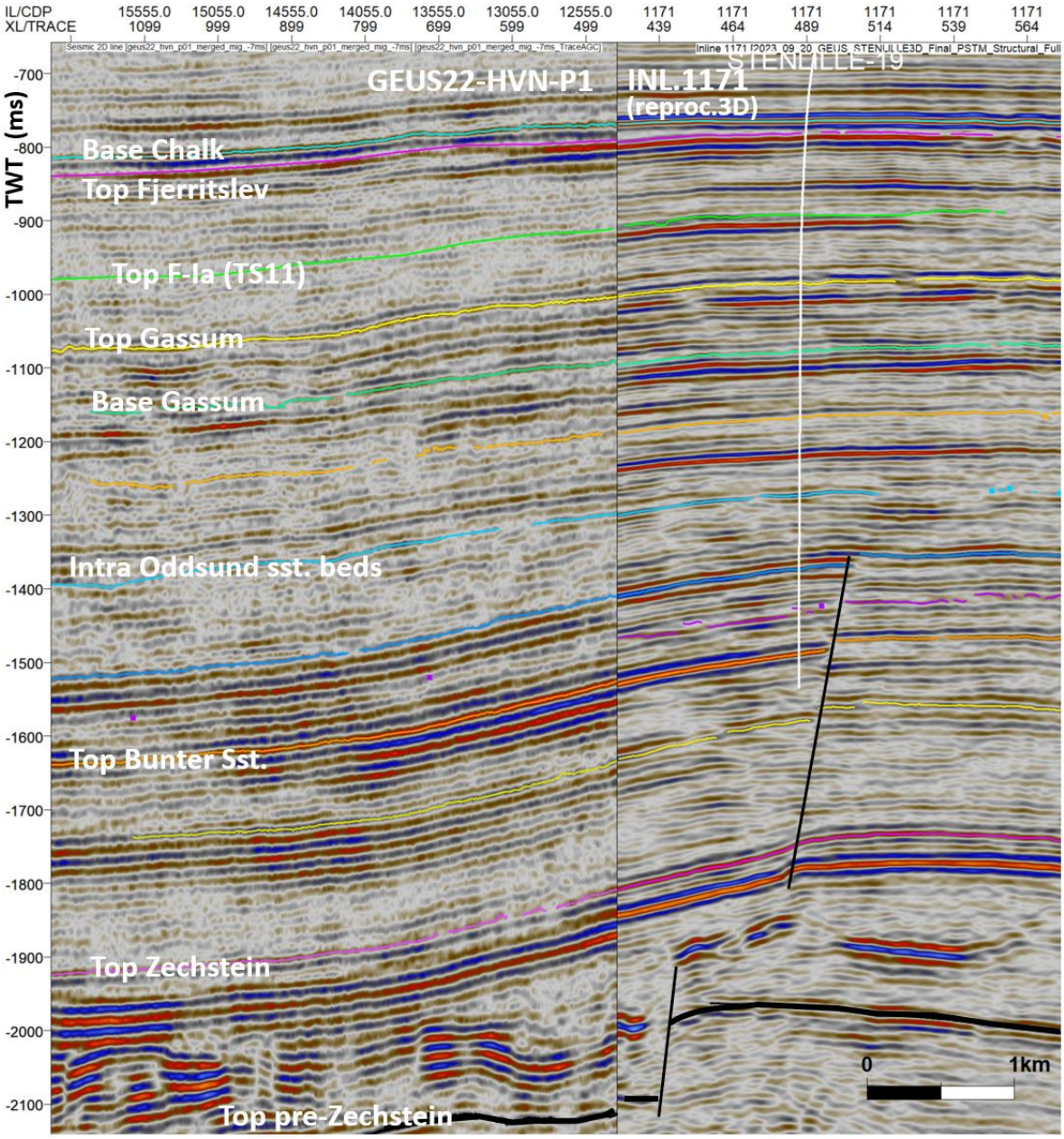

Figure 4.1.4. *The new GEUS22-HVN-P1 ('P1', left) line acquired, and processed by Uppsala University, is shifted -7 ms to fit the 3D Stenlille-97 survey (inline 1171), reprocessed by Realtime Seismic. Seismic interpretation of this study and the projected Stenlille-19 well are also shown.*

4.2 New seismic data acquired in this project

The new seismic survey: GEUS2022-HAVNSOE and reprocessing

The new GEUS2022-HAVNSOE 2D seismic survey acquired over the Havnsø structure from Stenlille to Havnsø in 2022 is organized by GEUS for the initial maturation described in this report, and with Uppsala University in charge of acquisition and first processing. Each of the survey profiles are named: GEUS22_HVN_P1, -P2, -P2.5, -P3, -P4, -P5, -P6, -P7, -P8, with line km lengths in total c. 130 km (130.7 km). The positions of the profiles are shown in Fig. 4.2.1, where they are abbreviated P1 – P8. Line extensions include a reference to the type of the geophone recording: streamer, wireless and merged (streamer & wireless together), and if the version is stacked (stk), or stacked and migrated (mig) - e.g., GEUS22_HVN_P1_merged_stk. Link to survey: Processing summary sheet (geus.dk)

In addition, GEUS issued a company reprocessing in 2023 of the GEUS2022-HAVNSOE survey: GEUS2022-HAVNSOE-RE2023 (Realtime Seismic 2023), also available from GEUS. Link to survey: Processing summary sheet (geus.dk). Contact to GEUS on data by email: info-data@geus.dk.

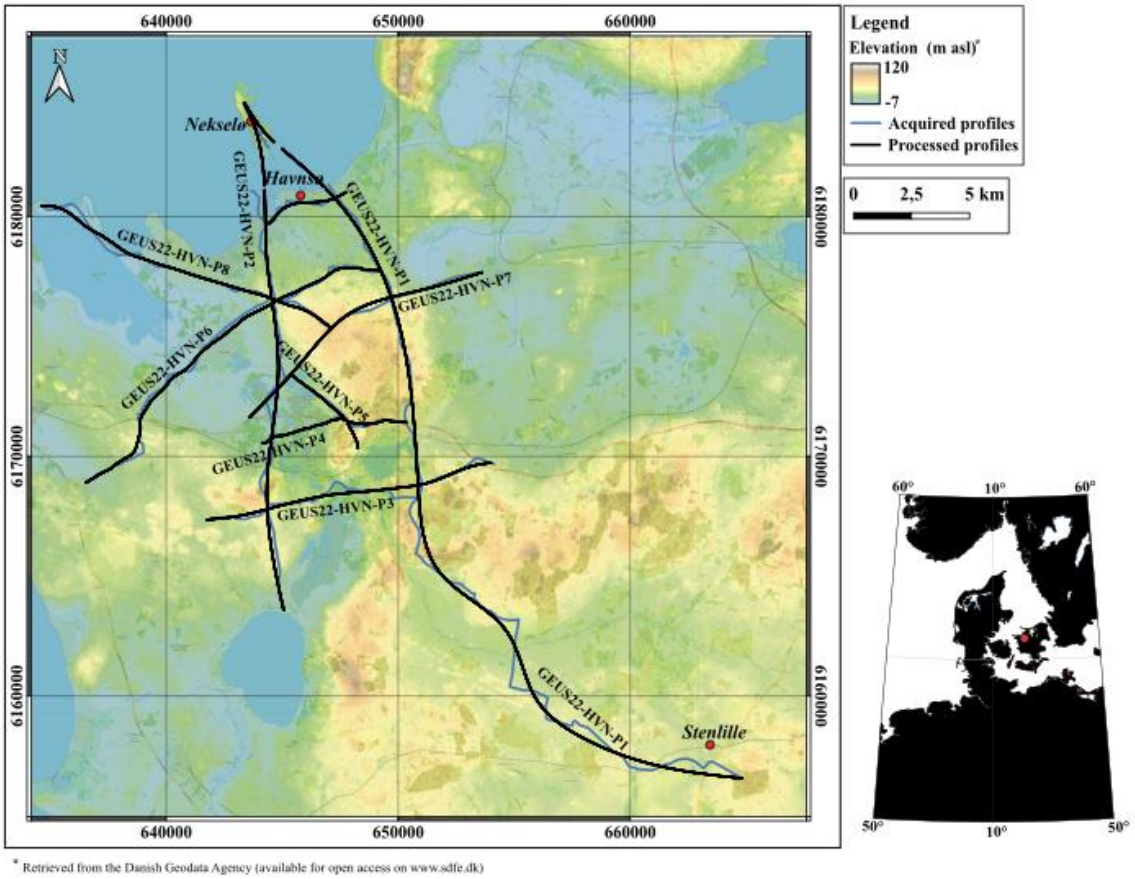

* Retrieved from the Danish Geodata Agency (available for open access on www.sdfe.dk)

Figure 4.2.1. *Map with locations of the seismic profiles from the acquisition and processing report (Malehmir & Papadopoulou, 2023). Black lines are locations of the final migrated seismic profiles (here the profiles of wireless and merged files). Blue lines are locations at the roads, or at the short marine strait to Nekselø, where the seismic data were acquired. For information of data contact GEUS (access from website or email to info-data@geus.dk).*

Acquisition of the survey by Uppsala University

Background and purpose

In November 2021, GEUS contracted Uppsala University to acquire and process a new small seismic survey with nine reflection seismic profiles of the survey GEUS2022-HAVNSOE, in a research and development cooperation. The survey was conducted from August 1st to October 10th 2022 (Fig. 4.2.1, 4.2.2) and is delivered and reported in the acquisition and processing report of June 2023 (final revision by Sept. 25th 2023) by Malehmir & Papadopoulou (2023) (Fig. 4.2.3).

The purposes of this cooperation acquisition project are mainly:
(1) to improve the database at the data-poor area between Stenlille and Havnsø to mature the Havnsø structure towards potential storage of CO_2;
(2) to acquire new seismic lines to improve the data coverage with modern data;
(3) to acquire modern high fold data for imaging and interpretation of the shallow and deeper subsurface, in particular the key reservoir (mainly Gassum Fm), seal (mainly Fjerritslev Fm), faults and the geometry of the Havnsø structure.
(4) to expand knowledge of CCS operations through research and education, here in cooperation with universities.

Collaboration partners

Uppsala University contracted the Polish company Geopartner Sp. zo.o with two small trucks with vibration hydraulic pistons as source for the vibro-seismic data. Students in Geophysics and Geoscience from both University of Copenhagen and Uppsala University were hired as field assistants to conduct field support, including handling, and moving the wireless geophones with Differential GPS surveying, adjusting the landstreamer, handling the road traffic signs, distributing information folders and flyers to citizens. COWI was contracted for acquiring permits, logistical planning, assessments in relation to landowners and supported on external contacts to authorities and citizens. Gas Storage Denmark A/S supported the acquisition with much help, including logistics of housing project meetings and storage of equipment.

Communication & meetings

Communication with the local community was provided through three public information meetings in June 2022, on June 16th (Jyderup hallen), on June 20th (Væksthus Havnsø), and on June 22nd (Gas Storage Denmark). Public visit days were on August 23rd and September 18th. Information flyers and folders were provided to landowners in the vicinity of the acquisition, and information mainly on the website of project. In addition, local medias made interviews and articles on the acquisition (NORDVESTNYT, April 28th, 2022; Sjællandske Nyheder, August 4th, 2022, August 31st, 2022; Jyllands-Posten, October 17th,2022), and in television (TV2 regionerne).

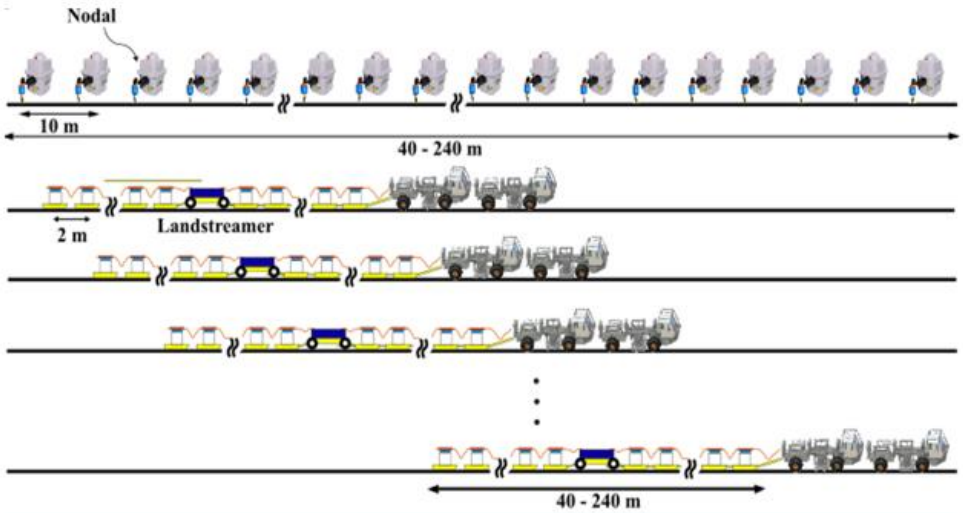
Nodal
10 m
40 - 240 m
2 m
Landstreamer
40 - 240 m

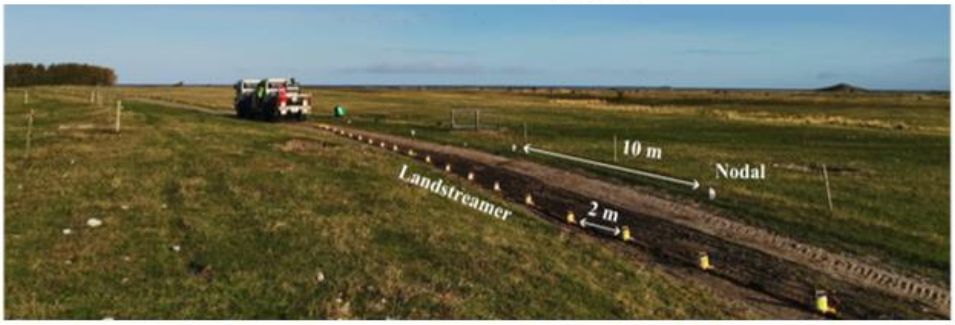
10 m
Nodal
Landstreamer
2 m

Figure 4.2.2 (previous page). *Survey design and equipment. Uppermost two rows: Survey design scheme and photo with two mini-trucks, and behind a landstreamer on the road and separate wireless geophones with a 10 m distance along the road. Middle row: The two mini-trucks NW of Stenlille, a close-up photo of a wireless geophone and a sensitive tool (Micro-Mate) to control-measure the vibration level to avoid too strong vibrations near properties. Lower row: Air photo of the acquisition trucks with the streamer approaching Havnsø and Nekselø in the horizon. The scheme, and the uppermost and lowermost photos are from the acquisition report (Malehmir and Papadopoulou, 2023), and middle photos: GEUS.*

The acquisition took place from August 1st to October 10th 2022 and the seismic data are recorded along the nine lines shown in Figure 4.1.1, with a total length of c. 130 km. The most crocked lines were later geometrically adjusted to become more straight lines, during the processing work to the final lines (Fig. 4.2.1).

As seismic source, two small trucks (INOVA UNIVIB-326; operating at peak-force: 95 kN) were used with synchronized vibrating hydraulic pistons lowered in firm contact with the road (Fig. 4.2.2). Each truck has a weight of 9 ton but were loaded to be 12 ton in total for a better ground contact. Before the acquisition, the field personnel followed a road-safety course, and were equipped with safety clothing during fieldwork.

On August 1st, after briefing of field personnel, equipment was checked, and acquisition tests were performed for optimal acquisition. The trucks generated simultaneous a sweep lasting 18 seconds, increasing in frequency from 10 Hz to 140 Hz (Fig. 4.2.4). At every shot-point location this sweep was repeated three times. The three sweeps were later stacked to one shot-point during the processing to improve signal-to-noise ratio. After each shot-point with three sweeps, the trucks move 10 meters (shot-point distance) to the next shot-point. The last truck drags the attached land-streamer, adjusted along the road by field assistants (Fig. 4.2.2). When passing close to properties, control measurements with a sensitive 'Micromate' devise were carried out at the properties to secure, that vibrations stay below a threshold, as defined by the German norm DIN 4150-3. If the vibrations approached the threshold, the vibrations were stopped or continued with smaller vibration level, and in some cases with sensitive properties the shot-point was skipped.

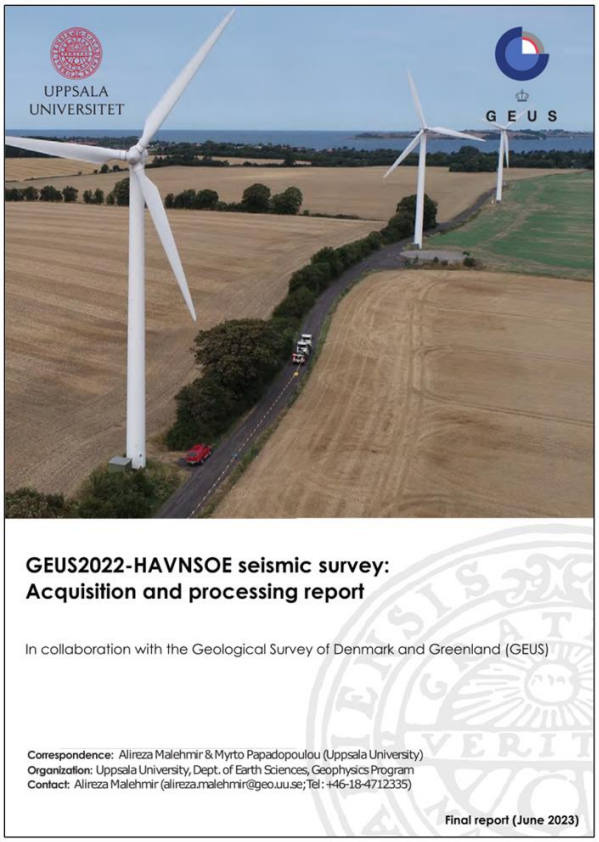

Table of Contents

Figure 4.2.3. *The front page and contents of the GEUS2022-HAVNSOE seismic survey: Acquisition and processing report (Malehmir & Papadopoulou, 2023), which can be purchased through GEUS (access via webpage, or email: info-data@geus.dk).*

As recording equipment connected to the truck data system was used both landstreamer mounted geophones attached to the last truck and road-side wireless geophones (Fig. 4.2.2) and the recording time of the geophones was 25 seconds. The wireless geophones were placed in the roadside with a 10-meter distance and used a frequency of 10 Hz and a 2 ms sampling interval (Table 4.2.1). The landstreamer has mounted a Micro-Electro-Mechanical (MEM) based geophone at every 2 meters with a sampling interval of 1 ms (Table 4.2.1). The landstreamer is developed by Uppsala University and is constructed of attached sections providing a flexible length up to c. 270 meter in this survey. It was shortened after logistical conditions, such as crookedness and other road conditions. From the shortest line (P2.5) to the longest line (P1) the receiver positions varied from 422 to 4,015, and the total number of traces (vertical component) from 21,440 to 219,293 (Table 4.2.1).

Papers, reporting and abstracts from Uppsala University present the results of the acquisition and processing of the GEUS2022-HAVNSOE survey, including: Malehmir & Papadopoulou 2023; Kucinskaite et al. 2023a,b; Papadopoulou et al. 2023a,b; Zappalá et al. in review.

Table 4.2.1. *Table showing the main onshore seismic data acquisition parameters from the 2D GEUS2022-HAVNSOE seismic survey: Acquisition and processing report (Table 1; Malehmir & Papadopoulou 2023).*

Survey Parameters	P1	P2	P2,5	P3	P4	P5	P6	P7	P8
Recording system	Sercel Lite	Sercel Lite	Sercel Lite	Sercel Lite	Sercel Lite	Sercel Lite	Sercel Lite	Sercel Lite	Sercel Lite
Source	INOVA UNIVIB-326 (1)	INOVA UNIVIB-326 (1)	INOVA UNIVIB-326 (1)	INOVA UNIVIB-326 (1)	INOVA UNIVIB-326 (1)	INOVA UNIVIB-326 (1)	INOVA UNIVIB-326 (1)	INOVA UNIVIB-326 (1)	INOVA UNIVIB-326 (1)
Survey geometry	Fixed / Land-streamer	Fixed / Land-streamer	Fixed / Land-streamer	Fixed / Land-streamer	Fixed / Land-streamer	Fixed / Land-streamer	Fixed / Land-streamer	Fixed / Land-streamer	Fixed / Land-streamer
No. of shots	4015(2)	1923 (+227 shots from P1) (2)	422(2)	1439(2)	697(2)	449(2)	1809(2)	1232(2)	1467(2)
Shot spacing	10 m	10 m	10 m	10 m	10 m	10 m	10 m	10 m	10 m
Geodetic surveying	DGPS	DGPS	DGPS	DGPS	DGPS	DGPS	DGPS	DGPS	DGPS
Nodal									
No. of Receiver positions	4015 (10001-14015)	1923 (20001-21923)	422 (25001-25442)	1439 (3001-31439)	697 (40001-40697)	449 (50001-50449)	1809 (60001-61809)	1232 (70001-71232)	1467 (80001-81467)
Receiver spacing	10 m	10 m	10 m	10 m	10 m	10 m	10 m	10 m	10 m
Max. offset	~7800 m	~7573 m	~2572 m	~7715 m	~6300 m	~4210 m	~4210 m	~8000 m	~5550 m
Geophone	10 Hz, Spike	10 Hz, Spike	10 Hz, Spike	10 Hz, Spike	10 Hz, Spike	10 Hz, Spike	10 Hz, Spike	10 Hz, Spike	10 Hz, Spike
Sampling interval	2 ms	2 ms	2 ms	2 ms	2 ms	2 ms	2 ms	2 ms	2 ms
Record length	25 s(3)	25 s(3)	25 s(3)	25 s(3)	25 s(3)	25 s(3)	25 s(3)	25 s(3)	25 s(3)
Nodal data harvesting	GPS time(4)	GPS time(4)	GPS time(4)	GPS time(4)	GPS time(4)	GPS time(4)	GPS time(4)	GPS time(4)	GPS time(4)
Total no. of traces	2,369,171	1,435,434	122,108	185,521	383,897	127,419	1,208,305	919,574	697,719
Landstreamer (SeisMove™)									
No. of receiver positions	4015 (10001-14015)	1923 (20001-21923)	422 (25001-25442)	1439 (3001-31439)	697 (40001-40697)	449 (50001-50449)	1809 (60001-61809)	1232 (70001-71232)	1467 (80001-81467)
Receiver spacing	2 m	2 m	2 m	2 m	2 m	2 m	2 m	2 m	2 m
Max. offset	~ 210 m	~ 240 m	~ 150 m	~ 270 m	~ 137 m	~ 134 m	~ 168 m	~ 210 m	~ 140 m
Sampling interval	1 ms	1 ms	1 ms	1 ms	1 ms	1 ms	1 ms	1 ms	1 ms
Record length	25 s(3)	25 s(3)	25 s(3)	25 s(3)	25 s(3)	25 s(3)	25 s(3)	25 s(3)	25 s(3)
Total no. of traces	219,293(5)	114,631(5)	21,440(5)	69,550(5)	31,135(5)	18,660(5)	92,773(5)	92,991(5)	66,140(5)

(1)Two trucks, 12 t, operating at 95 kN
(2)Three records / point
(3)7 s SEGY raw data, reduced to 5 s for processing
(4)ms accuracy
(5)Vertical component

Marine acquisition of the survey by Aarhus University - with sources from Uppsala University

The survey lines (line GEUS22–HVN–P1) had to cross a 2-km-wide marine strait (Sejerø Bugt) between the port of Havnsø and the island of Nekselø (Fig. 4.2.4). To bridge the water, marine receivers were used to record the onshore vibroseismic sources. Marine sources were not an option due to the shallow water and the protection status as Natura2000 area. With the additional marine data, it will be possible to connect the land data from Nekselø with those from Havnsø. In addition, existing offshore seismic lines can be tied to the new onshore data. The reporting by Funck & Nørmark (2023) describes the recording and initial processing of the marine data, including data examples. Ultimately, the data from the marine receivers have to be merged with those recorded on land, which is described in Malehmir & Papadopoulou (2023).

For the marine component of the acquisition, 18 ocean bottom seismometers (OBS) from the national Danish seismometer pool DanSeis were deployed at the seafloor between Havnsø and Nekselø (Fig. 4.2.5, 4.2.6). These short-period instruments are equipped with three-component geophones and a hydrophone. The latter one has the best data quality. Some stations stopped recording before all Vibroseis sweeps on the two segments (Nekselø and road towards the beach in Havnsø) were completed. However, the data quality of the recorded signals is good. After correlation with the source sweep, reflections can be seen from depths below 2 s two-way travel time.

A second type of receivers was used close to Havnsø. Here a 600-m-long marine streamer with 96 channels was deployed from a winch located on the beach (Fig. 4.2.6). After pulling out the streamer seaward, weight was added to it to lower it down to the seafloor. Data quality is good with exception of the channels close to shore and at the seaward end of the streamer. The poorer data channels are probably caused by increased noise levels due to the surge of waves at the beach and by motion that was transferred from the recovery buoy attached to the tail end of the streamer. Sweeps from the area close to Havnsø produce an almost complete record from the surface to depths greater than 2.5 s two-way travel time, while the larger shot-receiver offsets for the sweeps on Nekselø result in a lack of data in the upper 1.0 to 1.5 s of the record section.

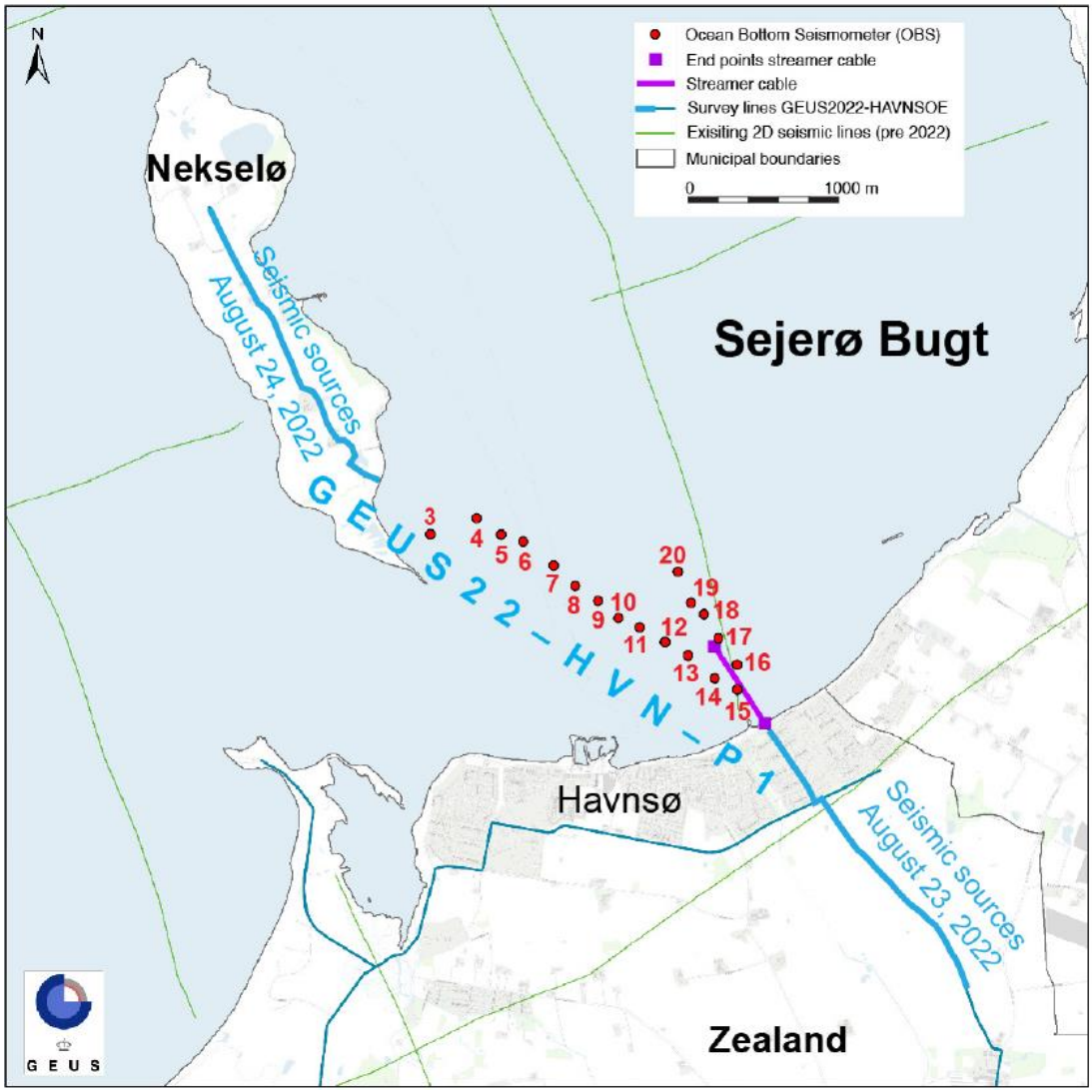

Fig. 4.2.4. *Map from Funck & Nørmark (2023) showing the location of the marine receivers: OBS' (red points) and marine streamer (purple line). The onshore acquired lines (blue lines: GEUS22-HVN-P1) are the nearby route of the source of the vibroseis.*

Fig. 4.2.5. *Photo from Funck & Nørmark (2023) with an OBS (Sercel MicrOBS_Plus) attached to an anchor-cross on the seafloor.*

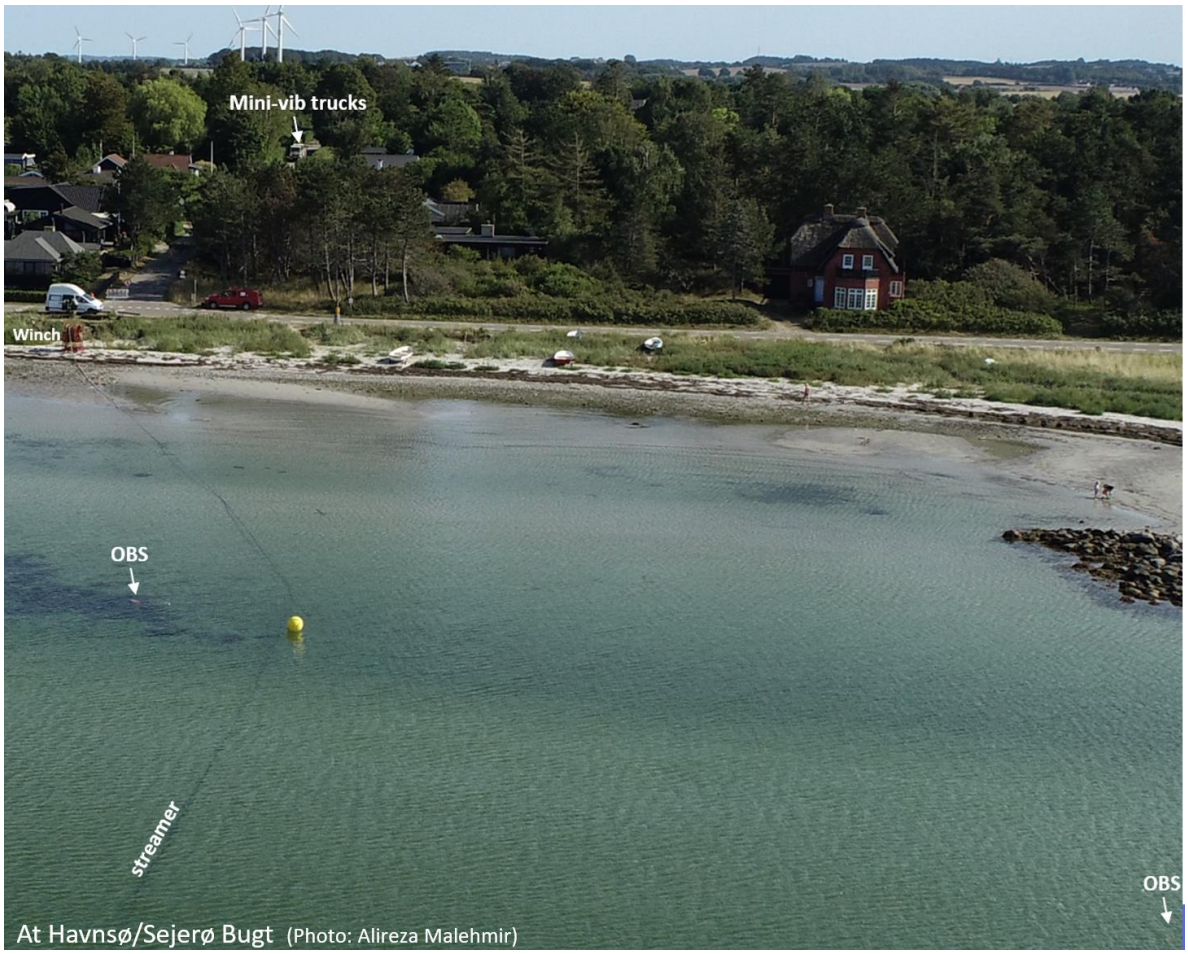

Fig. 4.2.6. *Arial view of the marine streamer and OBS. Onshore is the winch and in the background the approaching mini-vib trucks, which are the sources. Photo: Alireza Malehmir, 2022.*

Processing of the seismic survey by Uppsala University

Immediately after seismic data acquisition seismic processing from raw SEG-D field data to final post stack migration was performed at Uppsala University. Almost identical processing sequences have been applied to the wireless data recordings and to the short offset land-streamer recordings. In the first processing step shot and receiver geometry are included in the seismic trace header and output data are in SEG-Y data format. Secondly, cross correlation of the raw recorded vibrator signal with the theoretical source sweep has been applied to get the seismic response. Subsequently the 3 sweeps for each source location are then summed together to increase the signal to noise level.

The relatively small vibrator source (2x12 ton in total) is a big advantage in survey planning of line lay out and is also relatively easy to operate in the field in comparison to heavier equipment. In comparison to earlier reflection seismic surveys, the very short shot-point distance (10 m) and the long offset wireless receiver layout (10 m receiver distance) strongly supports noise attenuation tools both in source, receiver, and common offset domain.

The first run Uppsala University processing of the GEUS2022-HAVNSOE seismic survey is a relatively fast-track seismic processing of the dataset and the results have immediately been included in an updated seismic mapping of the Havnsø structure (Chapter 6). For getting this fast-track processing conventional post stack migration has been applied to the dataset. However, GEUS has issued a reprocessing including pre-stack time migration at Realtime Seismic (RTS) and results are presented in Section 4.3.

Landstreamer and wireless data were combined into a merged version (example for line P1 is shown in Fig. 4.2.7), for the sections: GEUS22_HVN_P1, -P2; -P2.5, -P3, -P4, P5, -P7. However, short streamer and poor data quality, caused that streamer data and consequently merged data are not available for two sections: GEUS22_HVN_P6 and GEUS22_HVN_P8. Wireless data are available for these sections.

Processing workflow for the wireless data from the Final Acquisition and Processing Report of the GEUS2022-HAVNSOE survey (Malehmir & Papadopoulou 2023):

1) Read SEGD
2) Theoretical sweep cross-correlation
3) Vertical stack
4) Minimum phase conversion
5) Geometry setup
6) First-break picking
7) Trace edit
8) Elevation statics
9) Frequency filter (BS 48-49-51-52)
10) Frequency filter (BP 20-30-70-90
11) Airwave attenuation (330 m/s)
12) Median horizontal filter (2200 m/s)
13) Median horizontal filter (1000 m/s)
14) DBS 16/150
15) Refraction statics
16) Constant Velocity Analysis
17) Residual statics (1 run)
18) Top mute
19) AGC (300 ms)
20) NMO corrections (60% stretch mute)
21) Stack (diversity)
22) Datum correction

23) Frequency filter (BP 15-30-90-110 Hz)
24) FX-deconvolution
25) Balance amplitude
26) FD migration

The processing workflow for the landstreamer data are almost identical to the workflow for the wireless data. Details are found in the Final Acquisition and Processing Report of the GEUS2022-HAVNSOE survey (Malehmir & Papadopoulou 2023)

The wireless and the landstreamer data resulting from the corresponding pre-stack processing works were merged together providing a unique dataset by combining the traces corresponding to each of the recorded shots. The stacked section generated from the merged dataset combines the detailed imaging from the landstreamer data in the uppermost part of the seismic section (down to c. 500–800 ms) with the better penetration depth from the longer offset wireless data. The wireless data shows better the deeper parts of the subsurface and reflects the target reservoir formations (below Top Gassum and Top Bunter Sst.), seal formations and even down to the pre-Zechstein basement (Fig. 4.2.7).

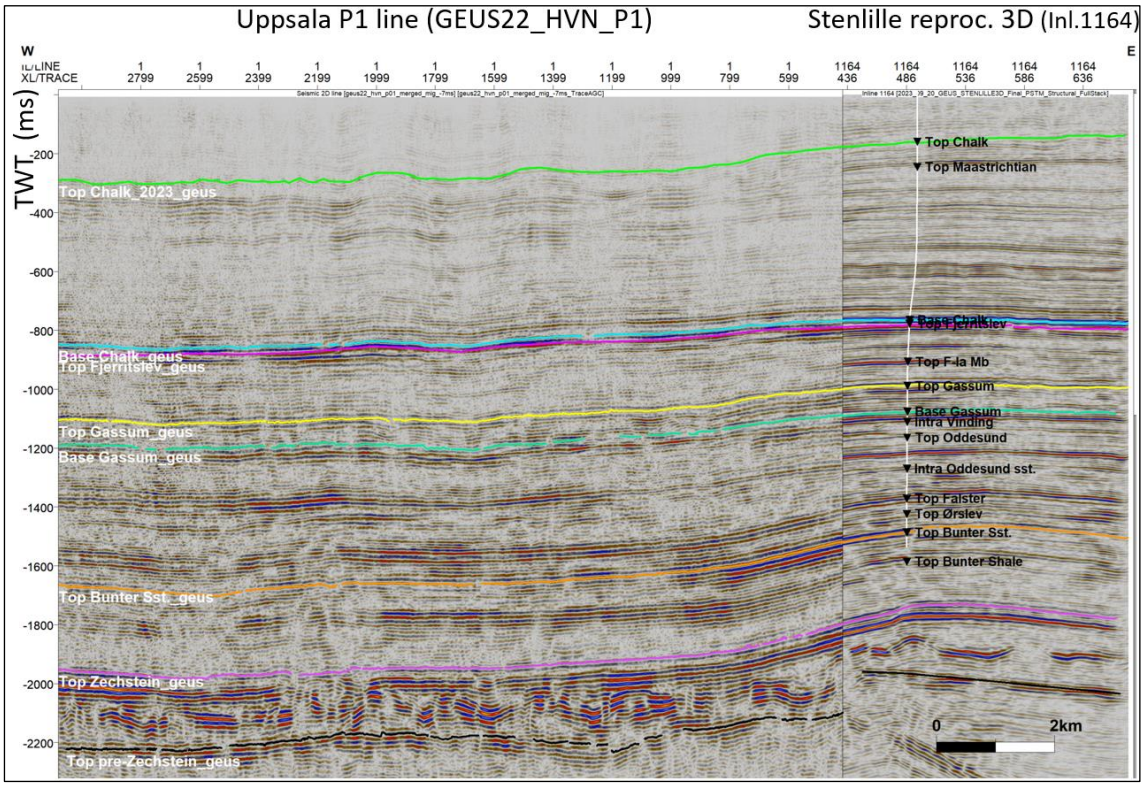

Figure 4.2.7. *Data example from the southernmost part of line P1 of the GEUS2022-HAVNSOE survey to the left with tie to the 3D STENLILLE-97-GEUS-RE2023 survey (Inline 1164) to the right. Horizons are shown from Top Chalk down to Top pre-Zechstein.*

Deliverables from Uppsala University

6. Deliverables

These items have been delivered (or available) as separate files:

1. Uncorrelated raw shot gathers (SEGD format) for both landstreamer and wireless recorders
2. Correlated and reduced time shot gathers (SEGY format) ready for processing incorporating important header information
3. Refraction model: weathering velocity, weathering thickness and refractor velocity, ASCII format
4. Static corrections:
    a. Source locations, ASCII format
    b. Receiver locations, ASCII format
    c. CMP locations (floating point statics), ASCII format
5. Unmigrated stack (SEG-Y format)
6. Post-stack time migrated stack (SEGY format)
7. Pre-stack time migrated CSP gathers (SEGY format) - Pending
8. Final processed, pre-stack time migrated stack and time-to-depth converted stack (SEGY format) ready for 3D visualizations and interpretation in standard software such as gOcad and Petrel - Pending
9. Advanced processing results for PostDoc position work on depth migration and on swath 3D imaging in separate report - Pending
10. Final report summarizing the acquisition and processing works

The list of deliverables is from the GEUS2022-HAVNSOE seismic survey: Acquisition and processing report (Malehmir & Papadopoulou 2023).

4.3 Reprocessed seismic data in this project

GEUS issued in 2023 the geophysical company Realtime Seismic (RTS) to reprocess the 2D seismic survey: GEUS2022-HAVNSOE in order to improve the data for interpretation and the reprocessed survey: GEUS2022-HAVNSOE-RE2023 was finalized in October 2023. Data and processing report are available from GEUS.

The objective of the reprocessing at RTS is to identify and select a robust processing sequence that improves the overall signal-to-noise ratio (S/N) and the resolution of the seismic data. Based on the experience from the STENLILLE-97-GEUS-RE2023 reprocessing at RTS a focused test program including PSTM migration for improving the GEUS2022-HAVNSOE-dataset were planned. The data is processed in such a manner that it should be optimized both for structural and sedimentological interpretations, as well as being prepared for input to pre-stack quantitative interpretation workflows, e.g. AVO inversion.

In the RTS reprocessing wireless recordings and landstreamer data were integrated together immediately after sweep cross-correlation. The main objective of the reprocessing was to apply PSTM migration in order to improve the seismic imaging and to improve the seismic resolution of the data for enhancing e.g. the identification of channels and other details in the Gassum Formation and to improve fault imaging. In general, the data quality was substantially improved both regarding continuity of seismic horizons and in seismic resolution (see comparison in Fig. 4.3.1 and Fig. 4.3.2). However, the crookedness of the lines caused in places vertical disturbances possibly may lead to suggestion of faulting. In comparison to the Uppsala processing the disturbances from crookedness in general seems to be stronger in the RTS reprocessing and are to some extent related to the PSTM migration. Different strength of smoothing in data gridding were tested, but these disturbances from crookedness of lines were not fully resolved and needs further evaluation outside the time available in the present project. In Fig. 4.3.3 an example of the disturbances caused by crookedness is shown for full stack of line P2 and in Fig 4.3.4 is shown an example of the disturbances from crookedness on near, mid, far and full stack from a small line segment from the southeastern part of line P1 in the vicinity of the Stenlille area. In particular, the mid stack shows continuous reflections and no displacements through the noise zones and not faults here.

Processing workflow for the reprocessing of the GEUS2022_HAVNSOE-RE2023 dataset:

1) Full data and geometry QC: Complete RTS QC module with RMS, LMO, statistical analysis of shots and receivers
2) First break picking: Three iterations of automatic picking using a robust sequence
3) Non-linear refraction tomography: 10 iterations of non-linear, 0.5 as smoothing parameter
4) Primary refraction statics: Surface consistent tomo statics, Floating datum in depth, Topography smoothed over 100 m, Intermediate datum at isovelocity 2000 m/s
5) Residual refraction statics: Surface consistent residual refraction statics, Model-based decomposition of residuals, Max shift 20 ms
6) Amplitude balancing: High Amplitude Noise Attenuation, Smoothing length 100 ms, Threshold 100%, Scale to 100%
7) Single trace deconvolution: Trace by trace deconvolution, Operator length 200 ms, Gap length 8 ms, Pre-whitening 0.1%
8) Time-Variant Spectral Whitening: Frequency: 8 - 150 Hz, Number of bands: 15, Taper 5 Hz

9) 2 iterations of reflection residual statics and horizonconsistent stacking velocity picking: Stacking velocity scans, from 1500 m/s to 6000 m/s, 50 m/s step, Stretch mute: 60%
10) Surface Wave Attenuation, (SWA): Radial filter, Minimum velocity (m/s) and Intercept time (ms): 150 m/s and, 100 ms, Maximum velocity (m/s) and Intercept time (ms): 1700 m/s and 0 ms, Operator length of median filter: 31, Frequency range: 0 Hz - 0 Hz - 35 Hz - 45 Hz
11) High Amplitude Noise Attenuation: FX Denoising, Noise threshold: 5, Number of filter points: 5, Number of estimation traces: 11, Window length: 200 ms, Frequency band: 0 Hz - 150 Hz, Add back: 5%
12) Surface Consistent Amplitude Correction: SCAC, Source domain: Decompose and apply, Receiver domain: Decompose and apply, Bin domain: Decompose only, Offset domain: De-compose only, Number of iterations: 50, Solver tolerance: 1E-8, White noise additive factor: 0.01
13) Surface Consistent Deconvolution: SC deconvolution, Decomposition domains: average, source, receiver, offset, bin, Apply domains: average, source, receiver, Offset bin size: 10 m, CMP supergather size: 5, Operator length 200 ms, Gap length 8 ms, Pre-whitening 0.1%
14) Time-variant filtering: Bandpass: Filter: 5 Hz - 8 Hz - 130 Hz - 150 Hz
15) 3D Regularization: Time patch: 200 ms, CMP patch: 71, Offset patch: 21, Maximum iterations: 80, Maximum frequency: 150 Hz
16) RMS migration velocity, picking on full scans, horizon consistent: Residual Kirchhoff pre-stack straight-ray migration scans, From 1500 m/s to 6000 m/s, 50 m/s step, Aperture (T, X, Y): 0 ms, 4000 m, 4000 m, Stretch mute: 60%
17) Kirchhoff PSTM Full Kirchhoff Pre-Stack Time Migration: Aperture: 4000 m x 4000 m, Dip limit: 75°, Maximum time: 7000 ms, Time increment: 2 ms, Max frequency of antialiasing: 140 Hz
18) RMO: Averaging window size: 100 ms, Depth slice AGC: 200 ms, Min/Max % change: -/+ 5%, CMP interval for picking: 3, RMO field - Vertical smoothing: 51 m/ms, RMO field - CMP smoothing: 101 bins
19) Spectral shaping: Frequency-amplitude pair: 0 Hz - 1 / 50 Hz - 1 / 80 Hz - 1.5 / 100 Hz - 1.3 / 140 Hz - 2 / 150 Hz – 1
20) Time-Variant Filtering: Window 1: 0 s - 2.6 s, Filter: None, Window 2: 2.6 s - 3.0 s, Filter: High-cut 70/40 dB, Window 3: 3.0 s - 7.0 s, Filter: High-cut 45/40 dB, Filter length: 500 ms
21) Trim Statics: Top horizon: 0 ms, Bottom horizon: 7000 ms, Frequency band: 30 Hz - 100 Hz, Maximum shift: 4 ms, Minimum cross-correlation coefficient: 0.1, Window length for time-varying trims: 500 ms, Window overlap for time-varying trims: 50 %
22) Outside mute: Outside mute at angle: 45°, Taper: 100 ms, preserve shallow up to offset: 100 m, Smooth interval velocities: 2000 ms
23) SOD: Dip field estimation, CMP search increment: 1, Time search increment: 8 ms, CMP search radius: 51 bins, Semblance search window: 50 ms Smoothing, Vertical: 11 ms, CMP: 21 bins, Smoothing table: 0.01
24) Post-stack enhancement: Bandpass:Filter: 5 Hz - 8 Hz - 130 Hz - 150 Hz, AGC (Structural only): Window: 500 ms

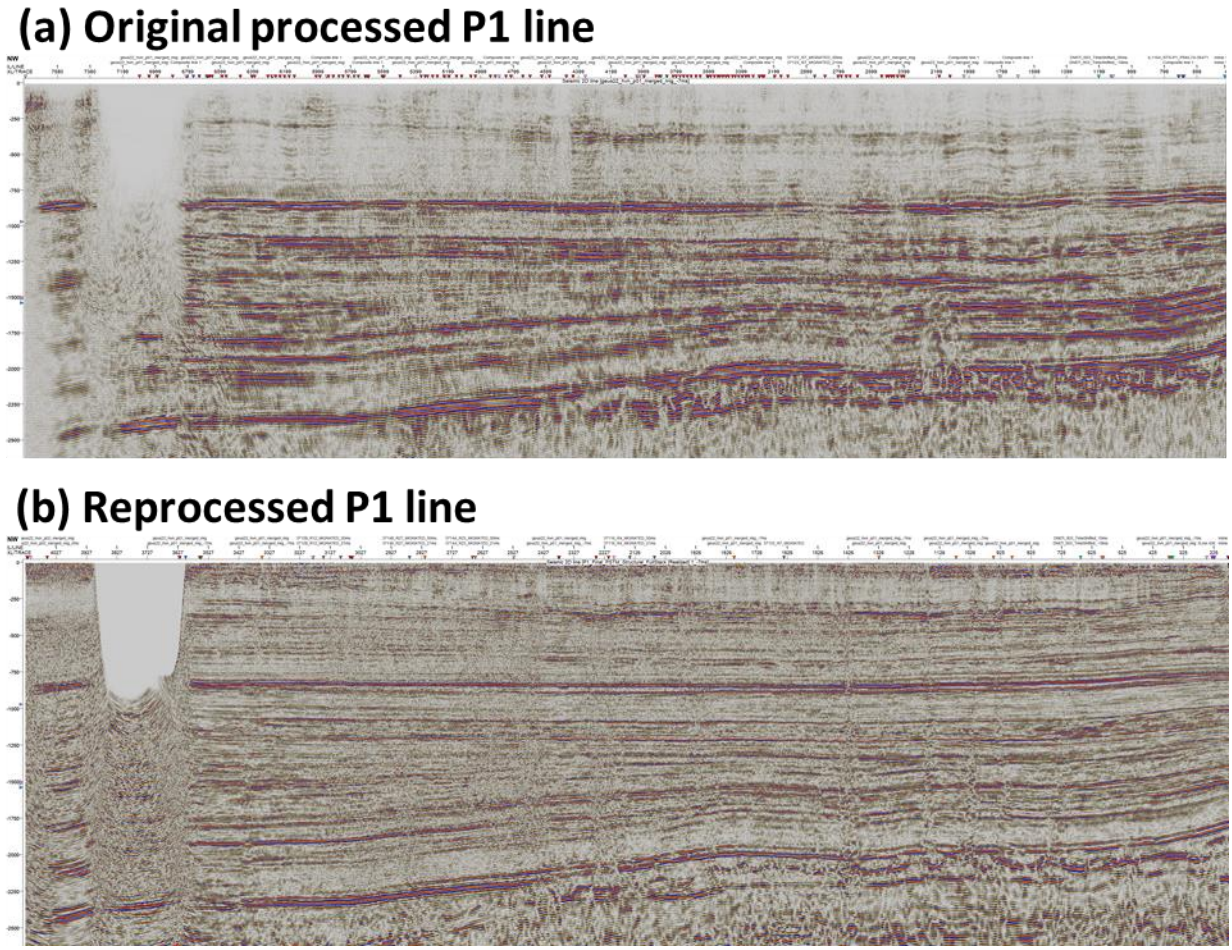

Figure 4.3.1. *Line P1, a) Original processing and b) reprocessing at RTS. In the reprocessing the seismic resolution has been substantially improved. Vertical section down to c. 2500 ms TWT. Profiles are c. 35 km long. The onshore landstreamer- and wireless data are merged with the marine OBS data, missing upper part. See also frequency spectre below. The same lines are shown in larger displays with interpretation in Fig. 6.1.4, 6.1.8.*

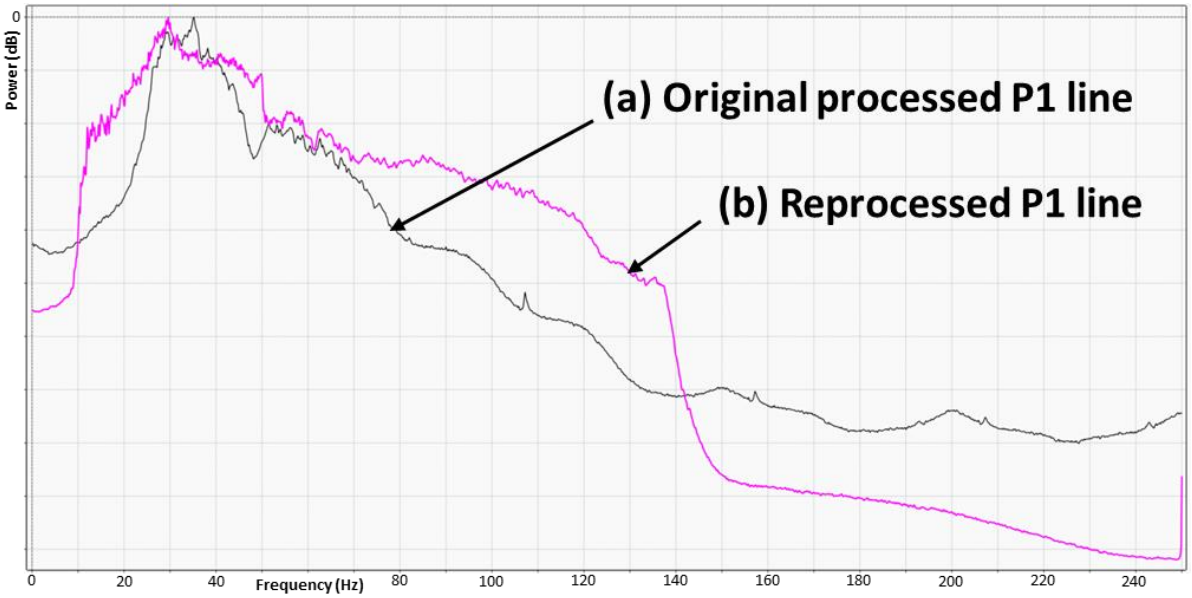

Figure 4.3.2. *Frequency spectre for the original line P1 and the reprocessed line P1. The big difference in the frequency spectre confirms the visual impression in Figure 4.3.1 of improvements in seismic resolution of the reprocessed line.*

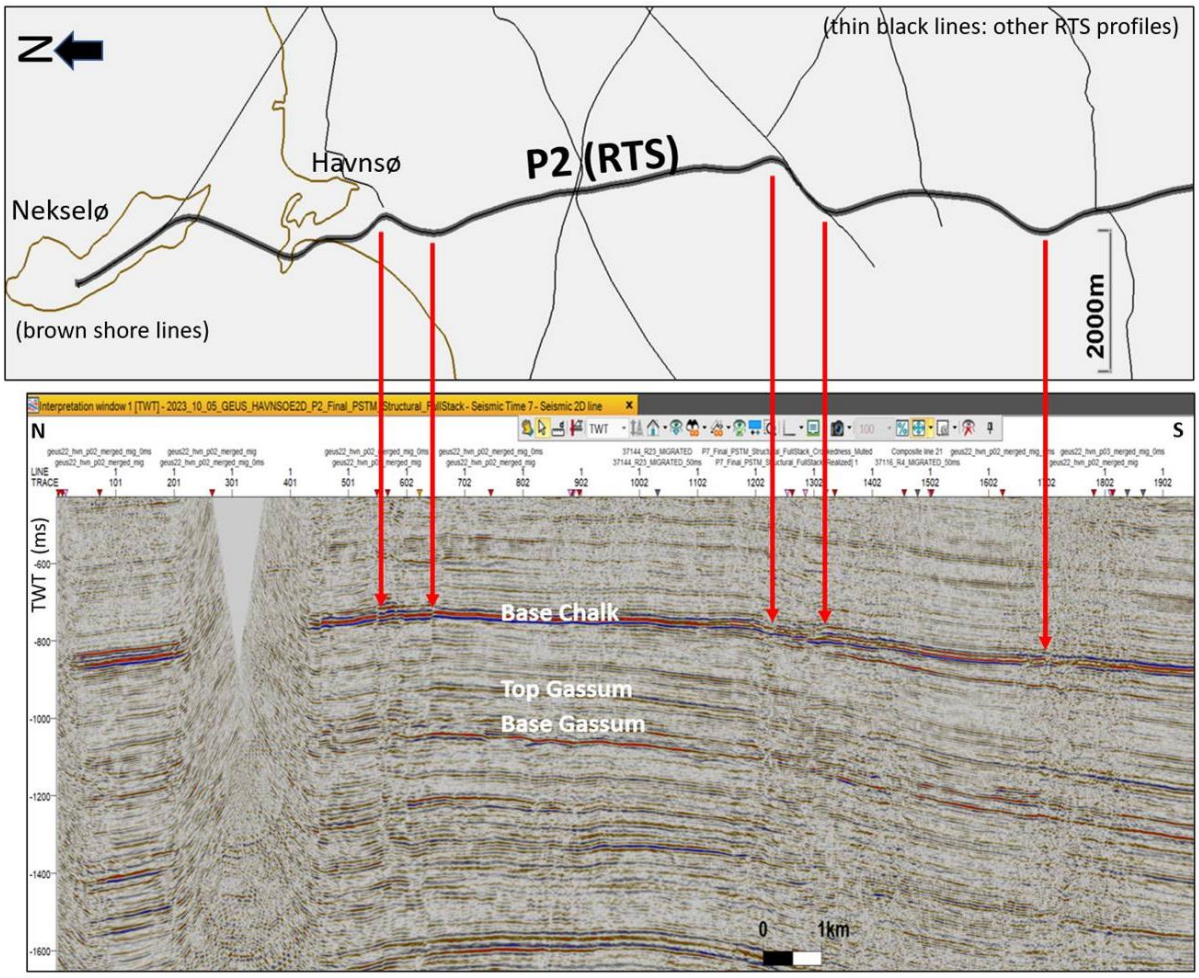

Figure 4.3.3. *The vertical disturbed zones for the RTS reprocessing of line P2 are closely related to line bends along the line.*

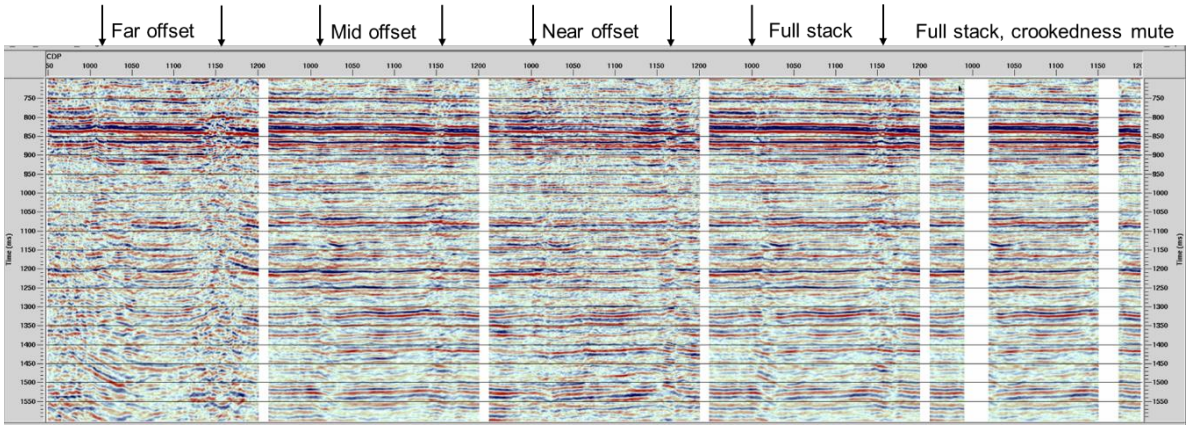

Figure 4.3.4. *Stack panels from 2-line bends along line P1. From left to right: far offset stack, mid offset stack, near offset stack, full stack, and full stack with mute at crookedness locations. The mid offset stack is less affected from the line crookedness than both the full stack and the far and near offset stack section and shows more continuous reflections and no marked faults.*

Acknowledgement – The new seismic data

The good cooperation with Professor Alireza Malehmir and his researcher team from Uppsala University, including Myrto Papadopoulou, Samuel Zappalá and Kristina Kucinskaite, and Geopartner Sp. zo.o (mini-vibs), on the planning, and during acquisition and completion of the GEUS2022-HAVNSOE seismic survey, and with Egon Nørmark and Per Trinhammer from Aarhus University on the marine acquisition are all highly appreciated. The great field assistance from all the students from the University of Copenhagen and Uppsala University are highly acknowledged and appreciated. Also, the good cooperation with COWI of applications and logistics and Gas Storage Denmark A/S of the logistics and meetings are highly acknowledged and appreciated. The good cooperation with the geophysics company Realtime Seismic during reprocessing for GEUS in 2023 to both the 2D survey GEUS2022-HAVNSOE-RE2023 and the 3D survey STENLILLE-97-GEUS-RE2023 is also appreciated.

4.4 Well data

The Stenlille structure is drilled by the 20 wells: Stenlille-1 to Stenlille-20 (ST-1 to ST-20), with 19 of the wells located within the 3D seismic survey area, and one (ST-6) just NE of the survey (Fig. 4.1.2). The first well ST-1 was drilled in 1980 and the latest well ST-20 is from 2009.

For this study additional wells surrounding the Havnsø structure have been included and tabulated in Table 4.4.1.

Well logs are used here for interpretation in particular of lithology, and selected logs are used for well log-based sequence stratigraphy, seismic to well ties and for seismic reservoir characterization and interpretation. See Chapters 5–7 for the specific used well logs.

Original logs: Caliper (CAL), Gamma-Ray (GR), Spontaneous Potential (SP), compressional Sonic (SON, DT, DTLF, DT4P), shear Sonic (DTS, DT4S), Resistivity (R_deep mostly used), Neutron Porosity (NPHI) and Density (RHOB) logs.

Derived (interpreted) logs: Shale volume (V_{shale}), Effective porosity (PHIE), and Permeability estimates. The latter were derived from porosity-permeability relationships, established based on an analysis of core analysis data.

Table 4.4.1. *List of the wells utilized in this study, with information on the year of drilling completed, operator, Kelly Bushing (KB, meter above mean seal level), Total Depth (TD, meter below Kelly Bushing, measured drilled depth), deviation and Chronostratigraphy of the TD units.*

Well	Year	Operator	KB a.msl (m)	TD b. KB (m)	Deviated	TD
Stenlille-1	1980	DONG	41.6	1664	no	Triassic
Stenlille-19	2000	DANOP	49.3	2570	yes	Triassic
Stenlille-4	1988	DANOP	38.4	1689	no	Triassic
Stenlille-5	1988	DOPAS	50.0	1717.5	no	Triassic
Stenlille-6	1988	DANOP	32.4	1723	no	Triassic
Stenlille-15	1995	DANOP	52.8	1701.0	no	Triassic
Lavø-1	1959	Dapco	28.3	2441	no	Triassic
Terne-1	1985	Amoco	37.3	3361	no	Cambrian
Rønde-1	1966	Gulf	35.1	5300	no	Silurian
Horsens-1	1958	Dapco	56.8	1729	no	Triassic
Løve-1	2011	GMT Exploration Co.	86.0	2461	no	Permian
Jelling-1	1992	Danop	97.6	2031	no	Permian
Ullerslev-1	1951	Gulf	25.3	1063	no	Triassic
Slagelse-1	1959	Gulf	40.9	2975	no	Cambrian

Well samples: Cores, SWC and ditch cutting samples

A number of cores, sidewall cores (SWC) and ditch cutting samples exist from the Stenlille wells and the cores and sidewall cores are listed in Table 4.4.2 below. Stenlille-4 is excluded from the list. The used samples and results are further discussed in Chapter 7.

Table 4.4.2. *Overview of the different cores, SWC and cuttings related to formation and well site. Chalk Group lower part is including the "Basal Chalk" and "Lower Chalk" and is of Cenomanian, Turonian and Coniacian age. Rødby Fm is Albian to lowermost Cenomanian age. Vedsted Fm is of late Hauterivian to late Aptian age. Fjerritslev Fm is of latest Triassic to Early Jurassic age.*

Cores at Stenlille	St-1	St-2	St-3	St-5	St-6	St-7	St-8	St-9	St-10	St-11	St-12	St-13	St-14	St-15	St-16	St-17	St-18	St-19	St-20
Chalk Group (lower part)	-	-	-	Core 1	-	-	-	-	-	-	-	-	-	-	-	-	-	-	-
Rødby Fm	Core 1	-	-	-	-	-	SWC	-	-	-	-	-	-	-	-	-	-	-	-
Vedsted Formation	Core 1 + SWC	-	-	-	-	-	SWC	SWC	SWC	-	-	-	-	-	-	-	-	-	-
Fjerritslev Fm	Cores 2; 3; 4; 5; 6	Cores 1; 2; 3	-	Cores 2; 3; 4	Cores 1; 2; 3; 4	-	SWC	SWC	SWC + Cores 1;2	-	-	-	-	-	-	-	-	-	-
Gassum Fm	Core 6	Cores 4, 5	-	Cores 4, 5; 6		-	SWC	-	Cores 3	SWC	Cores 1 and 2	Cores 1,2,3, 4	Cores 1,2,3, 4	Cores 1,2,3, 4,5,6	-	Cores 1,2,3,4 ,5,6	Cores 1; 2; 3	Core 1	-
Bunter Sandstone	-	-	-	-	-	-	-	-	-	-	-	-	-	-	-	-	-	Cores 2; 3	-
Cuttings	Yes	Yes	Yes	Yes	?	?	Yes	Yes	Yes	Yes	Yes	Yes	Yes	Yes	Yes	Yes	Yes	Yes	Yes

5. Methods

Seismic interpretation and well-ties (Chapter 6)

The Havnsø structure, its formation and stratigraphy with reservoir-seal pairs, are investigated and evaluated from structural and stratigraphic analysis, based on the available 2D- and 3D seismic data and well-ties. Seismic horizons, seismic successions and seismic facies are identified and interpreted, using seismic attributes and reflector terminations such as onlap, downlap and truncation. The seismic stratigraphic horizons are essential sequence stratigraphic and chronostratigraphic surfaces but in this limited area they can be regarded as near base or near top formation boundaries. Horizon names are for simplicity similar to the formation names tied from the wells, in particular the deep Stenlille-19 well. The seismic stratigraphic boundaries and sequence stratigraphic surfaces and units should on a regional scale have more neutral naming (as e.g., in Nielsen 2003; Boldreel et al. in review). At the same time, faults, salt structures, and folds were identified and mapped together with internal configuration and thickness patterns. A structural and tectonostratigraphic interpretation were carried out using the chronostratigraphic framework from the well ties.

Petrel (2022) software was used for establishing the database, seismic interpretation with manual and auto-tracking of the horizons and well-ties with synthetic seismograms. In total 14 regional seismic stratigraphic horizons were interpreted in the Stenlille–Havnsø area to determine the stratigraphy, geological evolution, and most important to define reservoir-seal pairs and structural closures (see Chapter 6). In addition, the deepest horizons (below Top pre-Zechstein) were interpreted on selected lines and correlated from Stenlille area to the Slagelse-1 well, in order to describe the earliest part of the tectonostratigraphic evolution of the region. However, the most comprehensive and detailed mapping of horizons and faults has been performed of the successions from the Top Vinding (Base Gassum) to the Base Chalk, comprising the primary reservoir (Gassum Fm), primary seal (Fjerritslev Fm) and part of the secondary seal to the Gassum Fm. In addition, the Gassum Fm are detailed described in special studies of sequence stratigraphy (with 8 internal sequence boundaries and transgressive surfaces) with well-logs and seismic lines, and reservoir properties. The methods used are described in each of these studies (see Chapters 6 and 7). Lithostratigraphic and sequence stratigraphic well-log boundaries (well-tops) are adjusted by time-depth relations to the seismic data and synthetic seismograms of the wells are used to constrain the seismic interpretation (see below; Fig. 5.1).

Well-to-seismic tie and synthetic seismogram (Chapter 6)

In order to utilize well log data and well tops (depth domain) with seismic data (time domain), seismic-well tie procedure have been performed on wells that contain sonic and density logs (Fig. 5.1). As no boreholes exist on the Havnsø structure, the study area therefore includes the previous investigated greater Stenlille area (GEUS RAPPORT 2022/26). Here, in total 13 wells contained density and sonic logs (see database section 4.4), though some wells only contained information in the vicinity of the reservoir section. In contrast to GEUS RAPPORT 2022/26 where the original 3D Stenlille processed seismic data was used from 1997, in this study we utilized the 2023 re-processed data, which required a new seismic-well-tie procedure due to a significant time shift (c. 40 ms). A statistical wavelet was extracted within the interval of the Fjerritslev – Gassum Formations, resembling a zero-phased wavelet with reverse polarity, and having several sidelobes due to the noisy seismic data (Fig. 5.1).

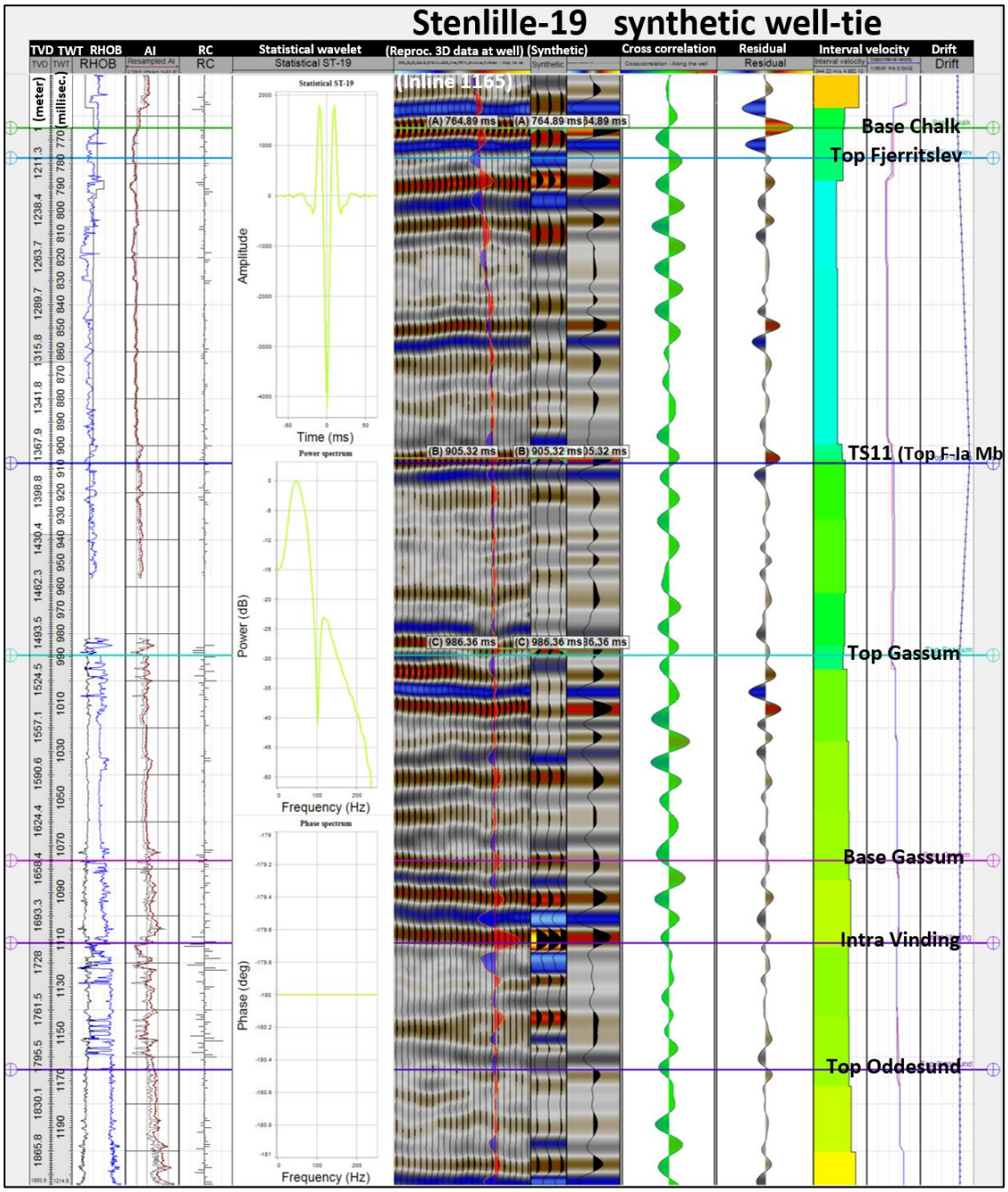

Figure 5.1. *Well to seismic tie of the Stenlille-19 well. Synthetic seismic trace is shown down along the well in red-white-blue display and on the 3D seismic inline 1165 close to the well. Well-tops and formations are also marked. Location of the projected well and inline 1165 and a larger seismic section are shown in Figure 6.1.3.*

Check shots were only available for the Stenlille-1 and -19 wells, which were used as an initial time-depth relationship, and using the density and sonic logs, a synthetic seismogram is produced for Stenlille-19 and compared to seismic data (Fig. 5.1). A combination of bulk shifts (initial shift to match Base Chalk Group reflection and Top Gassum reflection), and slight stretching or squeezing, QC'ed by observing reasonable interval velocities for the given lithologies, resulted in a good correlation of synthetic seismogram and seismic, thereby ensuring correct depths of well log information and well tops. For the other wells without check shot information, check shots from Stenlille-1 and -19 were used as well as initial time-depth

relationship. We evaluated this to be justified considering the relatively small distances (several kilometers at maximum), similar well trajectories and expected similar interval velocities due to the relative homogenous geological buildup. Some minor mismatch of the seismic-to-well tie in the gas saturated areas occur due to different years (data vintage) of drilling, seismic acquisition, and gas injection and volume. The Stenlille-1 to Stenlille-6 wells were drilled prior to the gas-injection initiated in 1989, and the Stenlille-18 was the latest well drilled prior to the 3D seismic survey in 1997. In addition, other factors may also affect the ties such as poor log data, the seismic datum, static correction, the level of the ground-water table, and other factors also affect the seismic velocities (e.g., lithology variations) and thus time-depth relations.

Seismic time to depth conversion (Chapter 6)

A regional velocity model was constructed to convert the interpreted horizons from the time domain to the depth domain. The model area was defined so that the velocity model includes a significant buffer around the Stenlille and Havnsø structures, which resulted in an area of 53 by 28 km (1484 km^2). Extra figures on the depth conversion process are available in Appendix A.

The data available include: 1) TWT seismic horizons of the main stratigraphic units, utilizing the 3D seismic survey and 2D lines (including new GEUS2022-STENLILLE and GEUS2022-HAVNSOE-RE2023 lines), gridded to 250x250m and well-adjusted to the Stenlille boreholes; 2) Well top markers; 3) Seismic migration (RMS) velocities from the 2D lines (GEUS2022-HAVNSOE-RE2023), and newly reprocessed 3D seismic volume (STENLILLE-97-GEUS-RE2023), which were Dix-converted to average velocities.

In order to account for vertical and lateral variations in average velocities found within the stratigraphic units as seen in the TDRs and 3D seismic migration velocities, the velocity model was constructed in two steps, followed by depth-conversion of the TWT seismic horizons:

1. First, seismic migration velocities from the 3D volume and 2D lines were upscaled into a structural 3D grid (using arithmetic mean), and subsequently extrapolated within each zone using full tension option in Petrel (Spline in Tension algorithm).
2. Second, a multi-layer velocity model was created using the modelled 3D interval velocities as velocity input, and 3D horizons and well tops to correct the velocity values to achieve a match between depth-converted horizon and well top.
3. Finally, TWT seismic horizons were depth-converted using the created velocity model.

The workflow was performed within Petrel (2022) by the following steps:

- QC of the input data:
    - seismic-well-ties; removing outliers in interval velocities observed in the TDRs originating from overstretching and squeezing in the seismic-to-well tie procedure.
    - adjusting the TWT seismic horizons to well markers since seismic peaks or troughs not necessarily coincide with the well tops, in order to get a good TWT to MD fit of main stratigraphic units (Fig. 5.1); checking TWT thicknesses for bull-seyes originating from horizon mis-picks or extrapolation, smoothening anomalies.

- Performing a dix-conversion of RMS velocity from seismic processing (STENLILLE-97-GEUS-RE2023 & GEUS2022-HAVNSOE-RE2023) to average velocities.
- Defining a 3D modelling grid (250x250m) based on the QC-ed TWT horizons using the Petrel structural modelling tool:
    - Model zonation according to the following horizons: MSL (0 ms), Top Chalk, Top Maastrichtian, Base Chalk, Top Fjerritslev, Top Gassum, Base Gassum, Top Oddesund, Intra Oddesund sst. beds, Top Falster, Top Ørslev, Top Bunter Sst., Top Bunter Shale, Top Zechstein (Fig. 5.2A).
    - Vertical layering was defined such that layer thickness is between 10 – 20 ms, with higher resolutions where large velocity changes occur (e.g. between Base Chalk Group and the Lower Cretaceous strata).
    - Upscaling of the 3D seismic average velocities into the 3D grid using arithmetic mean (Fig 5.2B)
    - Upscaling of the 2D seismic average velocities into the 3D grid using P1, P2, P5, P6, P7 and P8 lines since these lines showed average velocity values similar to the 3D seismic dataset. P2.5, P3 and P4 were removed from this step since the velocities were substantially higher (around 300 m/s) (Fig. 5.2B).
- Extrapolate the upscaled cells into the entire 3D grid using full tension option in the property operations (Spline in Tension) (Fig. 5.2C). As minimum curvature option gave poor results as it maintains trends, and therefore further away from the upscaled cells extreme low or high velocity values appear and are geologically unrealistic. Full tension extrapolation tends to flatten values and appears more realistic.
- Create an “advanced velocity model” using the same 3D seismic horizons (tied in TWT to boreholes from seismic-well-tie Time-Depth Relationship), well tops for calibration, and 3D average velocity grid from previous step as velocity model (Fig. 5.2D). Without applied correction, the average depth residual was in the order of 10 – 60 m. The final velocity model used the well tops (“global correction”) to improve to depth-converted horizons by adjusting the velocities (Fig. 5.2E).
- Depth-convert the TWT horizons using the constructed velocity model (Fig. 5.2F).
- The velocity model is called: 20231122_Havnsø_AvgVel 2D & 3D RTS (corrected)

To make the velocity model more accurate, the following steps could be undertaken:

1. Include additional velocity data from older seismic lines, as for some lines stacking velocities are documented.
2. Perform comprehensive data analysis on the upscaled cells to obtain geostatistical information of the upscaled cells for kriging purposes (variogram ranges, nugget, azimuths for each zone), and use kriging of the upscaled instead of full tension extrapolation.
3. Use the volume derived from point 2 and use co-kriging of average velocities from well TDRs and the 3D property grid as 3D trend.

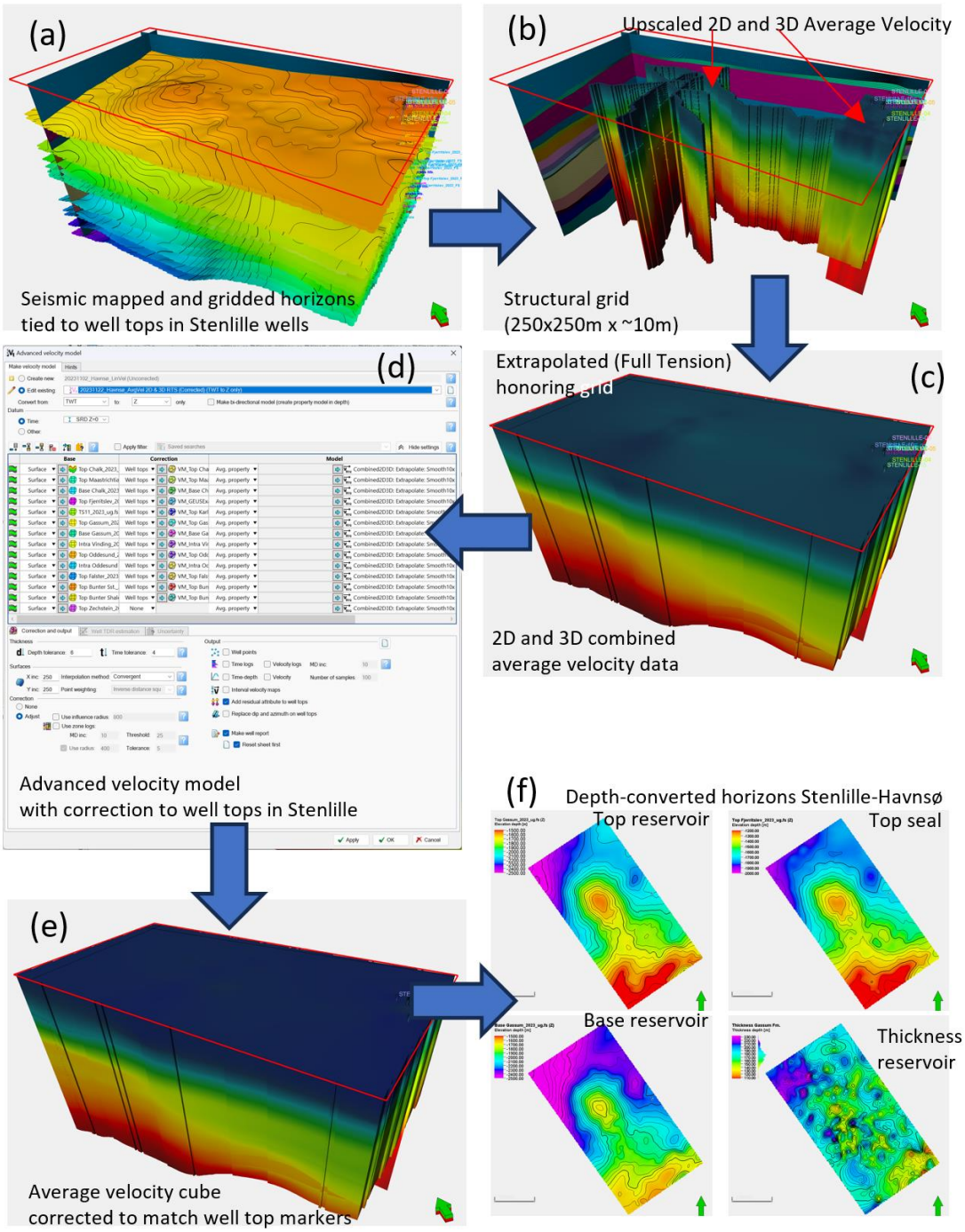

Figure 5.2 *(A) 3D perspective of the 14 horizons considered in the velocity model, which define the structural grid (250x250xc.10ms). The Stenlille structure is located on the righthand side where also the wells are indicated that were used to constrain the velocities. (B) The structural grid is indicated by the sections (0–3270 ms TWT), and the upscaled 2D and 3D Dix-converted RMS seismic migration velocities are shown (purple: 1500 m/s to red: 4000 m/s). (C) The data are interpolated within the grid using a full tension algorithm (Spline in Tension) and smoothened 10x to remove outliers where the 2D intersect. (D) An advanced velocity model is set up using the 14 horizons and associated well tops in Stenlille wells for correction. (E) Velocities are adjusted to find a match between depth-converted horizon and well tops. (F) This cube is then used to depth-convert the TWT horizons. (depth=average velocity*(surface TWT)/2).* (see Appendix A for enlargement).

Investigation of reservoir and seal (Chapter 7)

The geology of the reservoir and seal successions are described using well completion reports, publications, and in-house studies of well-logs and geological well samples mainly from cores. In addition, a limited number of studies focusing on lithology and biostratigraphy are available. The data used are from the wells closest to the Havnsø structure and mainly from the Stenlille area, which may to some extent be similar to the Havnsø area. The aim of these studies is to provide a more detailed understanding of reservoir and seal characteristics (see Chapter 7).

The reservoir characteristics presented below and discussed in Chapter 7 are derived mainly from the acquired wireline logs in Stenlille, that are calibrated against conventional core analysis, descriptions of cuttings and sidewall cores. Potential reservoir units were identified from wireline logs by low formation resistivity, characteristic neutron-density log responses, pattern of the spontaneous potential log, and low natural radioactivity as recorded by the GR log and documented by cuttings containing sand-sized quartz grains. Reservoir parameters were evaluated based on well data with emphasis on data from e.g., the ST-1, 2, 5, 6, 18 and 19 wells. In petrophysical terms, a sandstone reservoir is herein defined as a rock having < 50% volume of shale, and an effective porosity (PHIE) of > 10%. The permeability is estimated using in-house established relationships between porosity and permeability, which is based on conventional core measurements. These relations are derived from core analysis data, i.e., porosities and permeabilities measured on core samples originating both from the Gassum Formation and Bunter Sandstone Formation. Seal thickness and grain-sizes were similarly evaluated based on petrophysical logs. Mudstone sections that will act as seal were identified from wireline logs by several methods based on the availability of logs in the different wells drilled over a long period and for different purposes.

Storage Capacity Assessment (Chapter 8)

To be able to compare the potential CO_2 storage structures GEUS uses a simple widely accepted equation for saline aquifers. The storage capacity of reservoir units with buoyant trapping is estimated from:

$$SC = GRV * N/G * \varphi * \rho_{CO2R} * S_{Eff}$$

where:

SC	Storage Capacity or Mass of CO_2 (MT).
GRV	Gross Rock Volume is confined within the upper and lower boundary of the gross reservoir interval (h) and above of the deepest closing contour from where spillage from the trap will occur.
N/G	Average net to gross reservoir ratio of aquifer across the entire trap (GRV).
ϕ	Average effective reservoir porosity of aquifer within trap (GRV).
ρ_{CO2R}	Average CO_2 density at reservoir conditions across the entire trap.
S_{Eff}	Storage efficiency factor relates to the fraction of the available pore volume within the trap (GRV)that will store CO_2. This fraction depends on the size of storage domain, heterogeneity of formation, compartmentalization, permeability, porosity, and compressibility, but is also strongly influenced by different well designs and injection schemes (e.g., Wang et al. 2013).

Storage capacity (SC) is related to communication within the reservoir and the degree of pressurization. Pressurization depends on the difference between the fracturing pressure and the relation between pressure and volume increase, and compressibility of the rock and the fluids in the reservoir.

In open aquifers, as used here, a CO_2 storage injection is most likely pressure-limited during the entire operation, and the reservoir pressure will stay constant during injection, as the formation water will be pushed beyond the boundaries. The calculated stored CO_2 will be the amount injected until it reaches the boundaries of the storage complex (e.g. 'lowermost closed contour'). The calculation used here assumes a static approach where the pores in the trap is assumed to be 100% connected. However, it does not include dynamic pressure build-up and movement of CO_2 and in-place brine(water) in the saline aquifer, neither in-side nor out-side the trap. Furthermore, it does not consider the solubility of CO_2 in water, where more than 10% can normally be dissolved in the water.

A dynamic reservoir simulation will take these factors into account and will obviously produce different storage capacity results, depending on the selected parameters. A more realistic dynamic simulation of the potential storage capacity is normally carried out by the awarded

license holders and operators. Dynamic reservoir simulations should be used for local-scale CO_2 storage reserves estimates and should also consider operational and regulatory factors.

The CO_2 storage efficiency factor (S_{Eff}) was first introduced in 2007 in regional-scale assessments of storage capacity in the United States and Europe. The efficiency of CO_2 storage is regarded as a combination of factors, and many published papers show values from <1% to more than 20%, emphasizing that no single value or set of values can universally be used. Regional storage efficiency values are around 1–4 % (e.g., CO_2 Storage Atlas of the US and Canada 2008), while trap specific storage efficiency have values around c. 4–18% for clastic sediments (e.g. Craig et al. 2014; Gorecki et al. 2009); c. 3–10% (US-DOE; Goodman et al. 2011) and c. 5–20% for traps in German North Sea area (BGR, 2023 on-going project).

The storage efficiency factor represents the fraction of the total available pore volume of the saline aquifer that will be occupied by the injected CO_2 in the trap volume (i.e. the GRV) and is regarded as the fraction of stored CO_2 relative to the pore volume, - and has both a space and time dependency. It depends primarily on the relationship between the vertical and horizontal permeability, where a low vertical to horizontal permeability ratio will lateral distribute the CO_2 better over the reservoir than a high ratio. It will therefore be an advantage if the reservoir formation is internally layered with reservoir sandstone alternating with impermeable or poorly permeable clay acting as local seals. The Gassum reservoir is regarded as a multilayered formation with internal barriers, why a low ratio would be expected (Section 7.1).

Furthermore, the storage efficiency factor depends on the size of the storage domain, heterogeneity of the formation, compartmentalization, porosity, permeability, pressure, temperature, salinity and compressibility, but are also influenced by number of injection wells, design and injection strategy.

The Stenlille is the best-known case onshore Denmark, why a maximum value of 40% for a 4-way dip-closure is used here for the excellent and well known Gassum Fm sandstone reservoir. All other potential storage structures probably have lower storage efficiency values reaching more realistic values from 5 to 10%. For comparison reasons GEUS uses storage efficiencies from 40% in the Stenlille structure and 10% in all other potential structures.

To address the geological uncertainties associated with seismic data quality and density, interpretation and seismic well tie, depth conversion challenges, mapping, reservoir parameters assessment and fluid parameter, a number of assumptions in the reservoir have been applied. Ranges of min, mode and max for each input parameters have been chosen to reflect parameter uncertainty. By using distribution models, a simple Monte Carlo simulation in-house tool has used to estimate potential storage capacity. To achieve stable and adequate statistical representation of both input distribution and result output, 10.000 trials are calculated for each simulation. This methodology is simplistic and does not incorporate e.g., correlations of input parameters. However, for the purpose of estimating reliable screening volumes and CO_2 capacities, the methodology is considered relevant and adequate. The method is used for the calculations in Chapter 8.

6. Results of seismic and well-tie interpretation

6.1 Stratigraphy of the structure

In total fourteen regional seismic stratigraphic horizons ('horizons') were interpreted in parts of the study area and they are from the deepest to the shallowest: (1) Top pre-Zechstein (Base Zechstein or Top Rotliegende), (2) Top Zechstein, (3) Top Bunter Shale, (4) Top Bunter Sandstone (Sst.), (5) Top Ørslev, (6) Intra Oddesund sst. beds, (7) Top Oddesund, (8) Intra Vinding, (9) Base Gassum (Top Vinding), (10) Top Gassum (TS7), (11) Top F-Ia Mb (TS11) (intra Fjerritslev Fm horizon), (12) Top Fjerritslev, (13) Base Chalk, and (14) Top Chalk (Fig. 6.1.1−6.1.8).

In addition, eight detailed, internal sequence stratigraphic horizons of the Gassum Formation were interpreted in selected lines (Fig. 6.1.9) into the Havnsø structure, including: Sequence boundaries (SB): SB2, 3, 4, 5, 6; Transgressive surfaces (TS): TS3, 4, 5, 6, 7, where Base Gassum is here SB2 and Top Gassum is here TS7 – See Chapter 7 (Fig. 7.1.13) for more details and facies reservoir model. Also, older horizons are interpreted in the Stenlille area, and correlated to the Slagelse area: Top Pre-Cambrian basement, Top basal Palaeozoic (Cambrian), and Top Lower Palaeozoic, to interpret the oldest tectonostratigraphic evolution and to tie the deepest succession in the Stenlille−Havnsø area to the Slagelse-1 well that has TD in Cambrian rocks (See the reporting of the Stenlille structure: Gregersen et al. 2023).

Key horizons correlated into the Havnsø structure are the horizons: Top Zechstein, Top Bunter Sst., Base Gassum, Top Gassum, Top Fjerritslev, and Base Chalk. TWT grids of these horizons are published by Gregersen & Smit (2023) on November 28th 2023 with reference to the present report and can be accessed via the GEUS Dataverse (link). In addition, most of the other horizons were correlated to more limited extent, e.g., Fig. 6.1.4−6.1.8.

The uppermost horizon Top Chalk (Fig. 6.1.4) is mainly used for the Chalk Group isochore map for the time to depth conversion. Horizons from Top Bunter Sst. and shallower can be correlated to the Stenlille-19 (ST-19) well (Fig. 6.1.1, 6.1.3). Horizons from Base Gassum and shallower can be correlated to well-tops in nearly all Stenlille wells. The interpreted seismic stratigraphic horizons with well-ties documents the local stratigraphy of the Stenlille and the Havnsø structures with regional tie lines from Stenlille to Havnsø, in particular P1 and P2 of the Havnsø survey (Fig. 6.1.3−6.1.5).

The regional generalized lithostratigraphy to the deepest well Stenlille-19 is shown in Figure 6.1.1 with stratigraphy, possibly also applicable to the Havnsø structure from the seismic correlation. This study and the study of the Stenlille structure have indicated that parts of the Triassic lithostratigraphy should be revised in the future for this part of the Danish Basin.

The horizons are essentially interpreted as sequence stratigraphic (approximately chronostratigraphic) boundaries, which are traced in a certain reflection (here a trough or a peak) (Fig. 6.1.9). However, they are in most cases also, on a local scale, near-formation boundaries as correlated to the well-tops. Thus, the seismic horizons are here named after the approximate formation boundaries. More regionally, it may be considered to use lithostratigraphic independent naming such as letters or ages, as on a regional scale, some of the lithostratigraphic units are diachronous. For example: The top of the Gassum Formation is

late Rhaetian in age (at the sequence stratigraphic flooding surface TS7) in the Stenlille area, whereas it is of a younger Hettangian – early Sinemurian age in central to northern Jutland, where the formation top occurs at different sequence stratigraphic flooding surfaces e.g., TS9–TS11 (Nielsen 2003). However, here in this local area, the naming serves to more directly relate formations and thus key reservoir-seal pairs.

Synthetic seismograms have been produced to study and connect wells to seismic reflections for interpretation of the horizons (Fig. 5.1). Most seismic data, including 3D and most 2D lines are European SEG reverse polarity, where a peak is a soft kick with downward decreasing acoustic impedance (AI), such as the Base Chalk seismic reflection. Figure 5.1 shows a significant drop in velocity from chalk of the Chalk Group into lower velocity marl and chalk of the Rødby Fm. We use here mostly coloured profiles displayed in red-white-blue (red peaks and blue troughs) or black-grey-white (black peaks and white troughs) (Fig. 6.1.1–6.1.9).

We define here each interpreted horizon in either a peak or a trough seismic reflection (note the reverse polarity), where e.g., the Base Chalk follows a peak, the Near Top Fjerritslev follows a trough, and the Top Gassum follows a peak reflection (Fig. 6.1.4–6.1.8).

Several factors affect the seismic reflection responses (velocity and/or density), not only lithology variation, but also variations in e.g., compaction, cementation, fluids and gas. In the Stenlille structure close to the Havnsø structure, various amounts of natural gas have been stored in the Gassum Formation of the Stenlille structure, which in the seismic data impact locally decrease of the velocities and densities in the reservoir zones. The gas storage in the Stenlille structure shows a proven tight trap with more than 30 year of safe gas storage.

The relatively continuous seismic horizons and units with few marked faults indicate relative similar stratigraphy and tectonism in Stenlille and Havnsø areas in the uppermost Triassic (Gassum Fm) to Lower Cretaceous successions, although some differences and facies changes occur towards Havnsø. A close inspection of Gassum Fm reflections in the Stenlille area show local strong amplitudes (some related to gas), small progradations (clinoforms) and troughs, which may be interpreted as channels (Fig. 6.1.9) – see also Chapter 7 (Fig. 7.1.13) for detailed interpretation. The detailed study also shows that indications of progradation and channels in the formation become less frequent towards Havnsø, probably suggesting less sandstones, father from the coastal conditions that dominated the Stenlille area.

The seismic facies of the Gassum Fm with much reflectivity is very different from the overlying Fjerritslev Fm with more transparent and regular, continuous reflections. The Fjerritslev Fm comprises mudstones with thin sandstone and siltstone layers, mostly in the lower third, up to the Top F-Ia or TS11 surface (Fig. 6.1.8, 6.1.9). Local amplitude increases probably indicate sandstones or siltstones. Also, small progradations can be observed in the Bunter Sandstone Fm in few places, also if sufficient resolution allows, such as west of Stenlille towards Havnsø (Fig. 6.1.10). The progradations may also indicate sand-rich systems, although progradations are not always associated with sand-deposition.

In large scale, the Havnsø structure is underlain and formed by a salt pillow. The Triassic succession of Falster Fm and Oddesund Fm (Top Ørslev to Top Oddsund) thickens markedly from Stenlille to Havnsø (Fig. 6.1.8) probably related to increased subsidence in this part of the Danish Basin.

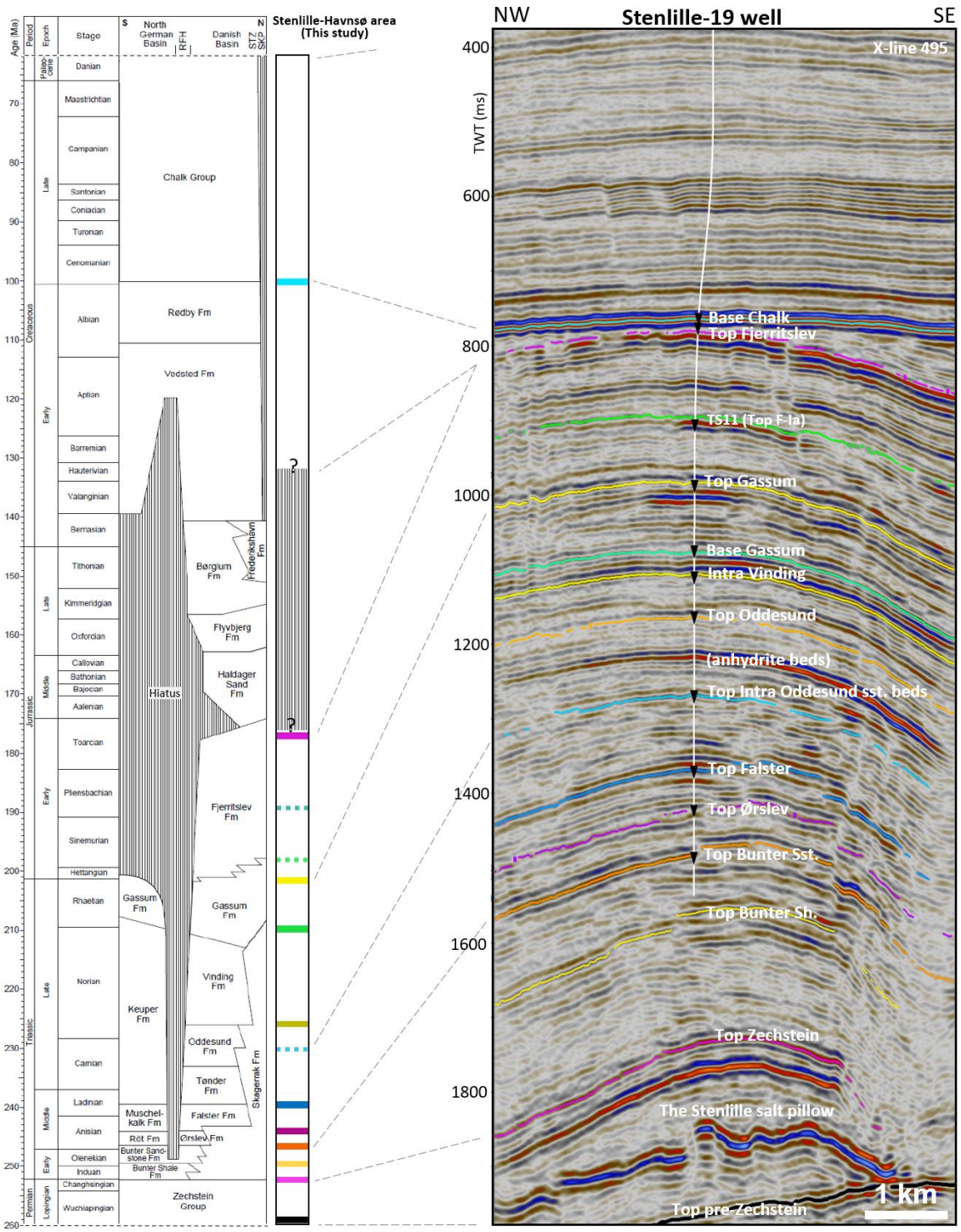

Figure 6.1.1. *Lithostratigraphy and seismic horizons with well-tie at the Stenlille-19 well in the eastern part of the Danish Basin, north of the Ringkøbing–Fyn High (RFH). The lithostratigraphic scheme, based on Bertelsen (1980) and Nielsen (2003), summarizes a more western part of the basin (Jutland), but most of the formations of the area just north of the RFH are partly comparable to the Stenlille region (excluding M.+U. Jurassic formations). Colored seismic stratigraphic horizons are shown in age in the separate stratigraphic column (this study), and in a seismic profile in two-way time (X-line 495 of the 2023 reprocessing – se Chapter 4 for location of the survey). The profile shows correlation to the Stenlille-19 well with well-tops (triangles, centers). Dashed horizontal lines at the top and base of the scheme (left) indicate omitted younger Cenozoic/Quaternary successions, and pre-Zechstein successions, respectively due to space limitation.*

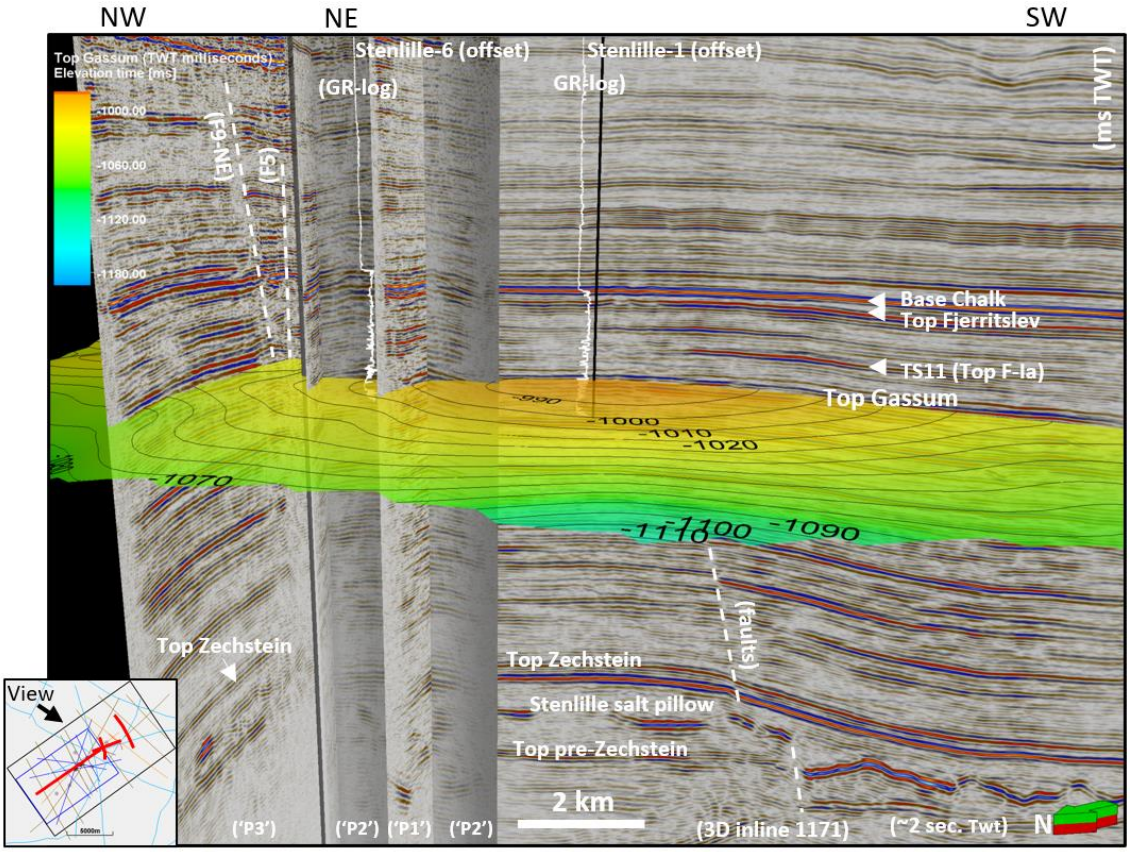

Figure 6.1.2. *3D perspective view with 3D inline 1171, aligned with the new 'P1', 'P2' and 'P3' (GEUS22-STL-P1,-P2,-P3) seismic sections, and a Top Gassum map (ms two-way time), with indicated positions of Top pre-Zechstein, Stenlille salt pillow, Top Zechstein,TS11 (Top F-Ia), Top Fjerritslev, Base Chalk, and faults. The Top Gassum structural closure towards NE was confirmed with the new Stenlille 2022 data, and faults were detected and mapped in the Gassum–Fjerritslev formations, but some also up into the Chalk Group. The 2D seismic sections are time-shifted to fit the reprocessed 3D survey (STENLILLE-97-GEUS-RE2023). Positions of sections (red) are shown in the small map and viewed towards SE. Modified from Gregersen et al. (2023).*

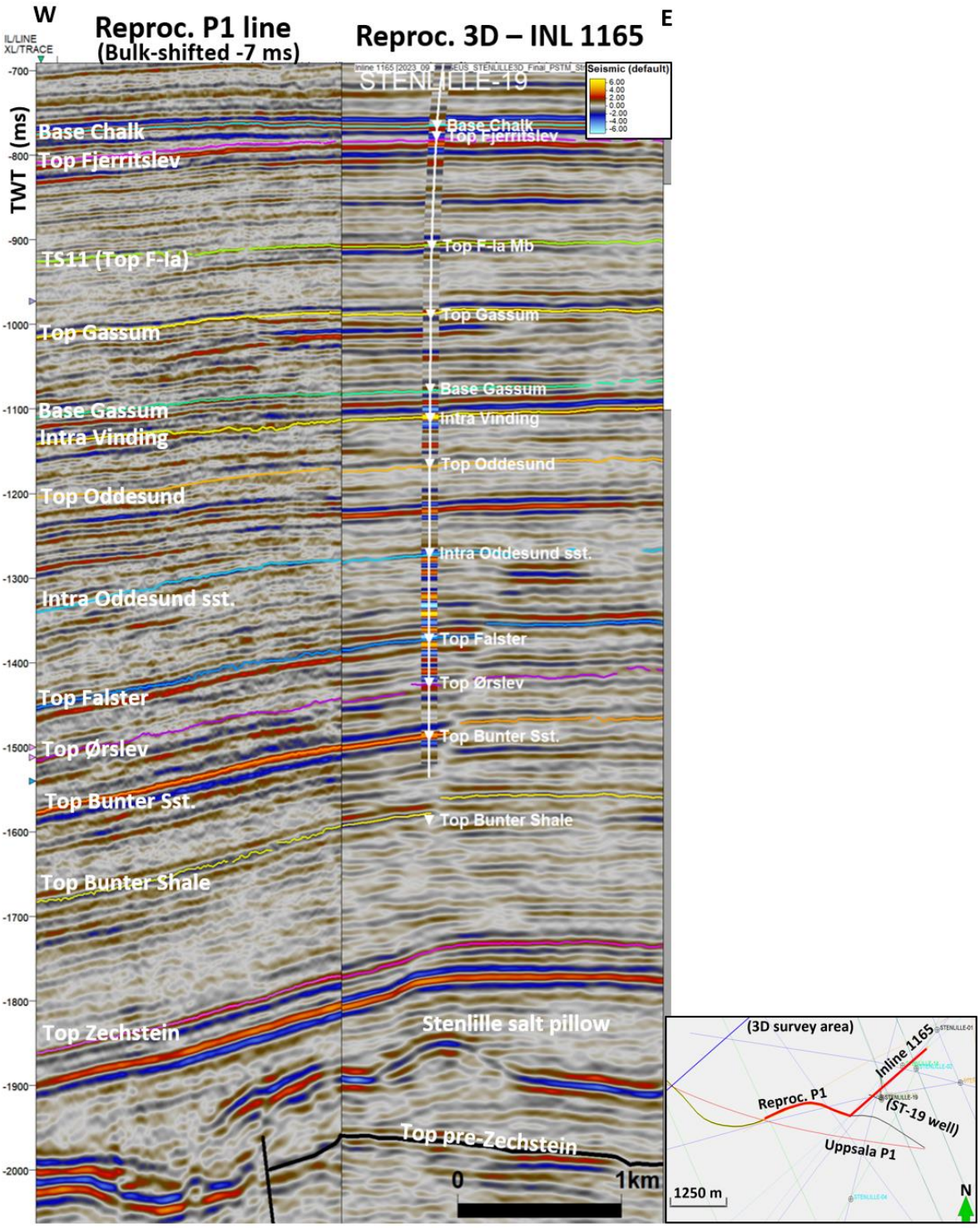

Figure 6.1.3. *Well to seismic tie with Stenlille-19 well at inline 1165 (reprocessed 3D) in a composite display with the P1 line (reprocessed, timeshifted -7ms). Synthetic seismic trace is displayed along the ST-19 well (see also Fig. 5.1). Well-tops and interpreted seismic horizons are also shown. Good correlation between the 3D and 2D data. The location of the line with the projected well is shown (red line) in the small map. Note that the reprocessed line is closer to the well (less smoothed).*

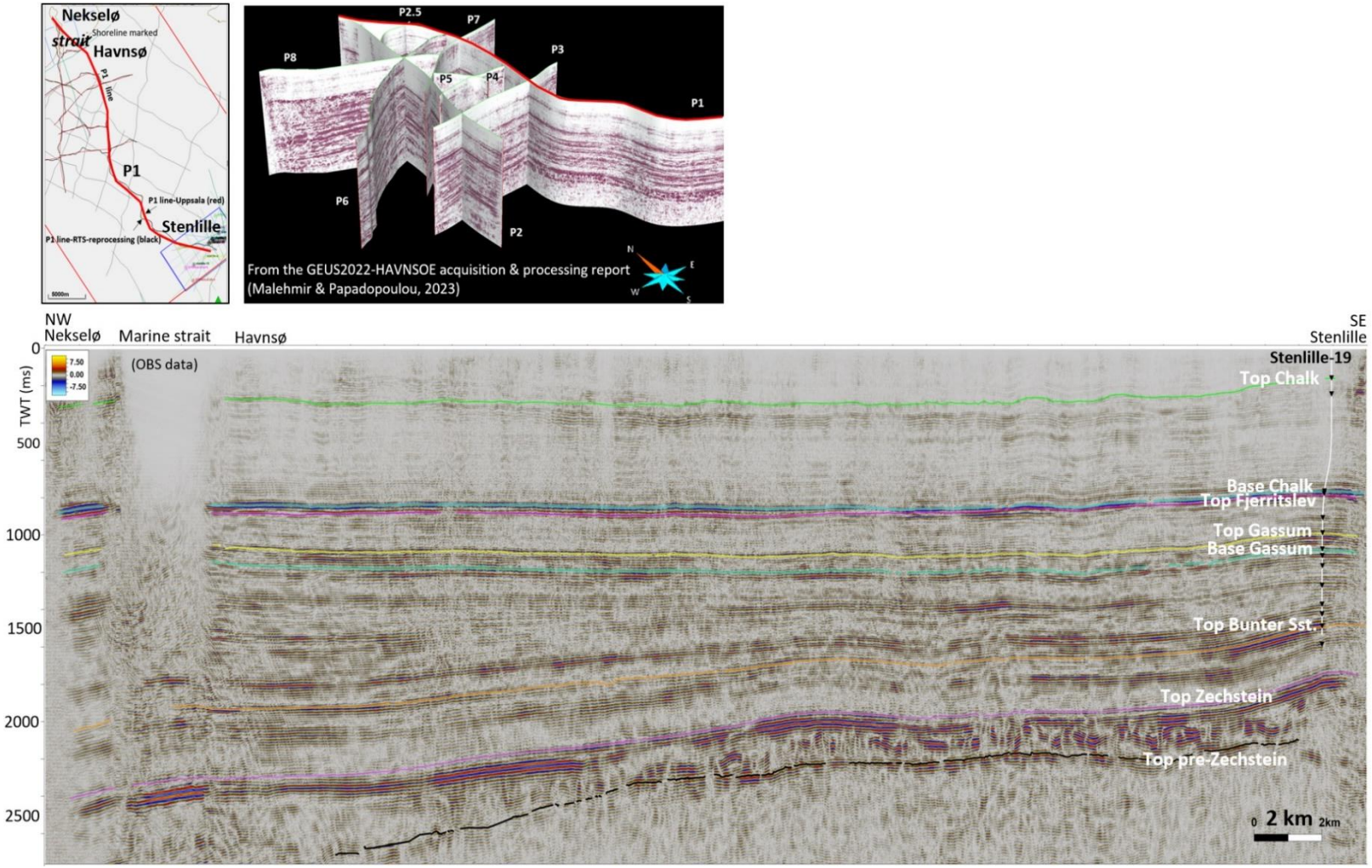

Figure 6.1.4. *2D seismic line GEUS22-HVN-P1 ('P1', with AGC) from the Stenlille area to the Havnsø area and the Stenlille-19 well (offset from the line, see map) with well-tops and interpreted horizons. The line is merged with marine (OBS) data and connects the data from the islands of Nekselø and Zealand. The location of the line is shown in the map and the 3D view.*

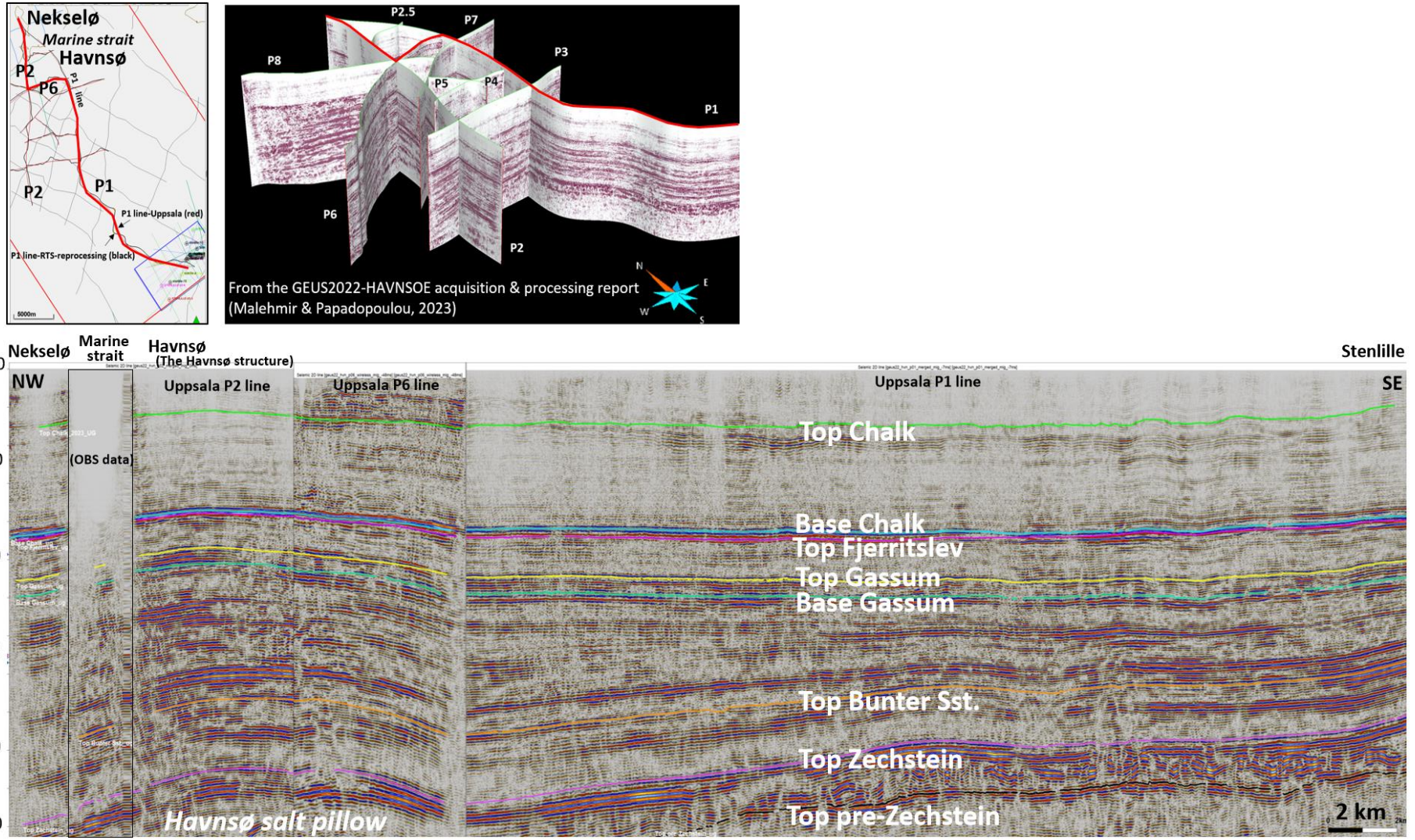

Figure 6.1.5. *Composite 2D seismic lines (GEUS22-HVN-P1,-P6,-P2) from the Stenlille area to the Havnsø area. The P2 line is merged with marine (OBS) data and connects the data from the islands of Nekselø and Zealand. The location of the lines are shown in the map and the 3D view. The deep Havnsø salt pillow growth elevated the Triassic–Jurassic successions, bounded at the top by an unconformity at the Top Fjerritslev.*

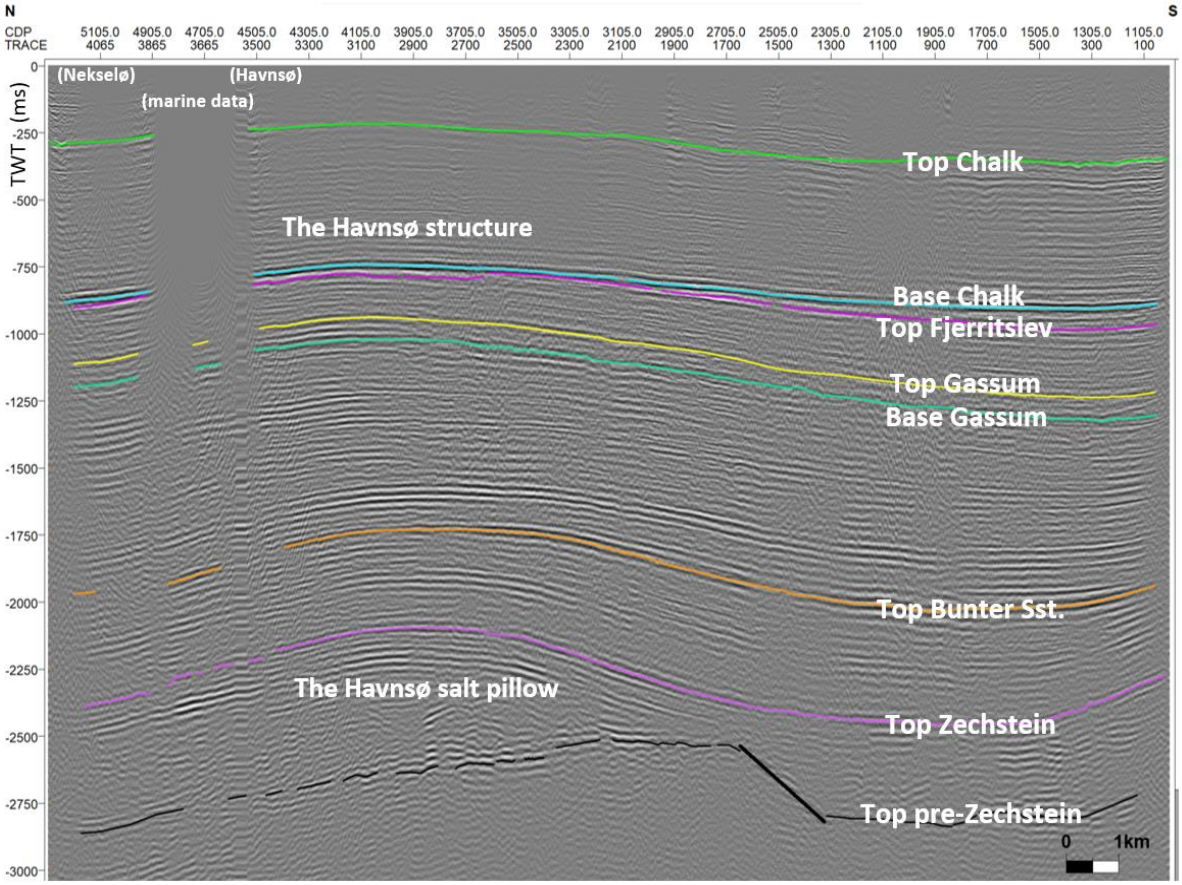

Figure 6.1.6. *2D seismic line GEUS22-HVN-P2 (two-way time) S-N into to the Havnsø structure. The line is merged with marine (OBS) data and connects the onshore data from the islands of Nekselø and Zealand at Havnsø. The location of the P2 line is shown in Fig. 6.1.5. The deep Havnsø salt pillow growth elevated the Triassic–Jurassic successions, bounded at the top by an unconformity (Mid-Cimmerian Unconformity, sensu Nielsen 2003) at the Top Fjerritslev. The Fjerritslev Fm thins towards the top of the Havnsø structure and may indicate growth of the structure. The unconformity at the Top Fjerritslev may as in Stenlille span a hiatus from latest Early Jurassic and into Early Cretaceous time. The unconformity is overlain by Lower Cretaceous Vedsted Fm and Rødby Fm, also thinning across the top of the structure. Growth of the structure probably continued during Middle to Late Jurassic, but also into the Cretaceous. The location of the P2 line is shown in Fig. 6.1.5.*

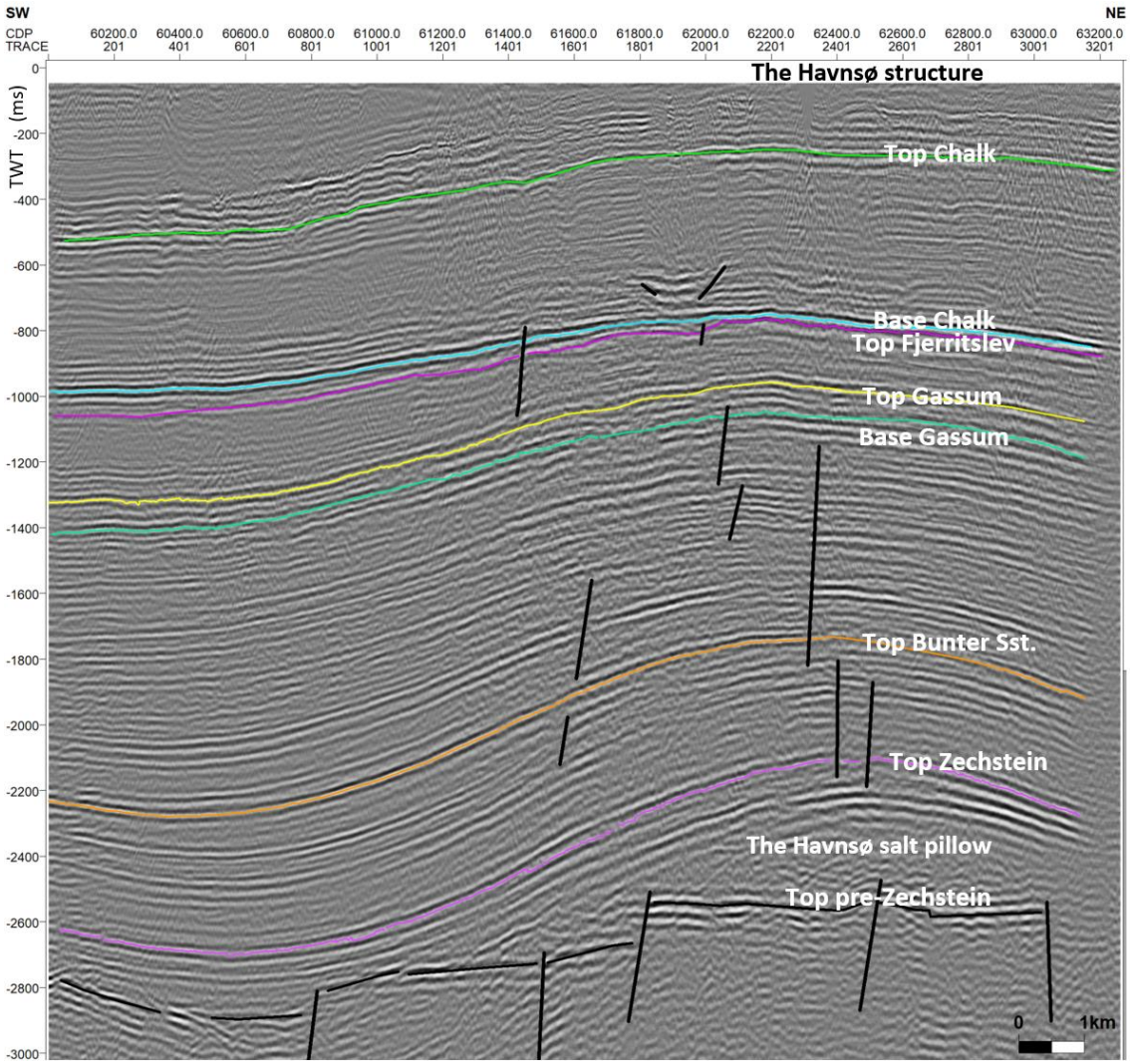

Figure 6.1.7. *2D seismic line GEUS22-HVN-P6 (two-way time) S-N into to the Havnsø structure. The line is merged with marine (OBS) data and connects the onshore data from the islands of Nekselø and Zealand at Havnsø. The deep Havnsø salt pillow growth elevated the Triassic–Jurassic successions, bounded at the top by an unconformity at the Top Fjerritslev. Minor faults are observed on line P6 and only a few of these in the Fjerritslev Fm and near Base Chalk. The small faults in Fjerritslev Fm have throws here less than 10 ms. Faults also deeper are probably related to growth of the salt pillow. The pre-Zechstein basement is affected by larger faults. Noise affects the data and zones of noise are e.g. observed from top and down into the Chalk and Fjerritslev to Gassum successions between CDP 61500 and 61800. The location of the P6 line is shown in Fig. 6.1.5.*

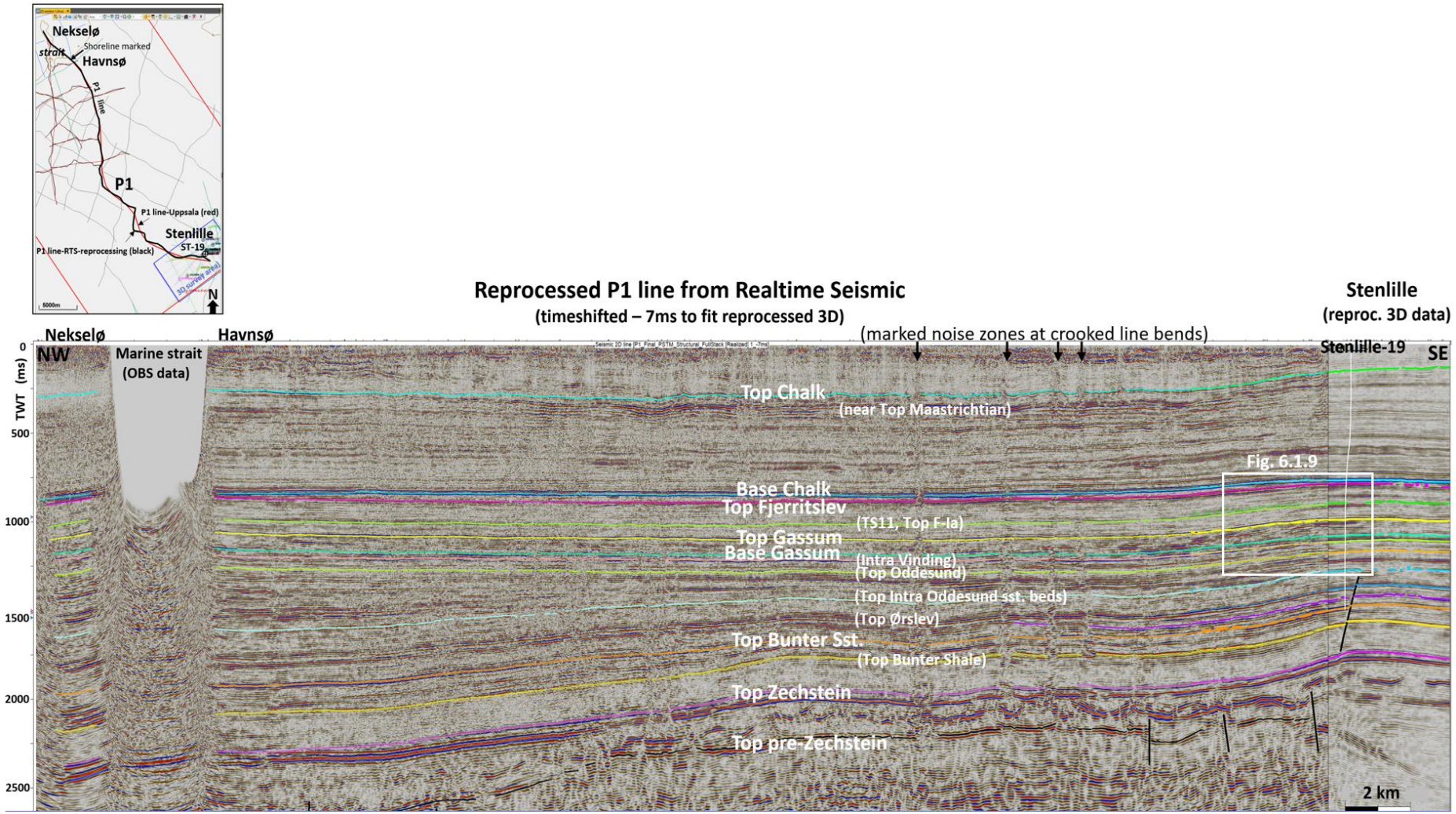

Figure 6.1.8. *2D seismic line GEUS22-HVN-P1 reprocessed by RTS from the Stenlille area to the Havnsø area. The P1 line is only time-shifted -7 ms and fits with the inline 1167 of the Stenlille-97 3D survey also reprocessed by RTS. The position of the Stenlille-19 well is also shown. The line is merged with marine (OBS) data and connects the data from the islands of Nekselø and Zealand at Havnsø. The location of the line is shown in the map. Note the narrow vertical noise zones occurring at marked road bends, where data was acquired (See Section 4; Fig. 4.3.3-4.3.4).*

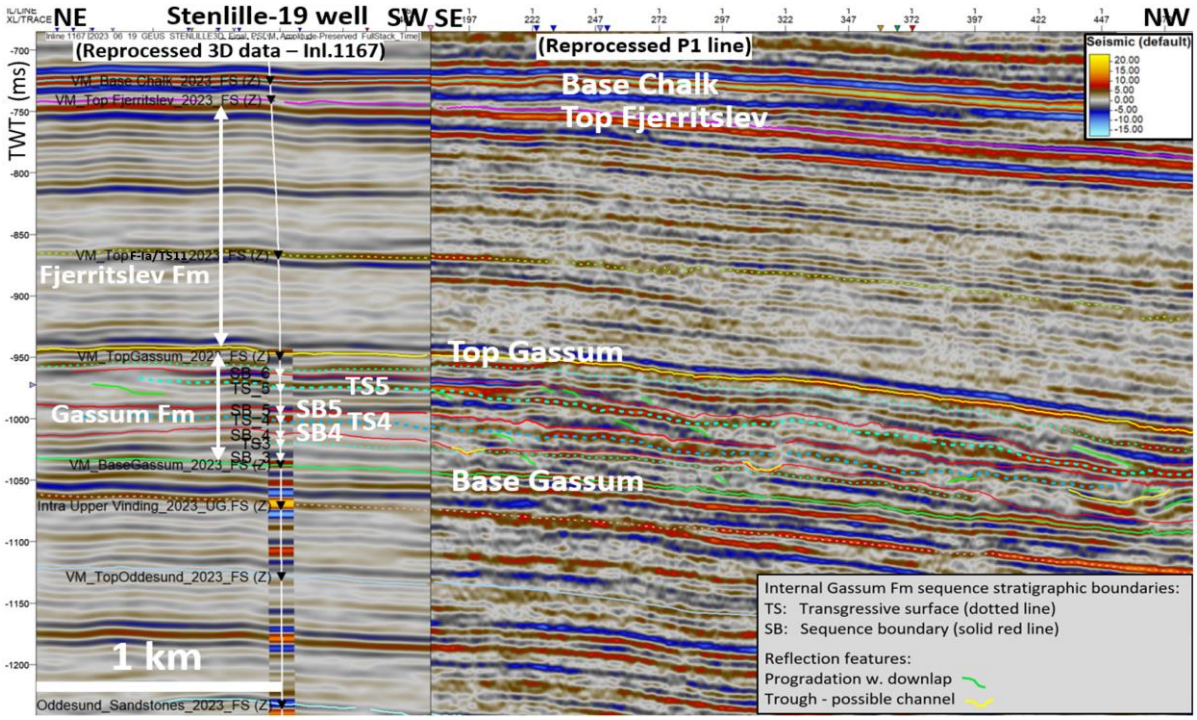

Figure 6.1.9. A zoomed, flipped part of Fig. 6.1.8 of *2D seismic line GEUS22-HVN-P1 reprocessed by RTS from the Stenlille area to the Havnsø area fitting with the inline 1167 of the reprocessed Stenlille-97 3D survey. The Stenlille-19 well is also shown with well-tops defined in the well, and with a synthetic seismogram along the well. Note the detailed subtle progradational reflections and troughs (channels) also known from the Stenlille area where they are sand-rich and represent fluvial to near-shore environments (Chapter 7). This P1 line has subsequently been interpreted further NW into the Havnsø structure and a facies reservoir model is described in Chapter 7 (Section 7.1; Fig. 7.1.13) and is further used in a scenario (no. 3) for storage capacity calculations in Chapter 8. The location of the line is shown in Fig. 6.1.8.*

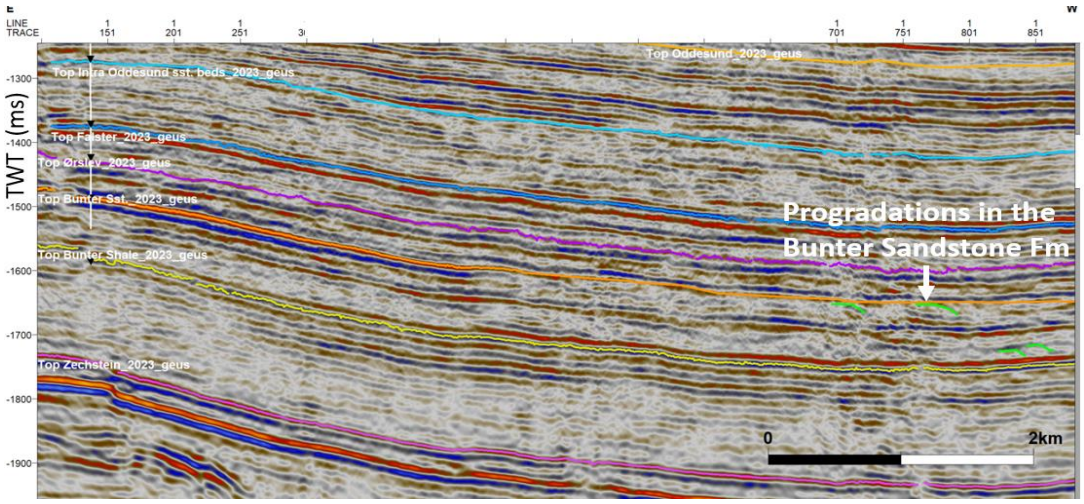

Figure 6.1.10. A zoomed, flipped lower part of Fig. 6.1.8 of P1 *reprocessed by RTS from the Stenlille area with the Stenlille-19 well. Note the subtle westward progradational reflections (green) in the Bunter Sandstone Fm, below Top Bunter Sst. horizon.*

6.2 Acoustic impedance modelling comparing the Gassum Formation in the Stenlille and Havnsø areas

This section shows results of an acoustic impedance modelling from the Stenlille to the Havnsø area. It gives an indication of the relative sandstone and mudstone volumes in the Gassum Fm along GEUS22_HVN_P1 (referred to as "P1" in this section). RMS-velocities are used to build a low frequent acoustic impedance model of P1. Results show that the acoustic impedance is generally higher in Havnsø compared to Stenlille, indicating a more mud-rich system.

Methods

The acoustic properties of sandstones, siltstones, and mudstones in Gassum Fm are investigated in the well Stenlille-19 (Fig. 6.2.1) from the density and sonic logs.

The RMS-velocities used are migration velocities, picked using a horizon-consistent method of straight and bending rays algorithms for the GEUS2022-HAVNSOE-RE2023 processing of P1 (Processing report: Realtime Seismic, 2023), Fig. 6.2.2a.

RMS velocities are converted to interval velocities using the Dix conversion,

$$v_n = \sqrt{\frac{v_n^2 \tau_n - v_{n-1}^2 \tau_{n-1}}{\tau_n - \tau_{n-1}}}$$

where τ_n and τ_{n-1} are the two-way zero offset times in the layer above and below the layer boundary *n* (Dix 1955), see Fig. 6.2.2b.

Acoustic impedance is calculated using Gardener's law calibrated to the Stenlille wells. First, densities are estimated, $\rho = 1.66 \cdot {V_{int}}^{0.25}$ (velocities in km/s and densities in g/cm^3), and then acoustic impedance is calculated, $AI = V_{int} \cdot \rho$ (Gardner et al. 1974). A mild lateral smoothing is applied to the acoustic impedance model, see Fig. 6.2.2c. The acoustic impedance model is converted to depth using the RMS-velocities, see Fig 6.2.2d.

Results

Mudstones and siltstones generally have a higher acoustic impedance than sandstones in the Gassum Fm in the Stenlille-19 well (Fig. 6.2.1). This is assumed to be the trend for the Gassum Fm in general along P1.

The acoustic impedance model shows lower values in the southeastern part of P1 (Stenlille) than in the northwestern (Havnsø). The change is occurring around CDP 1500, 15 km from the beginning of the line in Stenlille, see Fig. 6.2.2e. This is interpreted as more sand rich in Stenlille compared to Havnsø, which is also comparable to the sequence stratigraphical interpretation and facies model in Fig. 7.1.13.

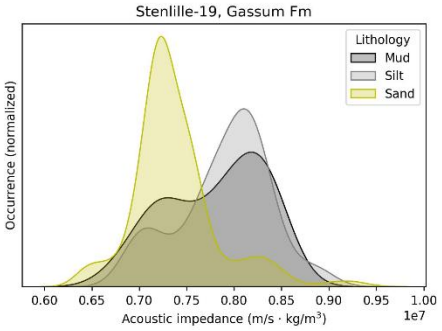

Fig. 6.2.1. *Acoustic impedance values for different lithologies of Gassum Fm in the Stenlille-19 well.*

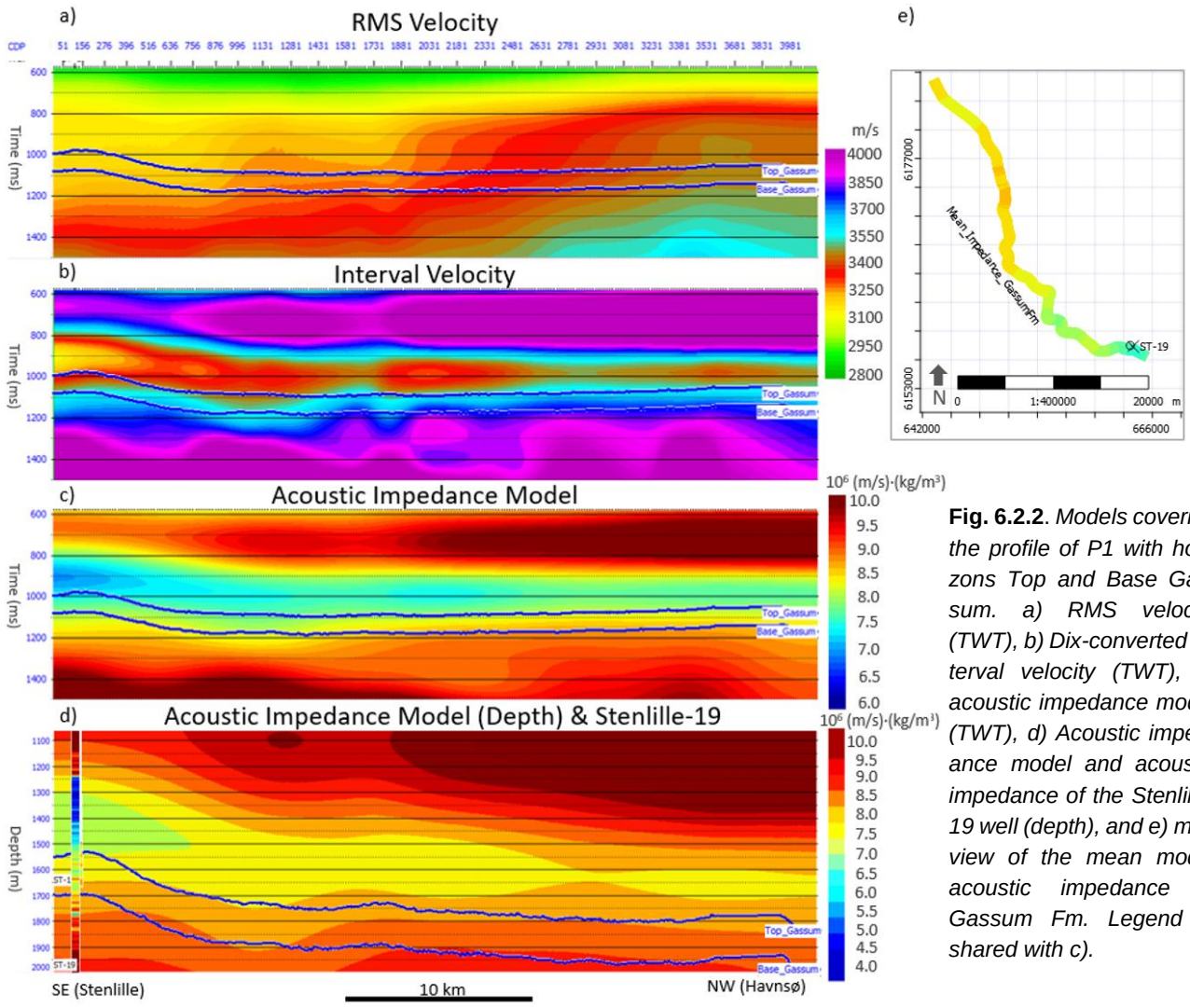

Fig. 6.2.2. *Models covering the profile of P1 with horizons Top and Base Gassum. a) RMS velocity (TWT), b) Dix-converted interval velocity (TWT), c) acoustic impedance model (TWT), d) Acoustic impedance model and acoustic impedance of the Stenlille-19 well (depth), and e) map view of the mean model acoustic impedance in Gassum Fm. Legend is shared with c).*

Discussion

The acoustic impedance model reflects the low frequency changes (0–2 Hz). The model thus does not contain the same details and as large range as the well log data, but it contains the overall trend (Fig. 6.2.2d). The thickness of the Gassum Fm is small compared to the wavelength (c. 1/5), so interval velocities above and below may affect the model.

Compaction also influences the acoustic impedance. The top of the Havnsø structure and in particular the Stenlille structure are therefore expected to have lower acoustic impedances relative to the surroundings, independent of the relative volumes of sandstones and mudstones. However, lateral changes are also seen at constant depth (Fig. 6.2.2d). In the top of the Stenlille structure, stored natural gas also decreases the acoustic impedances (Bredesen 2022). Other possible factors that may influence the acoustic impedances include cementation and pressure variations (Simm and Bacon 2014; Chapter 5). As the system is relatively consistent, these factors are expected to have a smaller contribution to the long wavelength, lateral variation in acoustic impedance, compared to changes in lithology.

In conclusion, the results show relatively higher velocity and acoustic impedance and thus probably a more claystone rich Gassum Fm is suggested from CDP 1500 of P1 and towards the Havnsø structure, compared to the Gassum Fm of the Stenlille structure. Results should be used only as an indication, as it relies on RMS-velocities and wells in Stenlille.

6.3 Structure description and tectonostratigraphic evolution

The seismic stratigraphic interpretation is tied to well-tops in the 3D seismic survey in most wells and extended further into the 2D seismic lines (fitted to the 3D survey) outside the 3D area. Figure 6.3.1 shows e.g., the two key-top reservoir surfaces in two-way time: Top Gassum and Top Bunter Sst. along the key seismic line (GEUS22_HVN_P1) from the Stenlille structure to the Havnsø structure. Maps in two-way time have been generated from horizons by gridding and smoothing - see each map in Fig. 6.3.2, where the most important for the gross stratigraphy, reservoir and seal are shown (shallow to deep): (A) Base Chalk, (B) Top Fjerritslev, (C) Top- & (D) Base Gassum, (E) Intra Oddesund sst. beds, (F) Top Bunter Sst., and (G) Top Zechstein is included to show a morphology affecting overlying horizons.

Figure 6.3.3 shows the depth converted maps of the four key horizons for the gross division of the Stenlille structure into top reservoir and seal containing formations (shallow to deep): (A) Base Chalk, (B) Top Fjerritslev, (C) Top Gassum, (D) Top Bunter Sst. For depth conversion procedure see Chapter 5.

Fig. 6.3.4 shows three key thickness maps including the (A) Chalk Group, important for depth conversion, and the primary seal and reservoir formations: (B) Fjerritslev Fm, and (C) Gassum Fm. The maps are used in the following descriptions of the geological evolution, stratigraphy and for calculation of storage capacity.

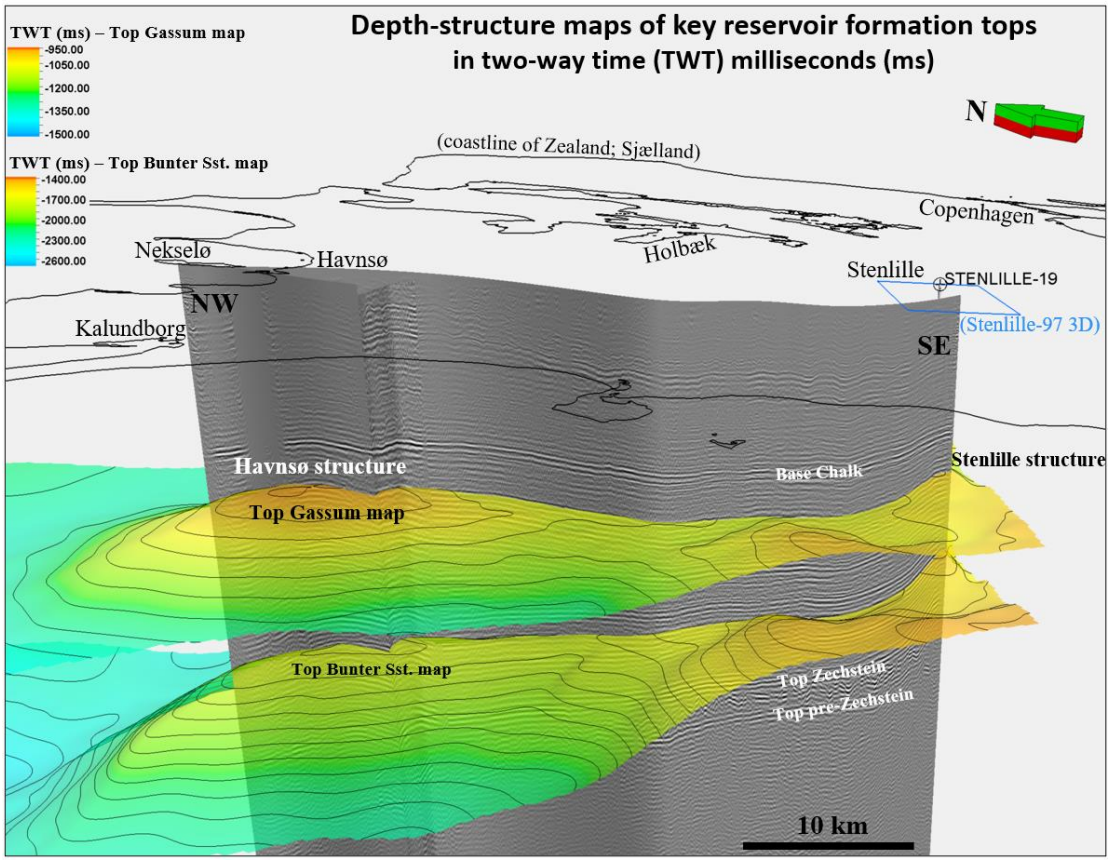

Figure 6.3.1. *Seismic section GEUS22_HVN_P1 with mapped key reservoir formation tops: The Top Gassum (upper) and Top Bunter Sst. (lower) in a 3D display in two-way time (milliseconds) and viewed towards NE below Zealand. Maps are also shown in Fig. 6.3.2C, F. Positions of the Stenlille-19 well and the Stenlille 3D survey area (blue square) are also shown.*

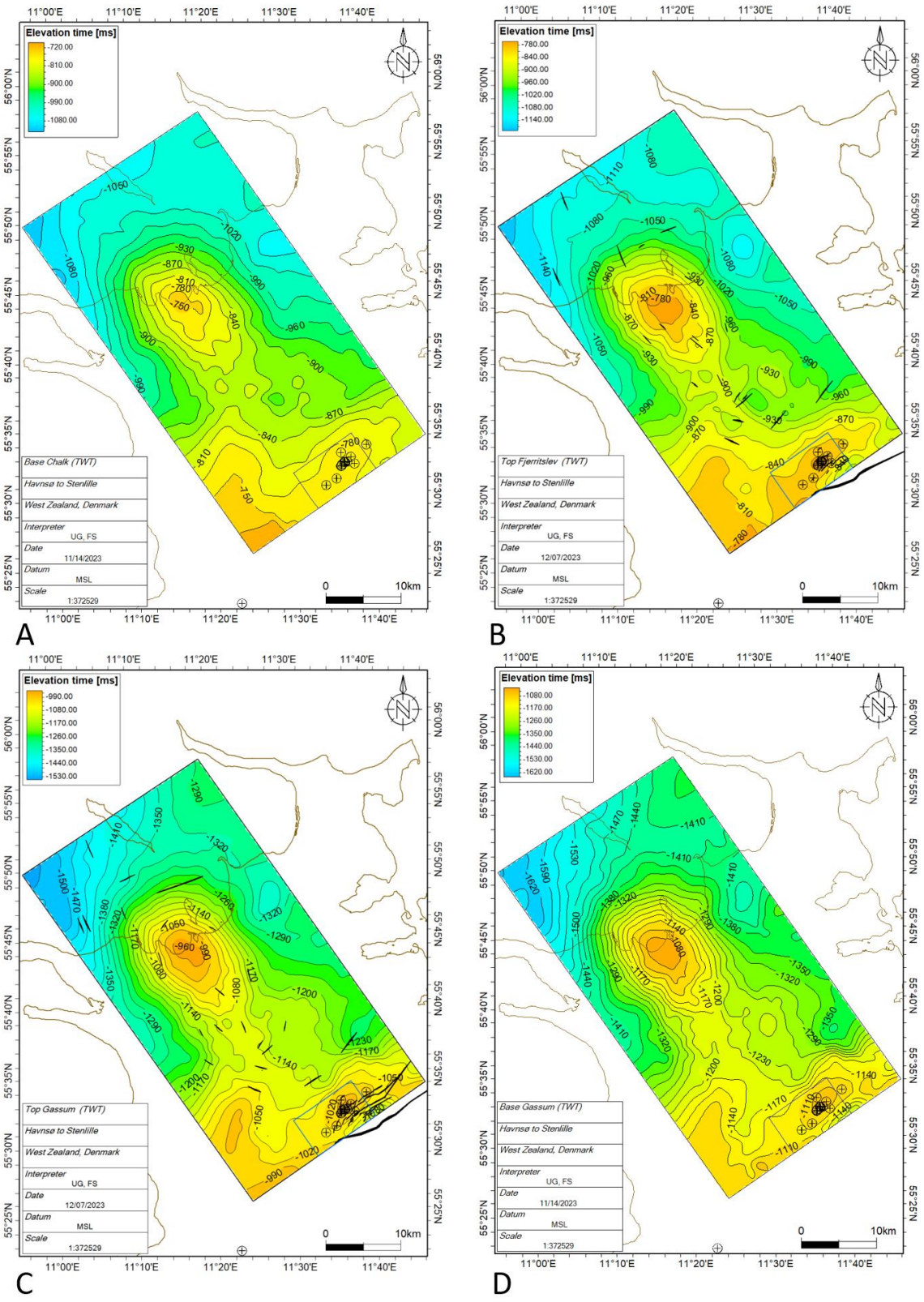

6.3.2. *Depth-structure maps in milliseconds (ms) two-way time (TWT) below mean sea level (b.msl. or MSL) with the largest faults (black polygons) shown at the Top Fjerritslev (B) and Top Gassum Fm (C). A: Base Chalk; B: Top Fjerritslev; C: Top Gassum; D: Base Gassum. The maps are produced with a 250 x 250 m grid and are mildly smoothed (mostly x2). The contour interval is 30 ms for the maps.*

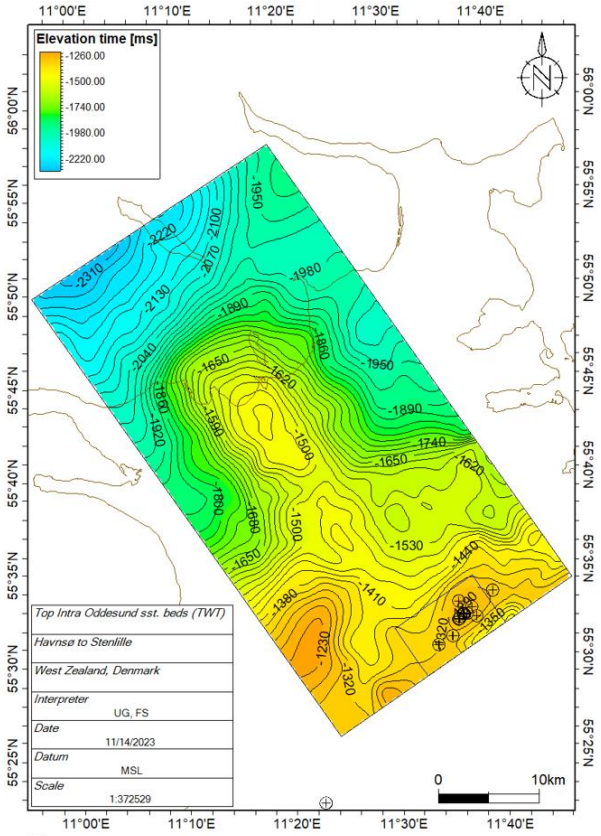

E

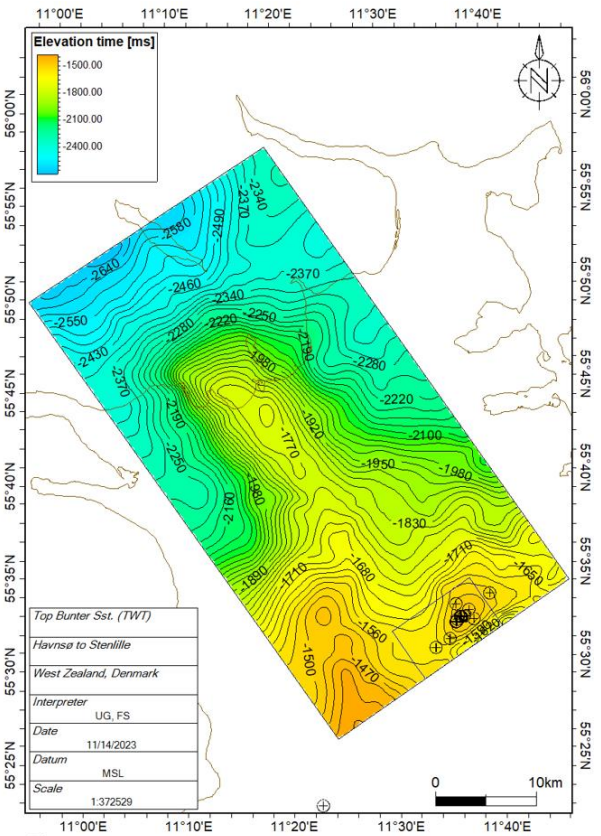

F

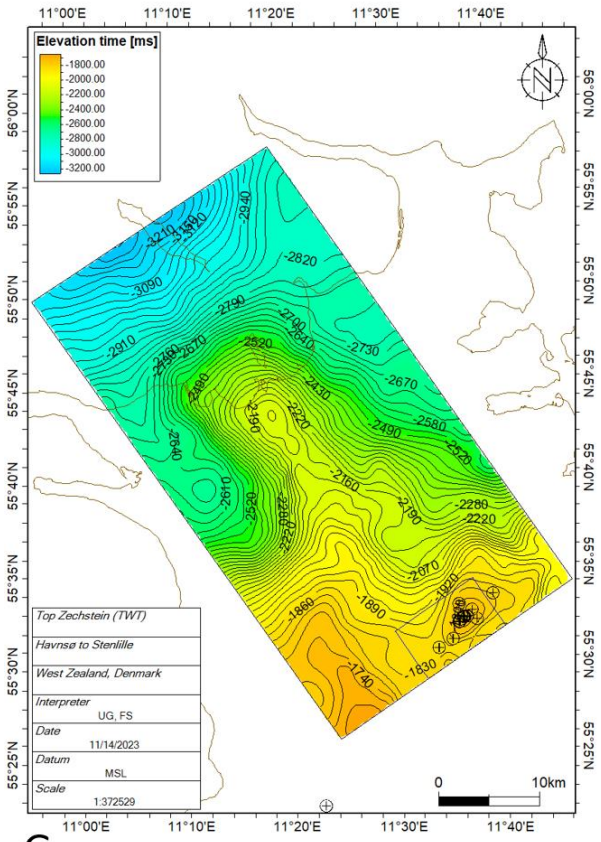

G

(**Fig. 6.3.2. – continued**).
Depth-structure maps (ms TWT) with no faults shown. E: Top Intra Oddesund sst. beds; F: Top Bunter Sst.; G: Top Zechstein. The maps are produced with a 250 x 250 m grid and are mildly smoothed (mostly x2). The contour interval is 30 ms for the maps.
The maps of Fig. 6.3.2A–G show approximately similar outlines of the central Havnsø structure, trending NW–SE, as a well-defined 4-way dip closed structure. The similar outline and similar position of the mapped structure overlying the domed Top Zechstein (G), which is cored by salt, support that the Havnsø structure is mainly formed by the salt pillow evolution. See also cross sections (Figs 6.1.5, 6.3.1). Mapping of E, F, G, includes PaleoScan™ in the 3D area.

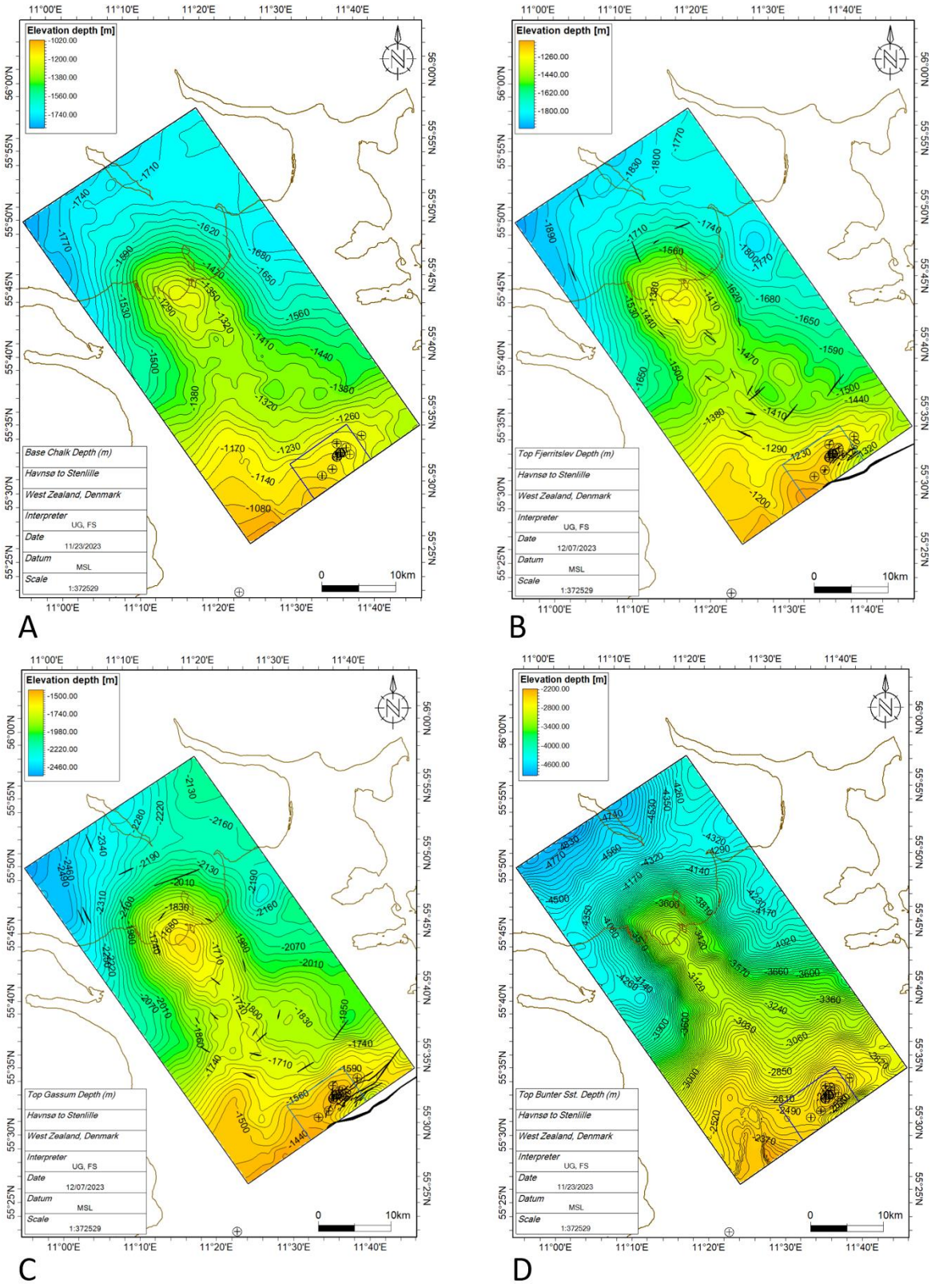

Fig. 6.3.3. *Key depth-structure maps in meter (m) MSL of A: Base Chalk; B: Top Fjerritslev; C: Top Gassum; D: Top Bunter Sst. The largest faults (black polygons) are shown at the Top Fjerritslev (B) and Top Gassum Fm (C). The contour interval for the maps is 30 meters. The Top Fjerritslev map has a top in the Havnsø structure of c. 1260 m. The Top Gassum map has a top in the Havnsø structure at c. 1550 m, a lower closure at c. 1710 m with an area of c. 70 km^2, and a relief of c. 160 m. The Top Bunter Sst. map has a top in the Havnsø structure at c. 3090 m, and two smaller, lower closures at c. 3120 m.*

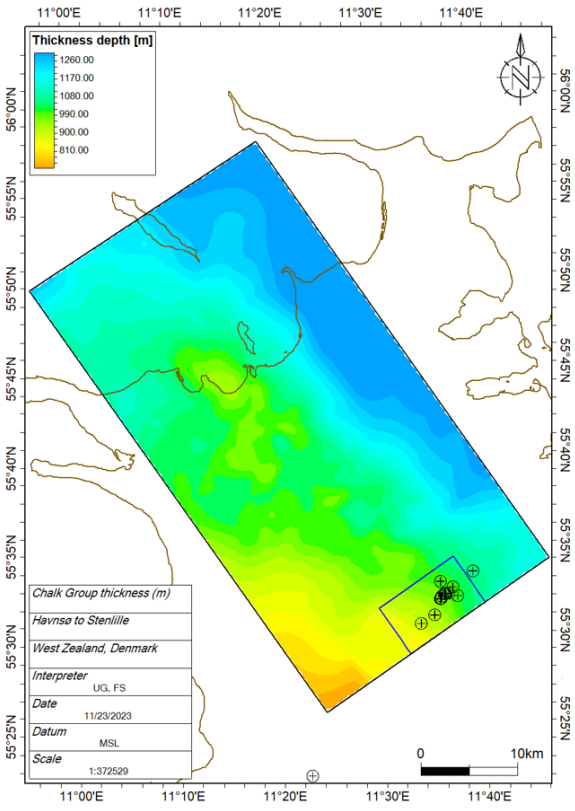

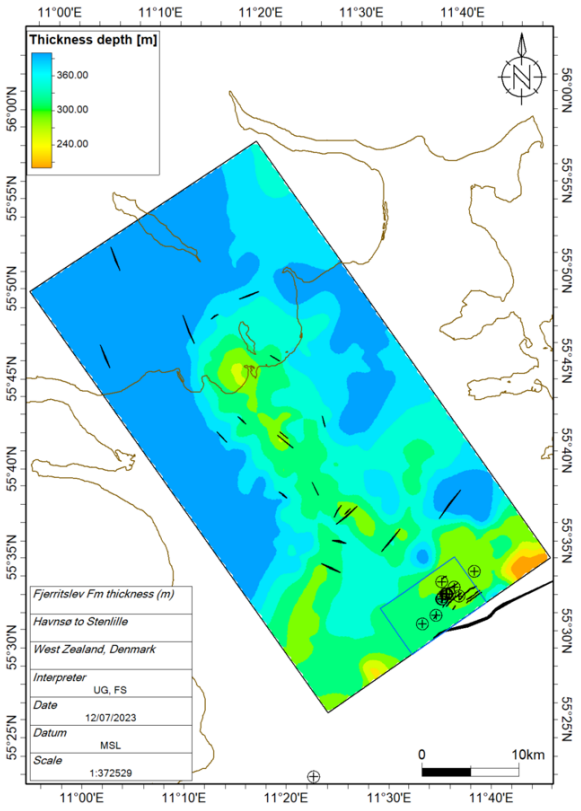

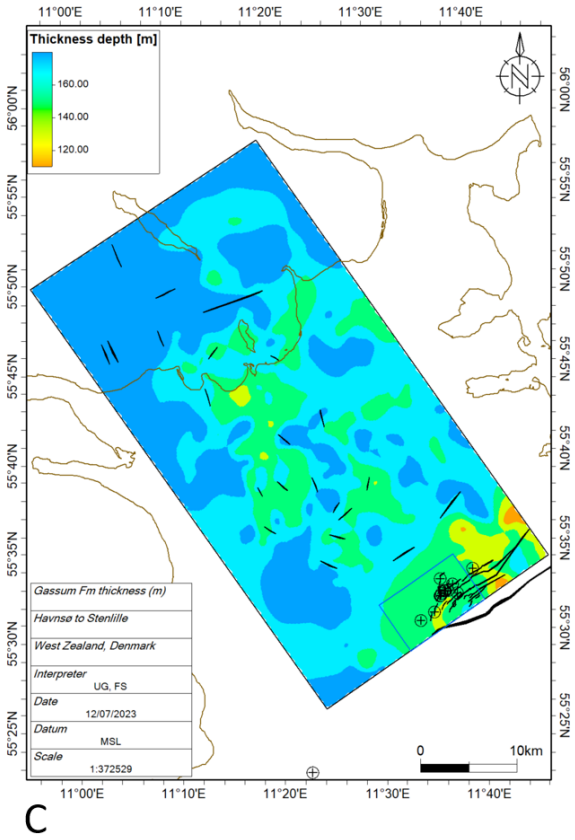

Fig. 6.3.4. *Key thickness (isochore) maps in meter (m) of A: Chalk Group; B: Fjerritslev Fm; C: Gassum Fm. The largest faults (black polygons) shown in the Fjerritslev Fm (B) and Gassum Fm (C). The contour interval is 30 meter for A and B, and 20 meter for C. In the Havnsø structure, the Chalk Group decreases towards the top from c. 1100 m to c. 950 m at the top. The Fjerritslev Fm thickness is more than 250 m in the Havnsø structure: c. 260 m in the top increasing to c. 350 at the flanks. The Gassum Fm is in the Havnsø structure c. 130 m in the top increasing to c. 170 m at the flanks, in average c. 150 m thick, which is similar to the Stenlille area. Faults are small and few in the Gassum and Fjerritslev Formations of the Havnsø structure and lager in the SE part of the Stenlille area. In the study area faults are mostly oriented SW–NE and in a NW–SE direction.*

Description of faults

Faults may act as potential leakage pathways, that could occur across and along faults, but faults may also act as potential barriers (compartments) for pore-fluids. Therefore, fault interpretation and mapping are important for evaluating reservoir fluid mobility and cap-rock integrity. Furthermore, mapping of faults provides insight into the geological evolution and setting of the investigated area.

A manual interpretation of the 2D and 3D reflection seismic sections is performed in the study area, and supported by various seismic attributes, including ant-tracking, semblance, and coherency. Only in the Stenlille-97 3D seismic survey Machine Learning has additional been conducted (see below). The focus was on larger faults in the primary reservoir succession in the Gassum Fm and the primary seal successions of the Fjerritslev Fm and in overlying secondary seal successions of the Vedsted−Rødby Formations and in the Chalk Group. The faults were interpreted vertically and laterally (Fig. 6.1.7, 6.3.2–6.3.4).

In particular, fault systems that appear to be connected vertically from top reservoir up through the seal successions are important to reveal for assessing the seal integrity. Some of the deeper faults near the top and above the Bunter Sandstone Fm and intra Oddesund Fm sandstone beds were also identified in connection to a possible secondary reservoir-seal potential, but not used for the maps and only shown on selected sections.

Faults in the Havnsø structure

We focus here on the Gassum and Fjerritslev Formations as the primary reservoir and seal successions, respectively. The regional interpretation of the Havnsø structure and surrounding areas shows in both formations few, small faults, less than a few km long (Fig. 6.3.2), and with throws mostly less than 10–15 ms (Fig. 6.3.5–6.3.7). Faults mainly occur with SW–NE and NW–SE orientations (Fig. 6.3.2–6.3.4). Faults are mostly rather vertical, slightly dipping, and mostly within the two formations, but some places they also continue up through lower part of the Chalk Group.

Faults were mostly small and difficult to interpret on the old seismic data due to noise. The new seismic lines show less noise and more continuous reflections than the vintage data, where noise zones can be misinterpreted as faults. Also, in the new lines noise zones occur, especially at marked bends of the roads of acquisition and may show more up in some processing types (Section 4.3; Fig. 4.3.3, 6.1.8) than in other (Fig. 6.1.4). A way to examine if noise zones reflect faults is to compare offset stack sections. Some tests of the reprocessed 2D Havnsø survey show, that the mid offset stack is less affected by noise from the line crookedness than both the full stack and the far and near offset stack section (Fig. 4.3.4). Sometimes it is possible in the mid stacks to follow the reflections with no displacements across the noise zones, thus not indicating faults. Also, the small faults were difficult to correlate and connect between seismic lines with noise and as lines are located at far distances.

Faults mostly trend parallel to the dominant orientation and flanks of the Havnsø structure outline (Fig. 6.3.2–6.3.4). Therefore, most of the faults in the two formations were probably formed during the Jurassic development of the Havnsø salt pillow. Salt movements were probably governed by increased temperature and pressure from the thick Triassic to Jurassic overburden and triggered partly from the Mid-Cimmerian Tectonic Phase. The structure formation is associated with development of an unconformity with a hiatus at the Top Fjerritslev (Lower Jurassic) onlapped by Lower Cretaceous successions Vedsted Formation.

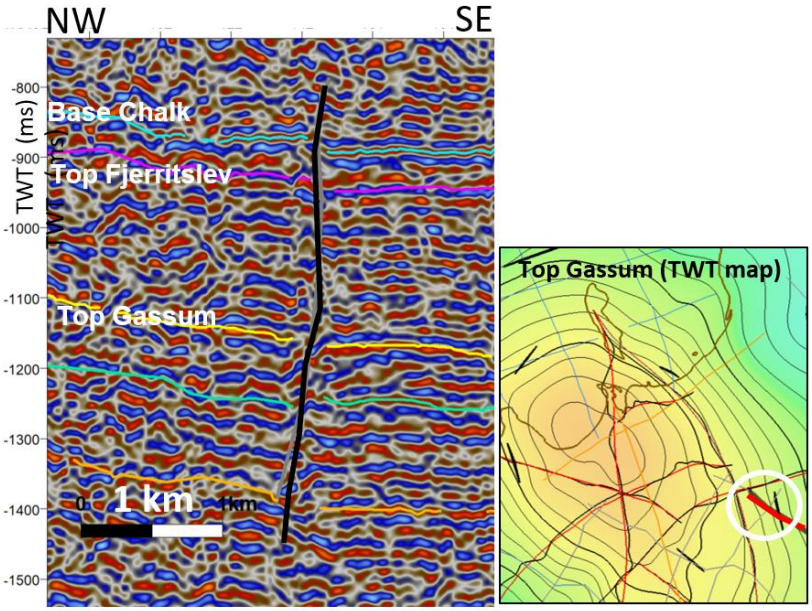

Fig. 6.3.5. *Fault in the SE part of the Havnsø structure with very small or no throw in the Gassum and Fjerritslev Formations, but a little throw on the Base Chalk horizon. Location of line (red) (SSL6267_R13) is shown on the map.*

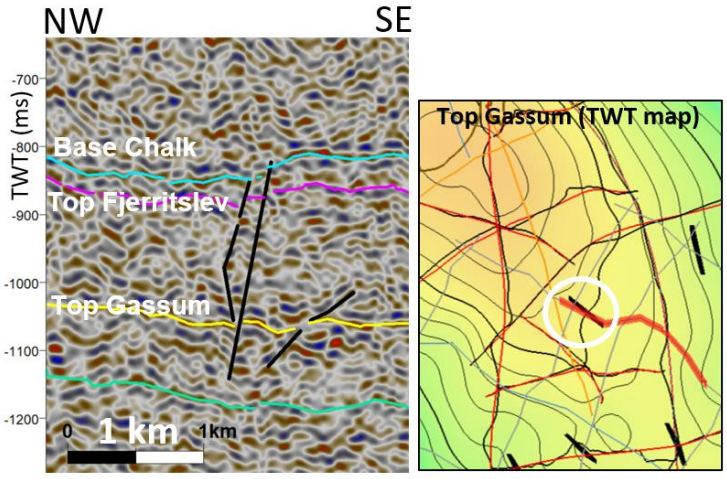

Fig. 6.3.6. *Faults in the southern part of the Havnsø structure with very small throws in Gassum and Fjerritslev Formations, little on Base Chalk. Location of line (red) (SSL6267_R23) on the map.*

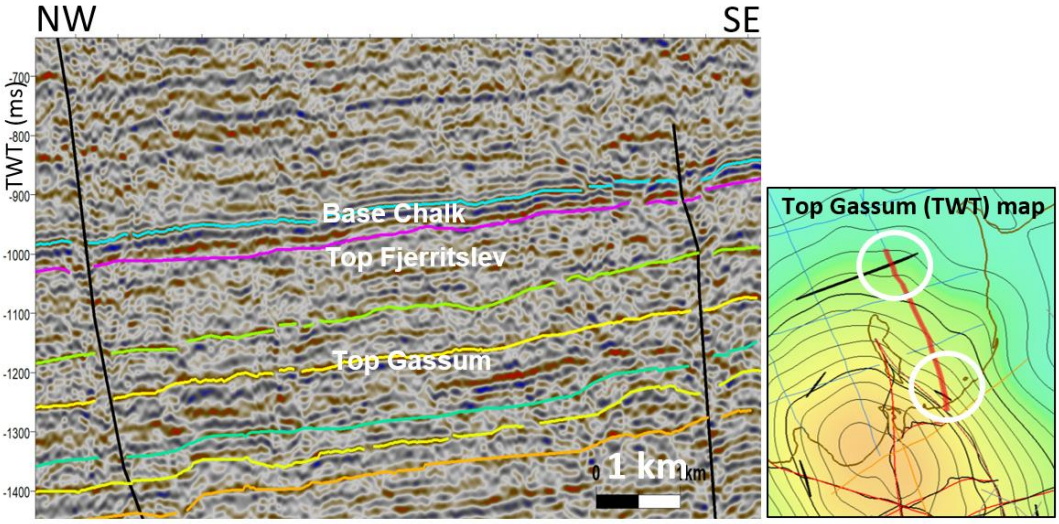

Fig. 6.3.7. *Faults in the northern part of the Havnsø structure with very small or no throws in the Gassum and Fjerritslev Formations, whereas a little throw is observed on the Base Chalk horizon. Location of line (red) (PRKL74A_38471) is shown on the map.*

Faults in the Stenlille structure – the southern part of the study area

Faults becomes larger in length and throw in the Stenlille structure, where they are more detailly studied in a much more comprehensive database including a 3D survey (Gregersen et al. 2023). The Stenlille structure has a number of faults in its top and eastern flank, in particular in the Gassum and Fjerritslev Formations, and less apparently in the overlying successions of the Vedsted to Rødby Formations and the lowermost part of the Chalk Group.

In large parts of the structure, most faults to the Top Fjerritslev horizon seem to displace more or less equal thicknesses in both the Gassum and Fjerritslev successions (Fig. 6.3.8, 6.3.9) and as the Gassum Fm has little thickness variations, this imply that most of the significant faults are formed after the deposition of the Gassum Fm and most of the Fjerritslev Fm.

As some of the significant faults continues up through the Fjerritslev Fm and more or less stops at the unconformable Near Top Fjerritslev horizon, they were probably formed during late part or after deposition of the Fjerritslev Fm, related to the doming of the structure, mainly caused by the salt pillow growth.

The Stenlille F1 fault SE in the study area, south of the Stenlille structure (Fig. 6.3.9, 6.3.10), is a large, deep normal fault, seated SE of the salt dome, which evolved from mid-Jurassic time. The F1 fault shows throw at the Top Gassum of c. 150−180 ms, with similar order of throws of the deeper horizons and units (c. 170−200 ms) down to Top Zechstein. The Stenlille structure was formed as response to the formation of the salt pillow, and faults at the flanks are probably related to the growth of the structure. At the fault zone to the SE (F1 fault) salt withdrawal and roll-over were also involved.

The Fjerritslev Formation between Top Gassum and Near Top Fjerritslev horizons thickens in the hanging wall syncline towards fault F1 (Fig. 6.3.10), indicating growth fault evolution of a primary syncline of salt doming. The throw near Top Fjerritslev is less than c. 70–80 ms and mostly 10–30 ms, possibly in part due to erosion (Fig. 6.3.8). Apparently, it is primary the uppermost part of the Fjerritslev Formation succession (probably the F-III and F-IV members), that thickens towards the fault. The top of the structure, south of the Stenlille-1 well is offset by faults (Fig. 6.3.8).

Most faults in Gassum and Fjerritslev Formations in the Stenlille structure have mainly minor, normal and in some cases reverse throws, mostly less than c. 30 ms or c. 30−50 m (Fig. 6.3.8). Most faults are located along the anticlinal NE−SW trending axis of the structure, in its top and its SE flank. A few faults trend N–S (Fig. 6.3.9). The deepest-seated faults occur along the SE structure flank, and some of these sole out deep into the salt pillow (Fig. 6.1.1, 6.3.8), indicating that they are related to the structural deformation due to the doming of the structure. The most prominent fault in the structure top SE of well ST-5, is the F5 fault (Fig. 6.3.8). Also, the shallower Gassum−Fjerritslev faults ending at the Near Top Fjerritslev horizon are mainly related to the doming of the salt pillow during Middle- to Late Jurassic times.

The manually interpreted fault polygons and ML fault trends both show consistent, mostly NE−SW fault directions at both the Top Gassum and Near Top Fjerritslev surface maps (Fig. 6.3.9c,d). Recent studies show that some of the near Top Gassum faults identified by mapping (F11, F13 and F14) and Machine Learning may compart the Gassum Formation reservoir zones and seem to restrict predicted natural gas in some cases (Bredesen et al. 2022).

At the Base Chalk surface (Fig. 6.3.9e) there are less faults, but still with NE−SW trends. This indicates relatively few clear fault connections between the Lower Cretaceous

successions and the Upper Cretaceous Chalk Group. However, breach of seals may occur even with few and subtle faults, and such risks should be investigated and assessed thoroughly before injecting CO_2. There as some faults in the Chalk Group, but faults in the shallow section is difficult to reveal, e.g., due to noise, and storage should in general be kept safely away from problematic faults. However, the long-term, safe storage of natural gas at Stenlille indicates competent sealing successions.

The Near Top Fjerritslev horizon is a significant seismic reflection trough with increasing acoustic impedance and the overlying successions (mostly of the Vedsted Formation) onlap this horizon (Fig. 6.1.1, 6.3.8). The Near Top Fjerritslev horizon is close to (or near below) a major unconformity (hiatus), separating Lower Jurassic (Toarcian age) deposits of the Fjerritslev Formation from the Lower Cretaceous Vedsted Formation (Fig. 6.1.1; see also discussion of ages in Section 7.2).

The youngest part of the Fjerritslev Formation in the Stenlille area is correlated to the F-III and F-IV members of the Fjerritslev Formation. In some of the Stenlille wells the uppermost preserved part of the Fjerritslev Formation (at or slightly above the seismic Near Top Fjerritslev horizon) seems to be of a latest Early Jurassic (Toarcian) age, whereas overlying deposits may belong to the Vedsted Formation of an Early Cretaceous age (Nielsen 2003; Pedersen et al. 2022) - see the discussion in Section 7.2. Thus, Middle and Late Jurassic deposits may be missing at the crest of the structure. The erosion and hiatus may be slightly different depending on the position on the structure, and the flanks of the structure were probably experiencing less erosion with more preserved successions, possibly also including uppermost parts of the Fjerritslev F-IV member. The major unconformity (hiatus) marks the formation of the Stenlille structure mainly due to formation of the underlying salt pillow, but possibly also due to regional uplift and erosion. The unconformity may be equivalent to the 'Base Middle Jurassic unconformity' or 'Mid-Cimmerian Unconformity' (Nielsen 2003) and is associated with uplift and erosion or nondeposition (a major Middle- to Late Jurassic hiatus) over structures and margins of the Danish Basin, including the Ringkøbing-Fyn High in central and southern Denmark.

The Lower Cretaceous Vedsted and Rødby Formations are part of the seismic stratigraphic wedge, which onlapped the Near Top Fjerritslev horizon after the formation of the elevated Stenlille structural dome. This wedge is only affected by a few faults (Fig. 6.3.8, 6.3.9). The Rødby Formation is overlain by the regional Upper Cretaceous Chalk Group, and around this transition and in basal parts of the Chalk Group (at Base Chalk), only few faults are observed from the ML method (Fig. 6.3.9). Slightly shallower, in the lower to middle parts of the Chalk Group (e.g., at 580 ms TWT), more extensional faults occur (Fig. 6.3.8, 6.3.9g) as sets of small half-grabens in and below the high-reflective succession (c. 550−600 ms) trending in three directions, mostly NW−SE and WNW−ESE, and less common NE−SW, due to renewed tectonism. Slight inversion may be recognized as gentle elevation over the top of the Stenlille structure (Fig. 6.3.8).

In the shallower successions above c. 600 ms TWT, faults are more difficult to track in the 3D seismic data mainly due to noise. Thus, data improvements and new data focused toward the shallow stratigraphic section is recommended for further evaluations. The new seismic data of the GEUS2022-STENLILLE and GEUS2022-HAVNSOE demonstrate, that some subtle faults can be detected in the shallow successions, not least due to the landstreamer data acquired.

Faults interpreted manually, are in 3D seismic data of the Stenlille area compared to Machine Learning (ML) derived fault probability, both vertically and laterally (Fig. 6.3.8, 6.3.9). In addition, deep faults to basement were interpreted at sections from the Stenlille area to the Slagelse-1 to investigate the regional structural evolution. See also description of these studies in Gregersen et al. (2022) and Lorentzen et al. (2022).

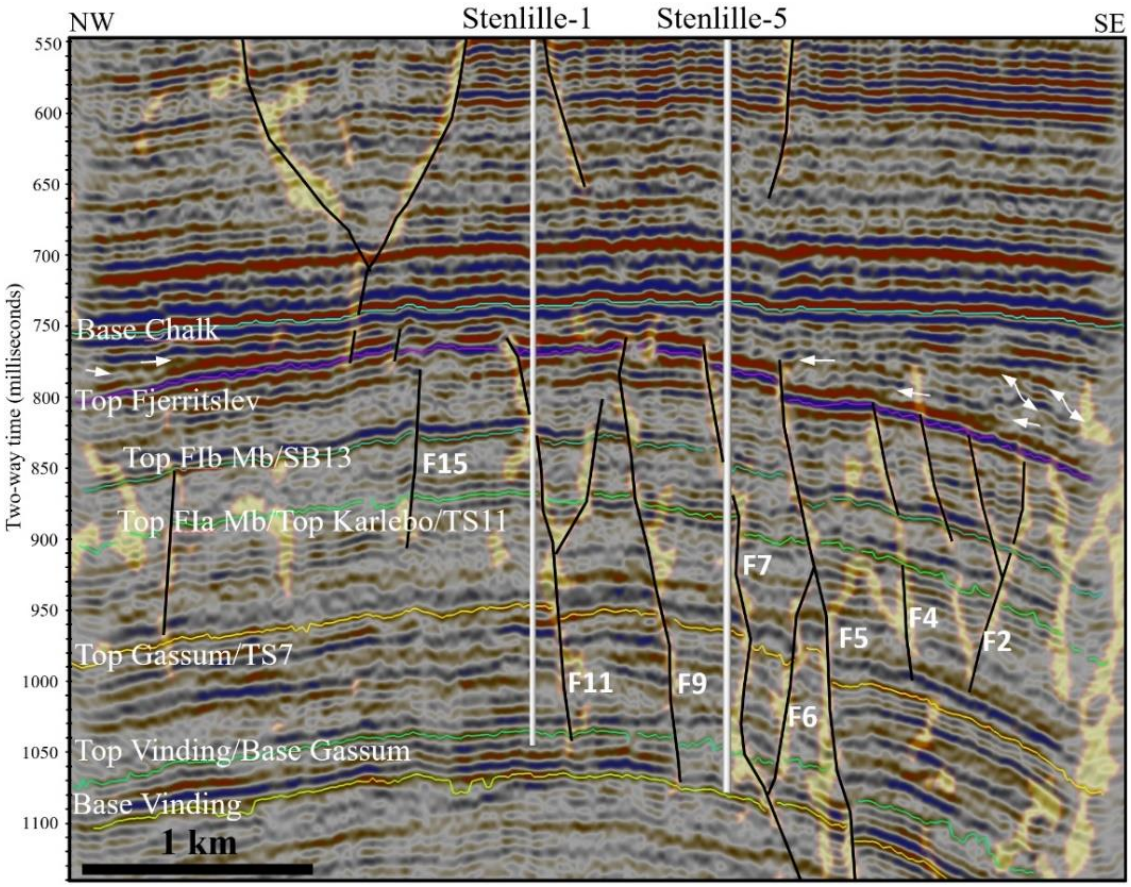

Figure 6.3.8. *X-line 578 (3D) with ST-1, -5 wells (projected) and details of the Stenlille structure. Interpreted horizons are coloured and manually interpreted faults (numbers – see Fig. 6.3.9) are vertical black lines. Vertical yellow zones mark fault probability (0.8−1.0) from a Machine Learning study by Lorentzen et al. (2022), which helped to predict fault patterns both vertically and laterally (Fig. 6.3.9). White arrows indicate onlap and toplap probably of the Vedsted Formation interval, that overlies the inconformity at the (Near) Top Fjerritslev horizon, where most deeper faults terminate. Cretaceous faults seem to have minor connections into the Fjerritslev Formation below Top Fjerritslev. From Gregersen et al. (2022).*

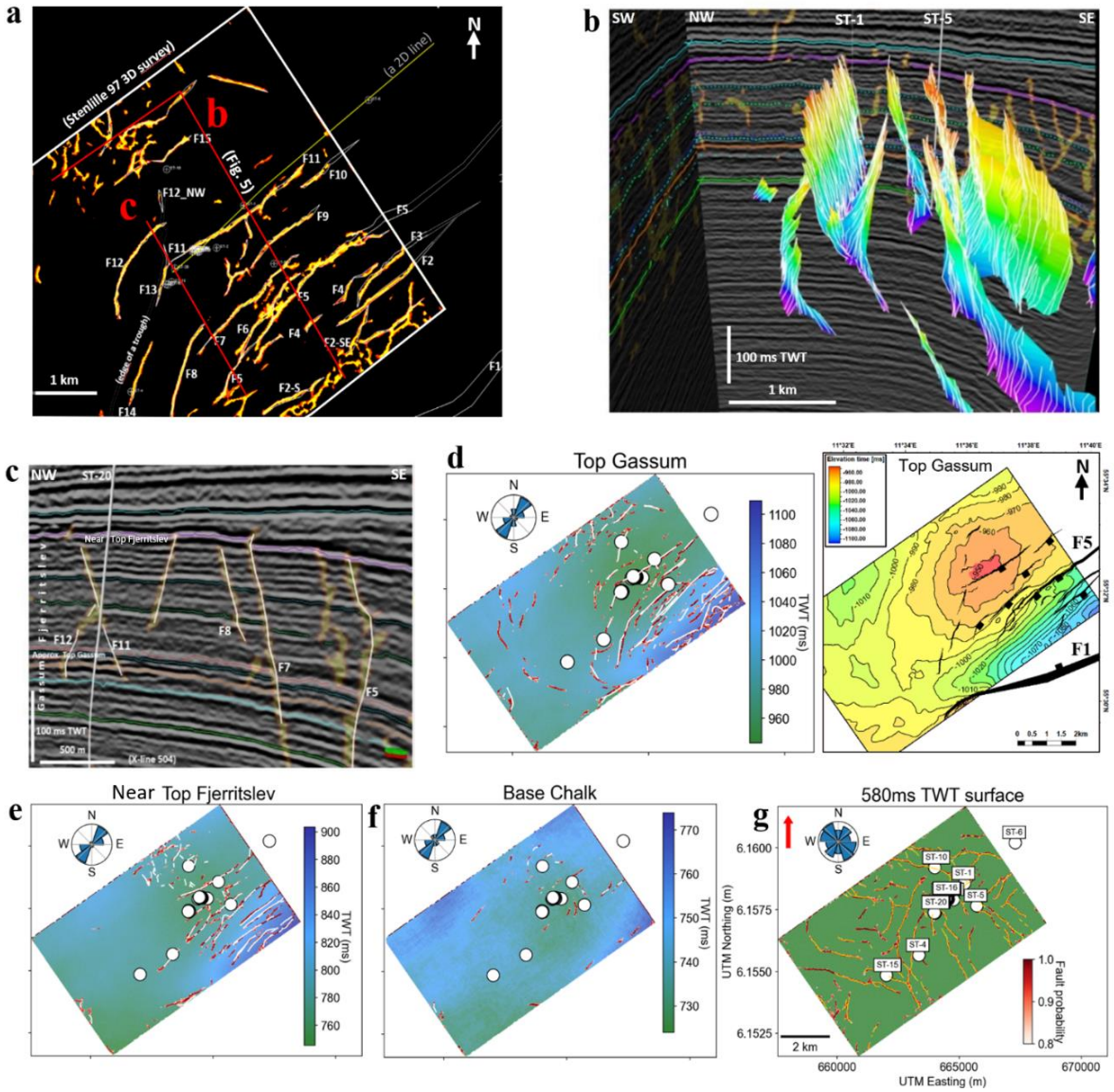

Figure 6.3.9. *More than fifteen manually interpreted fault polygons (thin white numbered lines) and numerous yellow Machine Learning (ML) faults of Gassum Formation-Fjerritslev Formation (5 ms below to 15 ms TWT above Top Gassum); b. Manually interpreted fault sticks (3D) coloured by TWT depth in Gassum-Fjerritslev Formations and yellow ML faults; c. Manually interpreted fault sticks (2D) and yellow ML traces on Xline 504 (location in 6a); d. Left: Map of Top Gassum with both fault stick traces (white) and ML fault traces (red). Right: Same horizon with manual interpreted fault polygons (black). Northing/Easting, km-scale and wells (white circles) are shown in g; e. Map of (Near) Top Fjerritslev with both fault stick-traces (white) and ML fault traces (red); f. Map of Base Chalk with both fault stick-traces (white) and ML fault traces (red); g. Map of 580 ms TWT (time slice) cutting through the lower part of the Chalk Group with ML fault traces (red) and Petrel generated fault traces (yellow). ML faults are generated and described by Lorentzen et al. (2022). Note the dominant NE-SW fault directions of Top Gassum-Fjerritslev, and the changed fault directions in the lower-mid (at 580 ms) Chalk Group, mostly trending NW−SE and WNW−ESE, and some NE−SW. From Gregersen et al. (2022).*

Tectonostratigraphic evolution at the Stenlille structure

The southern part of the study area comprises the Stenlille structure, which has a tectonostratigraphic evolution very similar to the Havnsø structure and is with the dense database and stratigraphic control from wells a key for understanding the Havnsø structure. Therefore, this description (mainly repeated from GEUS Report 2022/26, Gregersen et al. (2023) of the Stenlille structure is included here. The Stenlille area with a comprehensive database ties to the Slagelse area, which is shown in Figures 6.3.10 and 6.3.11. The key-tie composite profile in Figure 6.3.10 is chosen as it crosses the SE part of the Danish Basin towards the Ringkøbing–Fyn High and includes important deep and shallow structures. The interpreted tectonostratigraphic development is constrained by seismic stratigraphic horizons correlated to key wells, where lithostratigraphy and ages are defined. The tectonostratigraphic evolution of the area is summarized, based on the key profiles and well-ties, interpretation and mapping of horizons, units and faults, using among other tools horizon flattening and back-stripping (Fig. 6.3.11, 6.3.12). The tectonostratigraphic evolution of the area is described below, mainly from sections with flattened horizons, from the Palaeozoic to the Base of the Chalk Group (Base Chalk), including the formation of the Stenlille structure during the Jurassic time. The stratigraphy described here includes completion reports and GEUS work of the Slagelse-1 and Stenlille-19 wells.

Precambrian to Top Early Palaeozoic

The Precambrian basement (grey) and Lower Palaeozoic succession (turquoise colour) is affected by Early Palaeozoic extensional faults, which offsets the Top Basement horizon (black) and a thin uniform basal unit (below the lower green horizon) (Fig. 6.3.11a), which is onlapped by the thick upper turquoise unit, wedging out onto the two Slagelse structures. This indicates basin filling and deepening of basins connected between the Slagelse and Stenlille areas, which were partly divided by shallow structures and half-grabens (Fig. 6.3.11a). The Precambrian basement (grey) is likely crystalline as drilled south and north of the basin (Nielsen and Japsen 1991, Nielsen 2003, Vejbæk 1997), and is overlain by Cambrian quartzite, silt- and sandstones and Cambrian−Silurian mudstones, which are drilled in the Slagelse-1 well (Fig. 6.3.10) (Schovsbo 2011). The basins (Fig. 6.3.11a) probably subsided associated with tectonism due to the Caledonian Orogeny, with the central-north European deformation front moving towards north creating the deep foreland basin, with a thick Silurian shale succession (turquoise unit above the green horizon), drilled in the Slagelse-1 well (Schovsbo 2011 and references therein).

Late Palaeozoic

Extensional faults and large wedge-shaped basins developed after deposition of the Lower Palaeozoic unit, and an unconformity (turquoise colour) with truncation below and onlap above is interpreted at the base of the Upper Palaeozoic (red) succession both in the Slagelse area and towards the Stenlille area (Fig. 6.3.10, 6.3.11b). This indicates major rifting tectonism with fault blocks, erosional truncation, and syn-rift deposition. Thick Silurian shales are separated from Zechstein salt by a Rotliegende succession, and thus Devonian−Carboniferous rocks are absent here at the Top Lower Palaeozoic unconformity (blue horizon: Fig. 6.3.11b). The Rotliegende Group, including syn-rift successions of sandstones, mudstones, conglomerates and reworked volcanic rocks, are known from other wells drilled into tilted

hanging wall blocks (e.g., the Hans-1 well), in similar syn-rift wedges as in Fig. 6.3.10 north of the Slagelse-1 well, supporting significant Carboniferous−Early Permian regional tectonism and rifting (Vejbæk 1997, Michelsen & Nielsen 1991, Mogensen & Korstgård 2003).

The top of the Rotliegende succession is truncated by the regional Top pre-Zechstein (mid-Permian) unconformity (black horizon; Fig. 6.3.11b,c). The Top pre-Zechstein unconformity associated with basin-wide erosional denudation is the deepest and oldest basin-wide mappable horizon. Thus, on the elevated areas, such as rift-shoulders etc., it constitutes the base of the Danish Basin, whereas in the tilted fault blocks with syn-rift wedges the base of the basin is localised below the syn-rift successions. The Top pre-Zechstein surface separates the pre-rift and syn-rift successions from the post-rift basin succession and formed the seafloor of the restricted shallow northern Zechstein sea where evaporites later evolved (Vejbæk 1997). Lithosphere thinning and crustal extension during Late Carboniferous–Early Permian times possibly caused the widespread Rotliegende volcanism and block faulting as described by Frederiksen et al. (2001). This was followed by lithospheric thermal contraction creating subsidence and accommodation space for Zechstein evaporites and the overlying thick Triassic successions.

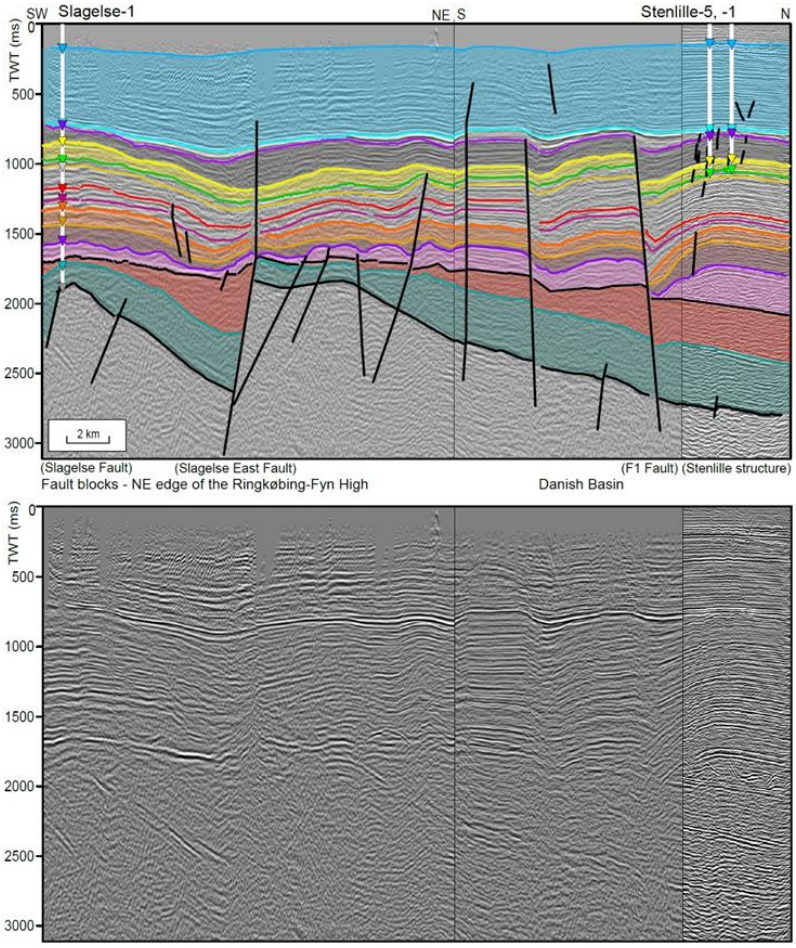

Figure 6.3.10. *Composite seismic sections in two-way time from the Slagelse-1 to the Stenlille-1,-5 wells (projected), with and without interpretation. Triangle positions mark lithostratigraphic well-ties. Major basin and structures are named. The upper blue unit indicates the Chalk Group and Danian. The Gassum (yellow unit) and Fjerritslev (dark-grey unit) Formations form the upper part of the Stenlille structure, which is formed by the deep Zechstein salt pillow (pink). Seismic sections are from SW to N: SSL72_001, SSL73_036 and DN94_D07. From Gregersen et al. (2022).*

The Zechstein Group (pink unit) is interpreted between the Top pre-Zechstein unconformity and the Top Zechstein (purple horizon), where the succession forms a number of minor mounds and in the Stenlille area a larger pillow. The unit ties into an evaporitic succession with halite, anhydrite, and dolomite in the Slagelse-1 well. The evaporites formed in an arid climate during the Late Permian time in large parts of the Danish Basin, where later mobilization led to numerous diapirs and pillows. Near the Permian−Triassic transition uplift took place which was followed by regional subsidence (Vejbæk 1997).

Triassic

The lowermost Triassic unit (brown) above the Zechstein shows variation in thickness (Fig. 6.3.11c), possibly due to incipient subsidence or secondary structures and later salt mobilization. It thickens considerably into the Stenlille area, and this seismic stratigraphic unit is interpreted as the Lower Triassic Bunter Shale Formation by correlation to the Slagelse-1 well (Fig. 6.3.10). The unit is separated from the overlying unit (orange) by an unconformity (light orange horizon) with downlap and is fairly uniform in thickness (Fig. 6.3.11c). This unit correlates to the Bunter Sandstone Formation in both the Slagelse-1 and the Stenlille-19 wells (Fig. 6.1.1, 6.3.10). However, the completion reports show fine-grained sandstones and dominance of claystones. Further east (in Copenhagen; Fig. 3.1) sandstones of this formation are reservoir for geothermal energy (the Margretheholm wells; Fig. 3.4).

Middle−Upper Triassic units (brown with red-orange-yellow horizons) show more or less uniform thicknesses across the area, though with some local fault activity with local thickening at faults, located at flanks of the underlying Zechstein unit (Fig. 6.1.1, 6.3.11d). This may indicate reactivation of Permian faults and/or incipient salt mobilization. The Middle to Upper Triassic formations (Ørslev, Falster, Oddesund and Vinding) are mostly clay-rich formations, that occurs widespread across much of the Danish Basin (Fig. 6.1.1). Contents of dolomites, limestones, anhydrites, etc. may cause some of the intraformational strong seismic reflections, e.g., anhydrites near c. 1200 ms (Fig. 6.1.1). The Middle to Upper Triassic successions thicken especially towards the Stenlille area (Fig. 6.3.11d,e). Claystones, calcareous in lower parts – more siliciclastic in upper parts, dominated the successions until the latest Triassic Rhaetian time (Slagelse-1 and Stenlille-19 completion reports).

Latest Triassic to Early Jurassic

The Gassum Formation (Rhaetian age) in the Stenlille wells can be tied to a seismic stratigraphic unit, bounded by top and base peak reflections and with internal reflectivity, occasional mounded or with troughs interpreted as channels (Section 7.1; Vosgerau et al. 2020; Smit et al. 2022). The total thickness of the formation in the Stenlille wells is approximately 140−150 meter, with the thickest and most sandstone-rich units preserved in lower part of the formation (below TS5) (Section 7.1; Vosgerau et al. 2020). The Gassum Formation can also be correlated in seismic sections from the Stenlille wells to the Slagelse-1 well, and the formation seems to have a more or less uniform thickness (average c. 150 m) in the mapped area of the structure.

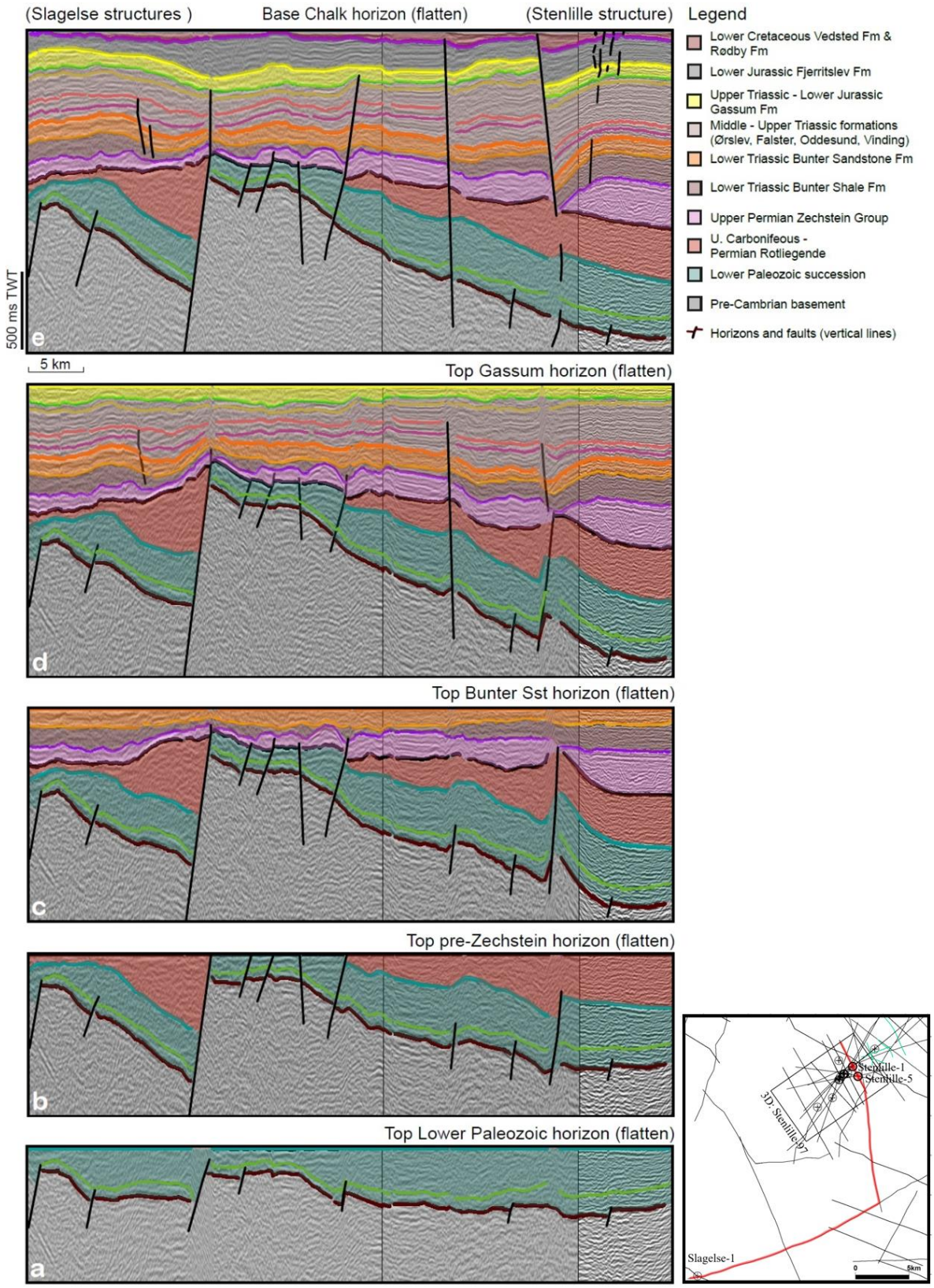

Figure 6.3.11. *Horizon flattening at key-horizons (a-e) of Fig. 6.3.10, illustrating the Palaeozoic to Cretaceous structural evolution between the Slagelse and the Stenlille structures, described in the text. See the insert map for location, and Fig. 6.3.10 for well-ties. From Gregersen et al. (2022).*

Channel positions mostly west of and partly across the present top of the Stenlille structure, lowermost in the successions, may indicate a paleo-topographical high, e.g., due to initial syn-depositional doming or sedimentary system build-up (Section 7.1; Vosgerau et al. 2020). However, the most significant doming of the structure is later occurring at the Near Top Fjerritslev horizon (Fig. 6.3.10e). The sedimentary systems of the Gassum Formation were dominated by fluvio-deltaic, estuarine, and shoreface environments also interpreted by new detailed seismic geomorphology, core facies, and sequence stratigraphic studies of wells and 3D seismic data (Smit et al. 2022; Section 7.1). These studies also revealed sand-rich, coastal-near systems (meandering fluvial channels, point bars, and sand plates) and indications of transport directions. In addition, seismic reservoir characterization is studied in the previous section (see also Bredesen et al. 2022). The improved reservoir characterization can be used in static reservoir modelling and simulation of CO_2 injection.

Zircon provenance analysis shows that the Stenlille area received input from long distance transported sediments sourced from both the Fennoscandian Shield (Caledonian Orogen and Sveconorwegian Orogen), and from south (Variscian Orogen). The thick mature sandstones indicate tectonism and denudation in the hinterlands as well as sufficient accommodation space at Stenlille for deposition of sand (Olivarius et al. 2022; See also Section 7.1).

The Stenlille structure has a number of faults in its top, in particular in the Gassum Fm and through the Fjerritslev succession, and less apparently in the overlying successions (Fig. 6.3.9). In large parts of the structure, faults seem to displace more or less equal thicknesses, though with minor variations, of both the Gassum and Fjerritslev Formations to the Near Top Fjerritslev horizon (Fig. 6.3.8, 6.3.9). This may indicate that these faults were active later than deposition of most of the Fjerritslev Fm, except for a thickening of the Fjerritslev Fm towards SE at the large F1 fault, close to the border of the mapped area (Fig. 6.3.9).

The Stenlille F1 fault SE in the study area, south of the Stenlille structure (Fig. 6.3.10), is a large, deep normal fault, seated SE of the salt dome, which evolved from mid-Jurassic time. The F1 fault shows throws at the Top Gassum of c. 160−180 ms, with similar order of throws of deeper horizons (c. 170−200 ms) down to Top Zechstein. The Fjerritslev Formation between Top Gassum and Near Top Fjerritslev horizons thickens in the hanging wall syncline towards fault F1, indicating growth fault evolution of a primary syncline of salt doming, and the throw at the Near Top Fjerritslev is only 70−80 ms, possibly a result of erosion (Fig. 6.3.10). Apparently, it is primary the uppermost part of the Fjerritslev Formation succession (probably the F-IV member), that thickens towards the fault. The structure top is offset by faults in particular south of the Stenlille-1 well, at the southern flank of the doming structure.

Most faults in Gassum and Fjerritslev Formations in the Stenlille structure have mainly minor, normal and in some cases reverse throws, mostly less than c. 30 ms or c. 30−50 m (Fig. 6.3.8, 6.3.9). Most faults are located along the anticlinal NE−SW trending axis of the Stenlille structure, in its top and its SE flank, and a few faults trend N-S (Fig. 6.3.9). The deepest-seated faults occur along the SE structure flank, and some of these sole out deep into the salt pillow (Fig. 6.1.1), indicating that they are related to the structural deformation due to the doming of the structure. The most prominent fault in the SE structure top, SE of ST-5, is the F5 fault (Fig. 6.3.8). Also, the shallower Gassum−Fjerritslev faults terminating at the Near Top Fjerritslev horizon are probably related to the doming of the salt pillow after late Early Jurassic time.

Faults interpreted manually, are compared to Machine Learning (ML) derived fault probability, both vertically and laterally (Fig. 6.3.8, 6.3.9; Gregersen et al. 2022, Lorentzen et al. 2022). The fault-probability shown in yellow are scaled to 80−100% probability (binary colour coded: '1'= 80-100% fault probability, whereas '0' (no colour) < 80%) of reflection discontinuity, which represents mostly faults. The ML fault predictions are created by training a convolutional neural network model on synthetic seismic data and was subsequently applied to the Stenlille 3D dataset (Lorentzen et al. 2022). This comparison improves the understanding significantly of the fault patches and will provide more accurate and detailed fault networks. Manually interpreted faults are mainly located at clear breaks/displacements in reflections and successions, whereas the ML fault predictions are also sensitive to less visible breaks and subtle features (Fig. 6.3.8, 6.3.9). Such features may also include boundaries of channels, mounds, seismic facies change due to changed lithology, fluids, etc., but also seismic noise. The significant details of ML fault-probability traces can provide important data for evaluations of fault risks, seal-integrity, etc., not least of prospects for storage CO_2 or other resources. The manually interpreted fault polygons and the ML fault trends show consistent NE−SW fault directions both at the Top Gassum and the Near Top Fjerritslev surface maps (Fig. 6.3.9d,e). Some of the near Top Gassum faults may compart the Gassum Fm reservoir and seem to restrict natural gas in some cases (See Seismic reservoir characterization section above; Bredesen et al. 2022). At the Base Chalk surface (Fig. 6.3.9e) there are less faults, but some still with NE−SW trends. This indicates relatively few clear fault connections between the Lower Cretaceous successions and the Upper Cretaceous Chalk Group. However, as breach of seals may occur at faults, such risks should be investigated and assessed thoroughly before injecting CO_2. The long-term, safe storage of natural gas at Stenlille indicates competent sealing successions.

The Near Top Fjerritslev horizon is interpreted at a marked trough with increasing acoustic impedance, in a significant seismic stratigraphic unconformity, with onlap from overlying successions and which defines the top of the Stenlille structure (Fig. 6.1.1). The preserved uppermost Fjerritslev Fm (Toarcian age) is overlain by the Lower Cretaceous Vedsted Fm near at or slightly above this horizon (Fig. 6.1.1), and the actual boundary in the sedimentary successions is thus a major hiatus – see also discussion in Section 7.2. The amount of erosion and thus the duration of the hiatus may be slightly different depending on the position on the structure, and the flanks of the structure probably experienced less erosion and have more preserved successions, possibly also including upper parts of the Fjerritslev F-IV Member. The major unconformity marks the formation of the Stenlille structure mainly due to formation of the underlying salt pillow. The unconformity may in part be equivalent to the 'Base Middle Jurassic unconformity' or 'Mid-Cimmerian Unconformity' (Nielsen 2003) associated with uplift and erosion (and a major hiatus) over structures and margins of the Danish Basin, including the Ringkøbing−Fyn High (Fig. 6.1.1).

Cretaceous

The Lower Cretaceous Vedsted and Rødby Formations are part of the seismic stratigraphic wedge, which onlapped the Near Top Fjerritslev horizon after the formation of the elevated Stenlille structural dome (Fig. 6.3.8). The dome formed primary due to salt pillow growth and probably caused erosional removal or non-deposition during Middle Jurassic to Early Cretaceous times. From the top of the Stenlille structure, closely above the Top Fjerritslev (at the Fjerritslev Fm/Vedsted Fm boundary), biostratigraphy shows, that the youngest Jurassic deposits are of Toarcian age (late Early Jurassic) and the oldest Early Cretaceous deposits are Hauterivian in age (see Section 7.2; Fig. 6.1.1). Parts of the Vedsted succession above the

Near Top Fjerritslev includes prograding reflections towards SE, away from the structural crest, and minor troughs (channels or fault related) occur towards the structure (Section 7.1). The Rødby Formation is overlain by the regional Upper Cretaceous Chalk Group. In the lower to middle parts of the Chalk Group extensional faults occur (Fig. 6.3.8, 6.3.9f) as sets of small half-grabens in and below the high-reflective succession (c. 550−600 ms) trending in three directions, mostly NW−SE and WNW−ESE, and less NE−SW, due to renewed tectonism. Slight inversion may be recognized as gentle elevation over the top of the Stenlille structure (Fig. 6.3.8). Most of the Cenozoic is missing over the Stenlille structure. Only a Paleocene succession shallow buried is described in the Final Well Report of well Stenlille-19. This succession includes the Lellinge Fm (Lellinge Grønsand of Selandian age) and the Ekofisk Fm (Danian age). The Paleocene succession is likely overlain by mostly Quaternary successions. Japsen & Bidstrup (1999) reported that c. 600 m Cenozoic successions are missing in some of the Stenlille wells.

Summary of the structural evolution – The Stenlille structure

The structural reconstruction of the development of the Palaeozoic and Mesozoic to the Base Chalk facilitated by horizon flattening at several key horizons shows that the Palaeozoic structures formed during several tectonic events with the Top pre-Zechstein as a base of the present Stenlille structure. The Stenlille structure mainly evolved by the growth of a salt pillow forming the overlying structural doming anticlinal. The formation of the structure was likely initiated during deposition of the Gassum Formation. However, the structure developed more pronounced under the subsequent burial of the thicker Fjerritslev Formation. The burial probably conditioned salt migration into the domal salt-pillow, which elevated the overburden structure during the Middle Jurassic to Early Cretaceous times. Normal faults and faults with reverse and compressional indications are observed and may be caused by doming and regional compressional related tectonics. More than fifteen faults were manually interpreted and show NE−SW trends in the Gassum-Fjerritslev Formations. Machine Learning increased the understanding of the 3D fault network. Shallower faults in the lower Chalk Group show three directions: NW−SE, WNW−ESE, and NE−SW. The Near Top Fjerritslev unconformity is onlapped by the Vedsted Formation and the Rødby Formation, which is overlain by the Chalk Group, and the structure was later affected by inversion and uplift episodes.

Summary of the structural evolution – The Havnsø structure

The Havnsø structure formed in a very similar way to the Stenlille structure and is also underlain by a salt pillow that mainly developed during the Jurassic to Early Cretaceous time, when buried by thick sedimentary successions (Fig. 6.3.12). The Havnsø structure is an oval 4-way dip closed structure, elongated with a NW−SE orientation. Nearly all successions overlying the Havnsø salt pillow core of the structure, form 4-way closures above the salt pillow. It is a large structure with a relief from top to base closure of the Top Gassum Fm of approximately 160 m, and with an area of the basal closure at the Top Gassum of c. 70 km^2.

Minor faults were developed during the growth of the salt pillow, partly triggered due to the Mid-Cimmerian Tectonic Phase. Faults are small in throw (mostly less than 15 ms), less than few kms long, and trend NW−SE and SW−NE, parallel to the outline and flank of the structure. Thinning of the Fjerritslev Fm over the top of the structure (Fig. 6.3.12) may indicate a larger amount of erosion of the Lower Jurassic succession over the structure and development of the structure during mid-early Jurassic–Early Cretaceous time. Onlap of the Lower Cretaceous Vedsted Fm on the Top Fjerritslev marks the Mid-Cimmerian Unconformity with a major hiatus, as in the Stenlille structure.

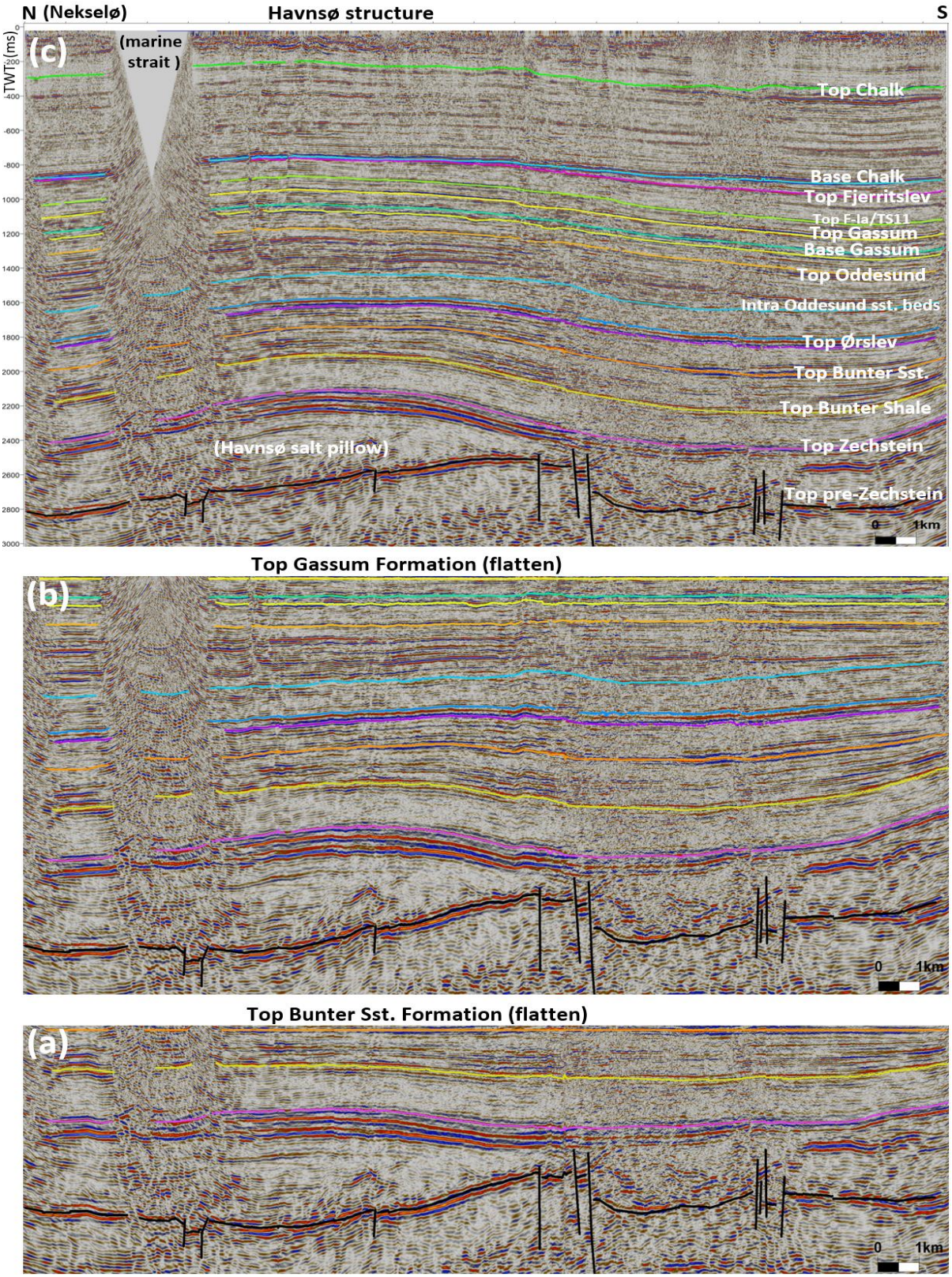

Fig. 6.3.12. *Horizon flattening at key horizons of line P2 (reprocessed) across the Havnsø structure. (a) Lower Triassic with Bunter Sst. basin formed, slightly thinning over Havnsø. (b) Middle-Upper Triassic thickening (Oddesund Fm) across Havnsø indicates subsidence, whereas Gassum Fm has a more uniform thickness, though it thins slightly at the top (Fig. 6.3.4C) and may indicate minor structure elevation. (c) Thinning of the Fjerritslev Fm across the Havnsø structure is topped by an unconformity, onlapped by the Lower Cretaceous Vedsted marks a hiatus and the main growth and formation of the Havnsø structure. Location of the P2 line is shown in Fig. 6.1.5.*

7. Geology and parameters of the reservoirs and seals

No wells penetrate the Havnsø structure and consequently well data information concerning reservoirs and seals must be obtained from the offset wells. The nearest wells are those that penetrate the Stenlille structure situated c. 25–30 km SE of the Havnsø structure (Figs. 1.1 and 3.1). Subsurface data from the Stenlille structure are comprehensive, including 2D seismic lines, a 3D seismic survey covering most of the structure and well data (e.g., petrophysical log-data and cores) from 20 wells (Figs. 4.1.1, 4.1.2). The comprehensive dataset has been acquired because the structure has been used for temporal storage of natural gas since the 1990's, with the gas being injected and stored in the upper sandstone intervals of the Gassum Formation. The seismic data, collected in the present study, links the Havnsø and Stenlille structures and the interpretation of the data emphasize the relevance of using the Stenlille data as an analogue for the Havnsø structure. Thus, seismic sections and thickness maps reveal that both the primary reservoir for CO_2 storage (Gassum Formation) and its primary seal (Fjerritslev Formation) extend from Stenlille to Havnsø with approximately continuous thicknesses (see section 6.1). Also, top of the secondary reservoirs (Top Bunter Sst. and Top Intra Oddesund sst. beds) and seals (Base Chalk, Top Ørslev, Top Oddesund) can be interpreted from Stenlille to Havnsø on seismic sections (see section 6.1). Borehole data from Stenlille are in the following therefore used as an analogue for the reservoirs and seals in the Havnsø structure. Consequently, the description of reservoirs and seals corresponds largely to the description of these in the CCS2022-2024 WP1 report dealing with the Stenlille structure (Gregersen et al. 2023). This is especially the case for the Gassum Formation as the description of its composition and the depositional environments in Stenlille forms the main input for evaluating the formation in the Havnsø structure. In doing so, the Stenlille data are adjusted to the Havnsø structure where lateral variations in the seismic data or simple proximal-distal considerations in the depositional environments, provides a basis for this. Also, data from selected wells that surrounds the Havnsø structure in the Danish Basin are included in order to elucidate regional lateral variations in the composition of the reservoirs and seals as an input for estimating their appearance in Havnsø structure. The Gassum-Fjerritslev interval in the wells has been subdivided into depositional sequences based on integration of sedimentological interpretations of cores and petrophysical log patterns and palynological data. The biostratigraphic zonations used include the ostracod zonation of Michelsen (1975), the dinocyst zonation of Poulsen & Riding (2003) and a combination of the spore-pollen zonations of Dybkjær (1991), Koppelhus & Nielsen (1994) and Lindström et al. (2023). The biostratigraphic database varies considerably from borehole to borehole. Thus, from some boreholes a solid biostratigraphic framework exists while hardly any data exists from others. In Appendix C, the available biostratigraphy is summarized for each well based on data from reports and publications combined with new data from some of the wells. In addition, links are given to stratigraphic summary charts for each well. The charts combine the chronostratigraphy, lithostratigraphy, biostratigraphy and sequence stratigraphy and further include the bio-events and biozonations.

7.1 Reservoirs – Summary of geology and parameters

The primarily reservoir for potential CO_2 storage in the Havnsø structure is the sandstone dominated Gassum Formation whereas the deeper lying sandstones of the Oddesund and Bunter Sandstone Formations may form secondary reservoirs (Fig. 7.1.1). In the following description of reservoirs, emphasis is on the Gassum Formation whereas the secondary reservoirs are only described briefly. The description of the Gassum Formation is based mainly on Vosgerau et al. (2020, in prep.) and Hovikoski & Pedersen (2020) which concerns the formation in the Stenlille structure. In Stenlille, the formation is subdivided into 6 Reservoir Zones and internal seals by DONG (DONG 2001), which is also used in the present reservoir characterization. The Gassum Formation and the identified Reservoir Zones are shown for the Stenlille-19 well in Figure 7.1.2. Interpreted well logs for selected Stenlille wells and wells that surround the Havnsø structure, however at large distances, are shown in the Appendix B. The Stenlille-19 well is to be considered as a key well since it contains the most comprehensive petrophysical data set of the Stenlille wells and furthermore it extends well below the Gassum Formation, having its TD within the Bunter Sandstone Formation (Fig. 7.1.1).

The primary reservoir: The Gassum Formation

The Gassum Formation is the best-known sandstone reservoir in the Danish onshore subsurface. It is used for geothermal energy in Thisted and Sønderborg and has also been used for seasonal storage of natural gas for more than 30 years in the Stenlille structure. The good reservoir properties of the formation have thus been proven at several places in Denmark. The formation is widespread in the Danish Basin and locally in the Danish part of the North German Basin (Fig. 7.1.3). It has a general thickness of 30–160 meters (Nielsen & Japsen 1991, Nielsen 2003). Locally it is missing due to uplift and erosion related to regional uplift in the Middle Jurassic, at the 'Base Middle Jurassic unconformity' or the 'Mid-Cimmerian Unconformity' *sensu* Nielsen (2003), and above structures formed by vertical salt movements. The Gassum Formation is of Late Triassic–Early Jurassic age with the upper boundary showing a significant younging towards the northern, north-eastern, and eastern basin margins (Fig. 7.1.3) (Bertelsen 1978, 1980; Michelsen et al. 2003; Nielsen 2003). The upper formation boundary is thus of latest Rhaetian age in the central parts of the basin, including the area of the Stenlille structure, whereas it is of Early Sinemurian age along the basin rims (Nielsen 2003 and references therein). This diachronic development of the boundary reflects an overall backstepping of the general coastline toward the basin margins during latest Triassic – Early Jurassic time owing to an overall rise in relative sea-level, interpreted as caused by a combination of regional basin subsidence and a eustatic sea-level rise (Nielsen 2003).

In general, the Gassum Formation is dominated by fine to medium-grained, in places coarse-grained, light grey sandstones, alternating with darker colored clay- and siltstones and locally thin coal layers (Bertelsen 1978, Michelsen et al. 2003, Nielsen 2003). The sediments were deposited during repeated sea-level fluctuations in Late Triassic – Early Jurassic times when the Danish Basin was a shallow marine area. Large quantities of sand were transported into the basin by rivers which were sourced by erosion of the Fennoscandian Shield and, to a lesser degree, locally from the Ringkøbing–Fyn High in periods when this was exposed (Nielsen 2003 and references herein).

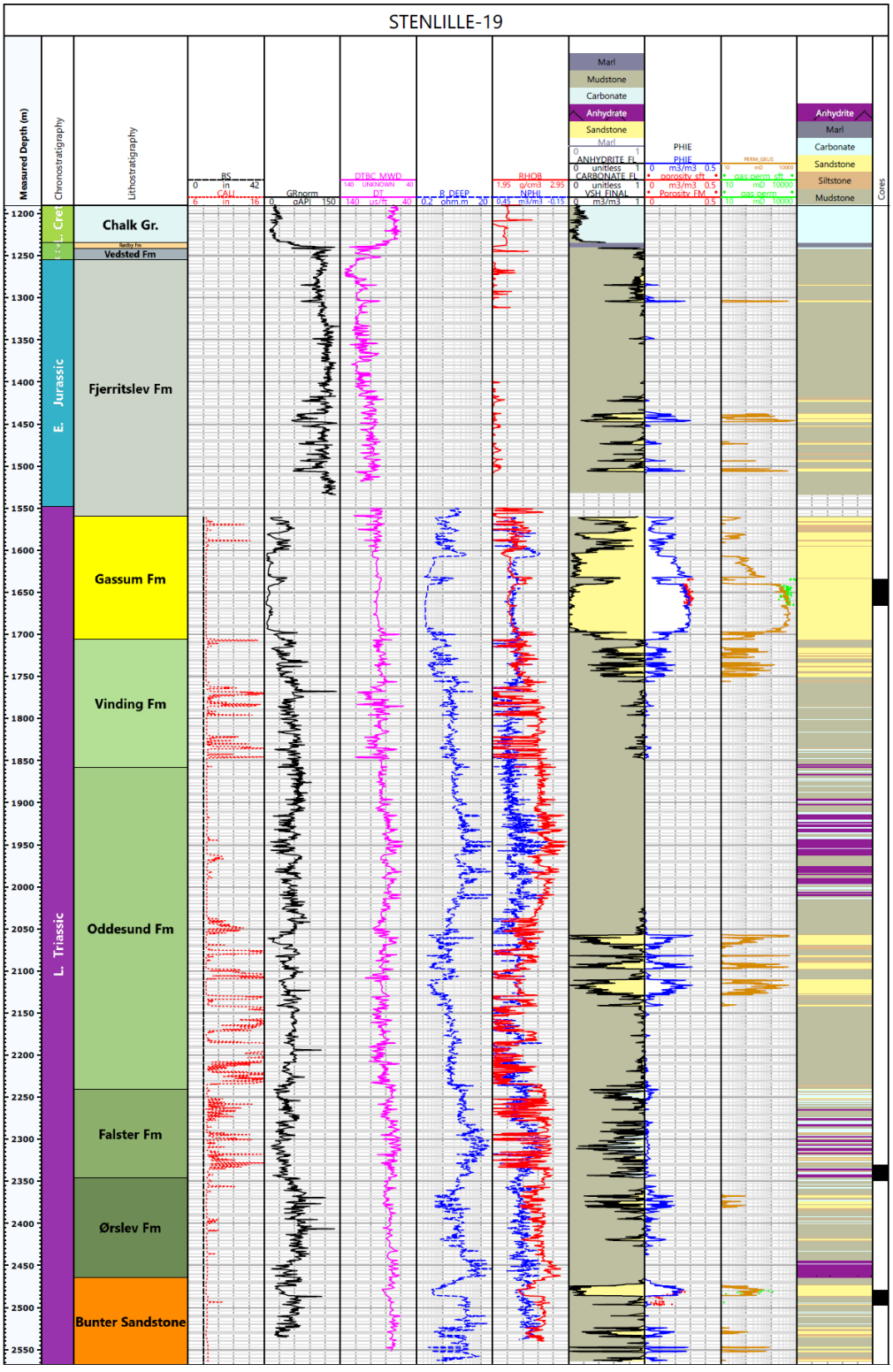

Figure 7.1.1. *Lithostratigraphic subdivision of the Stenlille-19 well with interpreted lithology and formations based on petrophysical log interpretation and information from core data, cutting samples etc. This well is the only Stenlille well that is drilled deeper than the Vinding Formation. Sandstones of the Gassum Fm is the primary reservoir, and sandstones of the Oddesund and Bunter Sandstone Formations are potential secondary reservoirs. The Fjerritslev Fm/Vedsted Fm boundary is at 1254.5 m MD and has been moved up from 1278 m MD based on new biostratigraphy (Gregersen et al. 2023) – see Section 7.2.*

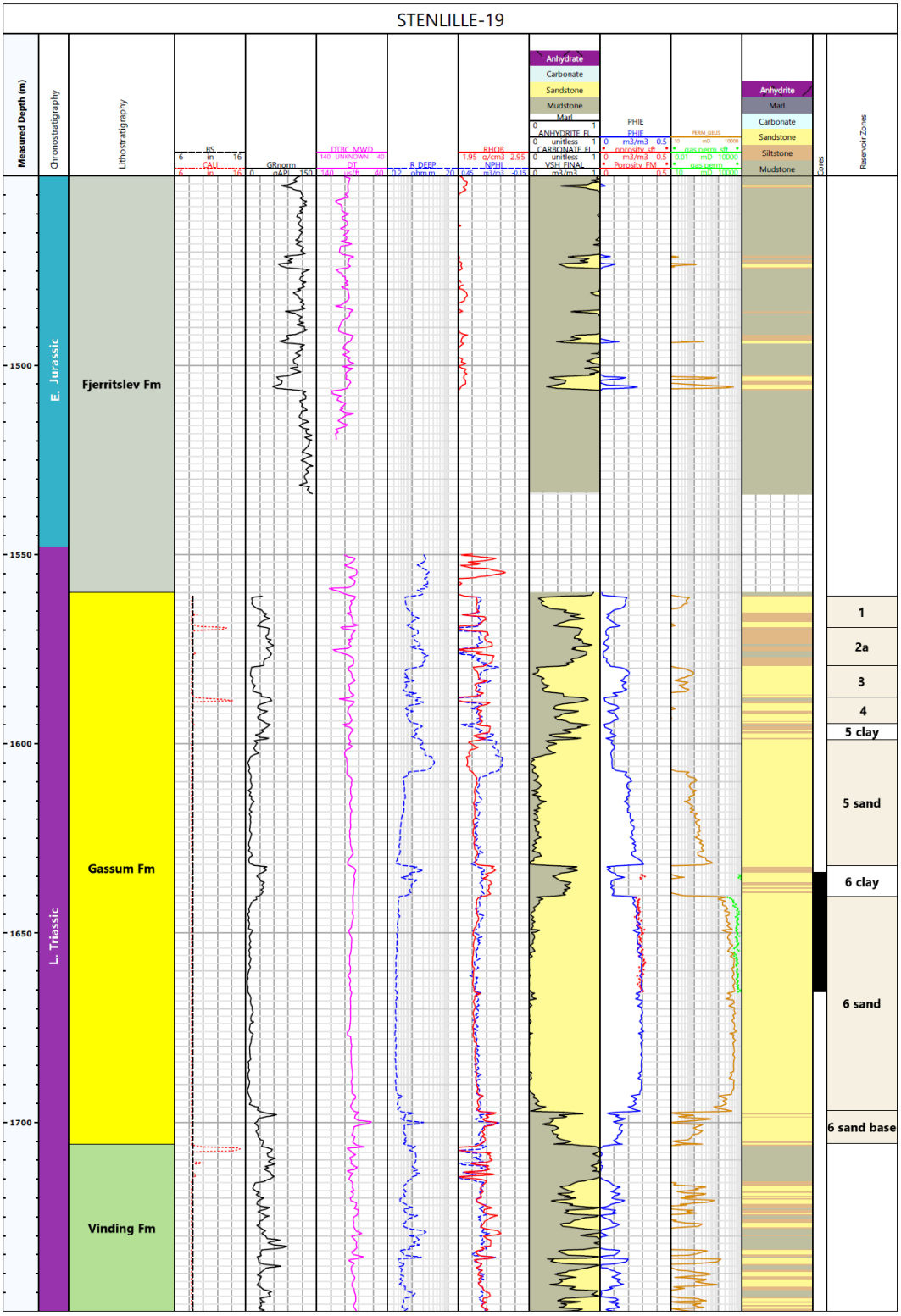

Figure 7.1.2. *The Stenlille-19 well with interpreted lithology and formations based on well-log interpretation. Zoom section of Fig. 7.1.1 to the Gassum Formation. Columns to the right mark reservoir zones (1–6) according to DONG (2001), and cored part of Zone 6 (black column). Note the good accordance between porosities derived from logs (PHIE column) and core measurements (red dots), and between permeabilities derived from logs (perm) and core measurements (green line), except in the Zone 6 clay.*

Recent provenance studies suggest that the basin was sourced also with sand from southerly Variscan source areas, perhaps transported into the basin through grabens intersecting the Ringkøbing–Fyn High such as the Øresund Basin and the "Storebælt trough".

However, a general mixed composition of zircon ages in samples from the eastern part of the basin suggests that rivers draining the Caledonian and Variscan Orogens met in the east and supplied mixed sediment towards west into the basin (Olivarius et al. 2020, 2022) (Fig. 7.1.4).

The high influxes of sediment almost balanced subsidence implying that the intracratonic basin largely remained shallow and almost flat-based, but with its deepest part located near its center (Hamberg & Nielsen 2000). Due to the flat, low-gradient basin floor and overall shallow water conditions, sediment accumulation was very sensitive to Late Triassic and Early Jurassic fluctuations in relative sea level which resulted in repeated long-distance progradation or retrogradation of the coastline. A large part of the sandstones in the formation therefore represents shoreface deposits, but significant amounts are also fluvial or estuarine in origin. This is especially the case for the lower part of the formation where pronounced high-order relative sea level falls led to the progradation of rivers into the central part of the basin and the establishment of estuaries during succeeding rise in relative sea level.

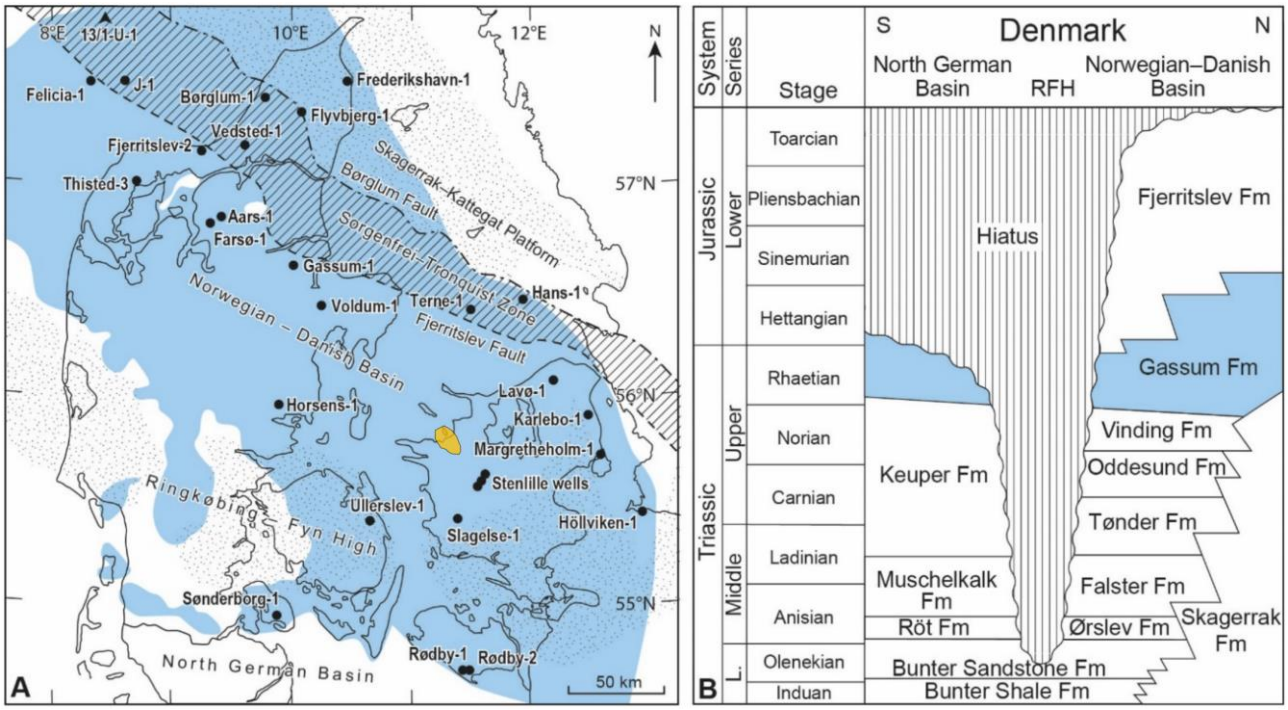

Figure 7.1.3. *A) Estimated distribution of the Gassum Formation in the Danish onshore and nearshore area shown in blue. Also shown is selected wells and main structural elements including the Norwegian–Danish Basin and the North German Basin which are separated by the Ringkøbing–Fyn High (RFH). Approximately location of the Havnsø structure is shown with orange polygon. B) Stratigraphic scheme of the Lower Triassic–Lower Jurassic succession onshore Denmark revealing among others the time-transgressive nature of the of the top of the Gassum Formation. From Olivarius et al. (2022).*

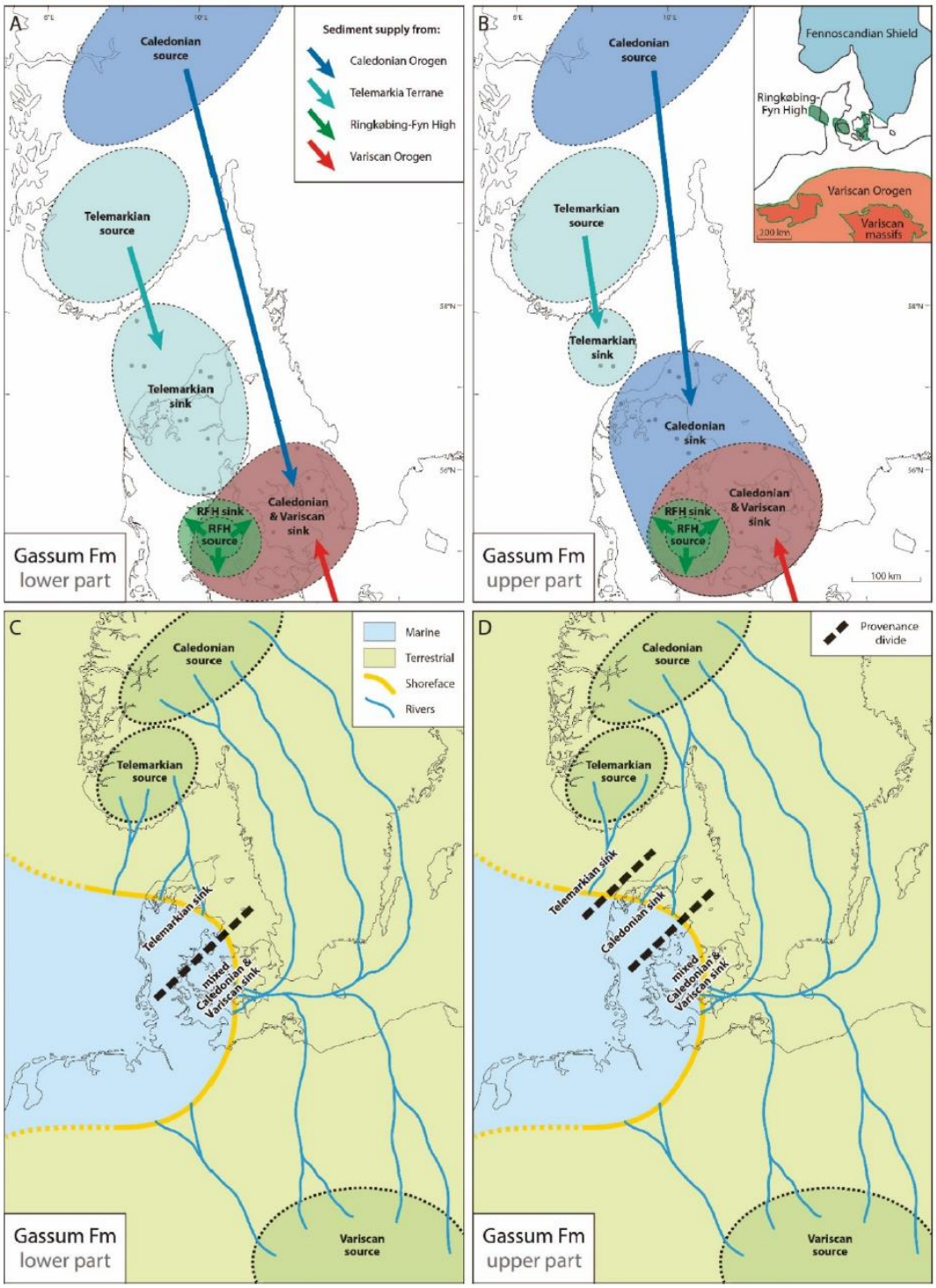

Figure 7.1.4. *Provenance of the lower (A) and upper (B) parts of the Gassum Formation showing the location of the primary source areas (Caledonian, Sveconorwegian, and Variscan) and the minimum extend of their sinks as evident from zircon U-Pb data from wells in the Danish Basin and the northern North German Basin. Sediments were locally supplied from exposed parts of the Ringkøbing–Fyn High. Tentative paleogeographic reconstructions for the lower (C) and upper (D) parts of the formation, where the primary difference is which of the Fennoscandian source areas that supplied most sediments to the basin. The maps represent snapshots since the coast-line moved back and forth due to repeated transgressions and regressions in time. From Olivarius et al. (2022).*

The Gassum Formation at Stenlille:

Depth, thickness and extent: At Stenlille, well data shows that the thickness of the Gassum Formation varies between 141 and 154 m, with a mean thickness of c. 146 m. The vertical depth to the top of the formation is slightly exceeding 1500 m at the central part of the domal structure and down to 1564 m at the flanks of the structure (Table 7.1.1). All Stenlille wells are located within the 3D seismic survey area, except ST-6 that is situated nearly 1 km NE of the north-eastern limit of the 3D survey area (Fig. 7.1.5). Seismic mapping and interpretation indicate that the Gassum Formation is present in the entire Stenlille area, with a thickness of approximately 140–160 m (Fig. 6.3.4C).

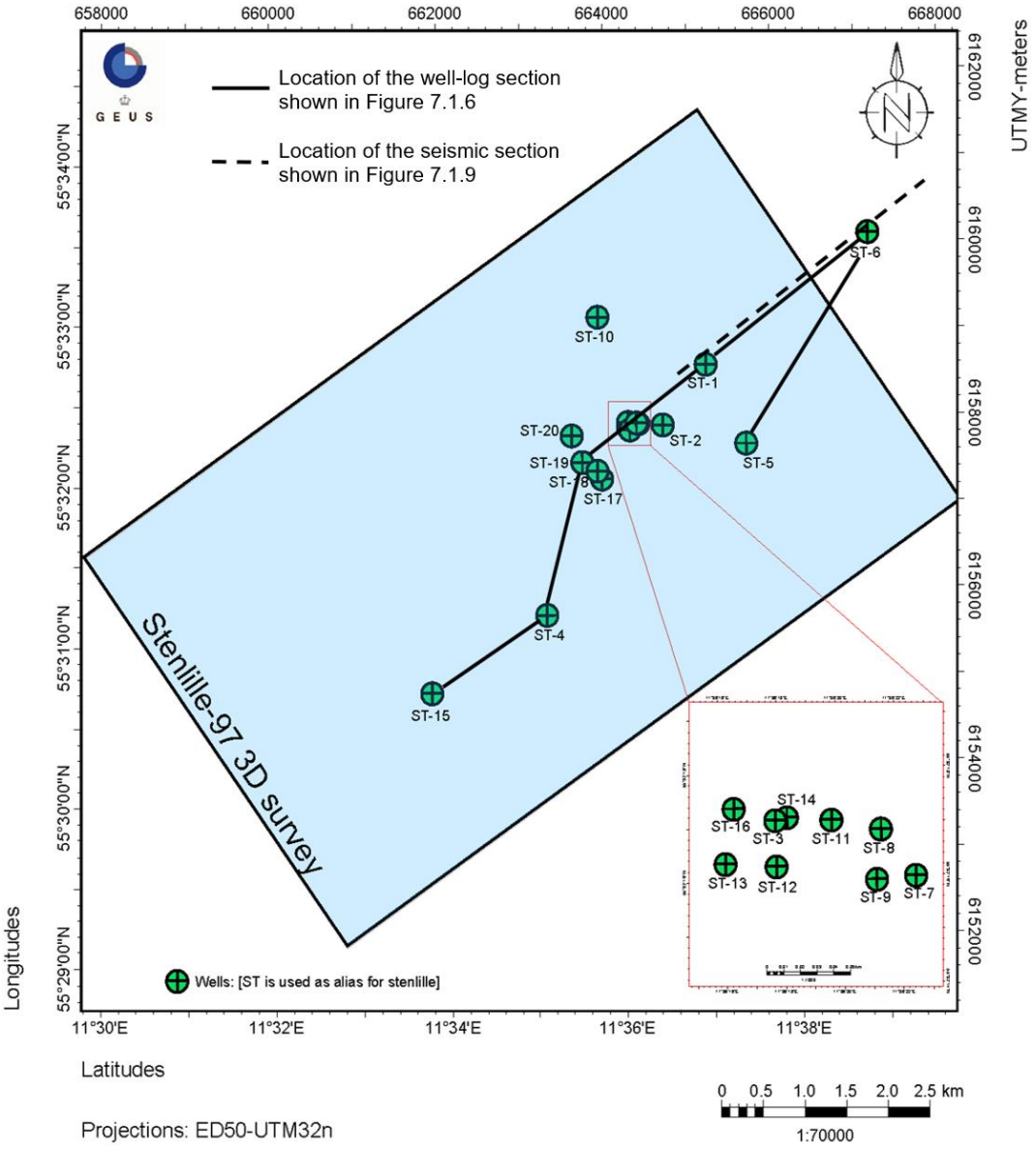

Figure 7.1.5. *Areal extent of the 3D seismic survey in Stenlille (blue rectangle) and the locations of wells of which only ST-6 to the NE is located outside the 3D survey. The marked log section (solid black line) is shown in Figure 7.1.6. Also marked, is the approximately location of a seismic section (dashed black line) shown in Figure 7.1.9.*

Table 7.1.1. *Approximately depths to the Top and Base of the Gassum Formation and its thickness in the Stenlille wells.*

Well	True Vertical Depth (meter below Kelly Bushing)		Thickness (m)
	Top Gassum Fm	Base Gassum Fm	
ST-1	1507	1650	143
ST-2	1512	1658	146
ST-3	Not penetrated		
ST-4	1514	1659	145
ST-5	1551	1692	141
ST-6	1564	1706	142
ST-7	1510	1657	147
ST-8	1505	1650	145
ST-9	1511	1653	142
ST-10	1524	1671	147
ST-11	1500	1647	147
ST-12	1503	1650	147
ST-13	1503	1650	147
ST-14	1501	1649	148
ST-15	1523	1677	154
ST-16	1503	1647	144
ST-17	1503	1649	146
ST-18	1503	1650	147
ST-19	1508	1653	145
ST-20	1505	1653	148

Subdivision: The formation is subdivided into 7 depositional sequences, SQ 1–SQ 7 (Fig. 7.1.6B), based on integration of sedimentological interpretations of cores and petrophysical log patterns, palynological data and interpretation of the 3D seismic survey (STENLILLE-97) covering a large part of the Stenlille structure (Hovikovski et al. 2020, Lindström 2020, Vosgerau et al. 2020) (Fig. 7.1.7). The numbering of sequences and their associated surfaces follows the sequence stratigraphic nomenclature in Nielsen (2003). This was developed for the Upper Triassic–Jurassic sedimentary succession in the Danish Basin and showed that individual sequences in most cases can be correlated basin-wide from well to well.

Each sequence is based by a sequence boundary (SB) formed at the time of maximum fall in relative sea level. Lowstand systems tracts (LST) form between sequence boundaries (SB) and the first transgressive surface (TS). Transgressive systems tracts (TST) form between the TS and the maximum flooding surface (MFS). Highstand systems tracts (HST) form between the MFS and the SB of the next sequence. This simple sequence stratigraphic approach (e.g., Payton 1977) is following the divisions of Nielsen (2003). There are also other

concepts (see e.g., Catuneanu 2019), but these are not discussed further here. Figure 7.1.6 shows how the depositional sequences link to depositional facies and environments.

DONG defined six reservoir zones with some internal mudstone seals in the Gassum Formation, but only the upper c. 40 m of the formation, covering Zones 1–4 and the upper part of Zone 5, is used for gas storage (Fig. 7.1.8). Overall, the lowstand systems tract (LST) and lower transgressive systems tract (TST) of the sequences consist of sandstone and correlates to DONG´s reservoir sand zones. In contrast, the remaining part of the TST of the sequences consists of mudstone and heteroliths correlating to DONG´s defined internal seals in the Gassum Formation (Fig. 7.1.8).

The seven sequences reflect an overall progradational stacking pattern from the base of the Gassum Formation and up to SB5. SQ´s 1–3 consist mainly of shoreface deposits, whereas thick lowstand systems tracts, up to 40 m thick, of the overlying SQ´s 4 and 5 are fluvial dominated with intercalations of shoreface sandstones. The upper part of SQ 5 is 15–20 m thick in many wells and is dominated by shoreface deposits (Fig. 7.1.6). An overall backstepping stacking pattern, above TS 5, is revealed by the depositional units becoming thinner and more fine-grained upwards in addition to offshore mudstone and shoreface sandstones becoming more dominant. SQ 6 has in several wells a thin fluvial succession at its base which marks the youngest event of fluvial deposition in the Stenlille area during deposition of the Gassum Formation.

High order sea-level variations formed the individual sequences and generated the complex internal reservoir architecture of the formation with lowstand intervals forming internal sandstone reservoirs and transgressive intervals of mudstone and heteroliths forming internal seals as mentioned above. Locally, these seals are truncated due to fluvial erosion related to fall in relative sea level and formation of sequence boundaries, implying that lowstand sandstones from different sequences are connected. The most intensive erosional event associated with basinward bypass of sediments relates to the formation of SB4. This sequence boundary in places led to a complete removal of the deposits of SQ 3, especially in the northeastern part of the 3D survey area (Fig. 7.1.9). Many sequences are thin, which preclude that all the sequence stratigraphic surfaces, identified based on the well data, can be idenfied in the seismic data due to resolution. Consequently, a subdivision of sequences into systems tract is generally not posible in the seismic data. Thus, it is mainly sequence boundaries that are linked to seismic reflectors whereas transgressive surfaces and maximum flooding surfaces are more difficult to map out laterally. However, the transgressive surface TS 7 corresponds approximately to the top of the Gassum Formation (Fig. 7.1.8B), which is marked by a decrease in the acoustic impedance from the Fjerritslev Fm to the Gassum Fm as a clear peak seismic reflection displayed in black or red color (Figs. 5.1, 6.1.3, 7.1.9).

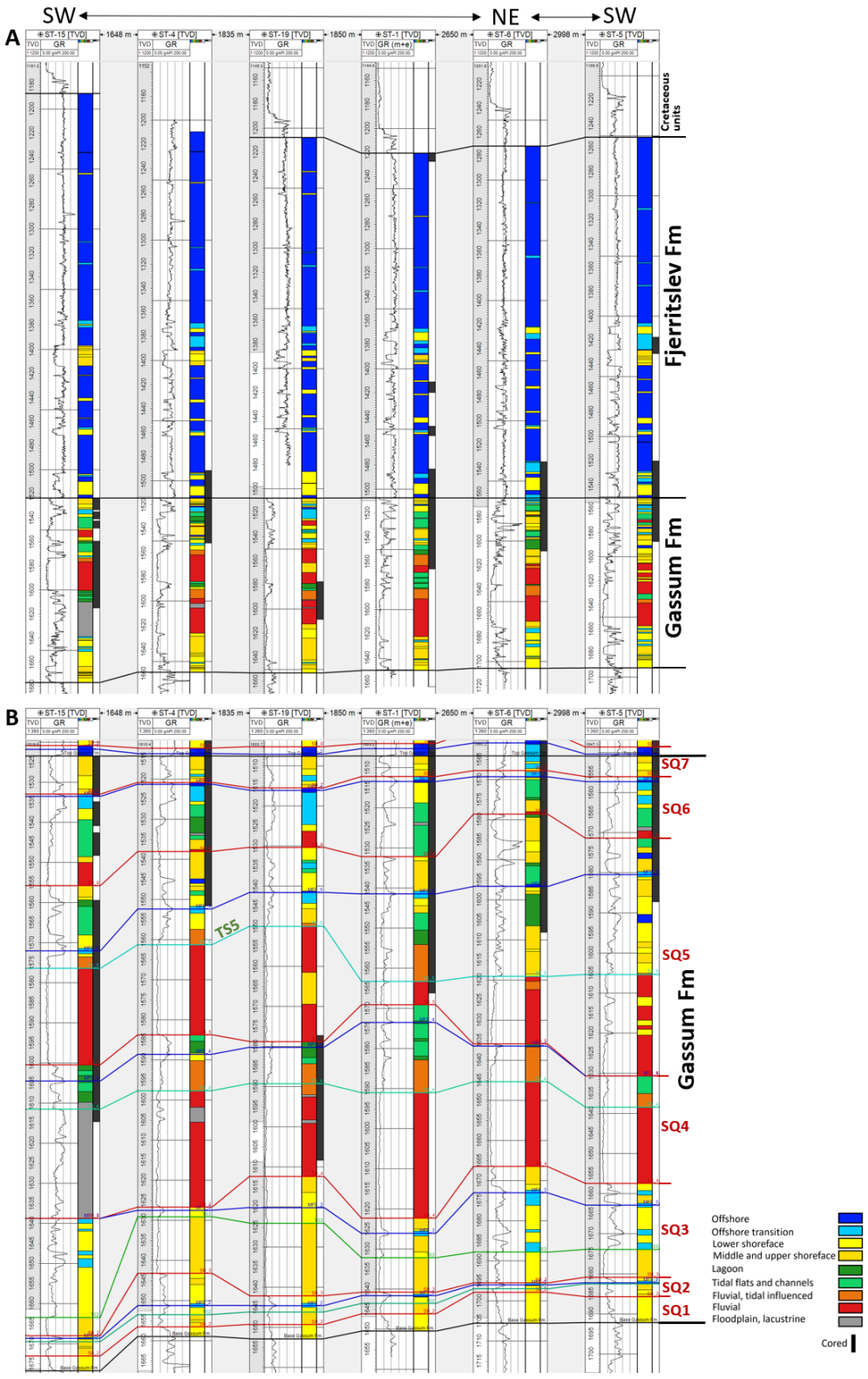

Figure 7.1.6. *A) Correlation panel of the Gassum and Fjerritslev Formations with interpreted facies associations. The top of the Fjerritslev Fm has been moved to a slightly shallower position in the wells based on new biostratigraphy and log correlation (Gregersen et. 2023). B) Correlation panel of the Gassum Formation showing sequence stratigraphic subdivision and interpreted facies associations. Location of log panels are shown in Figure 7.1.5.*

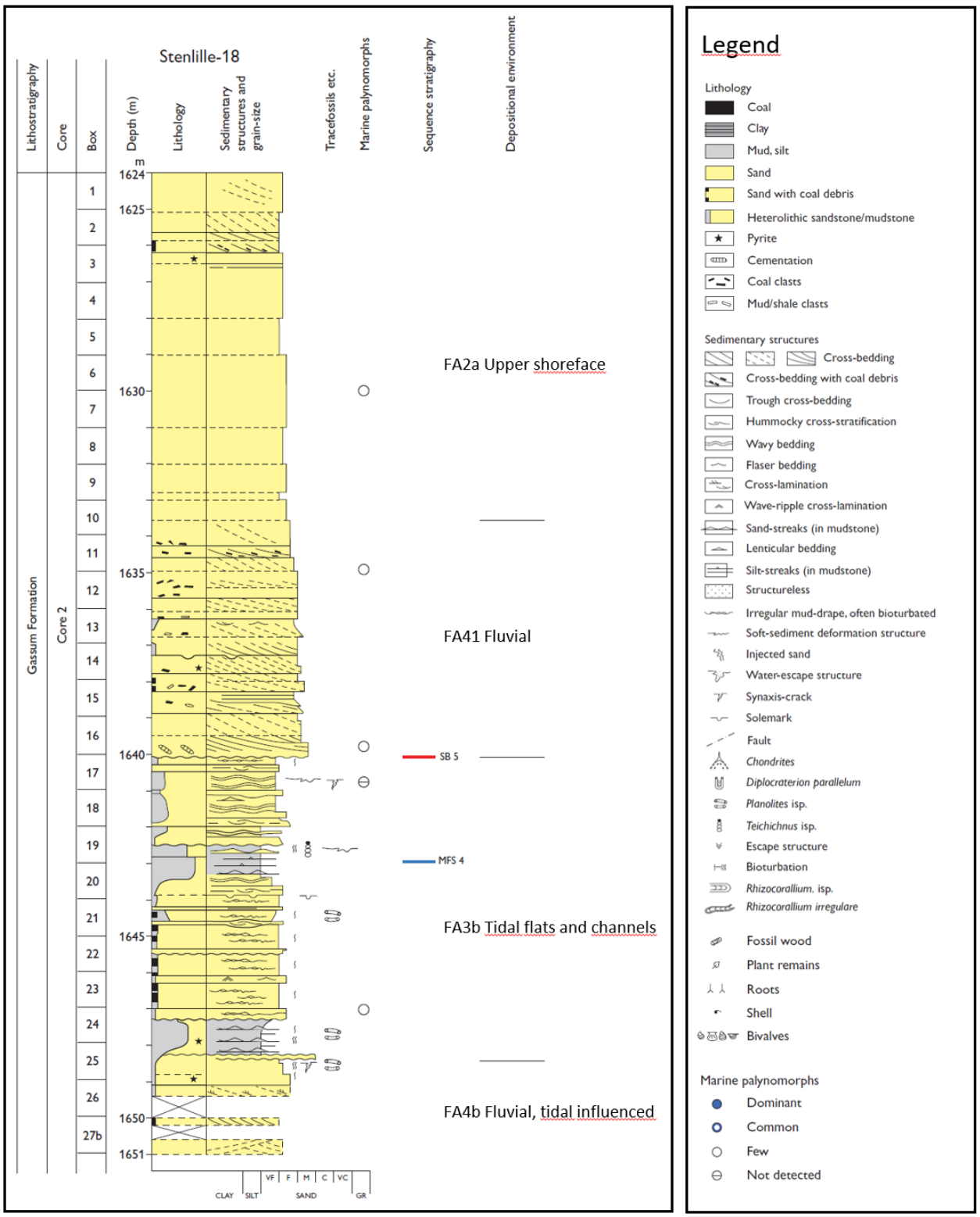

Figure 7.1.7. *An example of sedimentological description and interpretation of a core from the ST-18 well. Modified from Hovikoski & Pedersen (2020).*

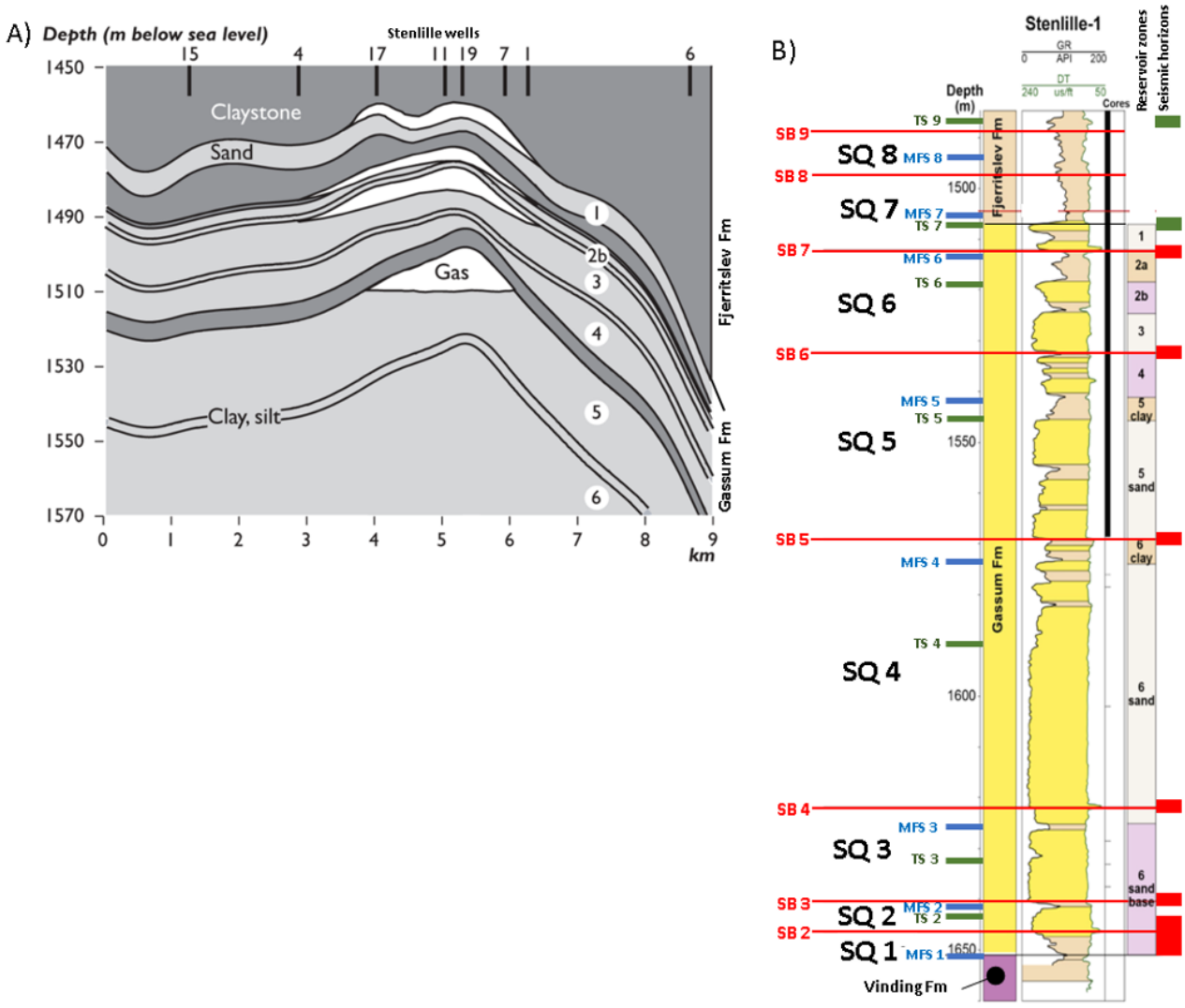

Figure 7.1.8. *A) Schematic cross-section (SW–NE) of the natural gas underground storage at Stenlille showing the various reservoir sandstone dominated zones (1–6) separated by relative thin mudstone dominated intervals (dark grey). From Laier & Øbro (2009). B) The Stenlille-1 well with gamma-ray log (GR) and sonic log (DT), well-tied sequence stratigraphic surfaces and sequences, reservoir zonation and to the right interpreted seismic horizons correlated to sequence stratigraphic surfaces. Yellow and brown, filling out the space between GR and DT logs, indicate intervals dominated by sandstones and mudstones, respectively. SB: sequence boundary, MFS: Maximum flooding surface, TS: Transgressive surface. The subdivision of the Gassum Formation into DONG´s reservoir zones are shown to the right (see also the well in Appendix B).*

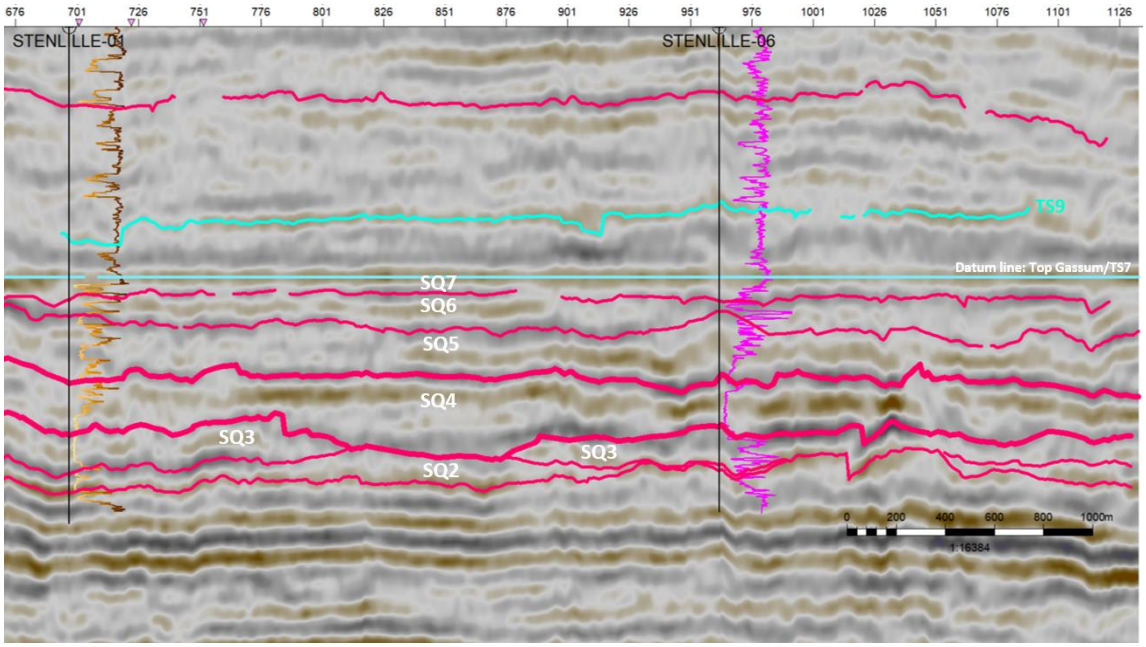

Figure 7.1.9. *SW–NE orientated 2D seismic line, DN94-D01, extending beyond the 3D survey area towards NE, and linking the ST-1 and ST-6 wells marked with their gamma-ray log motifs. The section is flattened on Top Gassum Fm (TS 7) to remove later halokinetic movement and bringing seismic reflections closer to original depositional geometry. Red lines are mapped sequence boundaries of the marked sequences. Note SB4 truncating through SQ 3 over a zone of c. 630 m forming an incised valley that is approximately up to 15 ms or c. 25–30 m deep. The incised valley provides extra accommodation space available for the deposition of fluvial sand, compared to the location of the ST-1 and ST-6 wells, where the LST of SQ 4 consists of fluvial sandstones in reservoir Zone 6 (Fig. 7.1.8B). Depth is in two-way travel time (milliseconds). Shown with a vertical exaggeration of 10. Location of the seismic profile is shown in Figure 7.1.5.*

Lithology, depositional environment, and provenance: The formation is interpreted to reflect a range of depositional environments including offshore, shoreface, lagoonal complex, fluvial, backshore, lakes and marsh (Fig. 7.1.6). The thickest sandstone intervals represent fluvial and shoreface LST deposits, whereas the intervening mudstone rich intervals represent offshore or lagoonal TST deposits.

Palynofacies analysis from facies below S5 5 in general indicate that the marine influence is low or absent, while the abundance of dinoflagellate cysts increases markedly above SB 5, thus reflecting the overall backstepping of the coastline towards the basin margins and accordingly stepwise enlargement of the marine areas during the latest Rhaetian. A shallow-marine to coastal-near position in Stenlille is shown near the time (earliest Jurassic) of transgressions at or near above the Gassum Fm in Figure 3.6C. The lowermost sequences, SQ´s 1–3, consist mainly of offshore to shoreface deposits followed by SQ´s 4 and 5 which also contain thick lowstand deposits of fluvial and subordinate shoreface sandstones (Fig. 7.1.6).

Seismic geomorphological analysis of SQ 5 using mapped sequence stratigraphic horizons within the 3D seismic volume and a frequency-filtering seismic attribute show concentric shapes associated with shingled reflections and channelized incisions in 2D sections, which suggest that the fluvial sandstones were deposited in sand-rich meandering river systems (Fig. 7.1.10; Smit et al. 2022).

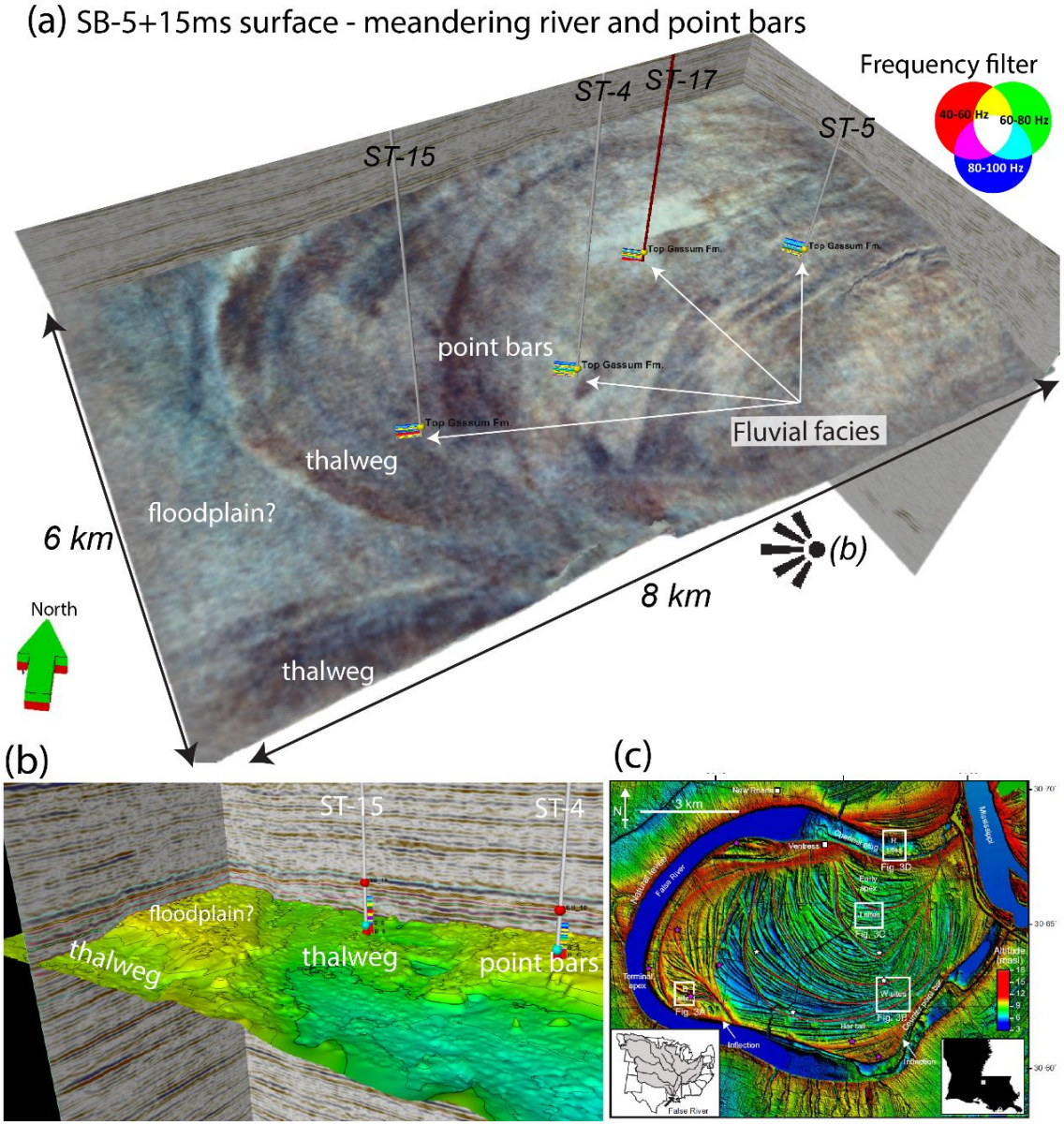

Figure 7.1.10. *A) Colour-rendering (with frequency-filtered data) of the time-shifted SB5 3D seismic horizon with 15 ms up. The concentric shapes are interpreted to reflect fluvial pointbars with the main channel (thalweg) furthest southwest. B) Time structure of mapped horizon SB5 showing the relief of the fluvial landscape. C) For comparison, an example from False River in Louisiana (USA) of similar concentric shapes representing pointbar migration formed by meandering rivers (from Clift et al. 2019).*

Incipient salt doming possibly controlled the pattern of fluvial erosion, as the 3D seismic data suggest this mainly to have occurred along the flanks of the present-day domal structure where nearly all the Stenlille wells are concentrated. Above TS 5, intervals of offshore mudstones and shoreface sandstones dominate (Fig. 7.1.6), and the backstepping pattern the sequences form culminates in the overlying thick succession of offshore mudstones of the Fjerritslev Formation. Lateral variations in facies associations within the sequence systems tracts as seen for some of the sequences in Figure 7.1.6 most likely reflect lateral variability of sub-environments in a costal setting where land meets the sea and barrier islands, lagoons, estuaries and nearby rivers may alternate within short distances.

Available dip-meter measurements from ST-3, -5, -6 and -11 were evaluated and compared to cored sections, when possible, to identify likely transport directions from sedimentary structures. Data from ST-5 seems to suggest a general N–S coastal trend in the section represented by the lower part of core 6 changing to a WNW–ESE trend in the upper part of core 6 and to a NE–SW trend in the section represented by core 5. One fluvial cross-bed above SB 6 suggest transport toward the SSW. Data from ST-11 may suggest westward transport in the thick fluvial to fluvial-estuarine sandstone-dominated intervals. However, it is mainly bedding planes of low inclination that are revealed by the dip-meter data, which make directional interpretations uncertain. Also, a variety of transport directions are expected in the depositional environments they are associated to, making it uncertain to draw conclusions on e.g., shoreline orientations based on the few data that show steep inclinations.

Zircon dating from SQ´s 4 and 7 suggest that the area received sediments from southern or south-eastern source areas apart from sediments from Fennoscandia (Olivarius et al. 2020, 2022). As mentioned above, this may have occurred as a mix of fluvial systems from the north and the south that merged east of the Danish basin and transported sediment into the basin from the east and southeast in the present Baltic Sea area (Fig. 7.1.4).

The Gassum Formation at Havnsø:

The Havnsø structure is situated c. 25–30 km NW of Stenlille (Fig. 1.1). A likely sediment supply from east and southeast, as mentioned above for the Stenlille area, implies that the Havnsø area probably represents a more distal depositional setting at the time the sediments of the Gassum Formation were deposited. Mapping with seismic data correlated from Stenlille reveals that the Gassum Formation has similar thicknesses in the Stenlille and Havnsø structures (average of c. 150 m; Fig. 6.3.4C) and that the transgressive surface TS 7 most likely also constitutes the top of the formation in Havnsø. The seismic data reveal no sign of a marked change in depositional slope from Stenlille towards Havnsø. This indicates the presence of a relative flat and low gradient basin floor at the time the sediments of the Gassum Formation were deposited. The sediments in Stenlille furthermore indicate overall shallow water or terrestrial conditions during deposition. Therefore, it sems likely that the shoreline and fluvial depositional systems behind experienced large distances of progradation and retrogradation during relative sea-level falls and rises, respectively. An optimistic reservoir prognostication of the Gassum Formation in the Havnsø structure would therefore be to assume that the depositional environments of the sandstone units in the Stenlille area also reach to the Havnsø structure. This approach will imply that the very good reservoir properties of the Gassum Formation in the Stenlille structure also characterize the formation in the Havnsø structure.

Another reservoir characterization approach is to include reservoir data of some of the nearest wells that surrounds the Havnsø structure in the Danish Basin (Fig. 7.1.11). This will include reservoir data from wells that represent both more proximal and distal depositional locations in “Gassum time” compared to the Havnsø structure. A simple average of the reservoir values from these wells could then be assigned to the Gassum Formation in the Havnsø structure. In doing so, only data that derives from the base Gassum – TS 7 interval in the surrounding wells should be included as this interval most likely corresponds to the Gassum Formation in the Havnsø structure (Fig. 7.1.12).

Finally, an attempt was made to map the sequences along a composite seismic line that link the 3D data set in Stenlille with the P1 seismic line that extends from Stenlille to the Havnsø

structure (Fig. 7.1.13). This is not straightforward as the resolution of seismic data is not high enough to reveal all the sequence stratigraphic surfaces identified in the Stenlille wells, and those that have been mapped are associated with uncertainty. Also, there are too much noise and too low resolution in offshore seismic data, vintage onshore data and new data from Nekselø to map and interpret internal seismic reflectors in the Gassum Formation. This is in general also the case for the new seismic lines that crosses the composite line. Also, the mapping and interpretation of the Gassum Formation along the composite line (Fig. 7.1.13) was done with a geological model in mind saying that the Havnsø area constituted a more distal depositional setting than the Stenlille area and that the sediment supply in this part of the Danish Basin mainly was from the SE and E (Fig. 7.1.4). Based on the geological model it is expected that:

- SQ´s 1–3: These sequences are expected to be thinner and the content of offshore mudstones and heteroliths to be larger on behalf of shoreface sandstones in the Havnsø area compared to the Stenlille area.
- SQ´s 4–5: The LST fluvial sandstones of sequences 4 and 5 in Stenlille may very well have reached the Havnsø area too due to the strongly progradational pattern these deposits reflect in Stenlille. Also, the relief of the basal sequence boundaries indicate marked erosion and basinwards bypass of sand into more distal parts of the basin. Consequently, the sandy LST of the sequences may even be thicker developed in the Havnsø structure than in Stenlille. The TST and HST of SQ 4 consist of lagoonal deposits in the Stenlille area implying that sandstones of a barrier island system may be present basinward in the direction of the Havnsø area.
- SQ's 6–7: It is likely that the LST´s of sequences 6 and 7 contain some sandstones, similar to those seen in wells located distally in the basin, whereas it is most likely that the TST´s consist of mudstones. Also, offshore mudstones may partly have replaced the sandy HST´s present in Stenlille due to the more distal depositional position of the Havnsø area and the less progradational depositional pattern of the HST's (compared to the LST 's of the sequences). Combined with the backstepping pattern the sequences form above TS 5 this implies that the number and thickness of sandstones in the upper part of the Gassum Formation is expected to be less in the Havnsø structure compared to the Stenlille structure.

The above-mentioned considerations implied that seismic reflectors representing possible channels and foresets were considered to reflect high-energy sandy depositional systems that should be assigned to the LST or possible HST of the sequences. In contrast, relatively consistent sub-horisontal reflectors were mapped as representing mudstones containing the transgressive or maximum flooding surfaces. Via the seismic 3D data, mappable reflectors were linked to the sequence stratigraphic surfaces identified in the Stenlille wells. The composite line was also investigated for any signs of sediment supply from other directions, e.g., from the Fennoscandian Shield. The interpreted seismic section is shown in Figure 7.1.13 together with a conceptual figure based on the interpretation. The conceptual figure predicts that sandstone dominated intervals in the Havnsø structure are mainly to be found in the LST´s of Sequences 4, 5 and 6 whereas sandstones of the highstands are interpreted to wedge out into mudstone before reaching the Havnsø area. This interpretation is supported by acoustic impedance modelling done on the P1 seismic line (GEUS22_HVN_P1) that extends from Stenlille to the Havnsø structure. This indicate that the Gassum Fm becomes more mudstone rich towards the Havnsø structure, compared to its composition in Stenlille as described in section 6.2. The sandy lowstands are probably of fluvial origin, as they are in Stenlille, due to the presence of seismic reflectors resembling channels and associated

foresets that may represent pointbar deposits similar to those described from Stenlille. Each of the LST´s may be linked roughly to a specific DONG reservoir zone as outlined in Figure 7.1.8. A reservoir characterization approach could therefore be to assign the mean reservoir parameter values of these zones to the presumed sandy LST´s in the Havnsø structure. However, of reasons mentioned above, some uncertainties are associated with the interpretation of the sedimentary lithology of the composite seismic section.

There are no distinct signs of sediment supply from other directions. However, the local occurrence of a relative deep channel at the base of SB 6 and close to the Havnsø structure, possibly reflects incision by fluvial channels that were orientated perpendicular or oblique to the orientation of the seismic section (Fig. 7.1.13). Based on the basinal setting, it seems most likely that this then would reflect a local sediment input from rivers sourced from the Fennoscandian Shield. The resolution of the crossing seismic 2D sections is not high enough to lend support to this and thus the interpretation remains speculative.

In summary, since no wells penetrate the Havnsø structure, three approaches are suggested to evaluate the reservoir properties of the Gassum Formation in the Havnsø structure:

Scenario 1: Use the average reservoir parameter values of the Gassum Formation in Stenlille, one to one, for the formation in the Havnsø structure.

Scenario 2: Use an average of the reservoir parameter values from the nearest wells that surrounds the Havnsø structure in the Danish Basin (from the interval covering the base Gassum to the transgressive surface TS 7).

Scenario 3: Use average reservoir parameter values of DONG reservoir zones that corresponds roughly to the LST sandstones that according to the conceptual model are present in the Havnsø structure.

These scenarios are discussed below.

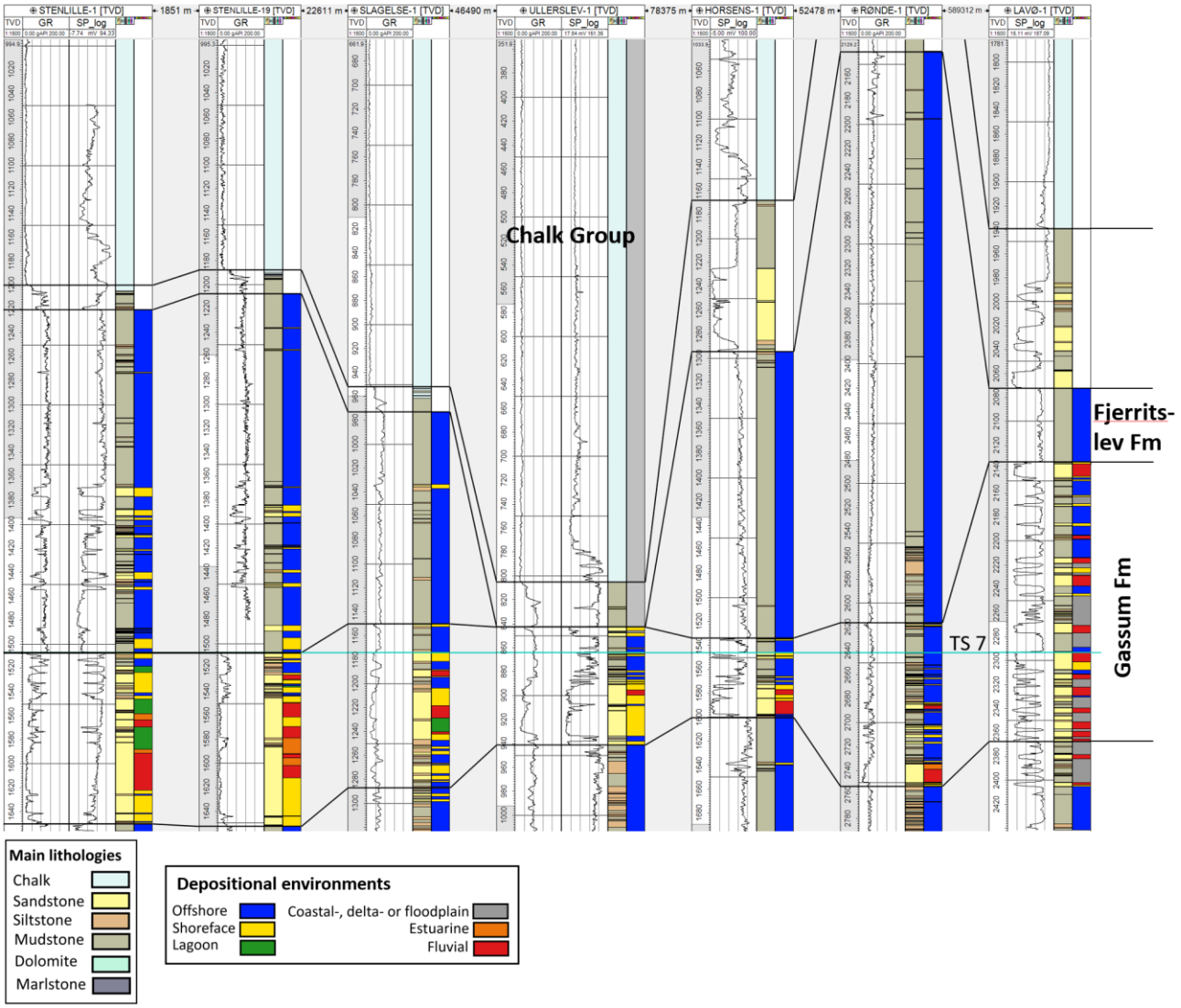

Figure 7.1.11. Correlation panel with selected wells that surrounds the Havnsø structure in the Danish Basin. Placement of formation tops are mainly based on depths given in Nielsen & Japsen (1991). Intervals between Top Fjerritslev and base Chalk Group consist of middle, upper or lower Cretaceous lithostratigaphic units depending on which well (see Nielsen and Japsen 1991). The transgressive surface TS 7 is used as datum line. Location of wells relative to the Havnsø structure is seen in Figures 3.1 and 7.1.3.

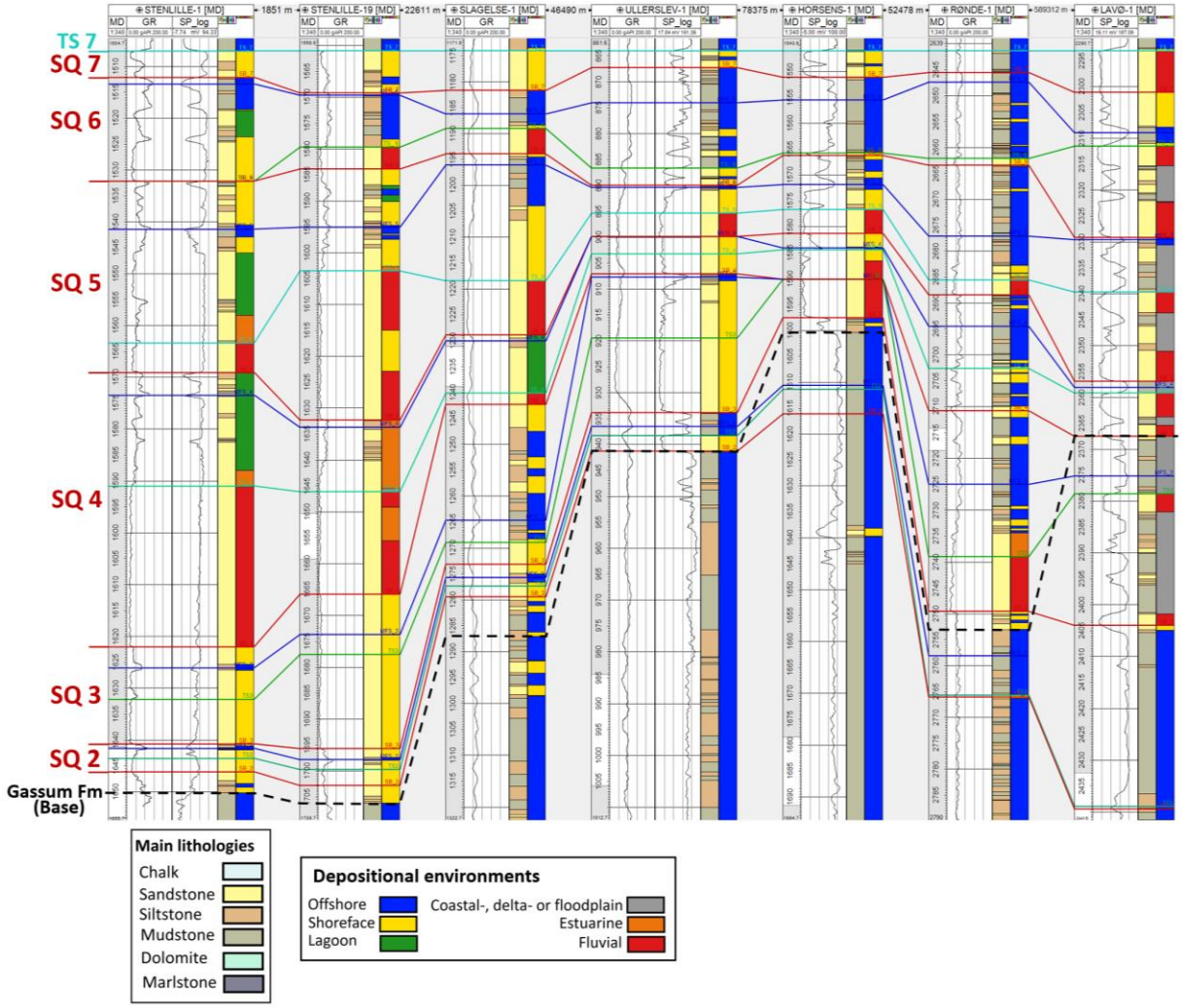

Figure 7.1.12. Correlation panel of selected wells that surrounds the Havnsø structure in the Danish Basin. Emphasis is on the interval from Base Gassum to the transgressive surface TS 7. This interval corresponds approximately to the Gassum Formation in the Stenlille structure and most likely also in the Havnsø structure. In reservoir estimates of the Gassum Formation in the Havnsø structure, based on the surrounding wells, data from this interval are therefore considered most relevant. The transgressive surface TS 7 is used as datum line. Location of wells relative to the Havnsø structure is seen in Figures 3.1 and 7.1.3.

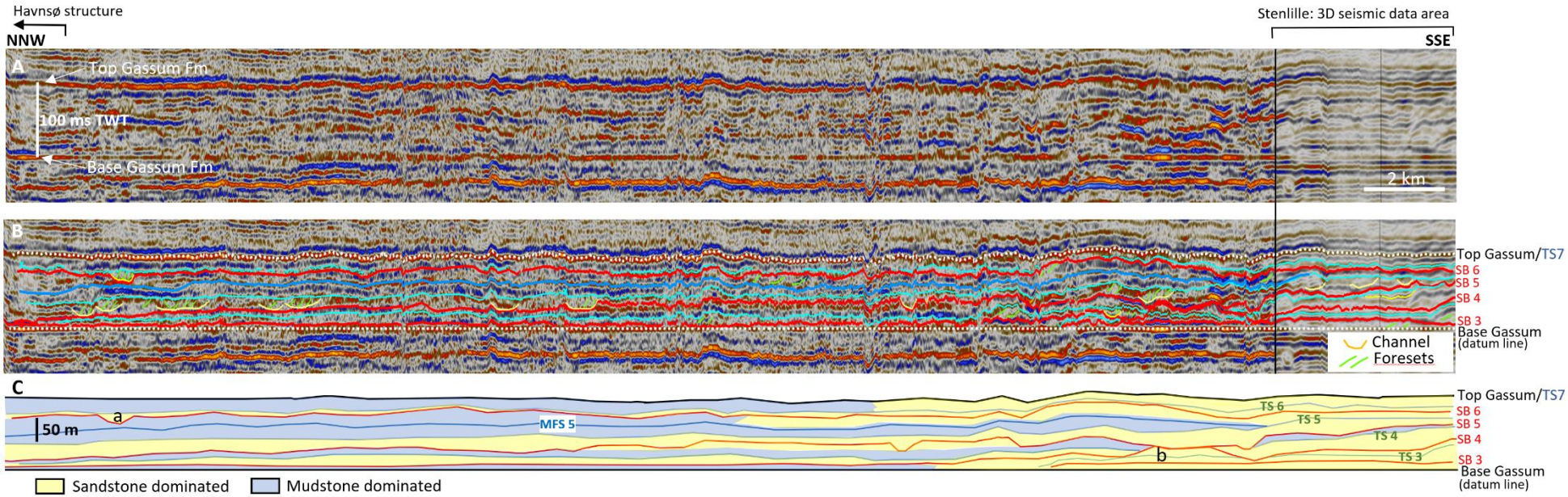

Figure 7.1.13. *A) Composite seismic section that links the 3D data set in Stenlille with the P1 seismic line that extends from Stenlille to the Havnsø structure (see section 6.1). Left of thin black vertical line: GEUS22_HVN_P1; right of thin black vertical line: composite 3D section in Stenlille. The seismic section is is flattened at the Base Gassum surface. B) Mapped sequence stratigraphic surfaces etc. are shown on the composite seismic section. C) Conceptual lithological model based on the interpretation of the seismic section. In this interpretation, only LST sandstones of SQ´s 4, 5 and 6 extends from the Stenlille area out into the Havnsø area whereas sandstones of the highstands are interpreted to wedge out into mudstone before reaching the Havnsø area. In the Stenlille area relatively thin mudstone intervals are associated with the maximum flooding surfaces (too thin to be shown on the figure). a: Possibly fluvial channel incision at the base of SB 6 and close to the Havnsø structure. b: Sequence 3 forms a positive relief that may have formed a barrier island at the time lagoonal sediments of the TST and HST of SQ 4 were deposited in Stenlille.*

Reservoir quality (porosity and permeability):

Previous studies performed by GEUS have shown that the key reservoir parameters of the Gassum Formation and the Bunter Sandstone Formation primary are dependent on the sediment source areas governing the mineralogy, the depositional environments determining the architecture of the reservoir sandstones, and the burial history of the Gassum Formation (e.g., Olivarius et al. 2022; Olivarius & Nielsen 2016; Kristensen et al., 2016; Weibel et al. 2017a, b; Olivarius et al. 2019; Weibel et al. 2020; Olivarius et al. 2022).

The porosity variations in the Mesozoic strata have been determined based on interpretation of well log data that are calibrated to the available core measurements. The permeability has not been logged in any of the wells, meaning that permeability has been evaluated from core permeability data and presumed porosity-permeability relations based on specific porosity-permeability relationships set up for sandstone units. Both with regards to the porosity and the permeability the core measurements correspond very well to the log derived values (Fig. 7.1.2). Thus, it is assumed that the log derived porosity and permeability also applies to the sections without cores.

The sandstones can be characterized by generalized reservoir parameters, including reservoir/net sand thickness, porosity (PHIE), shale volume (Vshale) and permeability (PERM) as tabulated below by using log data, core analysis data and presumed porosity-permeability relationships (Table 7.1.2). The table summarizes the results of existing well-log interpretations and current permeability assessments. The thickness of a particular sandstone unit varies across the structure and may pinch out. Similarly, the net sand thickness varies in terms of shale volume, porosity and well location. Herein 'Net sand' is defined as sandstone intervals characterized by porosities > 10 % and shale content < 50 %.

The porosities measured on the cores are the total porosities, i.e., including porosity within the clay minerals. The total porosity (PHIT) is also estimated from the logs; however, the effective porosity is used in the characterisation of the reservoirs. The total porosities measured on the cores and the logs are in good correspondence, but when the rock includes a high volume of shale the difference between the total porosity and the effective porosity is large. Contrary, in a clean sandstone, the total and effective porosities are similar.

The conventional core analysis data point to the presence of several porosity-permeability relationships in the Gassum Formation as the depositional environment varies throughout the Late Triassic time. Hence, the grain size and clay content of the Gassum Formation sandstones vary with depth and spatially. Accordingly, two distinct poro-perm models are suggested for the Stenlille area: one relation for the upper sand- and mudstone stone units (corresponding to DONG Reservoir Zones 1–5, SQ´s 5-7), and one relation for the lower clean sandstone unit (i.e., DONG Reservoir Zone 6, SQ´s 3-4). These correlations are used for estimating permeabilities in un-cored zones, meaning that the permeability assessments are derived from porosities estimated from log data and then transferred to permeabilities via the poro-perm relation.

In the following, reservoir characteristics are done for the three scenarios presented in the preceding.

Scenario 1

For the Scenario 1 reservoir prognostication of the Gassum Formation in the Havnsø structure assumes that the depositional environments of the sandstone units in the Stenlille area

also dominated around the Havnsø structure. In Stenlille, the composite cores from wells -1 and -19 constitute an almost complete coverage of the Gassum Formation, as only the lowermost 40 m are not cored, which forms a strong basis for calibrating the petrophysical interpretations in the Gassum Formation. Table 7.1.2 shows the reservoir characterization of the individual Reservoirs Zones as defined by DONG, as well as how these Zones relate to the sequence stratigraphic subdivision of the units within the Stenlille area. The table shows that best reservoirs in terms of porosity and permeability are located in the deeper units. Particular Reservoir Zone 6 sand that has average porosities of 27.1 %, corresponding to average permeabilities of 3496 mD. It is also seen that the best reservoir characteristics are found in the thick sandstone units.

Defining a reservoir zone as having permeabilities of at least 100 mD and porosities higher than 10 % leads to concluding on Scenario 1 that it could be expected that the Havnsø structure contains Reservoir Zones 1, 3, 4, 5 Sand, 6 Sand, and 6 Base, which will provide a combined reservoir thickness of 111 m. In particular the Reservoir Zone 6 sand could contain 42 m of reservoir sands with average porosities of 27.1 % and permeabilities close to 3500 mD.

Table 7.1.2. *Reservoir characterization of selected representative Stenlille-wells for each of DONG original Reservoir Zones, how these relate to the developed sequence stratigraphy based on the petrophysical interpretation that again is calibrated to the cored intervals. The last column shows the averaged values, which could be projected to be found in the Gassum Formation within the Havnsø structure. Note, in Stenlille-15 the Reservoir Zone 6 clay is set equal to 'Incised Valley Fill' as original proposed for this interval and based on the sequence stratigraphic subdivision the 'Incised Valley Base' is set equivalent to Reservoir Zone 6 Base.*

Sequences	Dong Reservoir Zones	Parametre	Stenlille-01	Stenlille-19	Stenlille-06	Stenlille-05	Stenlille-04	Stenlille-15	Havnsø
SQ 7	Reservoir Zone 1	Gross (m)	5.4	8.2	Not present	5.2	6.5	9.6	7.0
		Net Sand (m)	3.2	4.6		5	4.3	6.8	4.8
		N/G	0.59	0.56		0.96	0.66	0.71	0.7
		Ave PHIE (%)	23.6	15.9		20.4	23.9	21.8	21.1
		Ave PERM (mD)	232	32		115	217	133	146
		Ave Vshale	0.19	0.26		0.31	0.34	0.27	0.27
SQ 6	Reservoir Zone 2a	Gross (m)	6	10	5.7	7.9	5.0	5.0	6.6
		Net Sand (m)	0	0	2.4	0.3	0	0	0.5
		N/G	0	0	0.42	0	0	0	0.1
		Ave PHIE (%)	N/A	N/A	19.6	N/A	N/A	N/A	N/A
		Ave PERM (mD)	N/A	N/A	104	N/A	N/A	N/A	N/A
		Ave Vshale	N/A	N/A	0.25	N/A	N/A	N/A	N/A
	Reservoir Zone 2b	Gross (m)	6.1	Not present	5.3	5.5	5.6	8.0	6.1
		Net Sand (m)	3.5		5.0	4	5	7.9	5.1
		N/G	0.58		0.94	0.72	0.90	0.98	0.82
		Ave PHIE (%)	19.9		24.4	20.7	20.6	18.5	20.8
		Ave PERM (mD)	99		235	191	106	61	138
		Ave Vshale	0.35		0.07	0.38	0.26	0.29	0.27
	Reservoir Zone 3	Gross (m)	7.8	8.3	10.5	5.8	12.8	13.1	9.7
		Net Sand (m)	7.6	7.2	10.3	5.6	12.8	13.0	9.4
		N/G	0.98	0.87	0.99	0.97	1.00	0.99	0.97
		Ave PHIE (%)	24.2	17.2	25.5	21.3	25.1	24.8	23.0
		Ave PERM (mD)	223	43	266	184	256	234	201
		Ave Vshale	0.17	0.19	0.05	0.25	0.13	0.13	0.15
	Reservoir Zone 4	Gross (m)	8.7	7.0	10.5	10.6	7.0	8.9	8.8
		Net Sand (m)	4.9	3.3	9.1	4.9	5.2	5.3	5.5
		N/G	0.56	0.47	0.87	0.46	0.74	0.60	0.62
		Ave PHIE (%)	18.6	12.3	23.4	21.5	20.4	21.0	19.5
		Ave PERM (mD)	73	8	203	155	115	125	113
		Ave Vshale	0.39	0.39	0.12	0.29	0.32	0.19	0.28

SQ 5	Reservoir Zone 5 clay	Gross (m)	4.8	4.3	6.1	4.3	5.9	5.0	5.1
		Net Sand (m)	0	0	3.4	0	2.4	0	1.0
		N/G	0	0	0.55	0	0.42	0	0.2
		Ave PHIE (%)	N/A	N/A	18.3	N/A	0.15	N/A	9.2
		Ave PERM (mD)	N/A	N/A	76	N/A	20	N/A	48
		Ave Vshale	N/A	N/A	0.24	N/A	0.43	N/A	0.34
	Reservoir Zone 5 sand	Gross (m)	23.2	33.3	33.6	40.9	26.7	27.3	30.8
		Net Sand (m)	21.1	25.6	24.9	28.9	26.5	27.1	25.7
		N/G	0.91	0.78	0.74	0.71	0.99	0.99	0.85
		Ave PHIE (%)	24.0	21.5	27.1	24.6	26.8	26.1	25.0
		Ave PERM (mD)	224	139	405	275	350	298	282
		Ave Vshale	0.24	0.11	0.05	0.18	0.10	0.05	0.12
SQ 4	Reservoir Zone 6 clay	Gross (m)	4.9	8.2	5.3	4.8	6.8	47.0	12.8
		Net Sand (m)	1.5	2.1	4.2	4.8	2.5	14.3	4.9
		N/G	0.10	0.25	0.80	1.00	0.38	0.31	0.47
		Ave PHIE (%)	14.7	13.2	20.5	23.1	16.5	16.0	17.3
		Ave PERM (mD)	20	37	157	166	44	39	77
		Ave Vshale	0.45	0.38	0.16	0.25	0.38	0.34	0.33
SQ 4	Reservoir Zone 6 sand	Gross (m)	51.1	56.5	29.6	21.9	53.4	Not present	42.5
		Net Sand (m)	49.6	56.5	29.0	21.9	53.4		42.1
SQ 3		N/G	0.97	1.00	0.98	1.00	1.00		0.99
		Ave PHIE (%)	27.6	27.8	26.9	26.7	26.7		27.1
		Ave PERM (mD)	4189	3728	3253	3061	3249		3496
		Ave Vshale	0.11	0.03	0.04	0.03	0.13		0.07
SQ 2	Reservoir Zone 6 base	Gross (m)	25.0	8.6	35.5	62.8	15.4	29.5	29.5
		Net Sand (m)	20.9	6.6	23.5	18.5	12.5	21.6	17.3
		N/G	0.84	0.77	0.66	0.29	0.81	0.73	0.68
		Ave PHIE (%)	27.4	14.5	20.1	20.7	19.9	20.1	20.5
		Ave PERM (mD)	4463	287	972	1370	711	126	1322
		Ave Vshale	0.11	0.35	0.15	0.21	0.31	0.21	0.22

Scenario 2

For Scenario 2 the reservoir characterization approach includes reservoir data of selected wells surrounding the Havnsø structure in the Danish Basin. This will include reservoir data from wells that represent both more proximal and distal depositional locations in “Gassum time” compared to the Havnsø structure. An average of the reservoir values from these wells are assigned to the Gassum Formation in the Havnsø structure. In doing so, only data from the stratigraphic interval from the base Gassum – TS 7 interval in the surrounding wells are included (Figs. 7.1.11 and 7.1.12). In calculating the average values of the reservoir characterizations only the Stenlille-1 and -19 wells are included, as otherwise the dataset would be skewed toward the high data density in the Stenlille area compared to the surrounding regions.

Table 7.1.3 lists the general reservoir characterization of the Gassum Formation in the selected seven wells surrounding the Havnsø structure, and the lowermost row indicates the average values of the above columns, which in this scenario represent the expected values to be encountered in Havnsø. It is important to note, that for the wells outside the Stenlille area, only one porosity-permeability relation has been utilized, corresponding to the relation for SQ´s 4-7 in the Stenlille wells.

Despite of the variations of the sandstone units within the Gassum Formation, it can be generalized that the formation has excellent reservoir characteristics throughout the region. The top of the Gassum Formation is encountered in the depth range of 862 – 2613 m MD in the selected wells, which represent both basinal and marginal depositional settings. Based on the seismic data it could be expected to find the top of the Gassum Formation at 1550 m (below mean sea level) in the Havnsø area. The gross thickness of the Gassum Formation

ranges from 145 m in the Stenlille-19 well to 54 m in Horsens-1, which likely reflects a more proximal and distal depositional setting, respectively. Based on the seismic interpretation, the Gassum Formation is expected to be on average c. 150 m thick within the Havnsø structure (Fig. 6.3.4C). The net reservoir sand shows a similar pattern as the gross formation thickness, decreasing in a general east-west direction from 118 m in the in the Stenlille-19 well to 29 m in the Horsens-1 well. The average effective porosity (PHIE) within the reservoir sandstones in the surrounding wells ranges from 18 % to 26 % with an average of 23.6 %. It is important to notice that these variations in the PHIE seemingly does not represent a basinal versus marginal setting, as it varies both within the marginal and basinal settings, and also depends on other factors such as burial depth. The permeability as listed in table 7.1.3 varies between 2743 mD to 188 mD, however as mentioned above these numbers cover two porosity-permeability relations in the Stenlille-1 and -19 wells but only one relation in the remaining wells. Nevertheless, it can be seen that the Gassum Formation forms an excellent reservoir in all the shown wells. Even in the Rønde-1 well, where the present-day depth to the top of the Gassum Formation is more than 2600 m, there are excellent reservoir units, as for the 12 m thick LST sandstones within SQ 3 has average PHIE of 25 % and permeabilities exceeding 500 mD.

Table 7.1.3. *Generalized reservoir parameters for the Gassum Formation in wells surrounding the Havnsø structure. Due to the relative abundance of data in the Stenlille area it is possible to determine two porosity/permeability functions, however for the remaining wells this is not possible and therefore the permeabilities in these wells have been calculated based on a single function similar to the SQs 4 – 7 in Stenlille. Mean values assigned to the Gassum Formation in the Havnsø area, are a gross thickness of 105 m, of which 69 m are reservoir sandstone with a porosity of 23.3 % and 1087 mD permeability.*

Well	Top	Gross	Net	N/G	Av_Vshale	Av_PHIE	Av_PERM
Name	*m*	*m*	*m*	*v/v*	*v/v*	*%*	*mD*
Stenlille-19	1561	145	118	0.82	0.13	21.9	1829
Stenlille-1	1507	143	113	0.79	0.17	25.7	2743
Ullerslev-1	862	79	51	0.65	0.13	25.8	848
Horsens-1	1546	54	29	0.54	0.10	24.6	703
Terne-1	1158	134	89	0.67	0.09	25.5	753
Lavø-1	2293	74	50	0.67	0.16	21.8	547
Rønde-1	2641	109	34	0.31	0.11	17.9	188
Average (= Havnsø)		105	69	0.63	0.13	23.3	1087

Scenario 3

For Scenario 3, the reservoir prognostication of the Gassum Formation in the Havnsø structure utilizes a geological conceptual approach supported by the observations in the seismic data extending from the Stenlille area to the Havnsø structure. Figure 7.1.13 illustrates that only the LST sandstones of SQ´s 4, 5 and 6 extends from the Stenlille area out into the Havnsø area whereas sandstones of the highstand and transgressive system tracts are interpreted to wedge out into mudstone-dominated intervals in the Havnsø area.

Table 7.1.4 lists the thickness and reservoir parametres in the selected wells from the Stenlille area, which form the basis for the reservoir characterization of the Havnsø structure in Scenario 3. The selection of wells represents geographical dispersion across the stratigraphic closure constituting the Stenlille structure and therefore representing the variability

that could be expected in Scenario 3 in the Havnsø area. In the table, reservoir values of the Gassum Formation in the Havnsø area is represented by average values from the Stenlille wells. The LST sandstones in the Stenlille area in general are excellent reservoirs with porosities in the range of 17.7 – 30.5 % and a permeability range of 46 – 5634 mD (Table 7.1.4).

Based on an average of the three sequences (SQ 4–6; Table 7.1.4), 43.5 m of LST sandstone with a porosity of 26.5 % and permeability of 1516 mD can be assigned to the Gassum Formation in the Havnsø structure.

Table 7.1.4. *Generalized reservoir parameters for the LST sandstones of SQ 4-6 of the Gassum Formation in selected wells in the Stenlille area.*

Sequences	System Tract	Parametre	Stenlille-01	Stenlille-19	Stenlille-06	Stenlille-05	Stenlille-04	Stenlille-15	Havnsø
SQ 6	LST	Gross (m)	7.8	6.5	5.8	1.8	11.6	5.4	6.5
		Net Sand (m)	7.6	6.13	5.3	1.8	11.6	5.4	6.3
		N/G	0.98	0.99	1.00	1.00	1.00	1.00	1.00
		Ave PHIE (%)	24.2	17.7	26.4	27.1	25.8	26.2	24.6
		Ave PERM (mD)	223	46	305	402	276	298	258
		Ave Vshale	0.17	0.17	0.03	0.04	0.12	0.07	0.10
SQ 5	LST	Gross (m)	5.0	28.7	14.4	7.2	23.4	27.3	17.7
		Net Sand (m)	5.0	25.0	14.4	7.2	23.4	27.1	17.0
		N/G	1.00	0.87	1.00	1.00	1.00	0.99	0.98
		Ave PHIE (%)	28.1	21.8	29.1	28.0	27.4	26.1	26.8
		Ave PERM (mD)	427	143	498	410	377	298	359
		Ave Vshale	0.15	0.11	0.01	0.06	0.07	0.05	0.08
SQ 4	LST	Gross (m)	30	19.0	19.5	21.9	20.0	Not present	22.1
		Net Sand (m)	30	19.0	19.2	21.9	20.0		22.0
		N/G	1	1.00	0.98	1.00	1.00		1.00
		Ave PHIE (%)	30.5	27.8	26.9	26.7	28.6		28.1
		Ave PERM (mD)	5634	3660	3187	3061	4115		3931
		Ave Vshale	0.02	0.03	0.01	0.03	0.08		0.03

Conclusion on Reservoir Characterization

The interpretation of the seismic data (Chapter 6) indicates that the top of the Gassum is to be expected around 1420 m (b.msl.) and that the thickness is c. 140 – 160 m, thus closely resembling the thickness of c. 150 m in the Stenlille area. Three different scenarios predicting the reservoir units contained within the Havnsø structure have been presented based on incorporation of the acquired seismic data, sequence stratigraphic subdivision, and in particular log data from the Stenlille area and adjacent wells surrounding the Havnsø structure in the Danish Basin. The best reservoir units in the surrounding wells, including in the Stenlille wells, are encountered in the deeper depositional units of the Gassum Formation, and in particular the LST sandstones of Sequences 3 – 5 show promising characterizations. In addition, these LST sandstones are interpreted to be present regionally in the Danish Basin forming a basin ward stepping sequence set (Nielsen 2003), and it is thus likely that similar depositional sequences and reservoir units are also present throughout the Havnsø structure.

A single number for the potential of carbon storage potential in the Havnsø structure may be given by the transmissivity which is estimated by multiplying reservoir sand thickness with permeability. Table 7.1.5 shows that in all of the scenarios the transmissivity is high (> 72 Dm), thereby underlining that the Gassum Formation in the Havnsø structure probably exhibit an excellent carbon storage potential in the sense of reservoir characterization.

Table 7.1.5. *Summarizing the Scenarios 1-3 predicting the reservoir characteristics of the Gassum Formation within the Havnsø structure. All three scenarios show excellent reservoir qualities and thicknesses quantified by the transmissivity ranging from 72 – 89 Dm (Darcymeter).*

	Reservoir	Net to Gross	PHIE	PERM	Transmissivity
	m	*v/v*	*%*	*mD*	*Dm*
Scenario 1	111	0.75	21.9	805	89
Scenario 2	69	0.63	23.3	1087	75
Scenario 3	47.6	0.33	27.3	1516	72
Average	75.9	0.57	24.2	1136	79

The secondary reservoirs: Oddesund Fm and Bunter Sandstone Fm

In the estimation of the reservoir properties of the Oddesund and Bunter Sandstone Formations data from Margretheholm-1, Stenlille-19, Slagelse-1, Ullerslev-1, Horsens-1, Løve-1, Jelling-1 and Rønde-1 have been included with emphasis on the first two wells as these are located closest to the Havnsø structure.

The Oddesund Formation

The Oddesund Formation is largely dominated by variegated, calcareous, anhydritic claystones and siltstones and with a thick interval of evaporite beds and is interpreted as formed during prevailing brackish to hypersaline, arid conditions (Bertelsen 1980). Basically, it is thus not to be considered as a reservoir. However, locally the formation may contain intervals of sandstones as is also the case in Stenlille-19, the only Stenlille well which penetrate the formation (Fig. 7.1.1). Input of sandstones in the otherwise fine-grained formation may reflect increasing humidity leading to the deposition of deltaic or fluvial sand in basin-marginal areas.

The sandstones are in general fine-grained, silty or slightly clayey, greenish grey or red-brown, micaceous, mainly non-calcareous and locally they contain dispersed microlignite (Bertelsen 1978). The mudstones of the lower part of the formation are interpreted to reflect deposition on flat coastal plains which were not permanently covered by water as the mudstones are predominantly reddish, common in anhydrite and fossils are lacking (Bertelsen 1978). The sandstones from the upper part of the formation are interpreted to reflect fluvial deposition and a possible climatic change from semi-arid to more humid conditions (Bertelsen 1978).

The Oddesund Formation in the study area:

The Oddesund Formation is present in the Stenlille-19 well in the depth interval 1858 – 2241 m MD (Fig. 7.1.1). The formation is dominated by mudstones and secondary anhydrite beds but also contains an interval (c. 2257 – 2128 m MD) of well-defined sandstone layers embedded in the mudstones (Fig. 7.1.1). The three distinct sandstone layers range in thickness from c. 2 – 16 m with at least the lowermost and thickest sandstone layer probably being present in the entire Stenlille structure. The top of the sandstone beds, the 'Intra Oddesund sst. beds' horizon, has been interpreted in both the Stenlille structure and Havnsø structure from the seismic data, but no internal horizons (and possible sandstone beds) are interpreted in the succession in Havnsø (see section 6.1). The top 'Intra Oddesund sst. beds' surface in the Havnsø structure is, based on few interpreted seismic lines, located at c. 2440 m b.msl and the basal closing contour of this surface is c. 2500 m b.msl, and thus the structure at this surface has a relief of c. 60 m.

The lithological description of the sandstones in the completion report of the Stenlille-19 well is sparse, saying that the sandstones are very fine to fine grained, moderately sorted with subrounded grains, with calcareous cement and traces of pyrite. The color is white to light grey or olive green (DONG 2001).

In the Slagelse-1 well silt- and sandstones are present in three bundles of the interval between 1504 – 1567 m MD (Appendix B) with a combined net reservoir sand thickness of 12 m, which likely correlate to the three sandy intervals in the Stenlille-19 well. Due to the sparse logs available for the Slagelse-1 well it is only possible to estimate the volume of shale (Vshale) based on the gamma ray, and it is not possible to estimate neither the porosity nor

permeability. Based on the Vshale, the reservoir quality of the Intra Oddesund sandstone beds is expected to be poor in Slagelse-1.

In the Ullerslev-1 well, an interval in the Oddesund Formation contains siltstones and a thin layer of sandstone, as the net reservoir sand is estimated on the logs to be 0.3 m thick. Neither in the Horsens-1, Løve-1, Jelling-1, or the Rønde-1 wells are reservoir sands encountered within the Oddesund Formation. The Oddesund Formation is not encountered in the deep well of Terne-1 where the Triassic strata below the Gassum Formation consist of the Skagerrak Formation. Based on the information in these wells the intra Oddesund sandstone beds are thickest in the Stenlille area and may be pinching out towards west and north. This makes it less likely that the Oddesund sandstone beds form a significant reservoir in the Havnsø structure. However, for the sake of completeness, data on the reservoir properties of the sandstone beds are given below.

Reservoir quality (porosity and permeability): The reservoir quality of the three pronounced sandstone layers in the Oddesund Formation (Fig. 7.1.1) – located in the intervals 2057 – 2068, 2090 – 2097 and 2110 – 2126 m MD – is not fully documented as no cores are available, meaning that sandstone permeability cannot be measured in the laboratory. However, an evaluation of the well-log data indicates fairly low shale volume and porosities up to 30 % and averaging 18.9 %, suggesting fair reservoir quality. For this purpose, the porosity-permeability relation within the sandstones in the Oddesund Formation is expected to be similar to the SQ´s 5-7 in the Gassum Formation, further supported as the grain sizes are described as fine to very fine in the Final Well Report. Further, these sandstones are positioned between layers containing anhydrite and therefore there is a risk of the intra Oddesund Sandstone beds are well cemented, although the available logs do not necessarily indicate that this is the case.

The average reservoir parameters as derived from the petrophysical interpretation of the surrounding wells suggest that there would be 8.0 m of reservoir sand with an average porosity of 15.5 % and permeability of 435 mD in Havnsø, as summarized in Table 7.1.6.

Table 7.1.6. *Generalized reservoir parameters for the Intra Oddesund sandstone beds in wells surrounding the Havnsø structure. In Stenlille-19 the sandstones have a combined reservoir thickness of 28 m, while it is 12 m in Slagelse-1 and only 0.3 m in Ullerslev-1. The gross reservoir is here identified as the interval containing silt/sand and therefore not the full thickness of the Oddesund Formation.*

Well	Top	Gross	Net	N/G	Av_Vshale	Av_PHIE	Av_PERM
Name	*m*	*m*	*m*	*v/v*	*v/v*	*%*	*mD*
Stenlille-19	1858	38	28	0.74	0.28	18.9	852
Slagelse-1*	1334	63	12	0.18	N/A	N/A	N/A
Ullerslev-1	982	20	0.3	0.01	0.49	12.0	19
Rønde-1	2827	631	0	0			
Horsens-1	1645	84	0	0			
Average (Havnsø)			*8.0*		*0.38*	*15.5*	*435*

*Only the Shale cut off of 0.5 applied, as it is not possible to estimate PHIE

The Bunter Sandstone Formation

The Bunter Sandstone Formation is known from deep wells in Denmark and Sweden and is widespread in the Danish Basin and the North German Basin. The geothermal plant at Margretheholm in Copenhagen is designed to use hot water from sandstone layers in the formation. The formation is less than 300 meters thick in the southern Danish area, and over the Ringkøbing–Fyn High the formation is either thin or absent. The high and adjacent areas were probably partially exposed in the Early Triassic (Michelsen et al. 1981). The formation consists of reddish-brown and yellow-brown, fine- to medium-grained sandstones, in addition to thick intervening intervals of siltstones and claystones. Locally, the deposits are strongly calcareous, anhydritic and micaceous. In the Danish Basin, the formation is replaced to the north by coarse-grained sandstones belonging to the Skagerrak Formation (Fig. 3.3) (Bertelsen 1980). The Bunter Sandstone Formation was formed in the Early Triassic in a dry and hot desert climate (Fig. 3.5B). Ephemeral rivers transported sand, mainly from the Fennoscandian basement, into the central part of the Danish basin, where the sand was deposited in river channels. Vegetation was extremely sparse, and during the dry periods wind created sand dunes. Periodically eolian sand was supplied to the Danish Basin from the south (Olivarius et al., 2015). In between the river channel and dune sand, layers of clay were deposited in lakes.

In the North German Basin, the Bunter Sandstone Formation is divided into four members, each consisting of a sandstone succession followed by a relatively thick claystone succession (Fig. 7.1.14). Two of these members (Volpriehausen and Solling members), and partly the Defurth Member, can also be recognized in most of the deep Danish onshore wells that penetrate the Bunter Sandstone Formation (Bachmann et al. 2010, Michelsen & Clausen 2002).

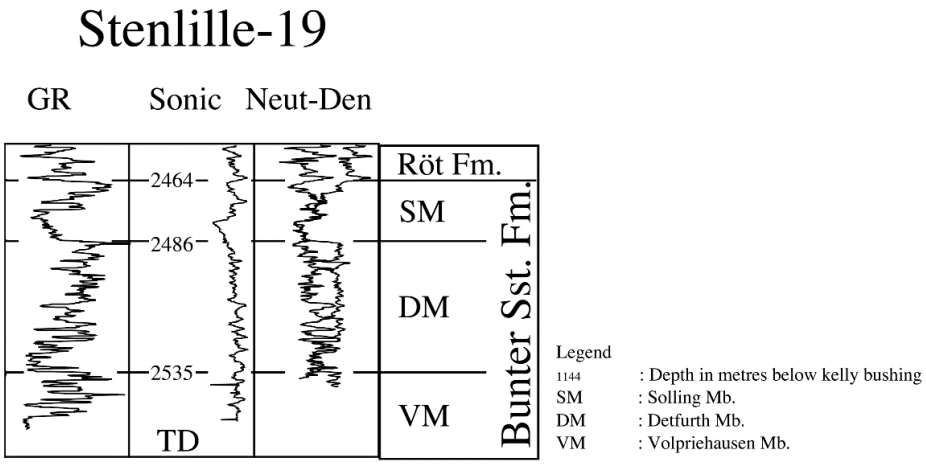

Figure 7.1.14 *Subdivision of the Bunter Sandstone Formation in the ST-19 well into the Volpriehausen, Detfurth and Solling Members. Modified from Michelsen & Clausen (2002).*

The Bunter Sandstone Formation in the study area:

Only one of the Stenlille wells (ST-19) is drilled deep enough to reach into the Bunter Sandstone Formation (Fig. 7.1.1). The ST-19 well penetrates the top of the formation at c. 2410 m TVD (2464 m MD). The well reveals a minimum thickness of the formation of 104 m as the base of the formation was not been penetrated. Michelsen & Clausen (2002) interpret the

Volpriehausen, Defurth and Solling members also to be present in the ST-19 well (Fig. 7.1.14). The lithological description of the sandstones published in the ST-19 completion report says that the sandstones are fine to medium grained, well sorted with rounded grains, and with calcite cement. The colour is described as red-brown to light grey to smokey (DONG 2001).

In the Margretheholm-1 well the Bunter Sandstone Formation is reached at 2368 m MD and has a thickness of 321 m and rest on weathered crystalline basement (DONG 2003). The studied wells to the west of the Havnsø structure it is only the Rønde-1 that reaches Lower Triassic, where the Bunter Sandstone Formation is encountered at 4058 m and has a gross thickness of 575 m. In order to have representative data for the reservoir characterization, the Løve-1 and Jelling-1 wells were included in the present study. In Løve-1, the Bunter Sandstone Formation is found at 1802 m and in Jelling-1 at 1636 m, while the gross thickness is 257 m and 114 m, respectively.

The Top Bunter Sandstone with underlying interval has been correlated in seismic lines from the Stenlille-19 well and into the Havnsø structure and the formation likely continues westwards (see section 6.1). Seismic interpretation indicates a widespread occurrence of the formation and a few places observations of subtle prograding/onlapping reflections and troughs, which may indicate depositional systems with sandstones and/or local tectonics at structure flanks near Stenlille-19 (see section 6.1). Such subtle features are also observed a few places in the new seismic data of the Havnsø structure (see section 6.1). The thickness of the formation may from seismic interpretation be in the order of c. 200 – 250 m within the Stenlille 3D survey area, and interpretation of selected seismic lines (in particular from new data) indicates thickening of the formation towards Havnsø (see section 6.1).

Individual sandstone units in the formation are not mapped from seismic data in this study.

Reservoir quality (porosity and permeability): In general, the reservoir quality of the Bunter Sandstone Formation is presumably good, since the aeolian deposits that characterizes the formation have a large lateral continuity, a fairly constant thickness, and only few cementing phases that are mostly clay-free. A smaller part of the Bunter Sandstone Formation was cored in the Stenlille-19 well (at 2479 – 2497m MD; Fig. 7.1.1) covering parts of the reservoir and the underlaying mudstone. The cored interval is approximately 19 m thick, and the conventional core analysis data are plotted in Figure 7.1.15. Within the reservoir zone of the Bunter Sandstone Formation the core measured porosity ranges from 15 % to 26 % and corresponds well with the log derived PHIE. The core measurements of the permeability within the sandstone vary from 17 to 1132 mD.

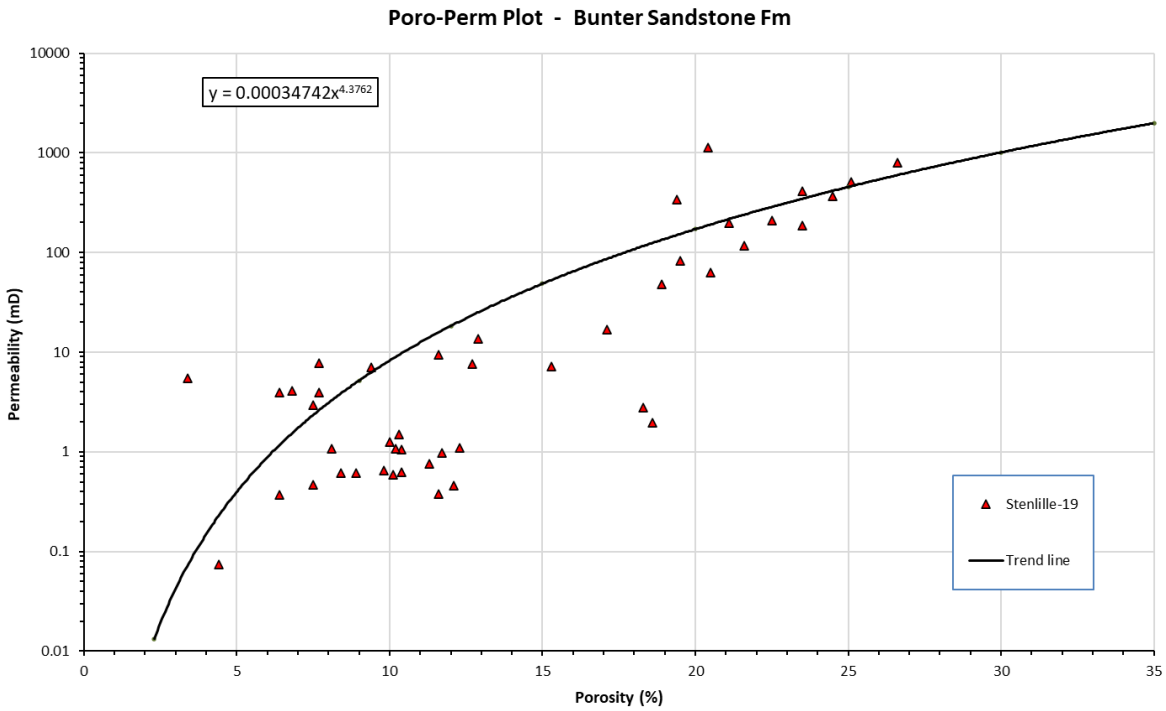

Figure 7.1.15. *Porosity-permeability relationships for the Bunter Sandstone Fm sandstones cored in the Stenlille-19 well. Based on conventional core analysis data. The black line represents the presumed trend line of the Bunter Sandstone Formation. This specific trend line is supported by core analysis data that are available from wells located outside the Stenlille area. Permeability values are gas permeabilities measured by the COREX Core Laboratory.*

In the Margretheholm-1 well, the reservoir sand units within the Bunter Sandstone Formation have a combined thickness of 106 m, and an average PHIE of 17.5 % corresponding to 149 mD permeability. The Løve-1 and Jelling-1 are located to the west of the Havnsø structure and have average PHIE of 23.0 % and 21.9 %, corresponding to permeabilities of 378 and 329 mD, respectively. In Rønde-1 the Bunter Sandstone Formation has been buried deeper to 4058 m MD and with accompanying deterioration of the reservoir characters with an average PHIE of 11.5, and average permeability of 16 mD (Table 7.1.8). Based on mapping of the seismic data the Bunter Sandstone Formation could be expected to be encountered at depths from c. 3090 m b. msl at the top of the Havnsø structure (see section 6.1). Thus, it is inferred that the reservoir parameters in Havnsø are closer to the parameters in Stenlille compared to the values found in Rønde-1.

The same approach to quantify the reservoir parameters for the Bunter Sandstone Formation is here used as was applied for the Gassum Formation. Two Scenarios are presented, where Scenario 1 assumes the same parameters as in Stenlille-19 and Scenario 2 is based on basin wide average parameters.

Adopting the methods contained within Scenario 1 and 2 above it is possible to estimate the reservoir characteristics of the Bunter Sandstone Formation in the Havnsø structure. Firstly, it can be assumed that the Bunter Sandstone Formation is present in the Havnsø structure, as this formation is widespread regionally and the depositional environment suggest only small lateral changes compared to the Stenlille-19 well. Therefore, in Scenario 1, characterizing the Bunter Sandstone Formation is to combine the parametres from Stenlille-19 and Slagelse-1 to Havnsø (Table 7.1.7). Unfortunately, the Stenlille-19 well terminates

approximately 100 m down into the Bunter Sandstone Formation without reaching the base, but the logs and cores provide the basis for evaluating the reservoir parametres. In the Slagelse-1 well the acquired log suite does not allow for other petrophysical interpretations than the formation thickness and volume of shale. Hence, for the purpose this characterization the thickness of the Bunter Sandstone Formation is copied from the Slagelse-1 well of 393 m, whereof 118 m are sand (no porosity cut-off applicable) and the reservoir parametres are copied from the Stenlille-19, where the combined reservoir thickness is 18 m with average porosities of 19.1 % and permeability of 129 mD could be expected in the Havnsø structure. Based on this scenario the estimated reservoir characters of the Bunter Sandstone Formation in Havnsø are summarized to a total thickness of reservoir sand of 118 m with average porosities of 19.1 % and permeabilities of 129 mD, as summarized in Table 7.1.7.

Table 7.1.7. *Generalized reservoir parameters for the Bunter Sandstone Formation based on a combination of the Stenlille-19 and Slagelse-1 wells, as these wells together constitute a petrophysical basis for reservoir characterization. The average PHIE ranges from 19.1 % and the permeability of 129 mD.*

Well	Top	Gross	Net	N/G	Av_Vshale	Av_PHIE	Av_PERM
Name	*m*	*m*	*m*	*v/v*	*v/v*	*%*	*mD*
Slagelse-1	1865	393	118	0.30			
Stenlille-19	2464				0.17	19.1	129
Havnsø		*393*	*118*	*0.30*	*0.17*	*19.1*	*129*

Scenario 2 includes the surrounding wells and uses an averaging statistical method to predict the reservoir characteristics within the Havnsø structure. Table 7.1.8 lists the reservoir parametres in the six wells where the Bunter Sandstone Formation has been encountered. Similar to the approach for the Gassum Formation, the characterization of the Bunter Sandstone Formation in the Havnsø structure is then assumed to be represented by a simple average of the surrounding wells. Thereby, it is expected that the formation has a combined thickness of reservoir sandstone of 90 m, with porosity of 18.6 % and permeability of 204 mD.

Table 7.1.8. *Generalized reservoir parameters for the Bunter Sandstone Formation from the wells surrounding the Havnsø structure. These wells encounter the Bunter Sandstone Formation at different depths and also the reservoir characteristics vary significantly, as the average PHIE ranges from 11.5 % to 23.0 % and the permeability ranges from 16 to 378 mD. On average the reservoir sand in the Bunter Sandstone Formation is 90 m, 18.6 % PHIE and 204 mD permeability.*

Well	Top	Gross	Net	N/G	Av_Vshale	Av_PHIE	Av_PERM
Name	*m*	*m*	*m*	*v/v*	*v/v*	*%*	*mD*
Margretheholm-1A	2368	321	106	0.33	0.07	17.5	149
Stenlille-19	2464	104	18	0.18	0.17	19.1	149
Rønde-1	4058	575	55	0.10	0.12	11.5	16
Løve-1	1802	257	151	0.59	0.25	23.0	378
Jelling-1	1636	114	91	0.80	0.19	21.9	329
Slagelse-1	1865	393	118	0.30			
Average (Havnsø)		*294*	*90*	*0.38*	*0.16*	*18.6*	*204*

Based on Scenario 1 and 2 regarding the Bunter Sandstone Formation, the transmissivity is calculated to be 15 Dm and 18 Dm, respectively (Tabel 7.1.9). Thus, it is estimated that the Bunter Sandstone Formation is a fair to good reservoir unit within the Havnsø structure.

Table 7.1.9. *Summarizing Scenarios 1 and 2 predicting the reservoir characteristics of the Bunter Sandstone Formation within the Havnsø structure. The scenarios show fair reservoir qualities and thicknesses quantified by the transmissivity ranging from 15 – 18 Dm (Darcymeter).*

	Reservoir	**Net to Gross**	**PHIE**	**PERM**	**Transmissivity**
	m	*v/v*	*%*	*mD*	*Dm*
Scenario 1	118	0.30	19.1	129	15
Scenario 2	90	0.38	18.6	204	18
Average	*104*	*0.34*	*18.9*	*167*	*17*

7.2 Seals – Summary of geology and parameters

The primary seal of the Gassum Fm: The Fjerritslev Fm

The Lower Jurassic Fjerritslev Fm is known from more than 60 deep wells in the Danish onshore and inland water areas and the well-sections show that the present distribution is largely controlled by Middle Jurassic and younger erosional events. The lithostratigraphy and positions of the wells drilled before 1990 were compiled by Nielsen & Japsen (1991). In addition to the many widespread wells, the formation is encountered in the 19 wells on the Stenlille structure close to Havnsø. In the Stenlille area sandstones of the Upper Triassic Gassum Fm are used for temporal storage of natural gas with the Fjerritslev Fm constituting the seal (Fig. 1.3). On the storage site in Stenlille the Fjerritslev Fm is known from seismic data and from 19 deep wells showing a thickness of c. 250–300 m (Fig. 6.3.4B; Table 7.2.1). There are no deep wells drilled in the Havnsø area, so data from the Stenlille wells and other wells in the Danish Basin that surrounds the potential storage site in Havnsø are included in this summary. Other wells are Terne-1, Lavø-1, Slagelse-1, Ullerslev-1, Horsens-1 and Rønde-1 (Fig. 3.1). However, none of the other wells have so detailed information about the Fjerritslev Fm as the Stenlille wells. The detailed and extensive data from Stenlille are therefore the main source of information in understanding the Fjerritslev Fm in the Havnsø area.

The Fjerritslev Fm is a succession of marine claystones and mudstones, interbedded with thin sandstone beds. It is present in the Danish Basin, north of the Ringkøbing–Fyn High, and in the North German Basin south of the Ringkøbing–Fyn High but absent on the high itself. In the central and eastern part of the Danish Basin (including the Havnsø and Stenlille areas) the fluvial to shallow marine Gassum Fm is of Rhaetian (latest Triassic) age and is overlain by the Fjerritslev Fm of latest Rhaetian – Early Sinemurian age (Fig. 7.1.3.).The Havnsø area represents a more distal depositional setting in the Danish Basin than the Stenlille area and consequently the Fjerritslev Fm is expected to be more fine-grained and with less sandstone layers in Havnsø.

However, in the Sorgenfrei–Tornquist zone and on the Skagerrak–Kattegat Platform deposition of sand continued through the Hettangian and into the earliest Sinemurian and is included in the Gassum Fm (Nielsen 2003; Fig. 7.1.1). Towards the SE and E (southern Sweden and Bornholm) the Fjerritslev Fm is replaced by sandstone-dominated formations deposited in non-marine and coastal depositional environments (Gravesen et al. 1982, Surlyk et al. 1995, Michelsen et al. 2003).

At Stenlille, Middle–Upper Jurassic and lowermost Cretaceous sediments are missing, and the Fjerritslev Fm is unconformably overlain by the Lower Cretaceous Vedsted Fm (Dybkjær 1991, Gregersen et al. 2023; Figs. 3.3, 7.2.1). In the Havnsø area the stratigraphy is interpreted to be similar as indicated by seismic data (see section 6.1). This contrasts with areas close to the Sorgenfrei–Tornquist Zone where the Haldager Sand, Flyvbjerg, and Børglum Formations were deposited in the Middle Jurassic to earliest Cretaceous (Michelsen 1989a; Michelsen et al. 2003; Nielsen 2003). Palaeogeographical reconstructions suggest that the Ringkøbing–Fyn High and adjacent areas, including the Stenlille and Havnsø areas, were characterized by deposition of terrestrial deposits or by erosion during Middle–Late Jurassic as well as in earliest Cretaceous times (Michelsen et al. 2003; Petersen et al. 2008; Fig. 3.6). The Stenlille area was also affected by growth of the Stenlille salt pillow and the regional, mid-Cimmerian tectonic phase (Gregersen et al. 2023). From the seismic interpretation (Chapter 6) the structural evolution of the Havnsø structure is like the Stenlille structure mainly formed due to growth of a salt pillow at the base of the structure. The seismic

correlation from the Stenlille area to the Havnsø area (Chapter 6) shows an overall similar appearance and thickness of the Fjerritslev Fm, but possibly the lower part of the formation (F-Ia mb) contains less sandstones in the Havnsø area. In the Havnsø structure, the Fjerritslev Fm is approximately 260–350 m thick and are thinnest towards the top of the structure (Chapter 6; Fig. 6.3.4B) but is of similar thickness as in the Stenlille structure (Table 7.2.1; Gregersen et al. 2023).

On Zealand, the Fjerritslev Fm is well documented in the Stenlille area, where 19 wells penetrate the formation with petrophysical logs, cores and cuttings samples, which have been investigated for sedimentology and biostratigraphy (Table 4.4.2). An overview of the many results is provided in the CCS2022-2024 WP1 report dealing with the Stenlille structure (Gregersen et al. 2023). In the Havnsø area, data from Stenlille-19 is primarily used as a reference. Most of the cores in the Stenlille area have been taken in the lower part of the Fjerritslev Fm and document the transition from the Gassum to the Fjerritslev Fm.

Age of the Fjerritslev Fm

The age of the Fjerritslev Fm is well-constrained by investigations of ammonites and bivalves (Sorgenfrei & Buch 1964), ostracods (Michelsen 1975, 1989a), and palynomorphs (Dybkjær 1988, 1991; Lindström 2020; Lindström et al. 2012, 2015, 2017, 2019, 2023) showing that the formation covers the latest Rhaetian to the Toarcian, and the upper parts possibly includes Aalenian deposits locally e.g., in Hans-1, Terne-1 and Rønde-1 (Table 7.2.1). In the Stenlille area the basal part of the Fjerritslev Fm is of latest Rhaetian age and the youngest part is Late Toarcian in age and is unconformably overlain by Lower Cretaceous deposits (Dybkjær 1991; Vosgerau et al. 2016; Lindström 2020; Gregersen et al. 2023). In Terne-1 the Fjerritslev Fm is complete including the members F-Ia to F-IV with no major unconformities and the basal part is of Early Sinemurian age and the youngest part of Early Aalenian age (Nielsen 2003) (Appendix C). In Lavø-1 a few cores existed from the Fjerritslev Fm, and the revised data display a basal part (F-Ia) of Hettangian age and a youngest part (F-III) of Toarcian age. Parts of F-III and all of F-IV are missing (Appendix C). The lower part of the Fjerritslev Fm (F-I) in the Rønde-1 well is of Hettangian to early Sinemurian age whereas the youngest part (F-IV) is possibly of Aalenian age (Appendix C). In Horsens-1 the oldest part (F-I) is of Hettangian age and the upper part has been removed by erosion and the top of the formation (F-II) is late Pliensbachian in age (Appendix C). In Ullerslev-1, situated close to the Ringkøbing-Fyn High, all Jurassic strata is missing and the Upper Triassic Gassum Fm is unconformably overlain by a Lower Cretaceous succession (Appendix C). In Slagelse-1, the oldest part of the Fjerritslev Fm is F-Ia of Hettangian age and the youngest part is F-Ib of Sinemurian age, and the formation is unconformably overlain by Lower Cretaceous strata indicating a hiatus corresponding to large parts of the Fjerritslev Fm and the Middle and Upper Jurassic. The large uniformity is indicated by lithostratigraphy and seismic data, but there is no biostratigraphic data to confirm this (Appendix C).

The well-dated end-Triassic mass extinction event (ETE) is documented in cores from the lowermost part of the Fjerritslev Fm between SB 8 and TS 8 in the Stenlille wells ST-1, ST-4, ST-5, and ST-6 and provides a well-defined correlation to the Lavø-1 and Rødby-1 wells and to the latest Triassic–earliest Jurassic succession in Scania (Lindström et al. 2012; Lindström et al. 2017; Lindström et al. 2023).The event is represented by characteristic grey siltstones in the Stenlille wells forming a distinct marker bed that is correlated to the GSSP section at Kuhjoch in Austria, and to several successions in northern Germany (Lindström et al. 2017).

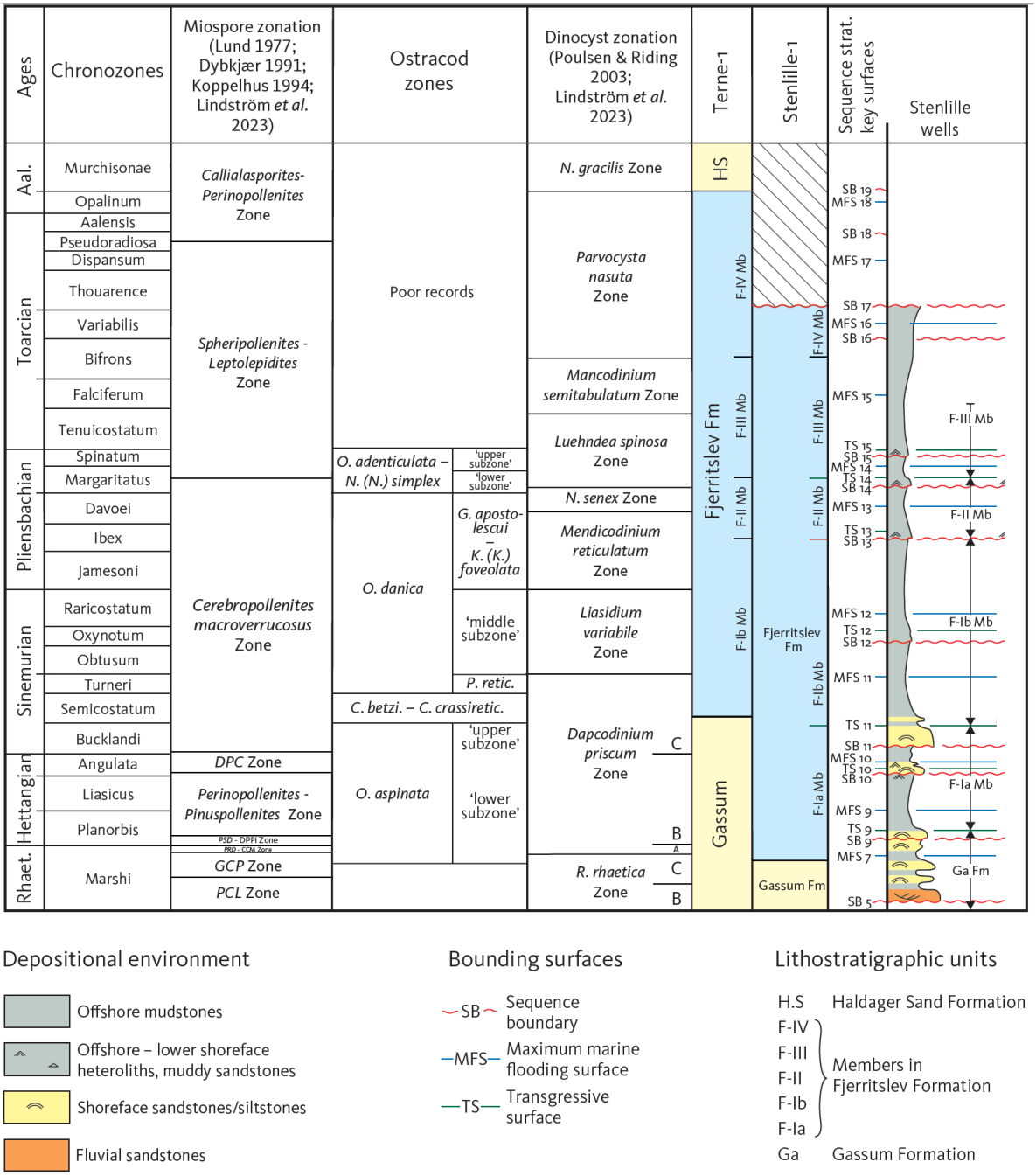

Figure 7.2.1. *Detailed litho-, bio-, and sequence stratigraphy of uppermost Upper Triassic to lowermost Middle Jurassic successions in the Danish Basin including the Stenlille-1 and Terne-1 wells. Modified from Nielsen (2003) and Pedersen et al. (2022). A major unconformity (hiatus) separates the Lower Jurassic Fjerritslev Fm from the overlying Lower Cretaceous Vedsted Fm (Fig. 6.1.1). The age gab from the uppermost preserved Fjerritslev Fm to the lowermost Vedsted Fm in the Danish Basin is varying due to different amount of erosion of the upper parts of the Fjerritslev Fm. Terne-1 well, located in the Sorgenfrei-Tornquist Zone, comprises the youngest preserved Fjerritslev Fm of early Aalenian age. The chronostratigraphy (ages and ammonite zones) is based on Gradstein et al. (1994). The right part of the scheme is copied from Nielsen (2003) and needs to be revised applying the latest timescale of Gradstein et al. 2020 and new biostratigraphic data (e.g., Lindström et al. 2023). Such a revision will include a thorough adjustment of the ages and duration of the biozones and depositional sequences; however, lithology, reservoir parameters and thus storage volumes will not be influenced by the changes.*

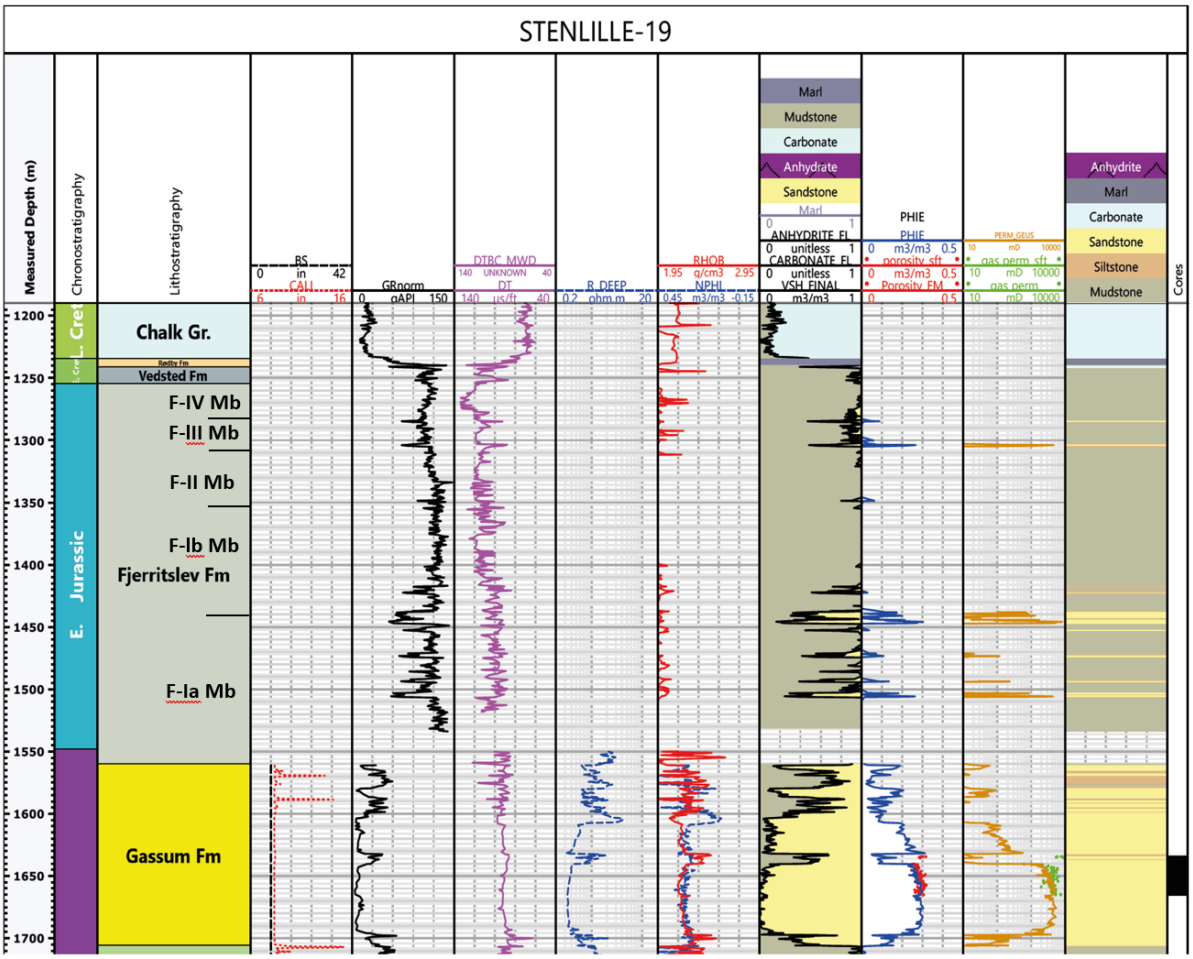

Figure 7.2.2. *Petrophysical logs from Stenlille-19 well with the primary reservoir sandstone successions of the Gassum Fm and the overlying mudstone seal successions of the Fjerritslev Fm (primary seal), followed by the Vedsted Fm to the Chalk Group (secondary seals). The Fjerritslev Fm is subdivided into informal members dominated by mudstones. Note that the lowermost F-Ia member contains a number of thin sand- and siltstone layers in contrast to the other members. The figure is a zoomed section from Fig. 7.1.1.*

Lithological subdivision

The Fjerritslev Fm was defined by Larsen (1966) and revised by Michelsen (1978, 1989a; Michelsen et al. 2003). The formation is divided into five informal members F-Ia, F-Ib, F-II, F-III, and F-IV using the Hyllebjerg-1 as reference section (Michelsen 1989a). A detailed correlation between wells located centrally in the Danish Basin shows that characteristic log-patterns can be traced across long distances suggesting that the formation comprises a high number of thin, but laterally continuous depositional units (Michelsen 1989b). A sequence stratigraphic division of the Gassum and Fjerritslev Formations was presented by Nielsen (2003). The base of Fjerritslev Fm is defined at TS 7 in the central part of the Danish Basin and in the Stenlille and Havnsø areas. The boundaries of the five members (F-Ia to F-IV) correlate to sequence stratigraphic surfaces (Table 7.2.1) (Nielsen 2003).

The log-patterns described by Michelsen (1989b) are difficult to recognize in the Stenlille wells. Here thin sandstones with large lateral continuity are present in the F-Ia member, separated by clay- and mudstones (Fig. 7.2.3). Deeper into the basin, the F-Ia member consists of claystones and mudstones only, whereas it is laterally equivalent and contemporaneous

with the Lower Jurassic part of the Gassum Fm toward the basin margins. Lateral variations in thickness of the Fjerritslev Fm in wells surrounding the Havnsø structure are shown in Table 7.2.1. The F-Ia member is the thickest of the members and is even thicker in Stenlille than further to the northwest in the Danish Basin. In contrast, the F-Ib to F-IV members are thin at Stenlille compared with central to northern Jutland (Table 7.2.1; Figs. 7.2.3, 7.2.4).

Fjerritslev Fm											Age
Location/wells				N. Jutland	Rø-1	Lavø-1	ST-19	Sl-1	Ul-1	Ho-1	
Depth (m) to		Top Fjerritslev Fm		~1920	2138	2072.3	1254.5	972.9	None	1294.4	Toarcian
		Base Fjerritslev Fm		~2400	2613	2133.9	1560	1150		1533.8	L. Rhaet.– E. Sinemurian
		Thickness (m)		~500	475	61.6	305.5	177.1		239.4	
		Sequence stratigraphy		Thickness (m)							
		Lower boundary	Upper boundary								
Lithostratigraphy	F-IV mb	SB 16*	SB 19	30 – 50	38	None	61.5	None	None	None	Toarcian
	F-III mb	TS 14	SB 16*	150 – 200	145	31.1					Early Toarcian
	F-II mb	SB 13	TS 14	30 – 80	73	30.5	39	None		21.9	Pliensbachian
	F-Ib mb	TS 11	SB 13	150	141	None	83	60.5		136,4	Sinemurian–E. Pliensbachian
	F-Ia mb	TS 7 / TS 9	TS 11	75 – 80	64		122	116.5		83	Rhaetian – Hettangian

Table 7.2.1. *Thicknesses of the members of the Fjerritslev Fm in wells from Danish Basin south of the Sorgenfrei-Tornquist Zone. Note that some of the wells have no core material in the unit of interest. This is discussed in the text. * The lower boundary of the F-IV member is positioned between MFS 15 and SB 16. The column N. Jutland is a compilation of characteristic thicknesses in Hyllebjerg-1, Kvols-1, Skive-1, and Hobro-1 wells south of the Sorgenfrei–Tornquist Zone (Michelsen 1989b). Rø-1, Rønde-1; ST-19, Stenlille-19; Sl-1, Slagelse-1; Ul-1, Ullerslev-1 and Ho-1, Horsens-1. The biostratigraphy in ST-19 are from Gregersen et al., 2023; the other biostratigraphic data is conducted in this study. Sequence stratigraphy after Nielsen (2003: fig. 31) and modified in this study also with the calculated thicknesses.*

The F-Ia member

The data from Stenlille are the main source of information in understanding the Fjerritslev Fm in the Havnsø area and are therefore presented here in detail. The main difference between the two depositional areas is that the sediments in Havnsø are interpreted to be deposited in a more central part of the Danish Basin compared to Stenlille and consequently the sediments are presumably finer grained. Thus, the lithology in Havnsø is probably muddier, more homogenous and contain less pronounced sandstone and siltstone beds. Seismic interpretation (Chapter 6) supports this hypothesis and indicates rather uniform seismic facies of the Fjerritslev succession towards Havnsø from Stenlille, indicating a rather uniform lithology (mudstone), with few local amplitude changes e.g., near TS 11 (Top F-Ia), which may indicate sandstone (see section 6.1).

In Stenlille, the F-Ia member is bounded by the sequence stratigraphic surfaces TS 7 and TS 11. The member is around 120 m thick, and the lithology and biostratigraphy in the lower part

of the member is well documented in cores from several wells (Fig. 7.2.3). The member comprises several sedimentary facies ranging from laminated claystones to heterolithic mudstones interpreted as deposited in lower offshore to lower shoreface environments (Pedersen 1985). It differs in lithology from the overlying members by containing a number (c. 7–10) of sandstone and siltstone units, 1–20 m thick, which can be traced laterally with varying thickness (Fig. 7.2.3; ST-1, ST-4, ST-5 and ST-6). Interpretation of the well-logs show that some sandstone beds are well-sorted with high porosities and permeabilities whereas other units, with intermediate values, probably are heterolithic (Vosgerau et al. 2016). The sandstones are interpreted as shoreface sandstones (Nielsen 2003). The lower part of the F-Ia member includes a series of grey siltstone beds between SB 8 and TS 8 (Lindström et al. 2015). The siltstones constitute a distinct chronostratigraphic marker bed with wave-ripple cross-lamination, water-escape structures and numerous soft-sediment deformation structures indicating deposition in a shoreface environment around fair-weather wave base. The siltstones mark a sudden shallowing compared to the black claystones below, which includes MFS 7, and to the mudstones above.

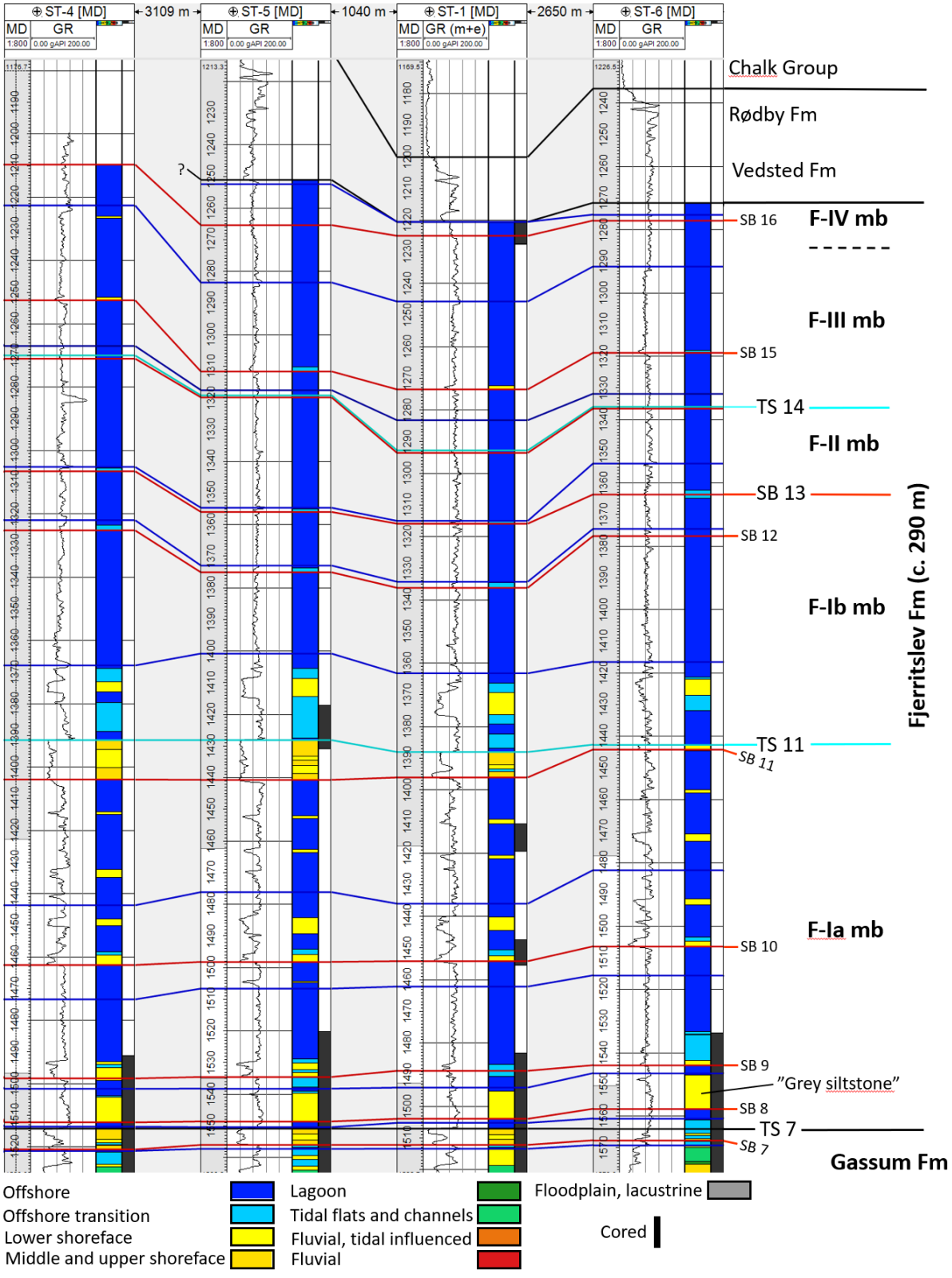

Figure 7.2.3. *Lateral changes in facies through the Fjerritslev Fm. Sequence stratigraphic surfaces define the boundaries between the members in the Fjerritslev Fm. Cored intervals are shown in black. Note that here are slight variations in the thickness of each member laterally. For location of the wells see Figure 4.1.2.*

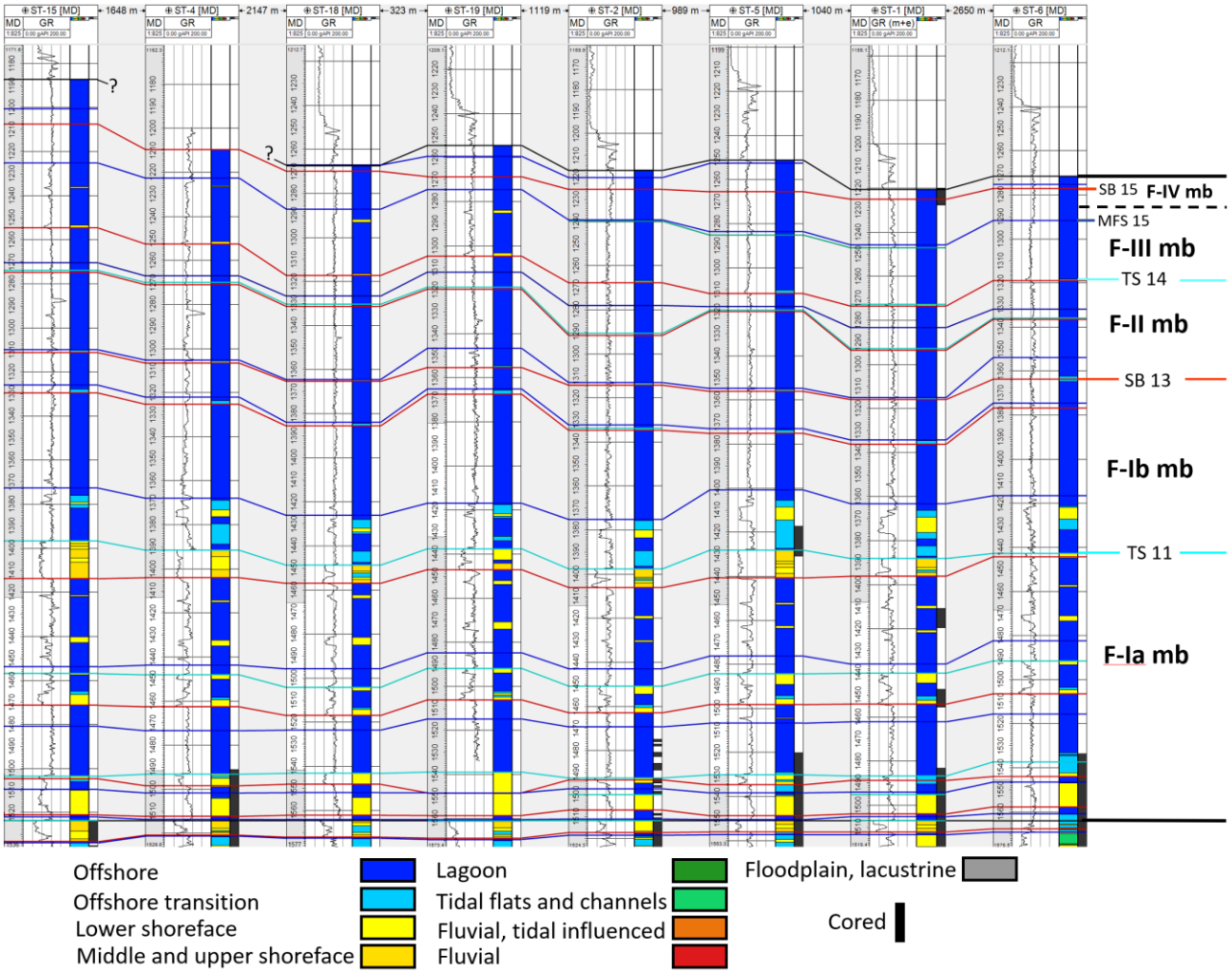

Figure 7.2.4. *Correlation of petrophysical logs and interpreted lithologies in the Fjerritslev Fm (members F-Ia to F-IV) in wells from the Stenlille area. The logs demonstrate lateral continuity, and minor variations in lithologies and thicknesses. Cores are available mainly from the basal part of the F-Ia member. The upper core in Stenlille-1 (core 2) contains the boundary between the Fjerritslev and Lower Cretaceous Vedsted Formations in its uppermost part.*

The siltstones contain the *Polypodisporites-Riccisporites-Deltoidospora* Zone, which formed during the global end-Triassic mass-extinction (ETE) that is linked to volcanic activity in the Central Atlantic Magmatic Province (CAMP), atmospheric changes, increased wildfire activity and deforestation causing increased erosion in the hinterland and larger influx of silt and sand (Fig. 7.2.5) (Petersen & Lindström 2012; Lindström et al. 2015, 2017, 2023).

The F-Ib member

In the Stenlille area the F-Ib member is characterized by a thin sandstone bed in the basal part overlayed by uniform fine-grained mudstones with a relatively high content of organic matter (Figure 7.2.3). Samples from the Gassum-1 well (Fig. 3.1, eastern Jutland) show that the marine fauna of benthic bivalves perished in the lower part of the F-Ib member probably caused by a change from normal marine to restricted (oxygen-poor) sea-floor environments (Pedersen 1986). The ostracod fauna also shows a major change in species (Michelsen 1975). The faunal changes in the F-Ib mb are interpreted to reflect a marine sea-level rise

during the Sinemurian to Pliensbachian that also led to a lithological change in Northern Jutland where deposition of coastal sand (Gassum Fm) was replaced by marine mudstones (Fjerritslev Fm; Nielsen 2003: figs. 25, 31). The transgression is also recorded in southern Sweden and at Bornholm (Frandsen & Surlyk 2003; Donovan & Surlyk 2003). The thin sandstone bed in the basal part of the F-Ib member followed by uniform mudstones is interpreted as formed during the sea-level rise and transgression. Similar lithological successions are interpreted to be deposited in the Havnsø constituting the F-Ib member.

The F-II member

In northern Jutland, the F-II member is characterized by influx of sand and silt, which resulted in deposition of heterolithic sand. This was not the case in the Stenlille area, where the member is fine-grained and difficult to distinguish from the F-Ib member below and the F-III member above. The Havnsø area was probably also experiencing deposition of fine-grained material. The F-II member is bounded by SB 13 and TS 14 surfaces (Figs. 7.2.3, 7.2.4). It may be speculated, that sand, supplied from the NE, E and SE was trapped in the Øresund Basin and that the eastern part of the Danish Basin was a starved basin during deposition of the F-II member.

The F-III and F-IV members

The gamma-log values recorded in the Fjerritslev Fm at Stenlille show very little contrast between the F-II, F-III and F-IV members (Fig. 7.2.3). The F-III mb is around 20 m thick, and clearly condensed in comparison with northern Jutland, where it is 150–200 m thick (Table 7.2.1). Petersen et al. (2008) examined the amount and composition of the organic matter contained in the Toarcian marine mudstones of the F-III and F-IV members in the central part of the Danish Basin. These members locally include intervals with hydrogen index (HI) values of 300–400 mg HC /g TOC (HC: hydrocarbons; TOC: total organic carbon) see also Michelsen (1989b). The high values indicate that the mudstones were deposited in deep-water with anoxic or oxygen-poor marine environments. This agrees well with the lack of benthic fauna in the F-III member in the Gassum-1 well (Pedersen 1986). The mudstones are probably very fine-grained with a low permeability.

The F-IV member is up to 45 m thick in the Stenlille wells (Figs. 7.2.3, 7.2.4). Palynomorphs from the F-IV member in the Stenlille-2 well indicate that deposition of marine mudstones continued into the Toarcian (Dybkjær 1991). The thickness is comparable to that of the member in northern Jutland (Table 7.2.1, Fig. 7.2.1). The major hiatus between the Lower Jurassic Fjerritslev Fm (Toarcian F-IV mb) and the Lower Cretaceous Vedsted Fm in Stenlille, and the faults in the Fjerritslev Fm, may have been caused partly by uplift and erosion due to growth of the Stenlille salt pillow, and partly by regional Mid Jurassic uplift. A similar tectonic evolution is probably the case for the Havnsø structure (Section 6.2; Gregersen et al. 2023). Similar hiati are recorded in Horsens-1, Slagelse-1 and Lavø-1 and are interpreted to reflect Mid Jurassic uplift and erosion (Nielsen and Japsen 1991; Nielsen 2003) (Appendix C).

Bulk mineralogy

The bulk mineralogy of the Fjerritslev Fm was examined in 12 samples from Stenlille-5 (Mathiassen et al. 1989). The data show a positive correlation between quartz and feldspars which suggest that both minerals dominate the coarse silt to sand fractions. This interpretation is supported by a negative correlation between quartz (and feldspars) and clay minerals.

The bulk mineralogy of mudstones from the Gassum and Fjerritslev Formations are shown in Vosgerau et al. (2016). Quartz is the dominant mineral in all samples followed by kaolinite and illite or mica. Feldspars are present in some samples. Calcite, siderite, or pyrite are present in some samples, mainly in the mudstones.

Clay minerals

Mathiassen et al. (1989) also examined the clay mineral assemblage in the mudstone facies, which are characterized by clay- to fine-grained silt sized particles. Total organic carbon (TOC) and pyrite (FeS_2) correlate with the clay content. The analyses of samples from the lower part of the Fjerritslev Fm in ST-5 and ST-6 show that the mudstones generally contain ≤ 60% clay minerals, quartz (≥20 %), feldspars (≤5%), pyrite (≤5%) and varying contents of calcite or siderite (Mathiassen et al. 1989). Clay mineral analyses from the Fjerritslev Fm are few, but some results were included in Vosgerau et al. (2016). They show that kaolinite is the dominant clay mineral followed by mixed-layer clays, and illite. Vermiculite is present in small amounts and smectite was not recognized. Ten samples from the Fjerritslev Fm in Kvols-1 (northern Jutland) shows little variation through the formation. All samples are dominated by kaolinite, followed by mixed-layer minerals, vermiculite, and mica. A similar mineral assemblage is reported from the Lower Sinemurian section at Örby (Scania, southern Sweden). Here the clay mineralogy is characterized by kaolinite and mica throughout the section and increasing amounts of chlorite and mixed-layer minerals occur in the marine deposits (Erlström et al. 1999).

Diagenesis, burial and exhumation

Vitrinite reflectance values are a proxy for maximum temperatures during burial. Petersen et al. (2008) measured 560 vitrinite reflectance (VR) values in samples from 26 wells in the Norwegian–Danish Basin and concluded that the Fjerritslev Fm experienced a significant post Early Cretaceous uplift in most of the basin. The data closest to the Stenlille and Havnsø areas are from the Rønde-1 well and it was estimated that the Fjerritslev Fm in this well was uplifted c. 400 m. Based on study of the sonic velocities measured in Stenlille wells Japsen & Bidstrup (1999) estimated that the Fjerritslev Fm was uplifted c. 600 m during Neogene time in this area. This extra burial depth may be considered when the capacity and quality of the Fjerritslev seal is evaluated.

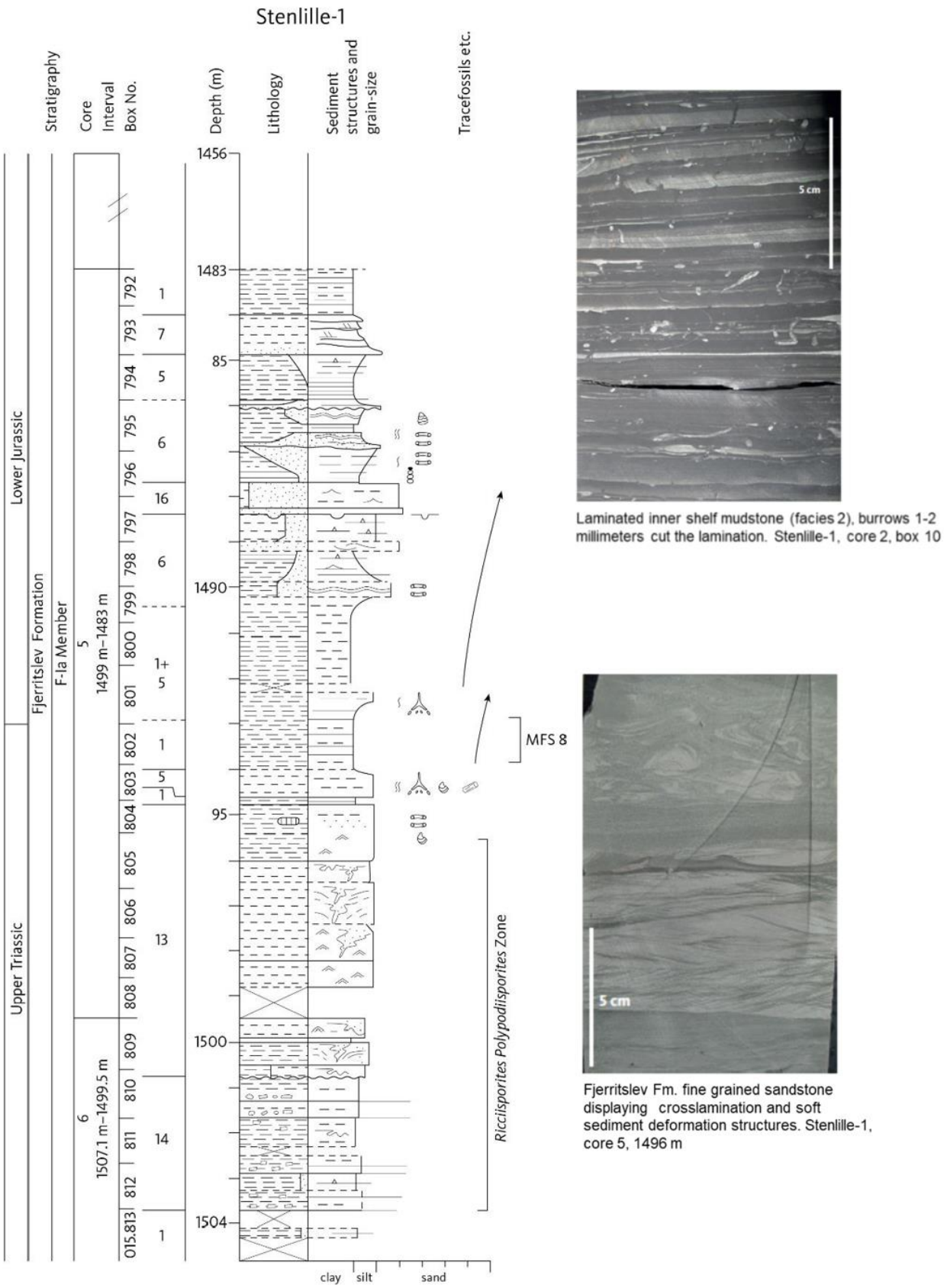

Figure 7.2.5. *Sedimentological logs of the transition from the Gassum Fm to the lowermost part of the Fjerritslev Fm (F-Ia mb) with examples of core photos from the Stenlille-1 well. From Pedersen et al. (2022).*

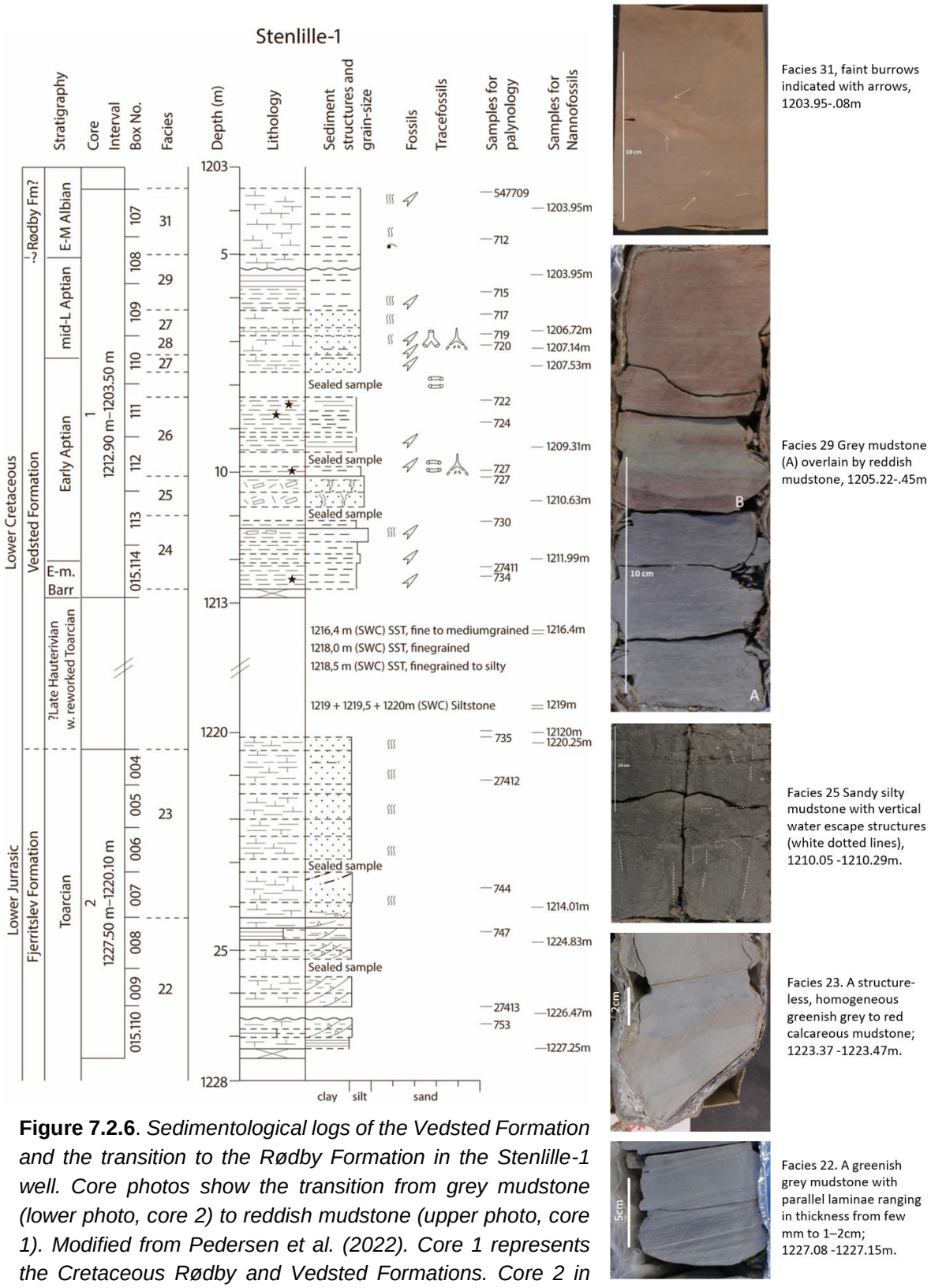

Facies 31, faint burrows indicated with arrows, 1203.95-.08m

Facies 29 Grey mudstone (A) overlain by reddish mudstone, 1205.22-.45m

Facies 25 Sandy silty mudstone with vertical water escape structures (white dotted lines), 1210.05 -1210.29m.

Facies 23. A structure-less, homogeneous greenish grey to red calcareous mudstone; 1223.37 -1223.47m.

Facies 22. A greenish grey mudstone with parallel laminae ranging in thickness from few mm to 1–2cm; 1227.08 -1227.15m.

Figure 7.2.6. *Sedimentological logs of the Vedsted Formation and the transition to the Rødby Formation in the Stenlille-1 well. Core photos show the transition from grey mudstone (lower photo, core 2) to reddish mudstone (upper photo, core 1). Modified from Pedersen et al. (2022). Core 1 represents the Cretaceous Rødby and Vedsted Formations. Core 2 in Stenlille-1 (1220.1-1227.5m MD) is shown with a revised Top Fjerritslev at the dashed black line (Gregersen et al. 2023). It is difficult to recognize a lithological boundary between the Fjerritslev and Vedsted Formations in two apparently similar fine-grained sediments.*

Seal capacity of the Fjerritslev Fm

The seal capacity of the Fjerritslev Fm was examined by Springer et al. (2020). They state, in their summary, that the sealing capacity of the Fjerritslev Fm has mostly been studied in the Stenlille area. Here, the seal succession is the c. 250–300 m thick Fjerritslev Fm, with interbedded porous sandy-silty layers (within the F-Ia member) that divide the seal into a lower and upper seal unit (Gregersen et al. 2023). Average porosity is 11%, and air-permeability is 160 µD. A single liquid permeability measured at in situ conditions in a massive mudstone layer from Stenlille reached a value of 3 nD, which is like the best petroleum caprocks known. A few other overburden measurements gave liquid permeabilities around 200 nD (Springer et al. 2020). Thus, the Fjerritslev Fm, and in particular its upper part above the F-Ia member, is an excellent seal in the Stenlille area, where natural gas has been stored in the Gassum Fm below the seal for more than 30 years. The good quality of the seal is probably a function of mineralogic composition, high content of organic material and the pre-Neogene maximum burial depth in combination with the great overburden thickness. The Fjerritslev Fm in the Havnsø area has probably gone through a similar geological history and the seal capacity in that area is most likely comparable to the Stenlille area. However only core data of the Fjerritslev Fm from the Havnsø area can confirm this.

Capillary entry pressure

The critical rock property for fluid entering the seal is the capillary entry pressure of the rock. Experiences from the petroleum industry confirms that shales in general are excellent caprocks. Capillary drainage displacement experiments by Mercury injection (MICP, Mercury Injection Capillary Pressure) is a fast technique to obtain entry pressures for caprocks. The governing parameters for the capillary entry pressure are the pore-throat size distribution and the wetting properties of the rock-fluid system.

One disadvantage for using MICP to evaluate seal capacity is the fluid system used: Mercury as the displacing fluid and air vacuum as the initially saturating fluid of the rock sample. Results from the mercury/air system must be converted into the CO_2 brine system, which depends on the ratio of the product of the contact angle and interfacial tension for the two fluid systems, which gives some uncertainties.

Using standard values for conversion of the capillary entry pressure to a brine/air system gave results in the range of 5–10 MPa (Springer et al. 2020). New MICP measurements on samples from the Fjerritslev Fm were conducted on both cores and cutting samples from the Stenlille-1 and Stenlille-2 wells. MICP measurements were also conducted on cutting samples from Stenlille-6. The new samples gave a somewhat lower range of 1–5 MPa.

The governing process for the seal capacity for CO_2 storage is the buoyancy force exerting on the caprock from the density difference between the formation water and the injected CO_2. The height of the CO_2 column in the reservoir below the caprock determines how high a pressure can be obtained (cf. Fig. 7.2.7).

Using the values from both Springer et al. (2020) and the newly obtained capillary entry data, a range of column heights can be calculated from approximate 290 m to more than 1000 meters.

With the relief on the Havnsø structure measured from the top of the structure (at the Top Gassum surface) and down flank near the lowest contour, a relief of approximate 200 meters can be determined. More data is needed from the Fjerritslev Fm, but it can be accessed that the formation is an excellent primary seal for the Gassum Fm with good sealing capacity.

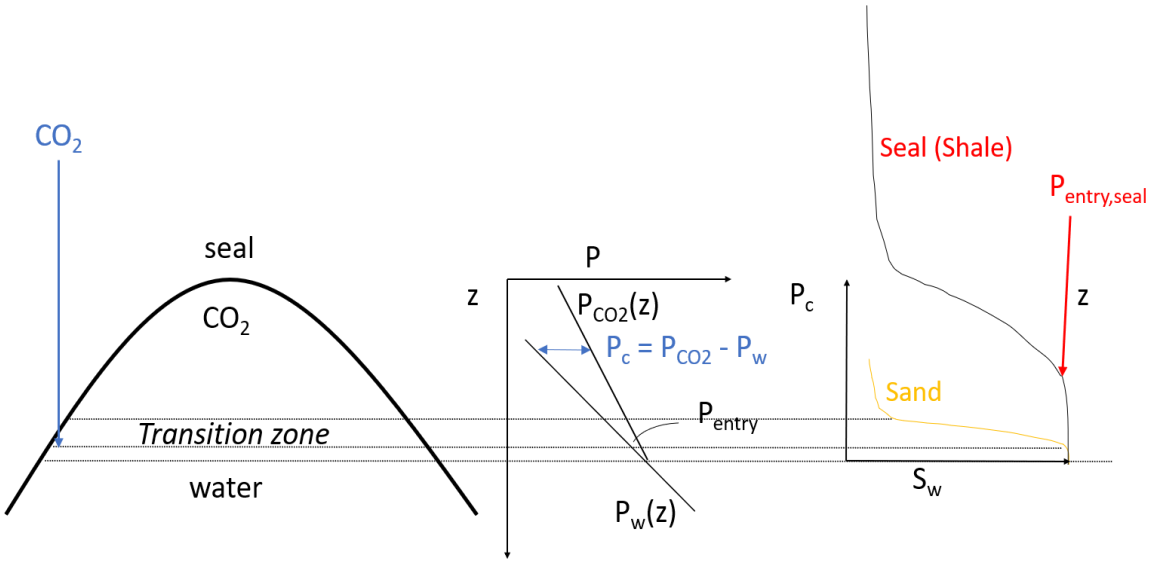

Figure 7.2.7. *Difference in the pressure gradients between the formation brine and the injected CO_2 determines the pressure or column height that the caprock can withstand ($P_{entry,seal}$). Seal (caprock) and sandstone have substantially different capillary entry pressures.*

Secondary seals of the Gassum Fm: The Vedsted Fm, Rødby Fm and Chalk Group

The seismic mapping indicates that in Havnsø the primary seal, the Fjerritslev Fm, is overlain by the Lower Cretaceous Vedsted and Rødby Formations and the Upper Cretaceous Chalk Group, which is around 1000 m thick. The Chalk Group is overlain by 230–300 m of Cenozoic to Quaternary strata including Danian limestones, Selandian greensand and marl, and Quaternary deposits. In Stenlille, the secondary seals of the Gassum Fm above the Fjerritslev Fm comprise the Lower Cretaceous Vedsted and Rødby Formations and the lower part of the Upper Cretaceous Chalk Group (Fig. 6.1.1). These formations have never been the main target for coring in the Stenlille area or in other areas in close vicinity to the Havnsø structure (Table 4.4.2). However, one core from the Stenlille-1 well potentially spans part of the Vedsted and Rødby Formations and a core from the Stenlille-5 well spans the lower part of the Chalk Group. Core 2 from Stenlille-1 has previously been dated as Lower Cretaceous but new palynological dating suggests a Lower Jurassic age (Toarcian) (Gregersen et al. 2023). Sparse biostratigraphic information from the Lower Cretaceous may be found from offset wells such as Ullerslev-1, where samples from 826-829 m are dated as Late Hauterivian (BC9-10) and samples from 2022-2027 m in Lavø-1 that is dated as Late Hauterivian (nannofossil Zones BC9-10 of Bown et. al 1998). From the Upper Cretaceous one sample from the1060-1065 m interval in the Horsens-1 well was dated as Early Campanian to Santonian, nannofossil subzones UC11c-UC14c (Burnett 1998), and a sample from the 1070-1071 m interval is dated as Santonian (UC11-13). In Lavø-1, a sample from the 1946.5-1951.8 m interval is dated as Late Turonian (UC8a-9a) (Fig. 7.2.8).

Results from studies of Stenlille-1, and -5 will be presented here with comments on a few other Stenlille wells because they are hitherto the most detailed studies of the Lower Cretaceous and basal Upper Cretaceous in close vicinity to the Havnsø area. The nannofossil zonation of Burnett (1998) and chronostratigraphy in Gale et al. (2020) is applied in the revised biostratigraphy of the Lower and Upper Cretaceous.

The Vedsted Fm of the Danish Basin spans the Valanginian to Albian. The lower boundary of the Vedsted Fm coincides with the transition from marine silty claystones to less silty claystones (Larsen 1966). The Rødby Fm, which overlies or in some places was deposited at the same time as the upper part of the Vedsted Fm, consists of marine red marlstones and marly chalks. Its base is suggested to be late Aptian or early Albian in age in the Danish Basin (Sorgenfrei & Buch 1964) and its upper boundary to the Late Cretaceous Chalk Group is late Albian to early Cenomanian in age (Lauridsen et al. 2022; Jensen et al. 1986). Mudstones and carbonate beds forming the upper part of the Vedsted Fm and the overlying Rødby Fm were deposited in a mixed siliciclastic-calcareous depositional system indicating lowstands when marly chalk and marl dominated deposition, and highstands when pure chalk was being deposited (Ineson 1993; Ineson et al. 1997). Onset of pelagic carbonate production started in the late Early Cretaceous (late Albian) and dominated the depositional environment in the Danish Basin from the Early Cenomanian. In the Lavø-1 well the siliciclastic sedimentation lasted into Early Cenomanian. The lower part of the Upper Cretaceous is characterised by white, hard chalk intercalated with marly beds.

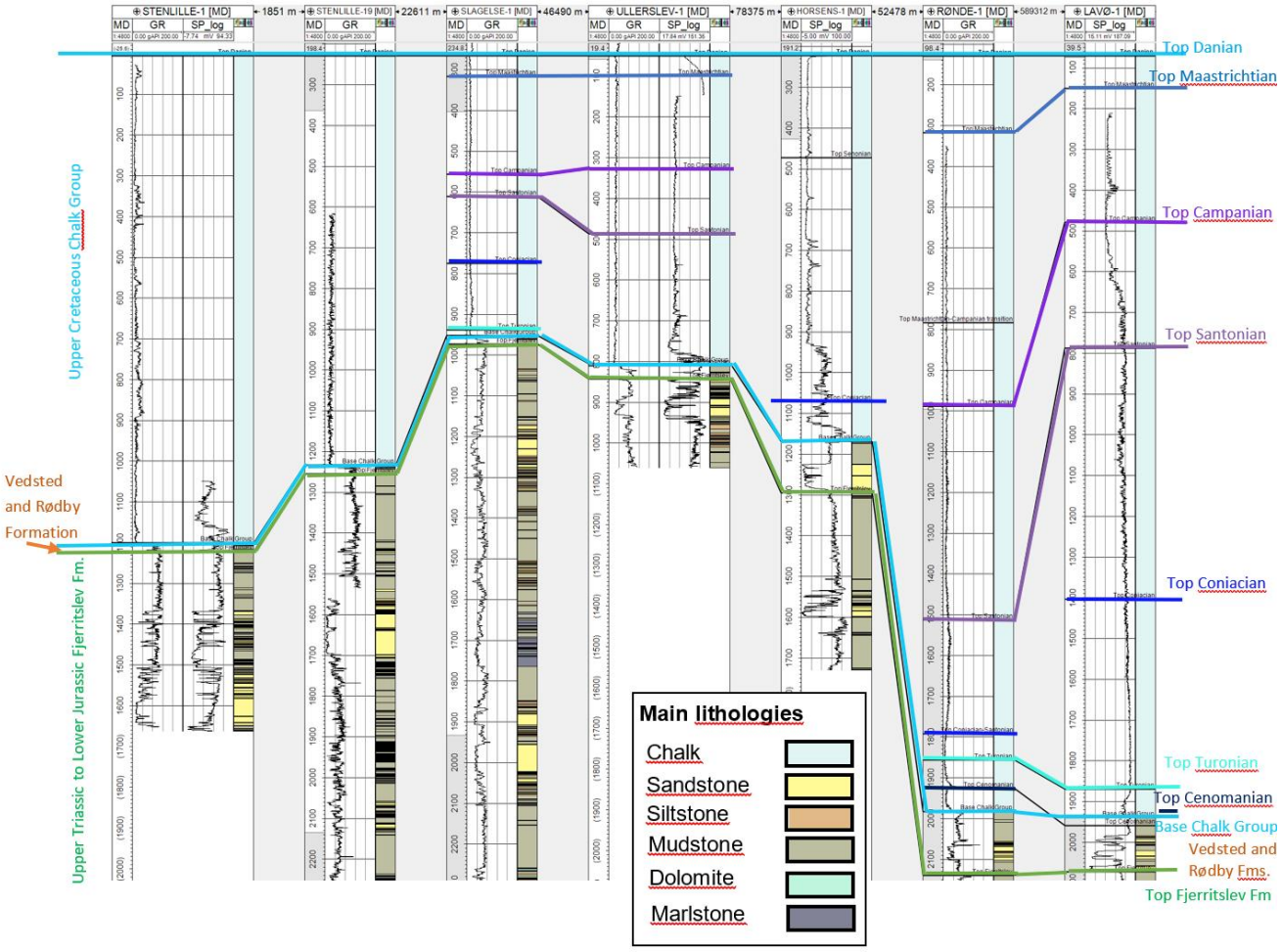

Figure 7.2.8. *Correlation panel of the Upper Cretaceous 'Chalk Group' and Lower Cretaceous succession with interpreted facies associations, flattened on Top Danian (top Chalk Group). Selected core chips were dated using nannofossil biostratigraphy (this study). More work is needed to compare data from the cored parts of wells representing the lower part of the Chalk Group to identify the exact position of the Basal and Lower Chalk.*

The Lower Cretaceous Vedsted Fm varies in thickness from a maximum of 700 meters in the Fjerritslev Trough in the northern Danish Basin to around 50 meters or less in the eastern and southeastern parts of Denmark (e.g., in the Slagelse-1 and Stenlille-1 wells where less than 23 m and 42 m, respectively, of Lower Cretaceous strata are preserved). An example of the vertical variation within the Vedsted Fm can be seen in a new core study of the Vinding-1 well located further to the west at the southern margin of the Danish Basin (Lauridsen et al. 2022). New biostratigraphy of the Vinding-1 cores indicates the presence of several hiati in the sedimentary record during the Lower Cretaceous suggesting a combination of discontinuous sedimentation and several erosional events. Erosion was most pronounced along the basin margins (e.g., only around 15 m of Lower Cretaceous strata is preserved in the Ullerslev-1 well). The Ringkøbing–Fyn High remained an uplifted landmass from Middle Jurassic to Early Cretaceous time and formed the southern border of the Danish Basin (Michelsen et al. 2003). Compared with the Lower Cretaceous successions in the central part of the Danish Basin in northern Jutland, the successions in the Stenlille wells, Slagelse-1, Horsens-1 and Vinding-1 are thinner, reflecting a location with less accommodation space along the

basin margin. The Rønde-1 well may represent a more central position in the basin, whereas the Lavø-1 well location may have experienced fault-controlled subsidence and accommodation due to the proximity to the Sorgenfrei-Tornquist fault zone. Seismic mapping indicates that the composite thickness of the Vedsted and Rødby Formations (Top Fjerritslev to Base Chalk) in the Havnsø area is mostly c. 30–60 m (thinnest at the top of the structure), and thus comparable to the thickness in the Stenlille structure. The formations are approximately up to 50 meters thick in the Stenlille and the Horsens-1 wells.

The upper boundary of the Vedsted/Rødby Formations towards the Upper Cretaceous Chalk Group is supposedly transitional, and the lower part of the Upper Cretaceous section is characterised by the presence of numerous marl layers in the lower 200–300 meters.

The Vedsted Fm in the Stenlille area

The Vedsted Fm in the Stenlille area has been studied in more details than in the cores from the surrounding wells and the Stenlille results are therefore presented here as the most likely analogue for the formation in the Havnsø area. In Stenlille, the Vedsted Fm is interpreted to have a thickness between 11.5 to 49 m based on petrophysical log interpretations (Fig. 7.2.9). The lower part of the Vedsted Fm comprises siltstones, mudstones, and sandy and silty mudstones, slightly changing in colour from grey to more reddish mudstones. The carbonate content increases upwards towards the Rødby Fm. According to the completion reports, the boundary between the Fjerritslev and the Vedsted Formations was picked at a distinct log marker recognisable in all Stenlille wells. This log marker apparently coincides with a minor change in lithology. Only one core (Stenlille-1, core 2) exists from this boundary interval to confirm this. However, our recent studies of the Stenlille wells, reveal that it is difficult to recognize a lithological boundary in two apparently similar fine-grained sediments (Fig. 7.2.6) (Gregersen et al. 2023). Detailed studies of palynomorphs and calcareous nannofossils in this boundary interval reveal a rich association of Lower Jurassic palynomorphs indicating the *Spheripollenites-Leptolepidites* Zone of Toarcian age with a few Early Cretaceous dinoflagellates in the lower parts of the well. A little further up in the well the samples contain a rather diverse Early Cretaceous palynomorph and dinoflagellate association of possible Hauterivian age. The nannofossils indicate an early Late Hauterivian age (nannofossil zones BC9-10 of Bown et. al 1998). The mixing of Early Jurassic and Early Cretaceous fossil associations is typical of a transgressive lag and is interpreted as the results of the Early Cretaceous transgression which eroded and redeposited Lower Jurassic sediments. The boundary of the Fjerritslev and the Vedsted Formations is therefore tentatively placed at 1220.5 m in Stenlille-1, supported by the marked decrease on the gamma ray log indicating a possible sequence boundary.

More work is needed to evaluate the age and consequently the sequence stratigraphic framework of all Stenlille cores, but the study of Gregersen et al. (2023) confirms a major hiatus spanning the latest Early Jurassic, Middle to Late Jurassic and the earliest part of Early Cretaceous (Late Hauterivian) in the Stenlille area and most likely also in the area around Havnsø. See also the logs (links in Appendix C).

The Rødby Fm in the Stenlille area

The Rødby Fm in the Stenlille area has been interpreted based on log patterns to measure between 4 and 8.2 m in thickness (Fig. 7.2.9). The Rødby Fm is only partly covered by a core in the Stenlille-1 well, by sidewall cores in Stenlille-8 and by ditch cutting samples of Stenlille-

5. The base of the Rødby Fm in the Danish Basin is suggested to be late Aptian to Early Albian in age and ranges possibly up into the Early Cenomanian in some areas. The Rødby Fm is represented by marlstones and marly chalks.

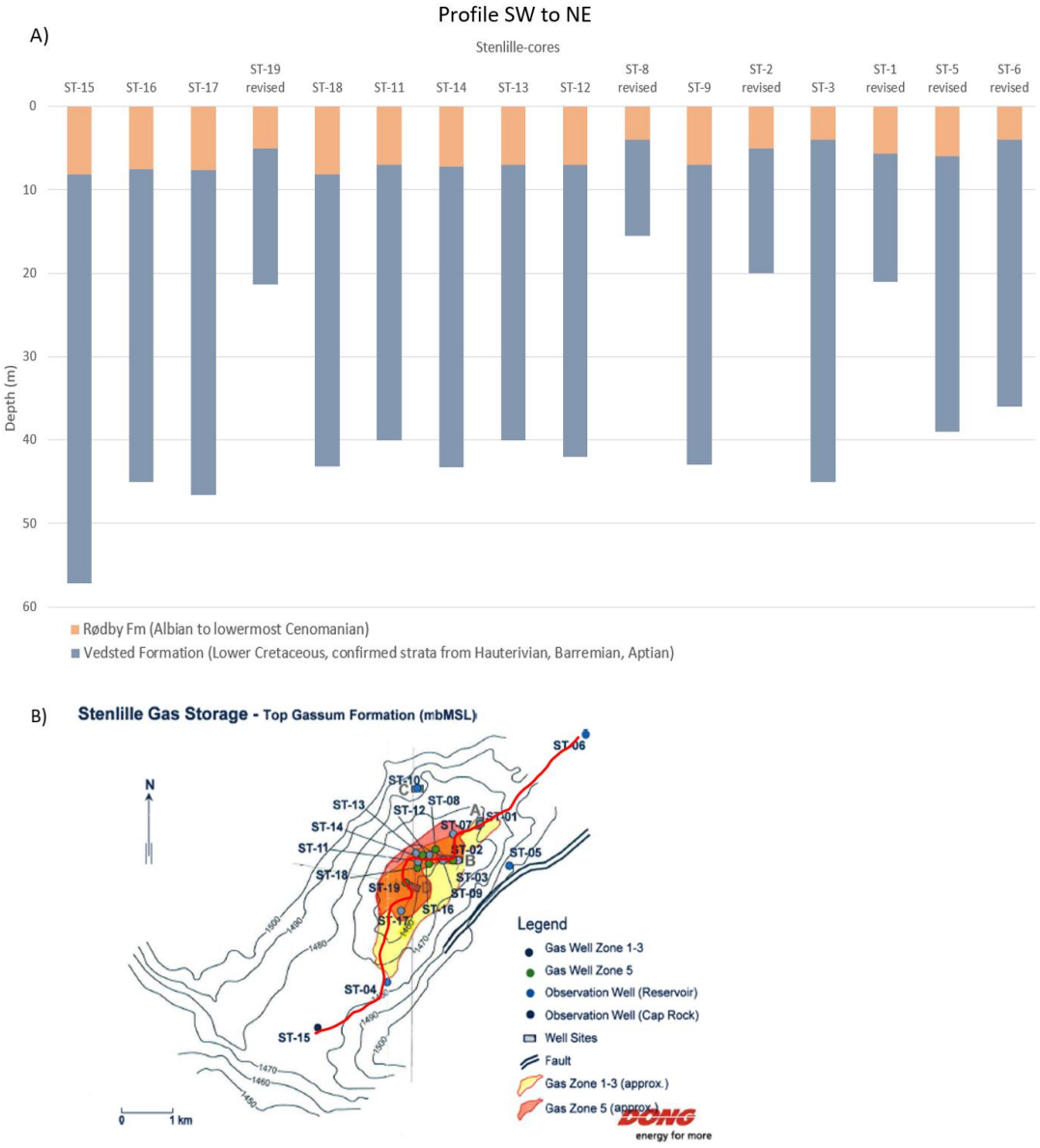

Figure 7.2.9. A) *Thickness of the Vedsted and Rødby Formations in the Stenlille area. Note that the Vedsted Fm of Stenlille-1, -5, and -8 has been revised based on biostratigraphy, and Stenlille-6 and -19 have been revised based on gamma ray log patterns. In all wells the revision has led to a significant reduction in the thickness of the Vedsted Fm. The variations and implications for this difference are discussed in the text. Note that the thicknesses of the formations are particularly thick in Stenlille-15 and -5 (also after revisions), probably reflecting these wells position on the flank of the structure. B) Position of the different wells in the Stenlille area and a red line showing the order they appear on the diagram in A). Map from DONG.*

The Chalk Group in Stenlille

The Chalk Group in the Stenlille area has been divided into a “Basal Chalk” representing the oldest parts of the Chalk Group followed by a “Lower Chalk”, “Campanian Chalk”, “Maastrichtian Chalk” and Danian Limestone. In this report only the “Basal and Lower Chalk” will be discussed in some detail, but a basic subdivision of the upper parts of the Chalk Group is shown on Figure 7.2.8 where chronostratigraphic subdivision is based on biostratigraphic or final well reports. However, more work is needed to compare data from the cored parts of wells representing the lower part of the Chalk Group to identify the exact position of the Basal and Lower Chalk.

The “Basal Chalk” includes pink, off white and green limestone with chert. The unit is locally hard to microcrystalline. This significant hard, lithified chalk likely causes locally increased seismic velocities in the lowermost part of the Chalk Group towards the Base Chalk seismic marker. On the sonic logs from Rønde-1 and St-1, St-5, and St-19, a slightly increase of sonic velocity towards the Base Chalk can be identified confirming this hard and lithified chalk. On Figure 7.2.10, only data from Rønde-1 and Stenlille-5 are presented. No cores appear to be present from the “Basal Chalk” neither from the Stenlille wells or any of the other wells discussed in this report. However, core 6 from the Lavø-1 well, east Zealand, could represent the “Basal Chalk” being dated as Late Turonian, but more work is needed to confirm this. In Stenlille-5 the possible “Basal Chalk” is dated as Cenomanian to possibly Turonian based on ditch cutting samples.

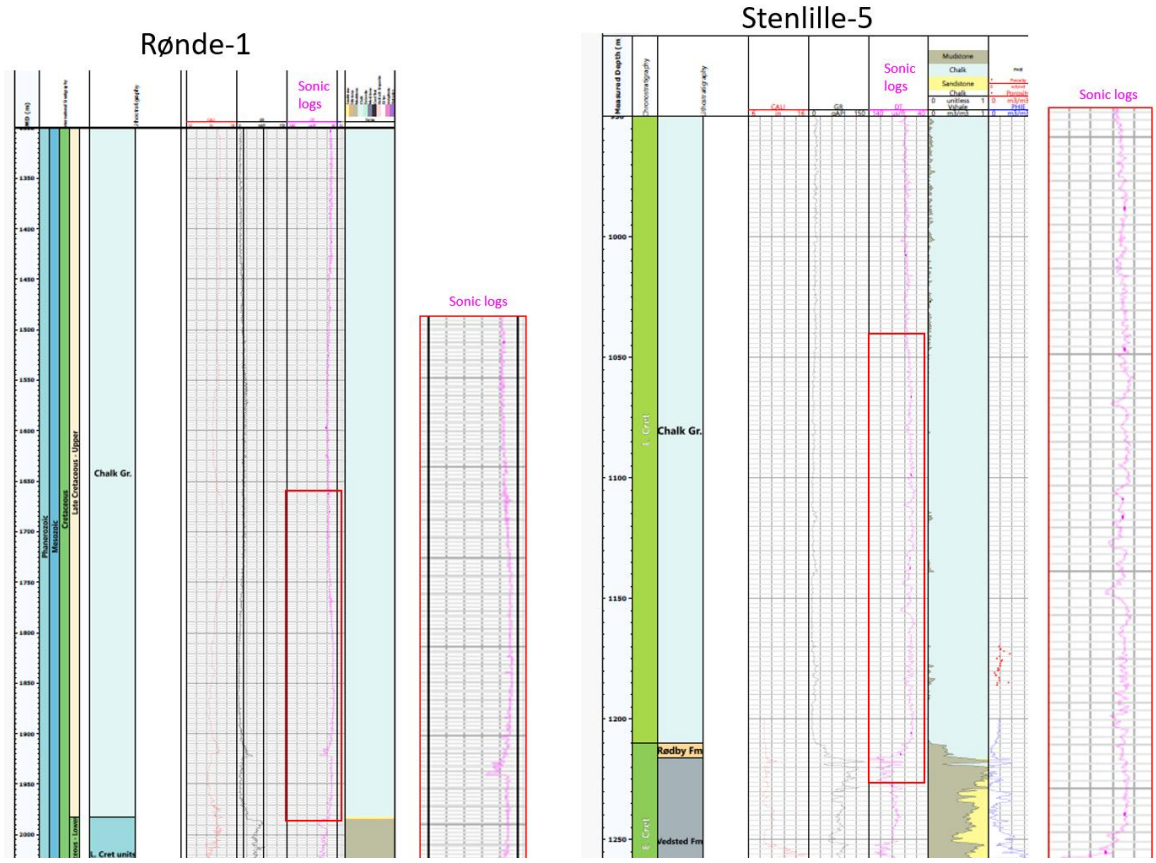

Figure 7.2.10. *Sonic logs of Rønde-1 and Stenlille-5. A detail of the log appears on the right side of the log and the zoomed part is marked with a red box. Note that the increase is most evident towards the base of the Chalk Group in Rønde-1. The location of the samples for porosity and permeability from Stenlille-5 plotted at Figure 7.2.12 is marked with a green box.*

The “Lower Chalk” consists mainly of limestone with a little chert and occasional marl horizons. Core 1 from Stenlille-5 is from this part of the Chalk Group has tentatively been divided into 5 different facies based mainly on the differences in sedimentary structures and carbonate and clay content and is dated as Coniacian to Early Santonian (nannofossil Zones UC10-11 of Burnett 1998) (Fig. 7.2.11) (see the Stenlille report, Gregersen et al. 2023, for more details on each individual facies). In general, the ‘’Lower Chalk’’ facies appear to be rich in biogenic grains, probably reflecting a relatively shallow marine depositional environment. Bioturbation related to the marl beds is not recorded. The marls beds are most likely very compacted. The presence of stylolites reflects chemical dissolution. The Stenlille-5 core is lithologically like the Stevns-1 core (Surlyk et al. 2013).

Figure

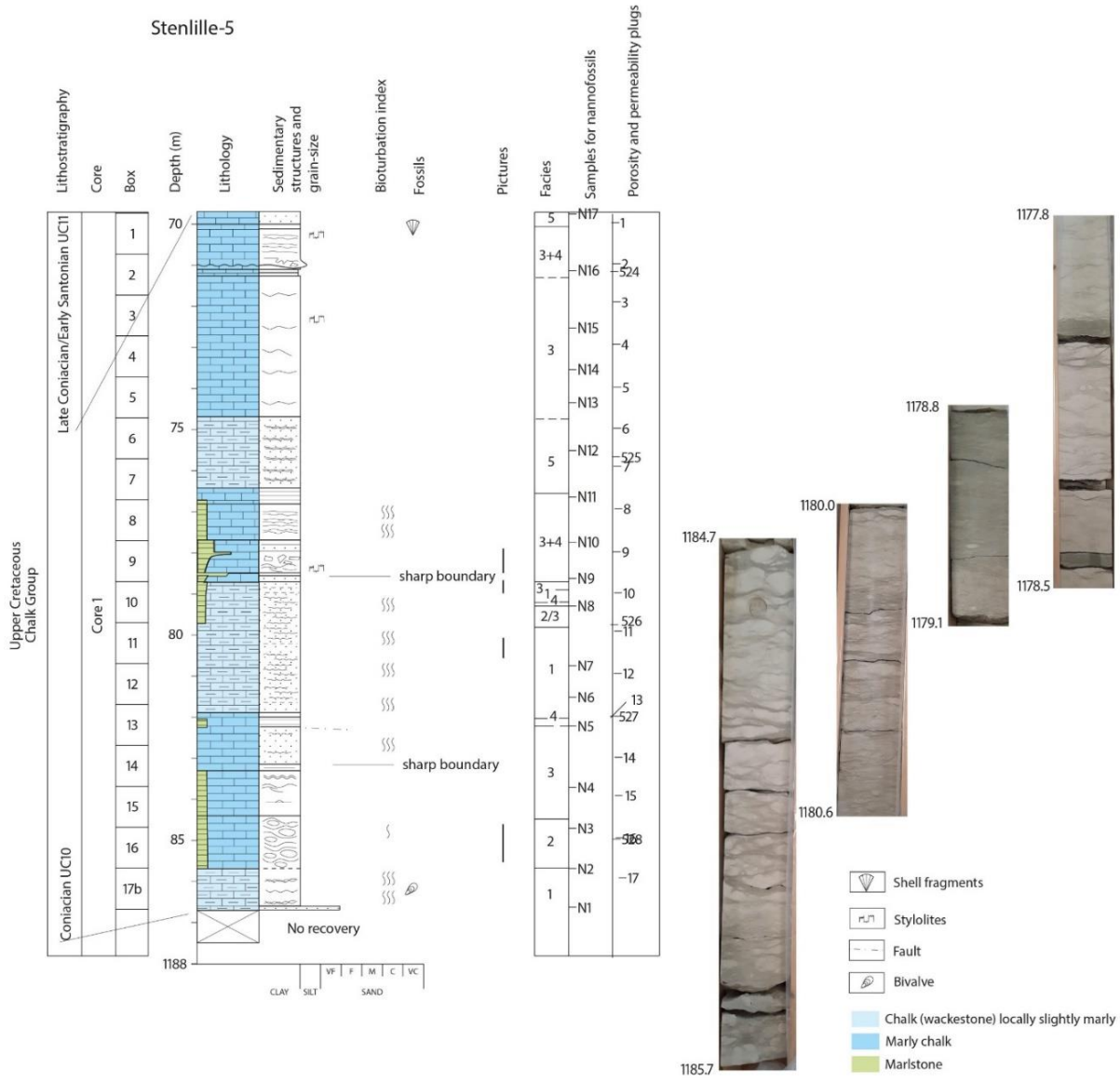

7.2.11. *Sedimentological logs of the ''Lower Chalk'' of the Chalk Group with core photos from the Stenlille-5 core. Only the lowermost and uppermost part of the core is dated. More work is needed to fully revise the core.*

The greatest Chalk Group thickness is identified in central parts of the Danish Basin, in the Lavø-1 well, where it measures 2000 m, of which 1200 m is dated as Campanian and Maastrichtian (Stenestad 1972). The Cenomanian chalk is at maximum 100 m thick, the maximum Turonian thickness is 50 m, and the maximum Coniacian thickness is 150 m (Stenestad 1972). The Stenlille and Havnsø areas are situated closer to the boundaries of the Danish Basin and the Ringkøbing–Fyn High in late Cretaceous time than the Lavø-1 locality. Consequently, the Chalk Group units are thinner in the Stenlille and Havnsø areas due to less accommodation space available for deposition than at the Lavø-1 locality. The early part of Late Cretaceous was most likely prone to many erosional events close to the rim of the Danish Basin in response to large regressions in the Late Cenomanian to Early Turonian.

Porosity and permeability data of the lower part of the Chalk Group in Stenlille-5

Data from the porosity and permeability tests of Stenlille-5 compiled in the mid 1980's are listed below (Fig. 7.2.12; their stratigraphic position appear on Figure 7.2.10 marked with a green box). The porosity and permeability values are generally very low in the chalk-rich facies 3 and 5 with an average porosity of 9.8% (facies 5) and 10.9% (facies 3) and an average permeability of 0.067 mD (facies 3) and 0.128 mD (facies 5). The stratigraphic positions of the different facies appear on Figure 7.2.11. The clay-rich facies have an even lower porosity of 6.6% (facies 4) to 7.4% (facies 1) and a permeability of 0.559mD (facies 4).

The porosity and permeability data are plotted against similar data from the Upper Cretaceous in the onshore Stevns-1 well and data from Upper Cretaceous in offshore wells. It is evident that the chalks in the Stenlille-5 well have the lowest porosity and permeability values. The relatively high porosity and permeability values from Stevns-1 (Upper Campanian to Maastrichtian) can be explained by the relatively shallow burial history of this site (between 450 to 600 m; Nielsen et al. 2011). The offshore chalks from the Danish Central Graben have been much deeper buried often exceeding 3000 m, but these chalk reservoirs have preserved a relatively high porosity due to retarded compaction caused by regional overpressure of the formations and the presence of oil and gas (e.g., Japsen 1998). The Stenlille data shows a normal burial compaction with no overpressure.

The non-reservoir chalks (low porosity and permeability) of the Central Graben have been investigated to understand their capability as a pressure seal (Mallon & Swarbrick 2002, 2008). Non-reservoir chalks have permeabilities which are like siliciclastic mudstones. The studies show that both in clean and argillaceous chalk, diagenetic alterations result in low permeability rocks. Further, the diversity of rock types that exhibit low permeability suggests that seals are pervasive throughout the Chalk Group. Non-reservoir chalks can therefore act as significant barriers to fluid flow and as significant pressure seals trapping high pressures beneath the Chalk Group.

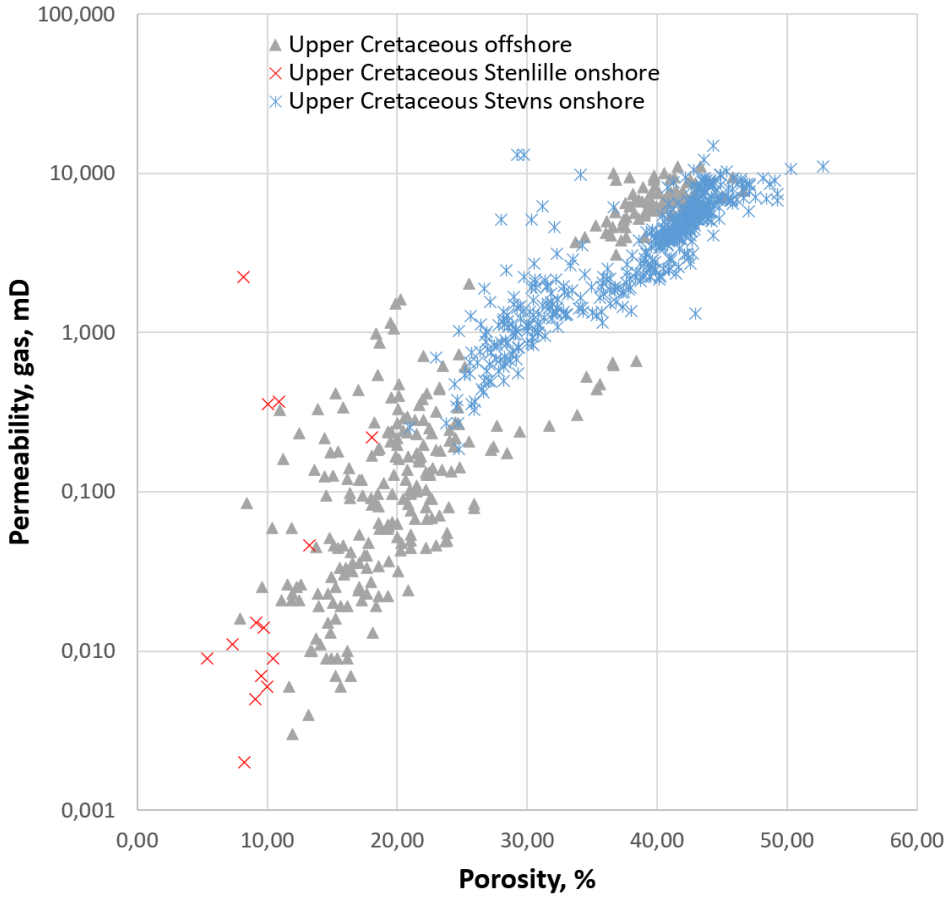

Figure 7.2.12. *Porosity and permeability plot of Upper Cretaceous chalks form onshore wells (part of the Stenlille-5 core and the Stevns-1 well) and from offshore in the Danish Central Graben (GEUS inhouse data). The data is discussed in the text.*

Concluding remarks on the secondary seal

The secondary seals of the Gassum Fm above the Fjerritslev Fm in the Stenlille area comprise the Lower Cretaceous Vedsted and Rødby Formations and the lower part of the Upper Cretaceous Chalk Group. Since these formations never have been the main target for coring in the Stenlille area or in other areas in close vicinity to the Havnsø structure this report summarize the present knowledge of these units based on data from the Stenlille area supplemented by available relevant data.

The Vedsted and Rødby Formations rest unconformably on top of the Lower Jurassic Fjerritslev Fm and a major hiatus spanning the latest Early Jurassic, Middle to Late Jurassic and the earliest part of Early Cretaceous (Late Hauterivian) in the Stenlille area is believed also to be present in Havnsø. The well-based stratigraphic boundary in the Stenlille area between the Lower Jurassic Fjerritslev Fm and the Lower Cretaceous Vedsted Fm is also mapped on seismic sections in the present study in the Havnsø structure as the Near Top Fjerritslev (see section 6.1). New studies need to be carried out to better define the more exact Fjerritslev Fm – Vedsted Fm (the Top Fjerritslev) boundary with more cored wells, well-ties and mapping. The thickness from the Top Gassum Fm to the near Top Fjerritslev Fm, estimated from seismic data, is a good approximation for the minimum thickness of the primary seal. Both

the Fjerritslev and the Vedsted Formations are expected to be excellent seals in the Stenlille and Havnsø structures as discussed in the text.

In the Stenlille area the Late Hauterivian to late Aptian Vedsted Fm consist of relatively homogenous mudstones with slight variations in silt content and with upwards increasing carbonate content. The formation possibly contains several hiati because of erosional events due to the proximity of the area to the basin margin. The Rødby Fm is represented by red marls with trace fossils and belemnites. It is dated as Early to middle Albian and possibly lowermost Cenomanian in the Stenlille area.

The Chalk Group in the Stenlille area has been divided into a “Basal Chalk” representing the oldest parts (Cenomanian to possibly Turonian) of the Chalk Group followed by a “Lower Chalk” (Coniacian to Lower Santonian), “Campanian Chalk”, “Maastrichtian Chalk” and Danian Limestone. The “Basal Chalk” is locally hard to very hard and appear with increased seismic velocities. The “Lower Chalk” consists mainly of limestone with a little chert and occasional marl horizons.

The porosity and permeability data for the lower part of the Chalk Group is listed in this report. Porosity and permeability values are generally very low and when compared with other onshore data from the Danish Basin (Stevns-1). The Stenlille Chalk Group data reveal an ordinary burial compaction with no overpressure. The properties of the lower part of the Chalk Group, in its potential capacity as a secondary seal, are compared with studies from the Danish Central Graben. It is very likely that the lower part of the Chalk Group will act as a significant barrier to fluid flow and high pressure from the underlying formations. It is probable that the potential sealing capacity of the lower part of the Chalk Group in the Stenlille and Havnsø areas will be similar due to their geographical proximity and similar geological history.

However, this can only be confirmed when core material from the Havnsø area becomes available and has been analysed. Core material from the closest deep wells (Lavø-1, Ullerslev-1, and possibly Horsens-1) could also be very useful and interesting to study in more detail for their sealing capacity.

8. Discussion of storage and potential risks

8.1 Volumetrics and Storage Capacity

Primary input for the estimation of potential CO_2 storage capacity has been the seismic interpretation of the Gassum Fm based on the newly acquired 2D seismic data (GEUS2022-HAVNSOE and GEUS2022-HAVNSOE-RE2023 survey) in combination with a reinterpretation of the formation on the old 2D-Survey lines. The detailed well analysis and a crucial element of revising the depth conversion impacts the understanding of the reservoirs (the Gassum and Bunter Sandstone fms) and their geometry in this gentle moderate-relief structure (see Figure 8.1.1).

The storage capacity estimations are average values for the whole structure. The well derived data in Table 7.1.5 is the primary input for the volume calculation. Therefore, the petrophysical and geological understanding of thicknesses and N/G in the wells is transformed into structure-specific average values for the storage capacity calculation that contains a spatial distribution/variation within GRV.

The Gross Rock Volume (GRV) is calculated first as a total volume between the top and the spill point contour line (see Figure 8.1.1.) The so-called Waste Rock Volume (WRV) (James et. al. 2013) is then subtracted from the total volume to give the resulting GRV. Average reservoir sandstone thickness (i.e., net sand thickness) is not just equal to the isochore thickness (or the relief) between top and base surfaces. Therefore, the Gross thickness is corrected with the N/G ratio to calculate the reservoir sandstone thickness for the GRV. Furthermore, the thickness correction could also incorporate potential thin sandstone wedges between top point and the spill point on the flanks of the structure, - if seismic data supports this.

For the storage capacity estimation at Havnsø, three scenarios have been evaluated where the structural closure (4-way closure only) is calculated so they can be compared to capacities of other structures across Denmark described in Gregersen et. al. (GEUS report 2022/26) and Hjelm et al. (GEUS report 2020/46).

The three scenarios related to three reservoir models are described Section 7.1., and an interpreted seismic section is illustrated in Figure 7.1.13. The scenarios should be assessed in more detail by 3D reservoirs simulation modelling to ensure optimal development, well configuration and filling of the reservoir units of the structure, and to ensure less uncertainty on storage capacity.

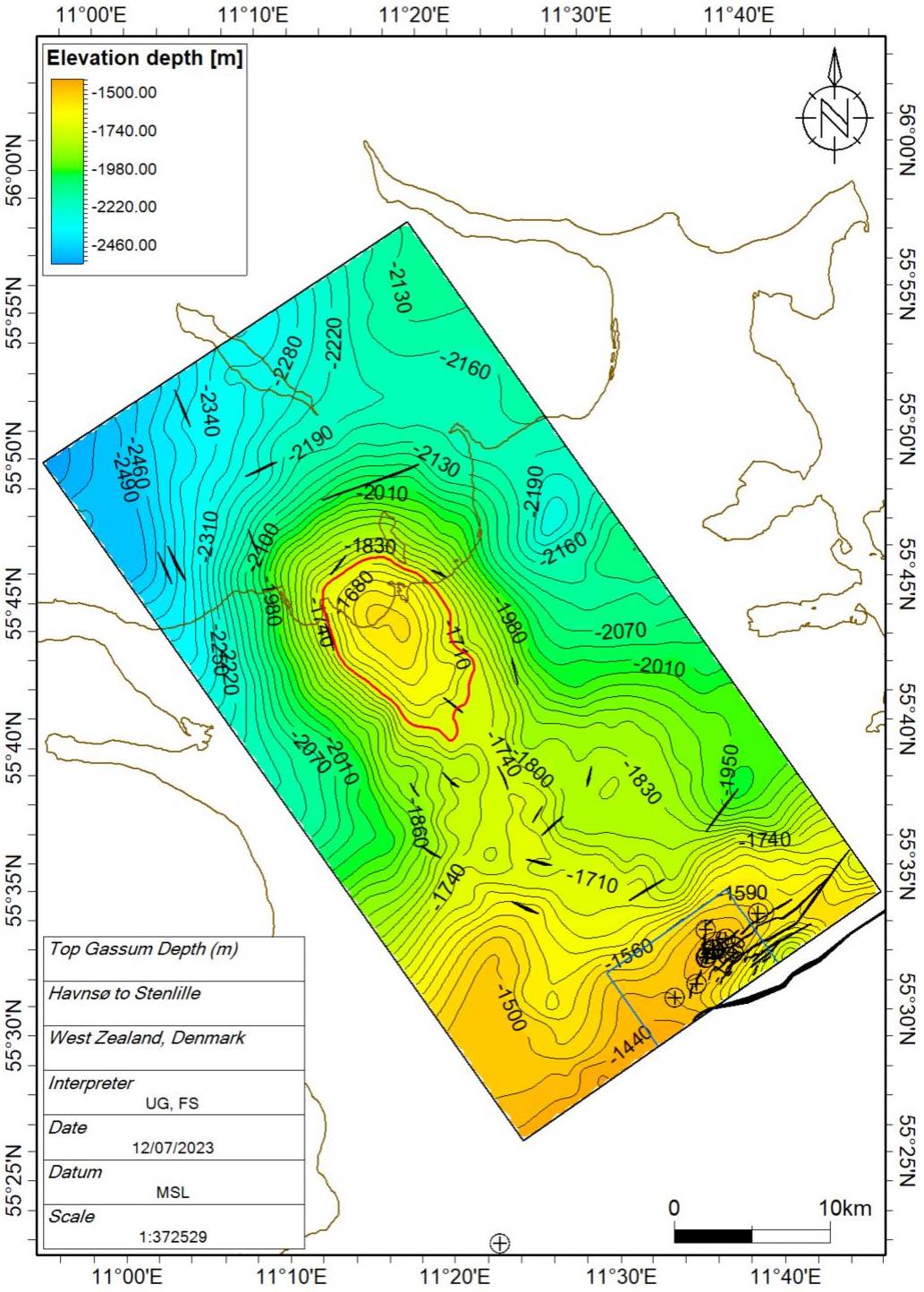

Figure 8.1.1. *The Top Gassum Fm depth structure map in meters (m) (generated in Petrel®) tied to Stenlille wells towards the SE and gridded by 250x250 meter – see Section 6.3; Fig. 6.3.3C) provides the primary input to the capacity assessment. The Havnsø structure has a structural spill point at c. 1710 m TVDSS located toward the SE (deepest closing contour, marked in red). The Top Gassum map shows, that the area within the spill point is c. 70 km², and with a top point at c. 1550 m; the structure height above spill point is c. 160 m. Note that faults are mainly small and mostly located around the Havnsø structure, and mainly trends SW–NE and a few NW–SE. See also Section 6.2 for fault analyses and map location. A conceptual profile (A–A') across the setting is shown in Figure 8.1.2 and 8.1.3.*

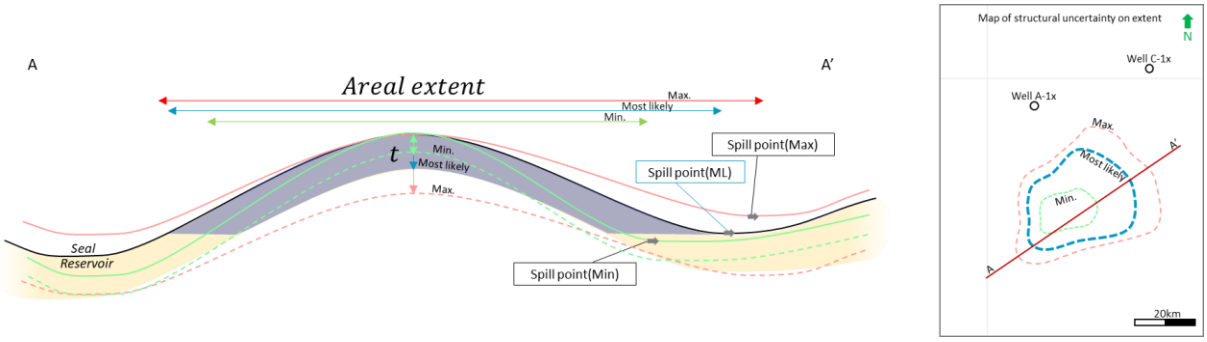

Figure 8.1.2. *Conceptual profile (A-A') across a potential structure. The uncertainty in mapping the structure results in the hypothetically min. and max. scenarios looking very different from the most likely mapped scenario. Variance in area and in thickness (t) will affect the Gross Rock Volume (GRV) of the structure. The uncertainty is addressed by applying uncertainty on the resulting GRV.*

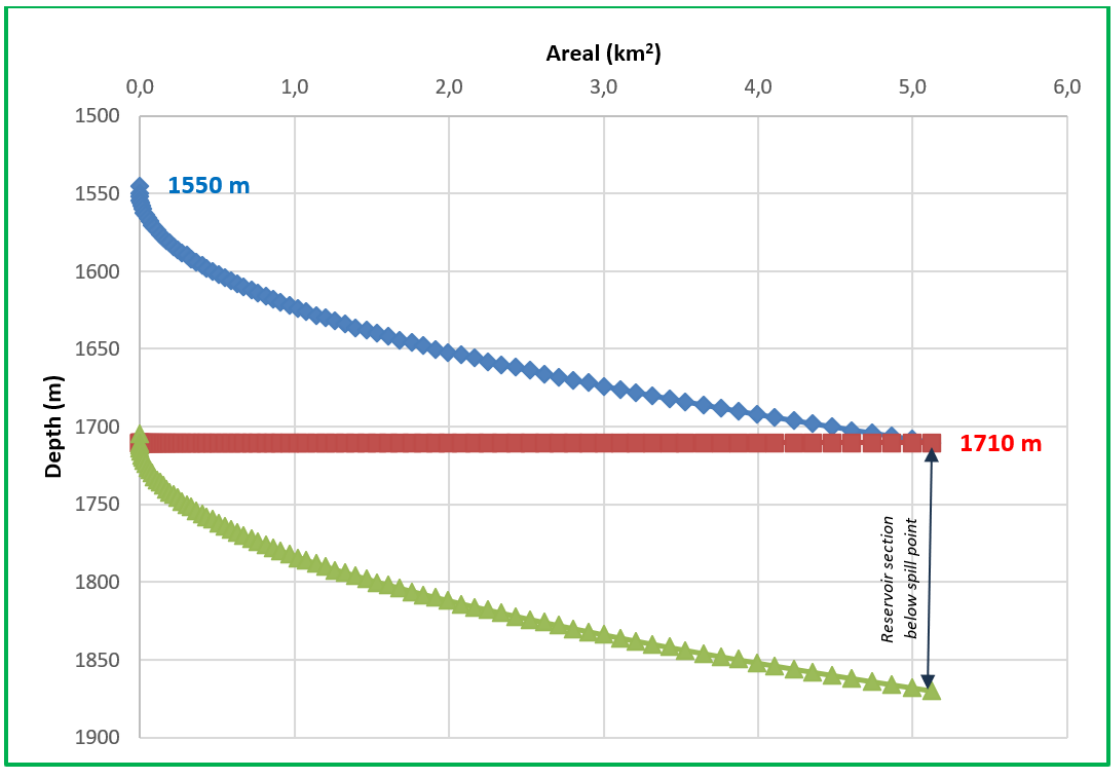

Figure 8.1.3. *Area and Thickness vs. Depth plot of the Havnsø structure. GRV is calculated from a top point (1550 m; blue) to the spill point at 1710 m (red line) and average thickness assumption with 2 meters depth increments for both the min., max. and the most likely (mode) cases. The green line represents the base of the reservoir, and the relief on the Havnsø structure shows that the 4-way closure only holds a part of the full reservoir potential within the structure. Only the most likely (mode) is shown.*

8.2 Volumemetric input parameters

Evaluation and maturation of a CO_2 storage site includes several steps. The maturation phase, carried out by GEUS, includes static calculation of theoretical storage capacity - primary based on gross rock volume (GRV), net/sand thickness, average porosity and density of the CO_2 (see also Section 5.1).

The current maturation phase does not provide dynamic capacity estimates of the potential CO_2 structures but focus on identifying and assessing extent and quality of reservoir aquifers. Furthermore, no attempts are made to address e.g., seal breach, fault leakage, fault reactivation etc.

In order to do detailed CO_2 storage capacity evaluation, it is important to assess aquifer quality and connectivity, i.e., to identify the existence of thick, high permeable sandstone aquifers with high connectivity with no major faults nor internal flow barriers. This will require dynamic reservoir simulation, that may result in different storage capacity than static calculations and will normally be the next step for potential license holders.

8.2.1 Gross rock volume

The Gross Rock Volumes of the Havnsø structure have been calculated using the Area and Thickness vs. Depth methodology described by e.g., James et al. (2013). The calculated Gross Reservoir Volume (GRV) is estimated from area vs depth tables extracted from seismic mapped and depth converted top and base reservoir surfaces (Figure 8.1.1.). The resulting volume of the structure together with the reservoir sand thicknesses estimated from petrophysical analysis is based on the nearest wells and is described in Section 7.1. Calculating GRV provides greater accuracy and flexibility that using various correction factors for geometries and overestimated wedge volumes. This is because it allows for uncertainty ranges on closure area and reservoir sand thickness to be modeled independently. Furthermore, the method allows for a rapid GRV calculation, that can be used in a Monte Carlo simulation, in order to establish an unbiased estimated range of GRV (James et. al. 2013).

To capture the uncertainty on the GRV across the Havnsø structure, a minimum and maximum case was also calculated as illustrated in Figure 8.1.2. GRV from area and thickness vs depth calculations were constructed defined by min., mode, and max. where mode is the data value that occurs most often in the data. This variation in GRV was set up for the areal extent to cover uncertainty in interpretations, seismic well ties, mapping, and depth conversion. To reflect this uncertainty, a distribution for the average GRV was constructed by defining the min. and max. of the distribution as ±20%. It is assumed that the GRV distribution follows a Pert distribution defined by the min., mode, and max. values. The Pert distribution is believed to give suitable representation for naturally occurring events following the subjective input estimates (Clark 1962).

For the Gassum reservoir the other input parameters is also given as min., mode, and max. values for porosity, N/G, CO_2 reservoir density and the Storage Efficiency factor, which are also assumed to follow a Pert distribution (see Table 8.2.1).

Table 8.2.1. *Gross Rock Volume assumption input and resultant GRVs for the three Scenarios 1-3 in the Havnsø structure. The Reservoir thickness (i.e. the Gross sand thickness) is taken from Table 7.1.5.*

Unit	Apex [m,TVDSS]	Spill point [m, TVDSS]			Area [km^2]			Reservoir TCK [Gross, m]			GRV [$1e^6m^3$]		
		Min.	Mode	Max.	Min.	Mode	Max.	Min.	Mode	Max.	Min.	Mode	Max.
Scenario S1	**1550**	1370	**1710**	2000	55	**70**	85	80	**111**	130	2.9	**5**	8
Scenario S2	**1500**	1370	**1710**	2000	55	**70**	85	55	**69**	85	2.9	**5**	8
Scenario S3	**1500**	1370	**1710**	2000	55	**70**	85	40	**47,6**	60	2.9	**5**	8

8.2.2 Net to Gross ratio

The N/G-ratios estimated from the petrophysical analysis of the nearest wells are evaluated and reasonable average N/G-values across the entire structure is defined as the mode of the distribution (see also Section 7.1). Some variance is expected due to lateral variation of deposition environment, facies distribution and diagenesis. To reflect these geological variations uncertainty, a distribution for the average N/G was constructed by defining the min. and max. of the distribution as c. ±20% (minor adjustments may occur). A Pert distribution has been applied.

8.2.3 Porosity

The porosity (ϕ) was estimated from petrophysical analysis of the Stenlille and surrounding wells as described in Section 7.1. The well-derived estimates are considered as reasonable average porosity across the entire structure (i.e., set as mode). Some variance is expected as lateral and depth variations may occur. To reflect this, an average porosity distribution has been constructed defining the min. and max. of the distribution as ±20% (minor adjustments may occur). A Pert distribution for this element has been applied.

8.2.4 CO_2 density

The average in-situ density of CO_2 was estimated using the 'Calculation of thermodynamic state variables of carbon dioxide' web-tool essentially based on Span and Wagner (1996) [http://www.peacesoftware.de/einigewerte/co2_e.html]. The average reservoir pressure was

calculated on the assumption that the reservoir is under hydrostatic pressure and a single pressure point midway between apex and max spill point was selected representing the entire reservoir. Temperature for this midway point was calculated assuming a surface temperature of 8°C and a geothermal gradient derived from Fuchs et al. (2020) to be c. 27–28 C°/km. Assumptions and calculated densities for the individual reservoir units are tabulated in Table 8.2.2. For a quick estimation of the uncertainty on CO_2 density, various P-T scenarios were tested and in general terms a -5% (min.) and +10% (max.) variation from the calculated mode was applied for building a Pert distribution. All calculations showed that CO_2 would be in supercritical state.

Table 8.2.2. *CO_2 fluid parameter assumption and estimated values*

Unit	Apex depth [TVDSS, m]	Spill point depth [TVDSS, m]	Structural relief [m]	Pressure HydroS.[MPa]	GeoThermal grad. [C/km]	Mid Res. Temp. [C]	CO_2 density (Kg / m^3)
Scenario S1	**1550**	**1710**	160	**15,99**	27	**52**	**698,8**
Scenario S2	**1550**	**1710**	160	**15,99**	27	**52**	**698,8**
Scenario S3	**1550**	**1710**	160	**15,99**	27	**52**	**698,8**

8.2.5 Storage efficiency

Storage efficiency is heavily influenced by local geological factors such as confinement, reservoir performance, compartmentalisation etc. together with injection design and operation (i.e., financially controlled factors) (e.g., Wang et al. 2013). A sufficient analogue storage efficiency database is not available to this study and accurate storage efficiency factor-ranges lacks at this early stage of maturation. This emphasises the need for further investigations of the local subsurface and development of scenarios and dynamic reservoir simulation to better understand the potential storage efficiency ranges. In this evaluation, a range from 5% to 20% with a mode of 10% is used as a possible range. The use of a mode of 10% assumes that sandstone reservoir in the Havnsø structure have good reservoir characteristics, however, it is emphasised that no wells penetrate the seal and reservoir in the structure itself. A Pert distribution for this element has also been applied.

Input summary

In tables 8.2.3. through 8.2.5, input parameter distributions are listed (all selected to follow Pert distributions defined by min, mode, and max). An example of input parameter distributions for the Scenario S1 is displayed in

Figure **8.2.4.**

Table 8.2.3. *Input parameters for the Havnsø structure -* ***Scenario 1***

Parameter	Assumption		
	Min	Mode	Max
GRV ($10^6 m^3$)	2.9	5	8
Net/Gross	0,6	0,75	0,9
Porosity	0,175	0,219	0,263
Storage eff.	0,05	0,1	0,2
In situ CO_2 density (kg/m^3)	663,86	698,8	768,68

Table 8.2.4. *Input parameters for the Havnsø structure -* ***Scenario 2***

Parameter	Assumption		
	Min	Mode	Max
GRV ($10^6 m^3$)	2.9	5	8
Net/Gross	0.6	0.63	0.9
Porosity	0.186	0.233	0.28
Storage eff.	0.05	0.1	0.2
In situ CO_2 density (kg/m^3)	663.86	698.8	768.68

Table 8.2.5. *Input parameters for the Havnsø structure -* ***Scenario 3***

Parameter	Assumption		
	Min	Mode	Max
GRV ($10^6 m^3$)	2.9	5	8
Net/Gross	0.6	0.33	0.9
Porosity	0.218	0.273	0.328
Storage eff.	0.05	0.1	0.2
In situ CO_2 density (kg/m^3)	663.86	698.8	768.68

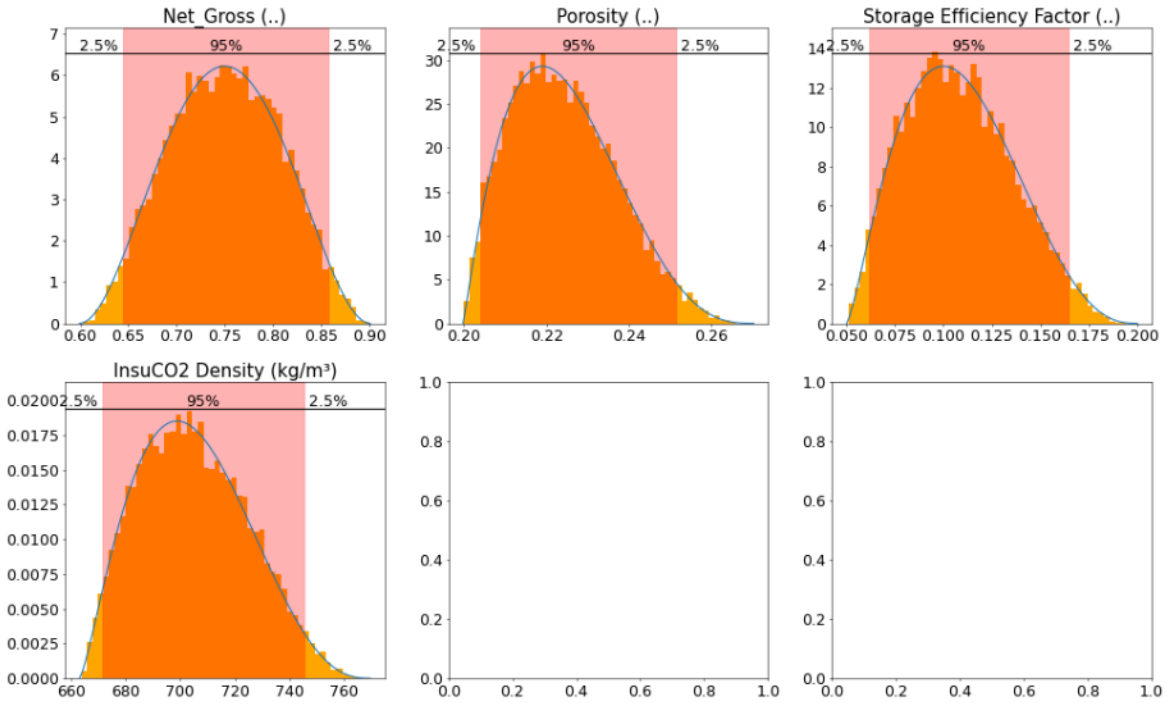

Figure 8.2.4. *Example of some of the distribution shapes (Pert distributions) for the 4 of the 5 input parameters for Scenario 1. Note that the first three distribution plots correspond to the GRV and that the two last input distribution plots are empty and not used.*

8.3 Storage capacity results

The modelled volumetrics was made on the assumption of the presence of an efficient reservoir/seal pair capable of retaining CO_2 in the reservoir, which needs to be tested by new 3D seismic data and further geological investigations. In tables 8.3.1 through 8.3.3, the results of the Monte Carlo simulations are tabulated. The tables indicate both the pore volume available within the trap (full potential above structural spill), the effective volume accessible for CO_2 storage (applying the Storage Efficiency factor to pore volume) and mass of CO_2 in mega-tons (MT) that can be stored. The tables present the 90%, 50% and 10% percentiles (P90, P50 and P10) corresponding to the chance for a given storage volume scenario to exceed the given storage capacity value. Mean values of the resultant outcome distribution are also tabulated and is considered the "best" single value representation for the entire distribution.

A mean storage capacity of c. 65 MT CO_2 is calculated for the Scenario 1; c. 58 MT CO_2 for the Scenario 2, while lower mean storage capacity of c. 35 MT CO_2 is modelled for the Scenario 3. For the Scenario 1 the unrisked storage potential of c. 65 MT CO_2 is calculated for Gassum reservoir with a range between c. 41 MT CO_2 (P90) and c. 90 MT CO_2 (P10) and a P50 of c. 63 MT CO_2 (Figure 8.3.1). Due to the variability-ranges of the behind-lying factors, the modelled storage capacity has a significant range and is associated with uncertainty. As illustrated in Figure 8.3.2, the storage capacity uncertainty is linked with especially the uncertainty in gross rock volume (GRV) and storage efficiency. In comparison, CO_2 density at reservoir conditions, is believed to be of minor significance.

Table 8.3.1. *The Havnsø structure – Gassum Fm,* ***Scenario 1*** *storage capacity potential*

Results	P90	P50	P10	Mean
Buoyant trapping pore volume (km^3)	0.699	0.843	1.021	**0.852**
Buoyant eff. storage volume (km^3)	0.059	0.089	0.128	**0.091**
Buoyant storage capacity (MT CO_2)	41.25	62.82	90.42	**64.81**

Table 8.3.2. *The Havnsø structure – Gassum Fm,* ***Scenario 2*** *storage capacity potential*

Results	P90	P50	P10	Mean
Buoyant trapping pore volume (km^3)	0.627	0.761	0.924	**0.769**
Buoyant eff. storage volume (km^3)	0.053	0.080	0.117	**0.083**
Buoyant storage capacity (MT CO_2)	37.04	56.34	82.80	**58.43**

Table 8.3.3. *The Havnsø structure – Gassum Fm,* ***Scenario 3*** *storage capacity potential*

Results	P90	P50	P10	Mean
Buoyant trapping pore volume (km^3)	0.365	0.451	0.533	**0.456**
Buoyant eff. storage volume (km^3)	0.031	0.048	0.069	**0.050**
Buoyant storage capacity (MT CO_2)	22.06	33.54	48.84	**34.73**

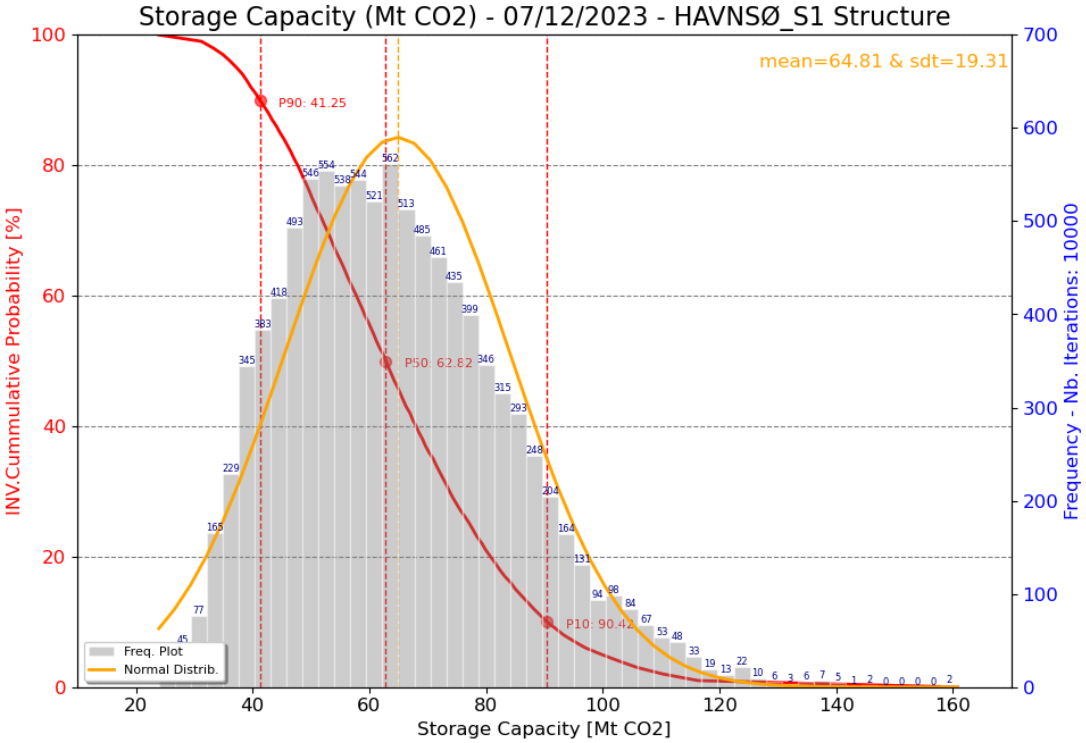

Figure 8.3.1. *Modelled statistical distribution of the combined storage capacity potential for the Gassum Fm,* ***Scenario 1*** *in the Havnsø structure.*

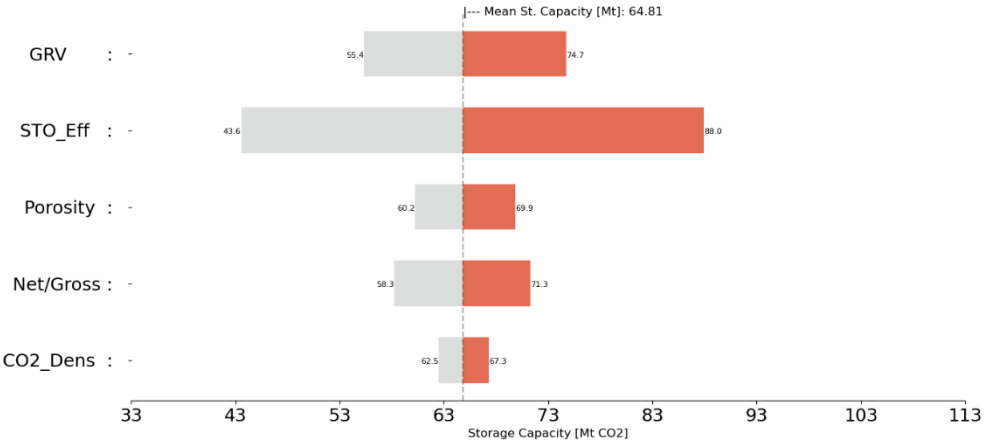

Figure 8.3.2. *Sensitivity or Tornado plot to how the various input parameters affect the estimate mean of storage capacity (c. 65 MT CO_2) of the Gassum reservoir. The horizontal bars for each parameter indicate change in storage capacity given that only that parameter is changed leaving all other constant (end levels being P90 and P10, respectively, in the parameter input range). The colours show the symmetric representation of the parameters on both sides of the mean storage capacity.*

Concluding Capacity Comments

To effectively store CO_2 in saline aquifer, the aquifer should contain the following main characteristics according to a new review by Yang et al. (2023):

(1) The saline aquifer should be situated at a depth more than 800 m for effective storage CO_2.
(2) It should have a porosity of minimum 10%.
(3) The reservoir thickness should be at least 20 m.
(4) The salinity property should be more than 10000 ppm.
(5) The caprock should have low permeability to avoid gas migration/leakage.
(6) There should be no fractures or faults.

Several studies have argued that injecting CO_2 into saline aquifers is a viable option for reducing climate changes by storing significant amounts of CO_2. Deep saline aquifers are present in sedimentary rocks all around the world, because of rocks with high permeability and porosity in many sedimentary basins (Yang et al. 2023).

Deep saline aquifers have been recognized for years in the Danish subsurface in sedimentary formations with high porosities and permeability (e.g., Michelsen et al. 1981; Weibel et al. 2020). In a basin wide screening study of the storage potential for CO_2 in the Danish subsurface it was suggested that the potential in the Havnsø structure was in the order of c. 306 MT CO_2 (Hjelm et al. 2022). The present study finds that the areal extent of the structure is smaller (70 km^2 compared to 119 km^2) than indicated on previous regional maps that was based on limited seismic data and that the structural relief is reduced from 200 m to 160 m due to a better constrained depth conversion applying data from the new seismic survey. This reduction in the rock volume of the structure together with an assumed storage efficiency factor of 10% compared to the previously assumed 40 % have reduced the estimated storage capacity.

The updated mean storage capacity estimate for a Gassum reservoir development on Havnsø, is estimated to be in the order of c. 65–34 MT CO_2. However, the capacity in connection to other possible scenario combinations should be investigated further by e.g., reservoirs simulation modelling to ensure optimal development, well configuration, and filling of the Havnsø structure, and to reduce the geological uncertainties.

Additional storage capacity may be available in the Havnsø structure, such as deeper reservoirs within the Oddesund and Bunter Sandstone Formations. However, this study has not evaluated the potential capacities of these deeper located reservoir sandstones and the associated upside storage capacity.

8.4. Potential risks

The present report provides an updated geological mapping describing reservoir-seal couples, the extent, thickness, closure, reservoir quality and volume of the primary reservoir formation, as well as larger faults, but does not comprise a dedicated study of risks or risk assessment of the structure for potential storage of CO_2. Thus, the report provides a geological characterization and maturation of these identified elements and points out geological related potential risk issues, that are recommended to be included for further evaluation and maturation, e.g., in risk assessment studies. Risks treated here are primary geological parameters incompletely understood, that may negatively affect the CO_2 storage potential. Not all risks can be identified at this early stage, while other risks identified at this stage will be mitigated by collection of new geophysical and geological data and further investigations, which together can shed new light on the critical parameters and risks. The few risks described below are not considered a full list, but rather emphasizes important points that needs further attention in future studies and data collections.

Faulting of the Gassum–Fjerritslev Fm reservoir-seal pair is considered the primary risk at the current level of understanding. Despite very thickly developed seals with minor detected faults, faults through the Fjerritslev Fm seal and some of them up to shallower successions may introduce a potential risk of vertical leakage from storage in the Gassum Formation, that needs to be addressed when maturing the structure further. Faults could also be a challenge to lateral migration such as reservoir compartmentalization, such as known from the Stenlille structure. The mapped faults are typically minor both in lateral extension (up to few km) and with small vertical throws (typical up to 10–15 ms) and they are also typical located kilometres apart. Faults may reduce reservoir communication and storage efficiency, and thus lower the storage efficiency and increase the number of injection wells required to fill the structure. The mapped faults are most densely mapped in 3D data in the nearby Stenlille area, but despite faults, there are not registered natural escape of gas at Stenlille. Havnsø may be a similar trap, but have to be investigated closely for any risks. Faults occur mostly up to near top of Fjerritslev Fm, and may in some cases connect further up into the Chalk Group, where faults of other directions are also detected. Thus, should it later be decided, CO_2 injection and the potential migration pathway should be safely away from faults.

Denmark is a low risk area for earthquakes though small earthquakes do occur (Fig. 8.4.1). Earthquake hazard for Denmark can be found in Voss al. (2015), where also lists of felt and damaging earthquakes can be found. In Figure 8.4.2 all known earthquakes on Zealand are shown. The largest is ML 4.0 (ML is the local magnitude or the local Richterscale) in 1930 ESE of Stevns (Lehmann 1931). Also, the smaller, but widely felt, earthquake in 2001 close to Holbæk is described (Larsen et al. 2008). Most earthquakes within Zealand are registered in the western part of Isefjord and the southern end of Roskilde fjord (Fig. 8.4.1). The depths of the earthquakes are very uncertain, but they are located within Earth's crust. A monitoring study was carried out around Gas Storage Denmark (GSD) gas storage facility close to Stenlille (Fig. 8.4.2). Six seismic stations were in operation for almost three years, and no local events were detected. The detection limit within the storage area was calculated to be at least ML 0.0 (Dahl-Jensen et al. 2021). Only few minor earthquakes have been registered at the Havnsø structure area NW of Stenlille (Fig. 8.4.2).

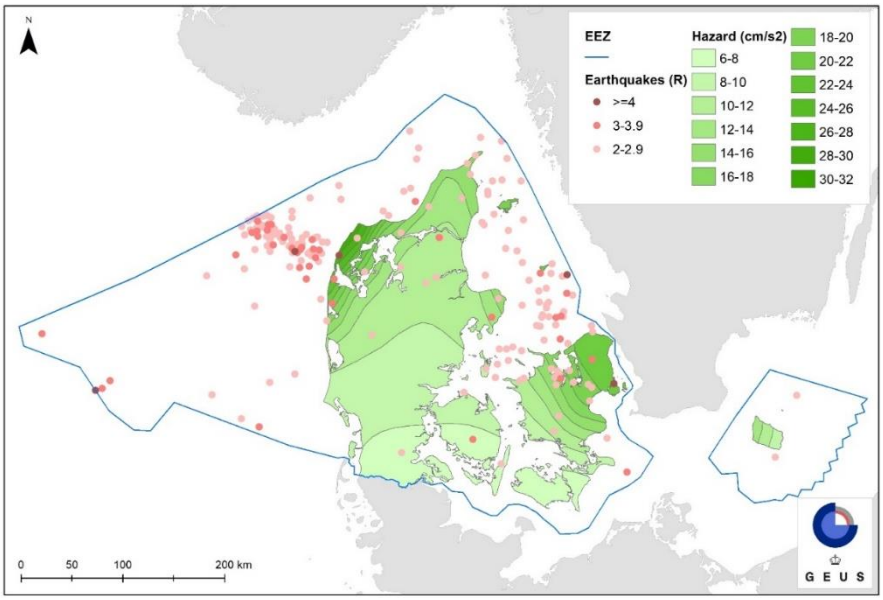

Figure 8.4.1. *The coloured contours are redrawn onshore from Voss et al. (2015) and show the estimated hazards given by the peak ground accelerations [cm/s2] for a return period of 475 years. This corresponds to a 90% non-exceedance probability in 50 years. Given values are only valid onshore Denmark. The contours are based on a validated catalogue of earthquakes over Magnitude 3 from 1960 to 2013. As the attenuation of earthquakes (ground motion prediction) has not been determined specifically for Denmark, the global reference model by Spudich et al. (1997) that describes attenuation from normal faults in hard-rock conditions was used.*

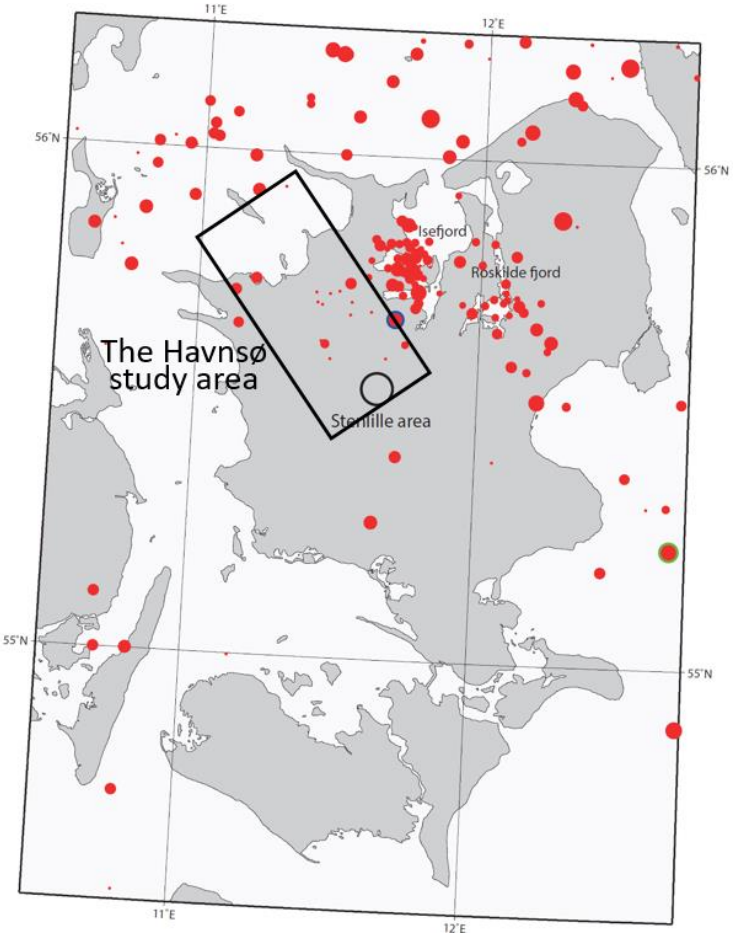

Figure 8.4.2. *All known earthquakes until the end of 2022, located since 1930 within 54.5–56.25N/10.5–12.75E. The magnitude (shown by the size of the red dots) varies from ML 4.0 and down. All known and assumed explosions have been removed, but some may remain, mainly offshore. 1930 Øresund ML 4.9 earthquake: green circle boundary; 2001 Holbæk ML 2.8 earthquake: blue circle boundary. The Havnsø study area of this report is marked with a black rectangle.*

9. Conclusions

This study shows that the Havnsø structure forms a well-defined structural anticlinal dome, cored by a Zechstein salt pillow that is overlain by a thick Triassic−Lower Jurassic succession, and younger strata. The structure is covered by vintage seismic data, and c. 130 km new seismic lines were acquired during August to October 2022 to increase the coverage of the structure. The primary reservoir is sandstones of the Late Triassic Gassum Formation whereas a thick mudstone succession of the latest Triassic−Lower Jurassic Fjerritslev Fm forms the primary seal. Both formations are well-known from several wells in the nearby Stenlille structure which resembles the Havnsø structure in its formation and composition. The Lower Triassic Bunter Sandstone Formation is considered to form a secondary reservoir in both structures with the overlying Lower Triassic Ørslev Formation forming the seal.

The Gassum and Fjerritslev Formations, the focus of this study, are mapped out on the new seismic data with a largely continuous thickness between the Havnsø and Stenlille structures. Since no wells penetrate the Havnsø structure, estimates of reservoir and seal properties largely relies on surrounding wells, in particular the nearest located Stenlille wells. Interpretation of the seismic data together with well data indicates that the Gassum and Fjerritslev formations are c. 140−160 m and c. 260−350 m thick in the Havnsø structure, respectively. The broad thickness interval of the seal (Fjerritslev Formation) reflects thinning towards the top of the structure related to regional uplift and erosion in the Middle Jurassic, probably enhanced by vertical movement of the deep-lying Zechstein salt. Based on knowledge obtained from the Stenlille structure (Gregersen et al. 2023), lateral variations in reservoir thicknesses, composition and properties of the Gassum Formation are likely to occur also within the Havnsø structure.

The reservoir properties of the sandstones in the Gassum Formation are prognosticated in three different scenarios: (1) As in the Stenlille structure; (2) As a regional average from selected Stenlille wells (ST-1, ST-19) and other wells surrounding the Havnsø structure in the Danish Basin; (3) From a sequence stratigraphic interpretation of the new seismic data as well as log data from Stenlille wells, showing that mainly lowstand sandstones of sequences 4, 5 and 6 are present in the Havnsø structure. In scenario 1, it is expected that the reservoir sandstones have a combined thickness of 111 m, an average porosity of 21.9% and permeability of c. 800 mD. For scenario 2, the estimated mean thickness of reservoir sandstone is 69 m, with an average porosity of 23.3% and a permeability of c. 1100 mD. In the more geological driven depositional model of Scenario 3, the combined thickness of the lowstand reservoir sandstones is 47.6 m, with an average porosity of 27.3% and a permeability of c. 1500 mD. In all three scenarios, the reservoir parameter values used to characterize the Havnsø structure are very good.

The mudstone dominated Fjerritslev Fm, is considered to form an excellent seal above the Gassum reservoir. Thus, it acts as an effectively seal for the seasonal storage of natural gas in the Gassum Fm in the nearby Stenlille structure. Above the Fjerritslev Fm, the Lower Cretaceous Vedsted and Rødby Formations form secondary seals, which furthermore are overlain by the km-thick Chalk Group and younger successions.

Faults are interpreted and described from the 2D seismic data with focus on their occurrence in the Gassum and Fjerritslev Formations. The faults are mainly trending NW–SE and SW–NE and have minor throws. As faults can result in compartmentalization of the reservoir and

a mechanical weakening of the seal, it is recommended to investigate this further by additional data acquisition and analyses.

The areal extent of the structure is estimated to be smaller (70 km^2) than indicated in the previous regional study (119 km^2 in Hjelm et al. 2022), which was based on a smaller amount of seismic data and velocity data. Also, the structural relief is reduced from 200 m to 160 m due to a better constrained depth conversion applying data from the new seismic survey. This reduction in the rock volume of the structure, together with an assumed storage efficiency factor of 10% compared to the previously assumed 40 %, have reduced the previous estimated storage capacity of 306 MT CO_2 in Hjelm et al. (2022) to c. 35–65 MT CO_2, depending on which of the above reservoir scenarios are used: (1) 65 MT CO_2; (2) 58 MT CO_2; (3) 35 MT CO_2. The calculations are for static reservoir models, but the capacity may be investigated further by more site-specific assessments and reservoir simulation modelling.

10. Recommendations for further work

New 2D seismic data has been acquired over the Havnsø structure and has improved the database considerably and have been used for the present updated mapping and analyses of the size, spill-point, volume, details of reservoir- and seal successions, and faults of the structure, for this initial maturation. However, it is recommended, that a further maturation of the structure should include new seismic acquisition, reservoir modelling and a risk assessment with seal integrity study, including leakage risk at faults and wells.

New 3D seismic acquisition over the potential injection- and storage areas is recommended, for more detailed interpretation prior to CO_2 injection. Acquisition of 3D seismic data over the structure can add important new data towards mitigating the fault related risks and develop scenarios for well design. It can also provide data for improved modelling of CO_2 migration. Later, repeated 3D surveys in same area can also contribute to monitor the extent of the CO_2 migration, together with other monitoring (e.g., via wells, seismometers, sampling, satellite, etc.). Such data will also enable a more precise definition of trap closures and reservoir outline, which again will feed into a refined storage volume calculation.

The modelled storage capacity is associated with variability-ranges and uncertainty, which e.g., are dependent on volume and closure definition. The geometry of the structure on the Top Gassum mapped surface and the relief from the deepest closure (spill-point) to the top structure is sensitive to mapping and depth conversion constraints despite the much-improved database. Thus, it is recommended to still improve the database and conduct a careful mapping and time-to-depth models. A further key element for the quantification of the storage potential of the structure is the understanding of the storage efficiency. The storage efficiency factor is mostly dependent on reservoir architecture and performance and thus potential heterogeneity, permeability, and compartmentalization, but also by economic aspects such as well density, well layout and injection design. Better understanding of the reservoir and simulation of reservoir flow could constrain storage efficiency better and thus narrow the estimated final capacity range.

In this study faults have been identified and described, mainly in the primary reservoir and seal. The study showed minor faulting in the Gassum and Fjerritslev Formations. Possible CO_2 injection in the Gassum Fm should be away from faults and the lowermost contour and saddle-point (spill-point) of the structure. Besides the potential storage of CO_2 within the structure as considered here, potential effects from injection and storage on reservoir and seal at the specific site(s) should also be considered, including mineral solubility, mineral trapping, pressure and stress effects, risks, etc.

New necessary data acquisition and sampling, analyses and evaluations should be carried out for further maturation, including risk analyses, to cover geological and other technical uncertainties and risks.

References

Anthonsen, K.L., Aagaard, P., Bergmo, P.E.S., Gislason, S.R., Lothe, A.E., Mortensen, G.M. and Snæbjörnsdóttir, S.Ó. 2014. Characterisation and selection of the most prospective CO2 storage sites in the Nordic region. Energy Procedia 63, 4884–4896. https://doi.org/10.1016/j.egypro.2014.11.519

Bachmann, G.H., Geluk, M.C., Warrington, G., Becker-Roman, A., Beutler, G., Hagdorn, H., Hounslow, M.W., Nitsch, E., Röhling, H.-G., Simon, T. and Szulc, A. 2010. Triassic. In: Doornenbal, J.C. & Stevenson, A.G. (eds): Petroleum Geological Atlas of the Southern Permian Basin Area. EAGE Publications b.v. (Houten), 149–173.

Bertelsen, F. 1978. The Upper Triassic – Lower Jurassic Vinding and Gassum Formations of the Norwegian–Danish Basin. Danmarks Geologiske Undersøgelse Serie B, Nr. 3, 26 pp. https://geusjournals.org/index.php/serieb/issue/view/927

Bertelsen, F. 1980. Lithostratigraphy and depositional history of the Danish Triassic. Geological Survey of Denmark. Series B, No. 4, 59 pp. https://geusjournals.org/index.php/serieb/issue/view/928

Boldreel, L.O., Andersen, M.S., Vosgerau, H., Mathiesen, A., Kamla, E. and Nielsen, L.H. *in review*. Late Palaeozoic-Cenozoic evolution of the onshore Danish area based on seismic reflection and well data. GEUS Bulletin.

Bown, P.R., Rutledge, D.C., Crux, J.A. and Gallagher, L.T. 1998. Lower Cretaceous. In: Bown, P.R. (ed.): Calcareous Nannofossil Biostratigraphy, 86–131. British Micropalaeontological Society Series. London: Chapman and Hall, London. https:// doi.org/10.1007/978-94-011-4902-0_5

Bredesen, K. 2022. Assessing rock physics and seismic characteristics of the Gassum Formation in the Stenlille aquifer gas storage – A reservoir analog for the Havnsø CO_2 storage prospect, Denmark. International Journal of Greenhouse Gas Control, 114, 103583. https://doi.org/10.1016/j.ijggc.2022.103583

Bredesen, K., Lorentzen, M., Smit, F.W.H. and Gregersen, U. 2022. Quantitative seismic interpretation of the Gassum Formation at the Stenlille aquifer gas storage. GHGT-16 Conference Proceedings (2022); SSRN Electronic Journal, November, 2022, 12 pp. https://doi.org/10.2139/ssrn.4276697

Burnett, J.A. 1998. Upper Cretaceous. In: Bown, P.R. (ed.): Calcareous Nannofossil Biostratigraphy. British Micropalaeontological Society Series. Chapman & Hall/Kluwer Academic, 132–199.

Catuneanu, O. 2019. Model-independent sequence stratigraphy. Earth-Science Reviews 188, 312–388.

CGG, 1998. Final report of seismic data processing. Survey: STENLILLE-97 3D survey. October, 1997-May, 1998. Conpagnie Générale de Géophysique for Dansk Naturgas A/S (DONG). France, May 1998.

Chadwick, R.A., Zweigel, P., Gregersen, U., Kirby, G.A., Holloway, S. and Johannesen, P.N. 2004. Geological reservoir characterization of a CO2 storage site: The Utsira Sand, Sleipner, northern North Sea. Energy, 29 (9−10), 2004. p. 1371–1381. https://doi.org/10.1016/j.energy.2004.03.071

Clark, C.E. 1962. The PERT model for the distribution of an activity Time. Operations Research 10, 405–406. https://doi.org/10.1287/opre.10.3.405

Clift, P.D., Olson, E.D., Lechnowskyj, A., Moran, M.G., Barbato, A. and Lorenzo, J.M. 2019. Grain-size variability within a mega-scale point-bar system, False River, Louisiana. Sedimentology 66, 2, 408–434. https://doi.org/10.1111/sed.12528

Craig, J., Gorecki, C.D., Ayash, S.C., Liu, G. and Braunberger, J.R. 2014. A comparison of volumetric and dynamic storage efficiency in deep saline reservoirs: an overview of IEAGHG study IEA/CON/13/208. Energy Procedia 63, 5185–5191. Doi: 10.1016/j.egypro.2014.11.549.

Dahl-Jensen, T., Jakobsen, R., Bundgaard Bech, T., Møller Nielsen, C., Nyrop Albers, C., Voss, P.H. and Larsen, T.B. 2021. Monitoring for seismological and geochemical groundwater effects of high-volume pumping of natural gas at the Stenlille underground gas storage facility, Denmark. GEUS Bulletin 47, 8pp. https://doi.org/10.34194/geusb.v47.5552

Dix, C.H. 1955. Seismic velocities from surface measurements. Geophysics, 20(1), 68–86.

DONG 2001. ST-19 (Stenlille-19). Final well report. H. Schokker, Copenhagen, 14-02-2001.

DONG 2003. Final well report. MAH-1, MAH-1A (Margretheholm).

Donovan, D.T. and Surlyk, F. 2003. Lower Jurassic (Pliensbachian) ammonites from Bornholm, Baltic Sea, Denmark. Geological Survey of Denmark and Greenland Bulletin 1, 555–583.

Dybkjær, K. 1988. Palynological zonation and stratigraphy of the Jurassic section in the Gassum No. 1-borehole, Denmark. Geological Survey of Denmark Ser. A, No. 21, 73 pp.

Dybkjær, K. 1991. Palynological zonation and palynofacies investigation of the Fjerritslev Formation (Lower Jurassic - basal Middle Jurassic) in the Danish Subbasin. Danmarks Geologiske Undersøgelse Serie A, no. 30, 150 p. https://doi.org/10.34194/seriea.v30.7050

Erlström, M., Sivhed, U. and Surlyk, F. 1999. A backstepping, fluviatile-paralic-marine succession, Sinemurian, Lower Jurassic, Skåne, southern Sweden. Bulletin of the Geological Society of Denmark 46, 1–12.

Frandsen, N. and Surlyk, F. 2003. An offshore transgressive–regressive mudstone-dominated succession from the Sinemurian of Skåne, Sweden. Geological Survey of Denmark and Greenland Bulletin 1, 543–554.

Frederiksen, S., Nielsen, S.B. and Balling, N. 2001. A numerical dynamic model for the Norwegian−Danish Basin. Tectonophysics, 343, 165−183. https://doi.org/10.1016/S0040-1951(01)00223-2.

Fuchs, S., Balling, N. and Mathiesen, A. 2020. Deep basin temperature and heat-flow field in Denmark – New insights from borehole analysis and 3D geothermal modelling. Geothermics, 83. DOI: http://doi.org/10.1016/j.geothermics.2019.101722

Funck, T. and Nørmark, E. 2023. CCS2022-2024 WP1: The Havnsø structure – Marine acquisition report. Offshore seismic acquisition Havnsø-Nekselø 2022, with seismic source from the onshore acquisition. Danmarks og Grønlands Geologiske Undersøgelse Rapport 2023/22. GEUS. 48 pp. https://doi.org/10.22008/gpub/34689

Gale, A.S., Mutterlose, J. and Batenburg, S. 2000. The Cretaceous Period. In: Gradstein, F.M., Ogg, J.G., & Ogg, G.M. (eds): Geological Time Scale 2020. 1023-1086. Amsterdam: Elsevier B.V. https://doi.org/10.1016/B978-0-12-824360-2.00027-9

Gardner, G. H. F., Gardner, L. W. and Gregory, A. 1974. Formation velocity and density—The diagnostic basics for stratigraphic traps. Geophysics, 39(6), 770–780.

Global CCS Institute: Global-Report-2022.

Goodman, A., Hakala, A., Bromhal, G., Deel, D., Rodosta, T., Frailey, S., Samll, M., Allen, D., Romanov, V., Fazio, J., Huerta, N., McIntyre, D., Kutchko, B. and Guthrie, G. 2011. U.S. DOE methodology for the development of geologic storage potential for carbon dioxide at the national and regional scale. International Journal of Greenhouse Gas Control, 5 (4), 952–965. https://doi.org/10.1016/j.ijggc.2011.03.010.

Gorecki, C.D., Holubnyak, Y.I., Ayash, S.C., Bremer, J.M., Sorensen, J.A., Steadman, E.N. and Harju, J.A. 2009. A New Classification System For Evaluating CO2 Storage Resource/Capacity Estimates. Paper presented at the SPE International Conference on CO2 Capture, Storage, and Utilization, San Diego, California, USA, November 2009. ISBN: 978-1-55563-267-0. https://doi.org/10.2118/126421-MS.

Gradstein, F.M., Agterberg, F.P., Ogg, J.G., Hardenbol, J., van Veen, P., Thierry, J. and Huang, Z. 1994. A Mesozoic time scale. Journal of Geophysical Research: Solid Earth, 99(B12), 24051-24074.

Gradstein, F.M., Ogg, J.G., Schmitz, M.D. and Ogg, G.M. (Eds.) 2020. Geologic time scale 2020. Elsevier.

Gravesen, P., Rolle, F. and Surlyk, F. 1982. LIthostratigraphy and sedimentary evolution of the Triassic, Jurassic and Lower Cretaceous of Bornholm, Denmark. Danmarks Geologiske Undersøgelse Serie B. No. 7, 51 pp.

Gregersen, U. and Smit, F.W.H. 2003: Two-way Time (TWT) grids from the Havnsø project. GEUS Dataverse V2, Geological Survey of Denmark and Greenland. Link to published data: https://doi.org/10.22008/FK2/ADIJKG

Gregersen, U., Vosgerau, H., Laghari, S., Bredesen, K., Rasmussen, R. and Mathiesen, A. 2020. Capture, Storage and Use of CO_2 (CCUS): Seismic interpretation of existing 2D and 3D seismic data around the Havnsø structure (Part of work package 5 in the CCUS project). Danmarks og Grønlands Geologiske Undersøgelse Rapport 2020/33; GEUS. 60 pp. https://doi.org/10.22008/gpub/34530

Gregersen, U., Smit, F.W.H., Lorentzen, M., Vosgerau, H., Bredesen, K., Hjelm, L., Mathiesen, A. and Laghari, S. 2022. Tectonostratigraphy and Structural Evolution of the Stenlille Structure in Zealand, Denmark – a Site for Natural Gas and CO2 Storage. GHGT-16 Conference Proceedings (2022); SSRN Electronic Journal Nov. 2022 & Geophysics eJournal 4 (85) Dec. 2022, 12 pp. SSRN: http://dx.doi.org/10.2139/ssrn.4275875

Gregersen, U., Hjelm, L., Vosgerau, H., Smit, F.W.H., Nielsen, C.M., Rasmussen, R., Bredesen, K., Lorentzen, M., Mørk, F., Lauridsen, B.W., Pedersen, G.K., Nielsen, L.H., Mathiesen, A., Laghari, S., Kristensen, L., Sheldon, E., Dahl-Jensen, T., Dybkjær, K., Hidalgo, C.A. and Rasmussen, L.M. 2023. CCS2022-2024 WP1: The Stenlille structure - Seismic data and interpretation to mature potential geological storage of CO2. Danmarks og Grønlands Geologiske Undersøgelse Rapport 2022/26. GEUS. 164 pp. DOI: https://doi.org/10.22008/gpub/34661

Hamberg, L. and Nielsen, L.H. 2000. Shingled, sharp-based shoreface sandstones: depositional response to stepwise forced regression in a shallow basin, Upper Triassic Gassum Formation, Denmark. In: Hunt, D. and Gawthorpe, R.L. (eds): Sedimentary Responses to

Forced Regressions. Geological Society, London, Special Publications, 172, 69–89. https://doi.org/10.1144/GSL.SP.2000.172.01.04

Hjelm L., Anthonsen K.L., Dideriksen K., Nielsen C.M., Nielsen L.H. and Mathiesen A. 2022. Capture, Storage and Use of CO2 (CCUS). Evaluation of the CO2 storage potential in Denmark. Vol.1: Report & Vol 2: Appendix A and B [Published as 2 separate volumes both with Series number 2020/46]. Danmarks og Grønlands Geologiske Undersøgelse Rapport 2020/46; GEUS. 141 pp. https://doi.org/10.22008/gpub/34543

Hovikoski, J. and Pedersen, G.K. 2020. Capture, Storage and Use of CO_2 (CCUS): Sedimentological description of Gassum and Fjerritslev Formations from cores in the Stenlille area, with interpretations of depositional environments (Part of Work package 6 in the CCUS project). Danmarks og Grønlands Geologiske Undersøgelse Rapport 2020/42, 60 pp. https://doi.org/10.22008/gpub/34539

Ineson, J.R. 1993. The Lower Cretaceous chalk play in the Danish Central Trough. Geological Society, London, Petroleum Geology Conference series, 4, 175–183.

Ineson, J.R., Jutson, D.J. and Schiøler, P. 1997. Mid-Cretaceous sequence stratigraphy in the Danish Central Trough. Danmarks og Grønlands Geologiske Undersøgelser Rapport 1997/109, 60 pp.

IPCC (Intergovernmental Panel on Climate Change) 2022. Climate Change 2022: Mitigation of Climate Change. Working Group III contribution to the Sixth Assessment Report of the Intergovernmental Panel on Climate Change. UN, New York. 2913 pp.

James, B., Grundy, A.T. and Sykes, M.A. 2013. The Depth-Area-Thickness (DAT) Method for Calculating Gross Rock Volume: A Better Way to Model Hydrocarbon Contact Uncertainty, AAPG International Conference & Exhibition. AAPG Search and Discovery Article #90166©2013, Cartagena, Colombia, 8-11 September.

Japsen, P. 1998. Regional velocity–depth anomalies, North Sea chalk: a record of overpressure and Neogene uplift and erosion. AAPG Bull., 82, 2031–2074.

Japsen, P. and Bidstrup, T. 1999. Quantification of late Cenozoic erosion in Denmark based on sonic data and basin modelling. Bulletin of the Geological Society of Denmark, 46, 79–99. https://doi.org/10.37570/bgsd-1999-46-08

Japsen, P., Green, P.F., Nielsen, L.H., Rasmussen, E.S. and Bidstrup, T. 2007. Mesozoic–Cenozoic exhumation events in the eastern North Sea Basin: a multi-disciplinary approach based on palaeothermal, palaeoburial, stratigraphic and seismic data. Basin Research 19, 451–490.

Jensen, T.F, Holm, L., Frandsen, N. and Michelsen, O. 1986. Jurassic-Lower Cretaceous Lithostratigraphic Nomenclature for the Danish Central Trough. Danmarks Geologiske Undersøgelse Serie A 12, 65 pp. https://doi.org/10.34194/seriea.v12.7031

Koppelhus, E.B. and Nielsen, L.H. 1994. Palynostratigraphy and palaeoenvironments of the Lower to Middle Jurassic Bagå Formation of Bornholm, Denmark. Palynology 18(1), 139–194.

Kristensen, L., Hjuler, M.L., Frykman, P., Olivarius, M., Weibel, R., Nielsen, L.H. and Mathiesen, A., 2016. Pre-drilling assessments of average porosity and permeability in the geothermal reservoirs of the Danish area. Geothermal Energy 4(6): 1–27.

Kucinskaite, K., Papadopoulou, M., Zappalà, S., Malehmir, A., Westgate, M., Gregersen, U. and Funck, T. 2023a. Near-surface effect on geological CO2 storage site characterization in Denmark. In 4th EAGE Global Energy Transition Conference & Exhibition.

Kucinskaite, K., Papadopoulou, M., Zappalá, S., Malehmir, A., Westgate, M., Gregersen, U., Hjelm, L., Funck, T. and Nielsen, L. 2023b. Novel land seismic studies for geological storage of CO2 in Denmark. Abstract. 81st International Scientific Conference of the UL, University of Latvia.

Laier, T. and Øbro, H. 2009. Environmental and safety monitoring of the natural gas underground storage at Stenlille, Denmark. Geological Society, London, Special Publications, 313, 81–92. https://doi.org/10.1144/SP313.6

Larsen, G. 1966. Rhaetic–Jurassic– Lower Cretaceous sediments un the Danish Embayment (A heavy-mineral study). Geological Survey of Denmark, II Series, No. 91, 127 p. plus plates. https://doi.org/10.34194/raekke2.v91.6882

Larsen, M., Bidstrup, T. and Dalhoff F. 2003. Mapping of deep saline aquifers in Denmark with potential for future CO2 storage. Geological Survey of Denmark and Greenland, Rapport 2003/39, 83 pp.

Larsen, T. B., Gregersen, S., Voss, P. H., Bidstrup, T. and Orozova-Bekkevold, V. 2008. The earthquake that shook central Sjælland, Denmark, November 6, 2001. Bulletin of the Geological Society of Denmark, 56. 1–11.

Lauridsen, B.W., Lode, S., Sheldon, E., Frykman, P., Anderskouv, K and Ineson, J. 2022. Lower Cretaceous (Hauterivian–Aptian) pelagic carbonates in the Danish Basin: new data from the Vinding-1 well, central Jylland, Danmark. Bulletin of the Geological Society of Denmark, 71, 7–29. https://doi.org/10.37570/bgsd-2022-71-02

Lehmann, I. 1931. Jordskælvet den 1. November 1930. Naturens Verden 15, 219–235.

Lindström, S. 2020. Capture, Storage and Use of CO_2 (CCUS): Palynology of the Gassum and lowermost Fjerritslev formations in the Stenlille area: biostratigraphic and palaeonenvironmental implications (Part of work package 5 in the CCUS project). Danmarks og Grønlands Geologiske Undersøgelse Rapport 2020/36, 35 pp. https://doi.org/10.22008/gpub/34533

Lindström, S., van de Schootbrugge, B., Dybkjær, K., Pedersen, G.K., Fiebig, J., Nielsen, L.H. and Richoz, S. 2012. No causal link between terrestrial ecoystem change and methane release during the end-Triassic mass extinction. Geology 40, 531–534. DOI: 10.1130/G32928.1 WOSUID: WOS:000304515000013

Lindström, S., Pedersen, G.K., van de Schootbrugge, B, Hansen, K.H., Kuhlmann, N., Thein, J.T., Johansson, L., Petersen, H.I., Alwmark, C., Dybkjær, K., Weibel, R., Erlström, M., Nielsen, L.H. Oschmann, W. and Tegner, C. 2015. Intense and widespread seismicity during the end-Triassic mass extinction due to emplacement of a large igneous province. Geology 43, 387–390. (publ. online 2015.03.19). DOI: 10.1130/G36444.1 WOSUID: WOS:000357619400025

Lindström, S., van de Schootbrugge, B., Hansen, K.H., Pedersen, G.K., Alsen, P., Thibault, N., Dybkjær, K., Bjerrum, C.J. and Nielsen, L.H. 2017. A new correlation of Triassic–Jurassic boundary successions in NW Europe, Nevada and Peru, and the Central Atlantic Magmatic Province: A time-line for the end-Triassic mass extinction. Palaeogeography, Palaeoclimatology, Palaeoecology 478, 80–102. [Available online 21 December 2016]. DOI: 10.1016/j.palaeo.2016.12.025 WOSUID: WOS:000402355900006

Lindström, S., Sanei, H., van der Schootbrugge, B., Pedersen, G.K., Lesher, C.E., Tegner, C., Heunisch, C., Dybkjær, K. and Outridge, P.M. 2019. Volcanic mercury and mutagenesis in land plants during the end-Triassic mass extinction. Science Advances 5, 13 p. (eaaw4018 23 October 2019). DOI: 10.1126/sciadv.aaw4018

Lindström, S., Pedersen, G.K., Vosgerau, H., Hovikoski, J., Dybkjær, K. and Nielsen, L.H. 2023. Palynology of the Triassic–Jurassic transition of the Danish Basin (Denmark): a palynostratigraphic zonation of the Gassum–lower Fjerritslev formations, Palynology 47 (4) 1–34. https://doi.org/10.1080/01916122.2023.2241068

Lorentzen, M., Bredesen, K., Gregersen, U., Smit, F.W.H. and Laghari, S. 2022. Fault Mapping of the Gassum Formation Reservoir and the Fjerritslev Formation Caprock Interval at the Stenlille Gas Storage Site Using a Pre-Trained Convolutional Neural Network. GHGT-16 Conference Proceedings (2022); Geophysics eJournal, 4(86), December, 2022, 12 pp. SSRN: http://dx.doi.org/10.2139/ssrn.4277405

Mallon, A.J. and Swarbrick, R.E. 2002. A compaction trend for non-reservoir North Sea Chalk, Marine and Petroleum Geology, 19, 10, 527–539.

Mallon, A.J. and Swarbrick, R.E. 2008. Diagenetic characteristics of low permeability, non-reservoir chalk from the Central North Sea, Marine and Petroleum Geology, 25, 10, 1097–1108. https://doi.org/10.1016/j.marpetgeo.2007.12.001

Malehmir, A. and Papadopoulou, M. 2022. Innovative land seismic data acquisition for geological CO_2 storage in Stenlille, Denmark. Final Acquisition and Processing Report of the GEUS2022-STENLILLE survey. Uppsala University, July 2022, 42 pp. Data and report available via GEUS: Processing summary sheet (geus.dk)

Malehmir, A. and Papadopoulou, M. 2023. GEUS2022-HAVNSOE seismic survey: Acquisition and processing report. Uppsala University. Final report (June 2023). 45 pp. Data and report available via GEUS: Processing summary sheet (geus.dk)

Mathiassen, D.R., Kristensen, L., Japsen, P., Rasmussen, E.S. and Michelsen, O. 1989. Evaluering af Gassum og Fjerritslev Formationerne på Stenlille strukturen. Bidrag til vurdering af gaslager. Danmarks Geologiske Undersøgelse, fortrolig rapport nr. 3, 1989.

Mathiesen, A., Dam, G., Fyhn, M.B.W., Kristensen, L., Mørk, F., Petersen, H.I. and Schovsbo, N.H. 2022. Foreløbig evaluering af CO_2 lagringspotentiale af de saline akviferer i Nordsøen. Grønlands Geologiske Undersøgelse Rapport 2022/15, 151 pp. + App.

Michelsen, O. 1975. Lower Jurassic biostratigraphy and ostracods of the Danish Embayment. Danmarks Geologiske Undersøgelse II. Række 104, 1-287. https://doi.org/10.34194/raekke2.v104.6895.

Michelsen, O. 1978. Stratigraphy and distribution of Jurassic deposits of the Norwegian–Danish Basin. Danmarks Geologiske Undersøgelse Serie B, Nr. 2, 28 pp. https://doi.org/10.34194/serieb.v2.7057

Michelsen, O. 1989a. Revision of the Jurassic lithostratigraphy of the Danish Subbasin. Danmarks Geologiske Undersøgelse, Serie A, Nr. 24, 23 pp.

Michelsen, O. 1989b. Log-sequence analysis and environmental aspects of the Lower Jurassic Fjerritslev Formation in the Danish Subbasin. Danmarks Geologiske Undersøgelse, Serie A, Nr. 25, 23 pp.

Michelsen, O. and Clausen, O.R. 2002. Detailed stratigraphic subdivision and regional correlation of the southern Danish Triassic succession. Marine and Petroleum Geology, 19, 563–587. https://doi.org/10.1016/S0264-8172(02)00028-4

Michelsen O. and Nielsen, L.H. 1991. Well records on the Phanerozoic stratigraphy in the Fennoscandian Border Zone, Denmark: Hans-1, Sæby-1, and Terne-1 wells. Geological Survey of Denmark – DGU Serie A, 29. 38 pp. https://doi.org/10.34194/seriea.v29.7049

Michelsen, O. and Nielsen, L.H. 1993. Structural development of the Fennoscandian Border Zone, offshore Denmark. Marine and Petroleum Geology Vol 10, 124–134.

Michelsen, O., Saxov, S. Leth, J.A., Andersen, C., Balling, N., Breiner, N., Holm, L., Jensen, K., Kristensen, J.I., Laier, T., Nygaard, E., Olsen, J.C., Poulsen, K.D., Priisholm, S., Raade, T.B., Sørensen, T.R. and Würtz, J. 1981. Kortlægning af potentielle geotermiske reservoirer I Danmark. Danmarks Geologiske Undersøgelse Serie B, Nr. 5, 96 pp.

Michelsen, O., Nielsen, L.H., Johannessen, P.N., Andsbjerg, J. and Surlyk, F. 2003. Jurassic lithostratigraphy and stratigraphic development onshore and offshore Denmark. In: Ineson, J.R. and Surlyk, F. (eds): The Jurassic of Denmark and Greenland. Geological Survey of Denmark and Greenland Bulletin 1, p. 145–216. https://doi.org/10.34194/geusb.v1.4651

Mogensen, T.E. and Korstgård, J.A. 2003. Triassic and Jurassic transtension along part of the Sorgenfrei-Tornquist Zone in the Danish Kattegat. GEUS Bulletin, 1. p. 437–458. https://doi.org/10.34194/geusb.v1.4680

Nielsen, L., Boldreel, L.O., Hansen, T.M, Lykke-Andersen, H., Stemmerik, L., Surlyk, F. and Thybo, H. 2011. Integrated seismic analysis of the Chalk Group in eastern Denmark – Implications for estimates of maximum palaeo-burial in southwest Scandinavia. Tectonophysics, 511, 14-26. doi:10.1016/j.tecto.2011.08.010

Nielsen, L.H. 2003. Late Triassic – Jurassic development of the Danish Basin and the Fennoscandian Border Zone, southern Scandinavia. In: Ineson, J.R. and Surlyk, F. (eds): The Jurassic of Denmark and Greenland. Geological Survey of Denmark and Greenland Bulletin 1, p. 459–526. https://doi.org/10.34194/geusb.v1.4681

Nielsen, L.H. and Japsen, P. 1991. Deep wells in Denmark 1935-1990. Lithostratigraphic subdivision. Danmarks Geologiske Undersøgelse, DGU Serie A, No. 31, 177 pp.

Olivarius, M. and Nielsen, L.H., 2016. Triassic paleogeography of the greater eastern Norwegian-Danish Basin: constraints from provenance analysis of the Skagerrak Formation. Marine and Petroleum Geology 69: 168–182.

Olivarius, M., Weibel, R., Hjuler, M. L., Kristensen, L., Mathiesen, A., Nielsen, L. H. and Kjøller, C. 2015. Diagenetic effects on porosity–permeability relationships in red beds of the Lower Triassic Bunter Sandstone Formation in the North German Basin. Sedimentary Geology, 321, 139–153.

Olivarius, M., Sundal, A., Weibel, R., Gregersen, U., Baig, I., Thomsen, T.B., Kristensen, L., Hellevang, H. and Nielsen, L.H., 2019. Provenance and sediment maturity as controls on CO_2 mineral sequestration potential of the Gassum Formation in the Skagerrak. Frontiers in Earth Science 7:312, 23 pp.

Olivarius, M., Heredia, B.D., Malkki, S.N., Thomsen, T.B. and Vosgerau, H. 2020. Capture, Storage and Use of CO2 (CCUS): Provenance of the of Gassum Formation: Implications for reservoir distribution and mineralogy (Part of Work package 6 in the CCUS project).

Danmarks og Grønlands Geologiske Undersøgelse Rapport 2020/38, 35 pp. https://doi.org/10.22008/gpub/34535

Olivarius, M., Vosgerau, H., Nielsen, L.H., Weibel, R., Malkki, S.N., Heredia, B.D. and Thomsen, T.B. 2022. Maturity Matters in Provenance Analysis: Mineralogical Differences Explained by Sediment Transport from Fennoscandian and Variscian Sources. Geosciences 2022, 12(8), 308. 24 pp. https://doi.org/10.3390/geosciences12080308

Papadopoulou, M., Malehmir, A., Zappalá, S., Gregersen, U., Nielsen, L. and Hjelm, L. 2022. Innovative land seismic data acquisitions for CO_2 and energy storage applications. EAGE – Near Surface Geoscience '22 conference, Belgrade, Serbia. Extended abstract. Vol. 2022, p. 1–5. https://doi.org/10.3997/2214-4609.202220098

Papadopoulou, M., Zappalá, S., Malehmir, A., Gregersen, U., Hjelm, L., Nielsen, L. and Haspang, M.P. 2023a. Innovative land seismic investigations for CO_2 geological storage in Denmark. Geophysics, 88, B251–B266. https://doi.org/10.1190/geo2022-0693.1

Papadopoulou, M., Zappalà, S., Malehmir, A., Kucinskaite, K., Westgate, M., Gregersen, U., Hjelm, L., Funck, T. and Nielsen, L. 2023b. Upscaling Innovative Land Seismic Acquisitions for Geological Storage of CO_2 in Denmark. European Association of Geoscientists & Engineers, Conference paper. Conference Proceedings Volume 2023, 1–5. https://doi.org/10.3997/2214-4609.202310385

Payton, C.E. 1977. Seismic Stratigraphy – applications to hydrocarbon exploration. The American Association of Petroleum Geologists – AAPG Memoir 26, Tulsa, Oklahoma, USA. 516 pp.

Pedersen, G.K. 1985. Thin, fine-grained storm layers in a shelf sequence: an example from the Lower Jurassic in the Stenlille 1 Well, Denmark. Journal of the Geological Society of London 142, 357–374. DOI: 10.1144/gsjgs.142.2.0357; WOSUID: WOS:A1985AFN5800010

Pedersen, G.K. 1986. Changes in the bivalve assemblage of an early Jurassic mudstone sequence (the Fjerritslev Formation in the Gassum 1 Well, Denmark). Palaeogeography, Palaeoclimatology, Palaeoecology 53, 139–168. DOI: 10.1016/0031-0182(86)90042-8 WOSUID: WOS: A1986A988800002

Pedersen, G.K., Lauridsen, B.W., Sheldon, E. and Midtgaard, H.H. 2022. Studies of geological properties and conditions for deep disposal of radioactive waste, Denmark. Phase 1, report no. 4. Jurassic and Lower Cretaceous claystone distribution, sedimentology, and properties. Danmarks og Grønlands Geologiske Undersøgelse Rapport 2021/55; GEUS. 105 pp and appendices. https://doi.org/10.22008/gpub/34615

Petersen, H.I. and Lindström, S. 2012. Synchronous wildfire activity and mire deforestation at the Triassic–Jurassic boundary. PLoS ONE 7(10): e47236. Doi:10.1371/journal.pone0047236

Petersen, H. I., Nielsen, L. H., Bojesen-Koefoed, J. A., Mathiesen, A., Kristensen, L. and Dalhoff, F. 2008. Evaluation of the quality, thermal maturity and distribution of potential source rocks in the Danish part of the Norwegian–Danish Basin. Geological Survey of Denmark and Greenland Bulletin, 16, 66 pp. https://doi.org/10.34194/geusb.v16.4989

Poulsen, N.E. and Riding, J.B. 2003: The Jurassic dinoflagellate cyst zonation of Subboreal Northwest Europe. Geological Survey of Denmark and Greenland Bulletin 1, 115–144.

Rasmussen, E.S. and Nielsen, A.T. 2020. Danmarks Geologi – En kort introduktion. Junior Geologerne. https://junior-geologerne.dk/wp-content/uploads/2020/06/Junior-Geologerne_Danmarks_geologi.pdf

Realtime Seismic, 2023. GEUS2022-HAVNSOE-RE2023. Reprocessing of the GEUS2022-HAVNSOE 2D Seismic Survey for the Geological Survey of Denmark and Greenland. Realtime Seismic Pty. Ltd., France. 57 pp. Link to info: Processing summary sheet (geus.dk)

Schovsbo N.H. 2011. The Lower Palaeozoic sequence in the Slagelse-1 well. Stratigraphical, lithological and geochemical evaluation. Danmarks og Grønlands Geologiske Undersøgelse Rapport 2011/84; GEUS. 49 pp. https://doi.org/10.22008/gpub/28811.

Simm, R. and Bacon, M. 2014. Seismic amplitude: An interpreter's handbook. Cambridge University Press.

Smit, F.W.H., Gregersen, U., Lorentzen, M., Bredesen, K., Pedersen, G.K., Hovikoski, J. and Vosgerau, H. 2022. Seismic Geomorphology of the Upper Triassic – Lower Jurassic Gassum Formation – Improved Reservoir Characterization in the Stenlille (Denmark) CCS Demonstration Site. GHGT-16 Conference Proceedings (2022); Geophysics eJournal, 4 (83), December 2022, 11 pp. SSRN: https://papers.ssrn.com/abstract=4277360

Sorgenfrei, T. and Buch, A. 1964. Deep Tests in Denmark 1935–1959. Danmarks Geologiske Undersøgelse, Række III, Nr. 36, 146 p. https://doi.org/10.34194/raekke3.v36.6941

Span, R. and Wagner, W. 1996. A new equation of state for carbon dioxide covering the fluid region from the triple-point temperature to 1100K at pressures up to 800 MPa, J. Phys. Chem. Ref. Data, 25, 1509–1596.

Springer, N., Didriksen, K., Holmslykke, H.D., Kjøller, C., Olivarius, M. and Schovsbo, N. 2020. Capture, Storage and Use of CO2 (CCUS): Seal capacity and geochemical modelling (Part of work package 5 in the CCUS project). Danmarks og Grønlands Geologiske Undersøgelse Rapport 2020/30; GEUS. 42 pp. https://doi.org/10.22008/gpub/34527

Spudich, P., Fletcher, J., Hellweg, M., Boatwright, J., Sullivan, C., Joyner, W., Hanks, T., Boore, D.M., McGarr, A. and Baker, L. 1997. SEA96—A new predictive relation for earthquake ground motions in extensional tectonic regimes. Seismological Research Letters 68(1), 190–198.

Stenestad, E. 1972. Træk af det danske bassins udvikling i Øvre Kridt. Dansk Geologisk Forening Aarsskrift, 1971, 63–69.

Surlyk, F. Arndorff, L., Hamann, N.E., Hamberg, L., Johannessen, P.N., Koppelhus, E.B., Nielsen, L.H., Noe-Nygaard, N., Pedersen, G.K. and Petersen, H.I. 1995. High-resolution sequence stratigraphy of the Hettangian–Sinemurian paralic succession, Bornholm, Denmark. Sedimentology 42, 323–354. DOI: 10.1111/j.1365-3091.1995.tb02105.x WOSUID: WOS:A1995QR46100007

Surlyk, F., Rasmussen, S. L., Boussaha, M., Schiøler, P., Schovsbo, N. H., Sheldon, E., Stemmerik, L. and Thibault, N. 2013. Upper Campanian-Maastrichtian holostratigraphy of the eastern Danish Basin. *Cretaceous Research*, *46*, 232-256. https://doi.org/10.1016/j.cretres.2013.08.006

THOR, 1997. 3D Stenlille-97 Final acquisition report. THOR Geophysikalische Prospektion GmbH seismic acquisition report for DONG A/S. Germany, December 1997.

Vejbæk O.V. 1997. Dybe strukturer i danske sedimentære bassiner. Geologisk Tidsskrift 1997/4; p. 1–31. https://2dgf.dk/xpdf/gt1997-4-1-31.pdf.

Vejbæk, O.V. and Britze, P. 1994. Geological map of Denmark 1:750.000. Top pre-Zechstein. Danmarks Geologiske Undersøgelse Map series, 45, 9 pp.

Vosgerau, H., Gregersen, U., Hjuler, M.L., Holmslykke, H.D., Kristensen, L., Lindström, S., Mathiesen, A., Nielsen, C.M., Olivarius, M., Pedersen, G.K. and Nielsen, L.H. 2016. Reservoir prognosis of the Gassum Formation and the Karlebo Member within two areas of interest in northern Copenhagen. The EUDP project "Geothermal pilot well, phase 1b". GEUS Rapport 2016/56. 138 pp + app 1–5. https://doi.org/10.22008/gpub/32477

Vosgerau, H., Gregersen, U. and Laghari, S. 2020. Capture, Storage and Use of CO2 (CCUS): Seismic interpretation of existing 3D seismic data around the Stenlille structure within the framework of sequence stratigraphy and with focus on the Gassum Formation (Part of Work package 6 in the CCUS project). Danmarks og Grønlands Geologiske Undersøgelse Rapport 2020/34; GEUS. 53 pp. https://doi.org/10.22008/gpub/34531

Vosgerau et al. *in prep*. Reservoir architecture of the Upper Triassic–Lower Jurassic Gassum Formation at two potential CO2 storage sites, the Stenlille and Havnsø structures, Denmark.

Voss, P., Dahl-Jensen, T. and Larsen, T. B. 2015. Earthquake Hazard in Denmark. Geological Survey of Denmark and Greenland report 2015/24, 53 pp.

Wang, Y., Zhangb, K. and Wua, N. 2013. Numerical Investigation of the Storage Efficiency Factor for CO2 Geological Sequestration in Saline Formations, Energy Procedia, Volume 37, 5267–5274.

Weibel, R., Olivarius, M., Kristensen, L., Friis, H., Hjuler, M.L., Kjøller, C., Mathiesen, A. and Nielsen, L.H., 2017a. Predicting permeability of low enthalpy geothermal reservoirs: examples from the Upper Triassic−Lower Jurassic Gassum Formation, Norwegian–Danish Basin. Geothermics 65: 135–157.

Weibel, R., Olivarius, M., Friis, H., Kristensen, L., Hjuler, M.L., Kjøller, C., Pedersen, P.K., Boyce, A., Mathiesen, A. and Nielsen, L.H. 2017b. The influence of climate on early and burial diagenesis in Triassic and Jurassic sandstones from the Norwegian–Danish Basin. The Depositional Record 3(1): 60–91.

Weibel, R., Olivarius, M., Vosgerau, H., Mathiesen, A., Kristensen, L., Nielsen, C. M. and Nielsen, L. H. 2020. Overview of potential geothermal reservoirs in Denmark. Netherlands Journal of Geosciences, 99, e3, 14 pp.

Yang, B., Shao, C., Hu, X., Ngata, M.B. and Aminu, M.D. 2023. Advances in Carbon Dioxide Storage Projects: Assessment and Perspectives, *Energy & Fuels 2023,* 37, 3, 1757–1776 (Review). DOI: 10.1021/acs.energyfuels.2c03826

Zappalá, S., Malehmir, A., Papadopoulou, M., Gregersen, U., Funck, T., Clausen, O. R. and Nørmark, E. *in review*. Practical aspects of a dual-element seismic data acquisition system for CCS applications across onshore and offshore transition areas at Havnsø, Denmark. *Geophysics*.

Appendix A – Depth conversion (see Chapter 5)

Appendix A – Velocity model and depth-conversion, additional figures

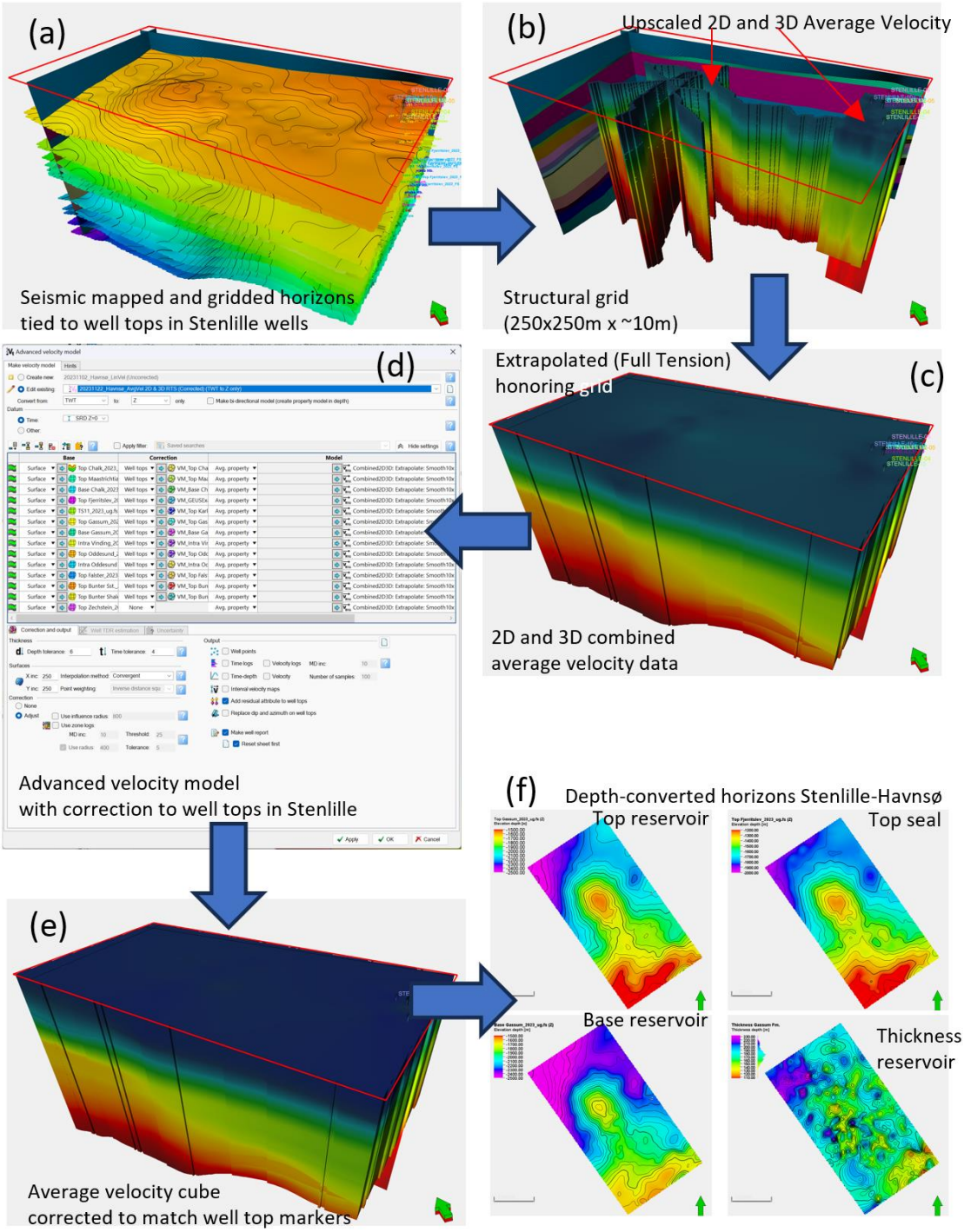

A1. *(A) 3D perspective of the 14 horizons considered in the velocity model, which define the structural grid (250x250xc.10ms). The Stenlille structure is located on the righthand side where also the wells are indicated that were used to constrain the velocities. (B) The structural grid is indicated by the sections (0–3270 ms TWT), and the upscaled 2D and 3D Dix-converted RMS seismic migration velocities are shown (purple: 1500 m/s to red: 4000 m/s). (C) The data are interpolated within the grid using a full tension algorithm (Spline in Tension) and smoothened 10x to remove outliers where the 2D intersect. (D) An advanced velocity model is set up using the 14 horizons and associated well tops in Stenlille wells for correction. (E) Velocities are adjusted to find a match between depth-converted horizon and well tops. (F) This cube is then used to depth-convert the TWT horizons. (depth=average velocity*(surface TWT)/2).*

Appendix A – Velocity model and depth-conversion, additional figures

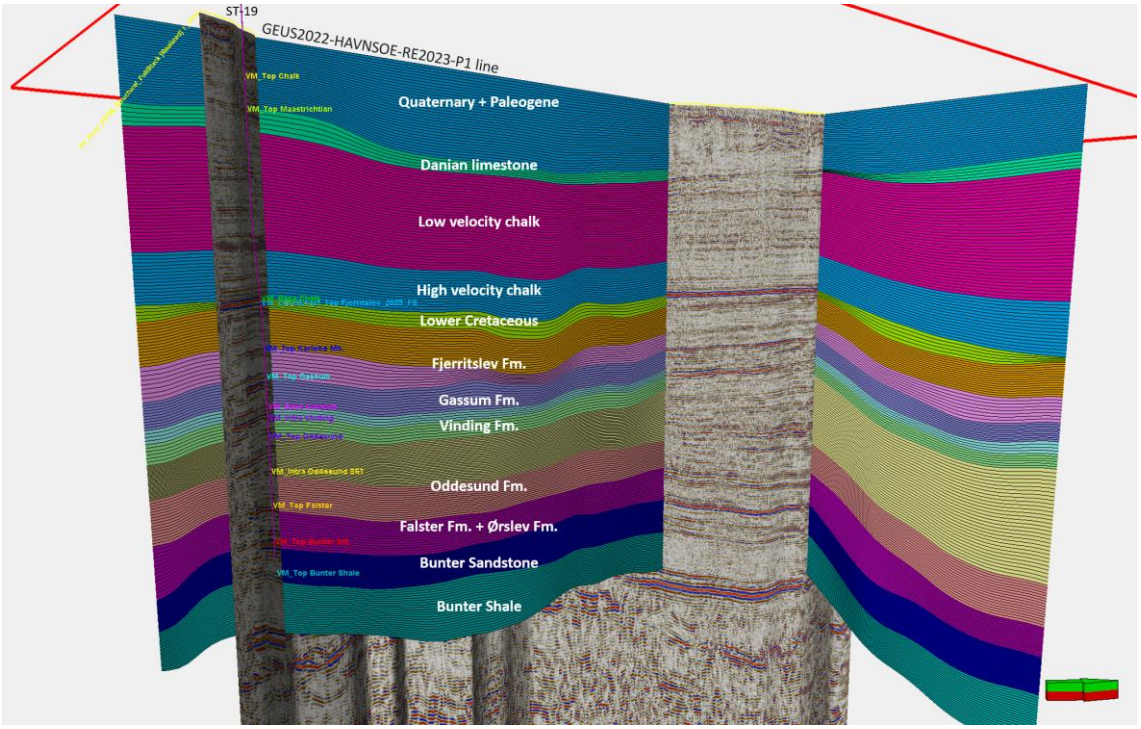

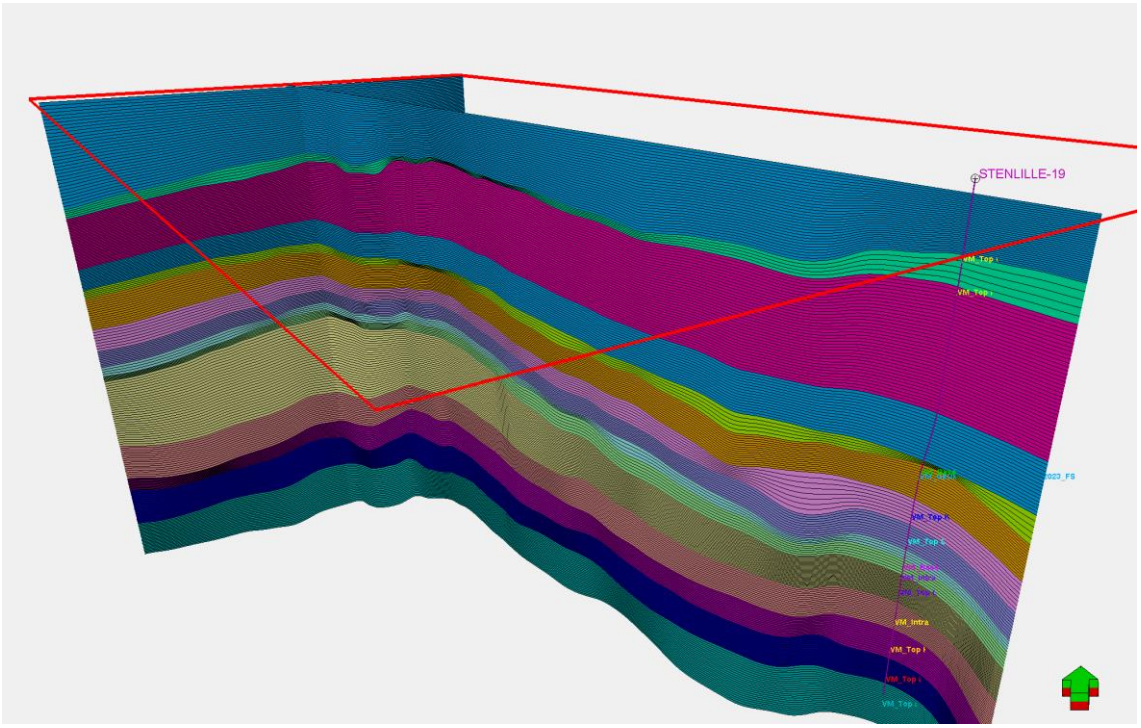

A2. *Mapped seismic horizons were input to generate a 3D structural grid that was used for modelling the seismic velocities from 2D and 3D data. Top of the model was sea-level (0 ms) and base Top Zechstein Fm. A cell size of 250x250m was used, and average thickness of the zones between 10 and 20 ms.*

Appendix A – Velocity model and depth-conversion, additional figures

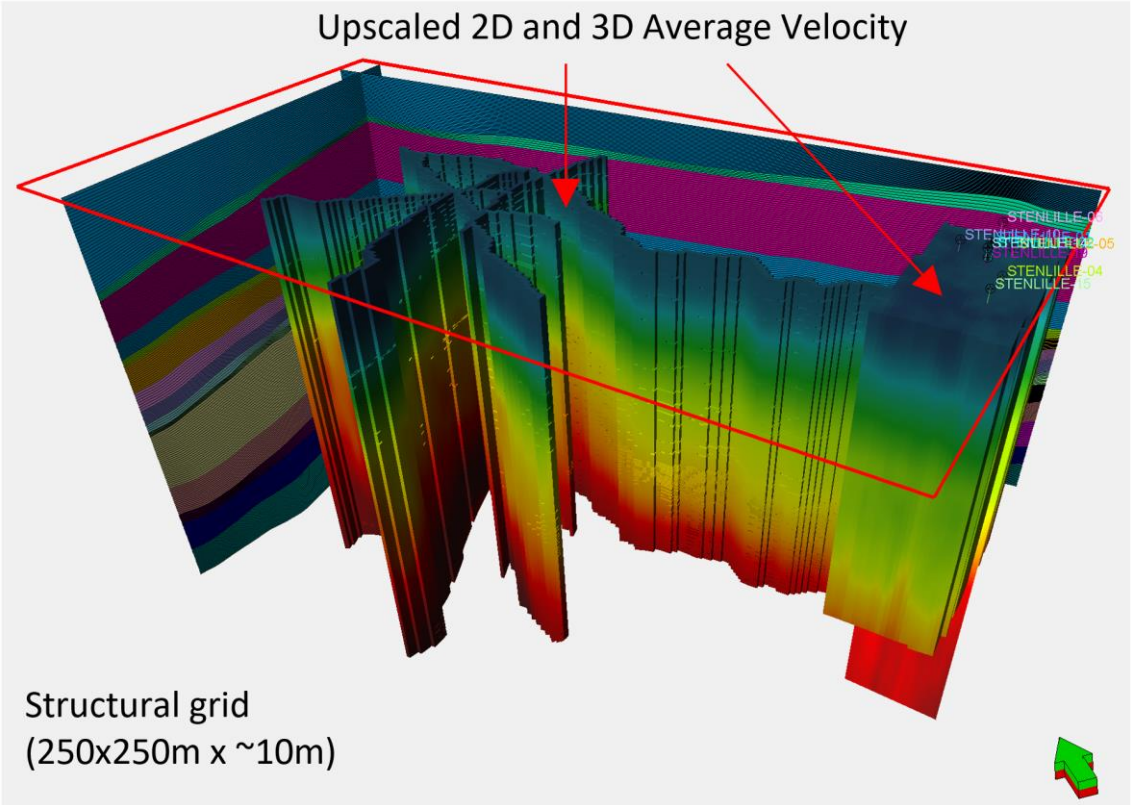

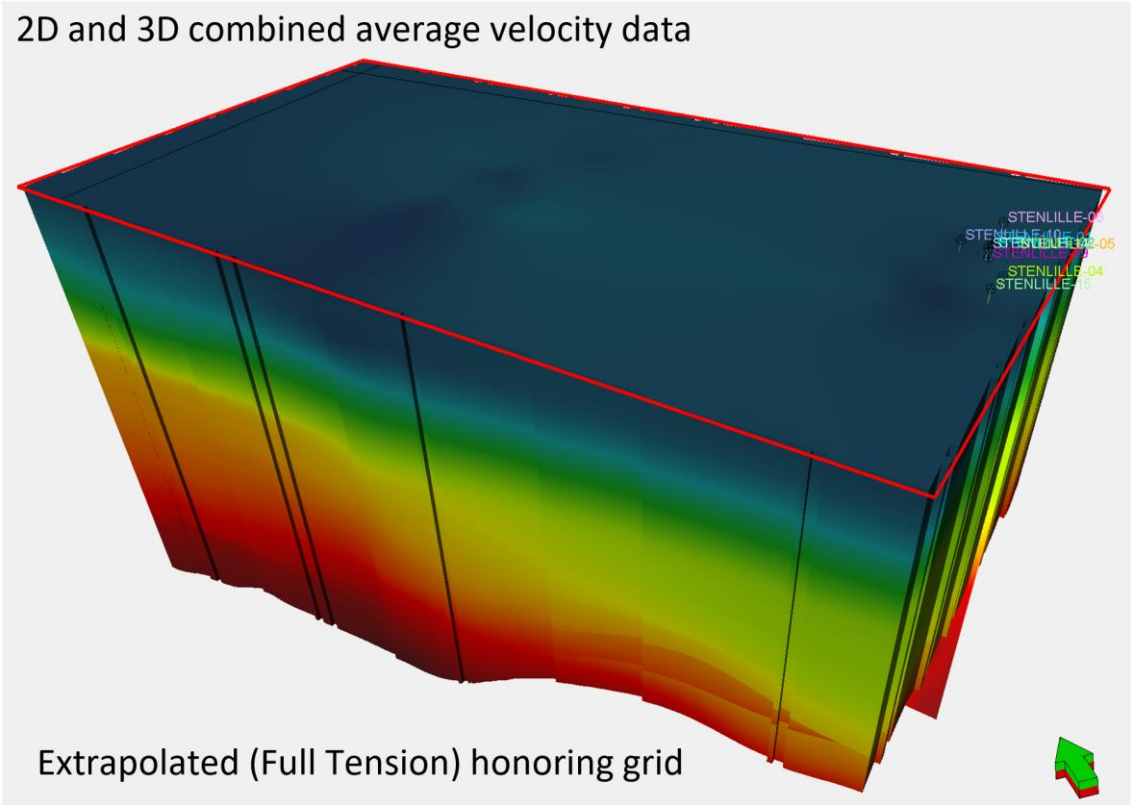

A3. *Average velocities from 2D and 3D seismic data were upscaled into the grid using arithmetic mean. The data were extrapolated within each zone using a full tension algorithm (spline in tension).*

Appendix A – Velocity model and depth-conversion, additional figures

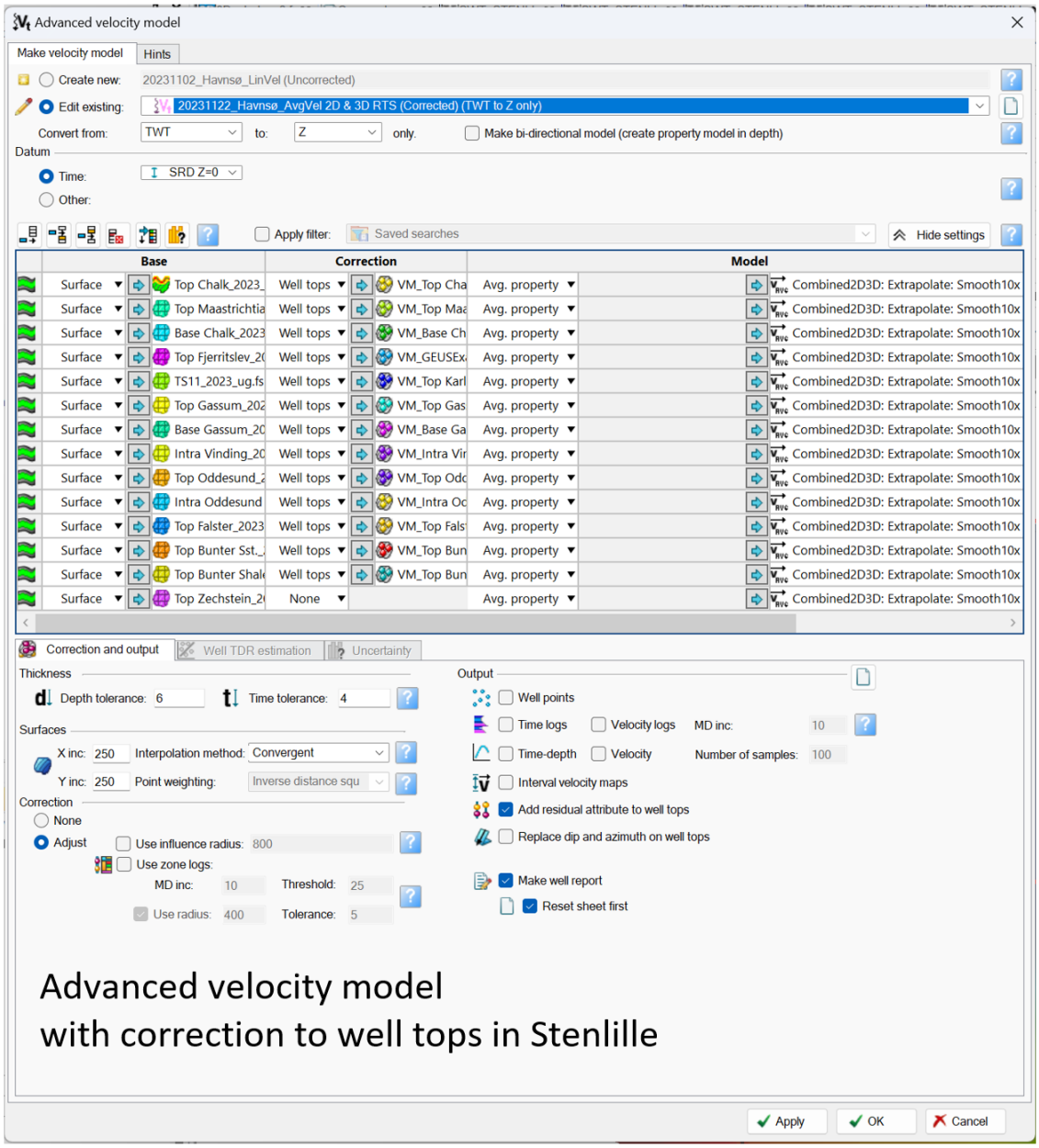

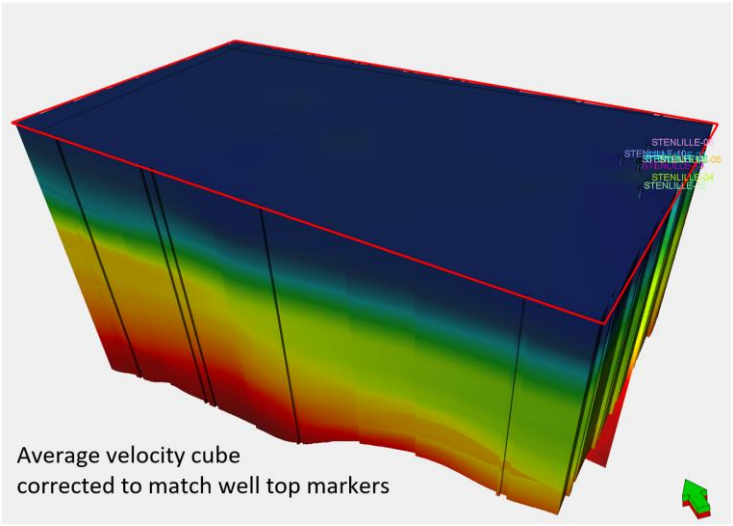

A4. *An advanced velocity model was set up using the 3D gridded surfaces (tied to well tops in TWT), associated well tops in depth, and as velocity model the 3D average velocity property. A global correction to well tops was used to improve the average velocities and get a good tie between depth-converted surface and well top in depth.*

Appendix A – Velocity model and depth-conversion, additional figures

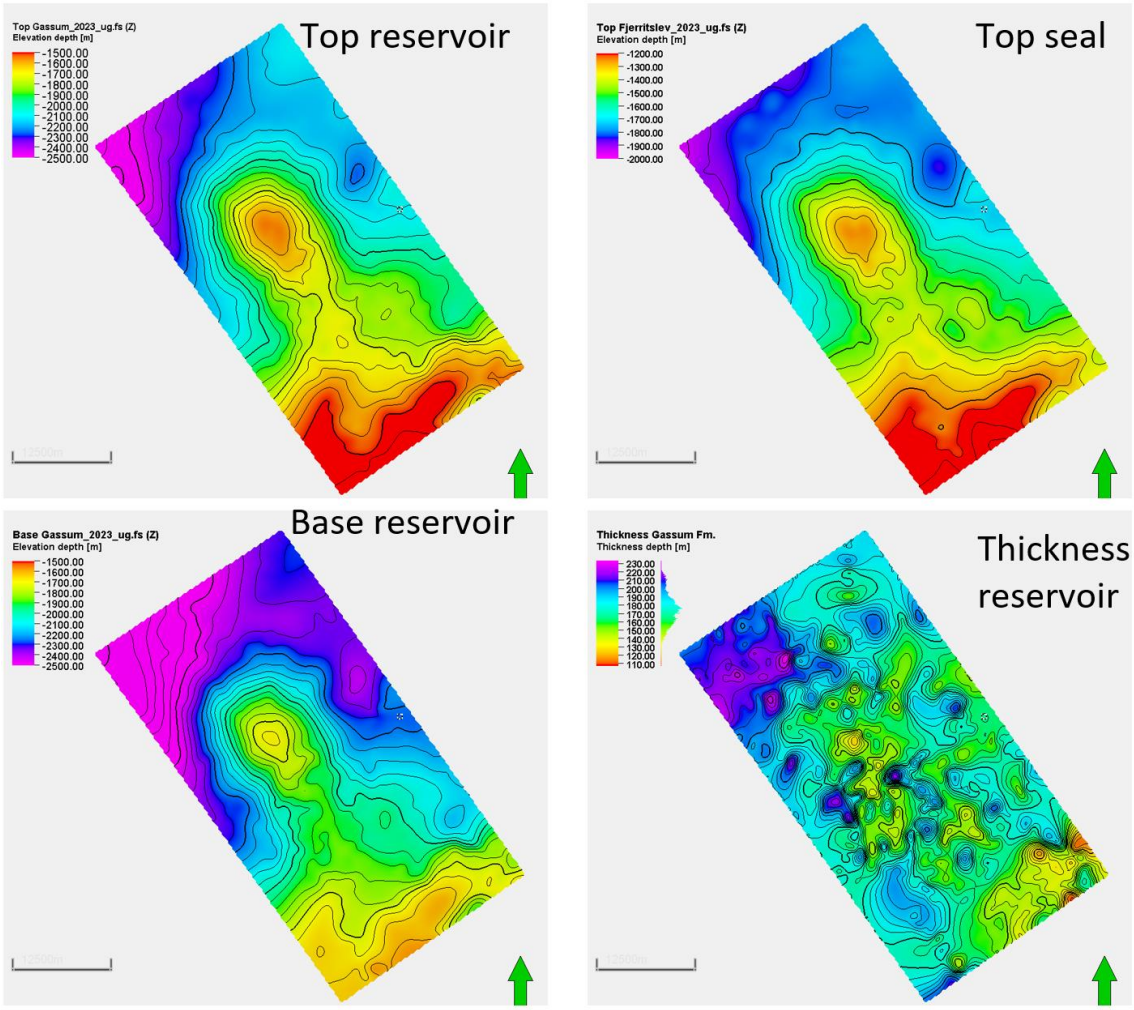

Depth-converted horizons Stenlille-Havnsø

A5. *The velocity model used to depth-convert horizons is called: 20231122_Havnsø_AvgVel 2D & 3D RTS (corrected). Using this velocity model, the TWT surfaces were depth-converted and used to generate depth structure maps, thickness maps, and perform volumetric calculations.*

Appendix B – Well-log interpretation (Stenlille & surrounding wells)

Link to the well-log interpretation of Appendix B:

- Stenlille-1
- Stenlille-4
- Stenlille-5
- Stenlille-6
- Stenlille-15
- Stenlille-19
- Slagelse-1
- Margretheholm-1A
- Lavø-1
- Terne-1
- Ullerslev-1
- Løve-1
- Jelling-1
- Horsens-1
- Rønde-1

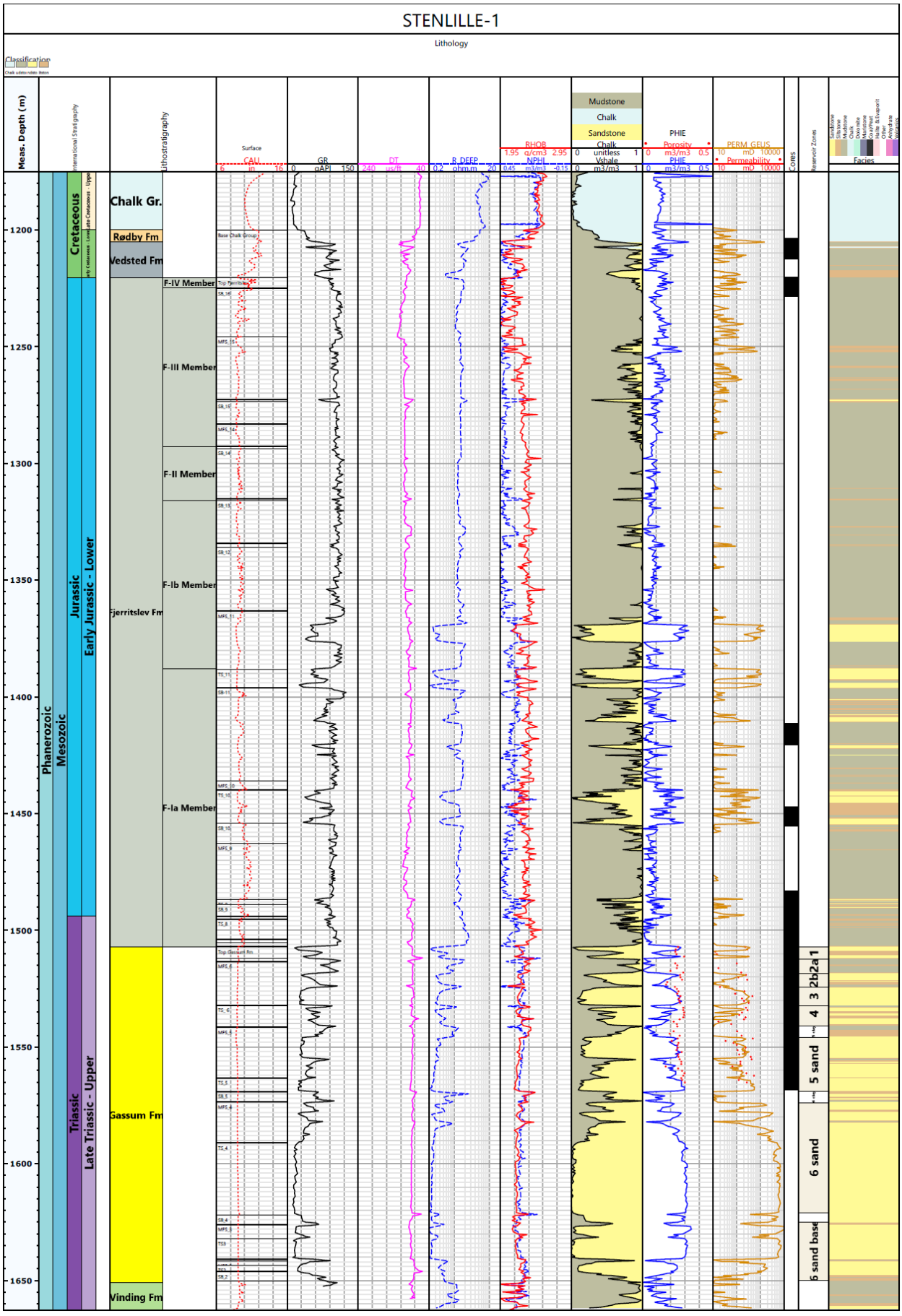
STENLILLE-1
Lithology
Classification
Meas. Depth (m)
International Stratigraphy
Lithostratigraphy
Surface
CALI
GR
gAPI
DT
us/ft
R_DEEP
ohm.m
RHOB
g/cm3
NPHI
m3/m3
Mudstone
Chalk
Sandstone
PHIE
Porosity
Vshale
PERM_GEUS
Permeability
Cores
Reservoir Zones
Facies
Phanerozoic
Mesozoic
Cretaceous
Jurassic
Early Jurassic - Lower
Triassic
Late Triassic - Upper
Chalk Gr.
Rødby Fm
Vedsted Fm
F-IV Member
F-III Member
F-II Member
F-Ib Member
F-Ia Member
Fjerritslev Fm
Gassum Fm
Vinding Fm
1200
1250
1300
1350
1400
1450
1500
1550
1600
1650
1
2b
2a
3
4
5 sand
6 sand
6 sand base

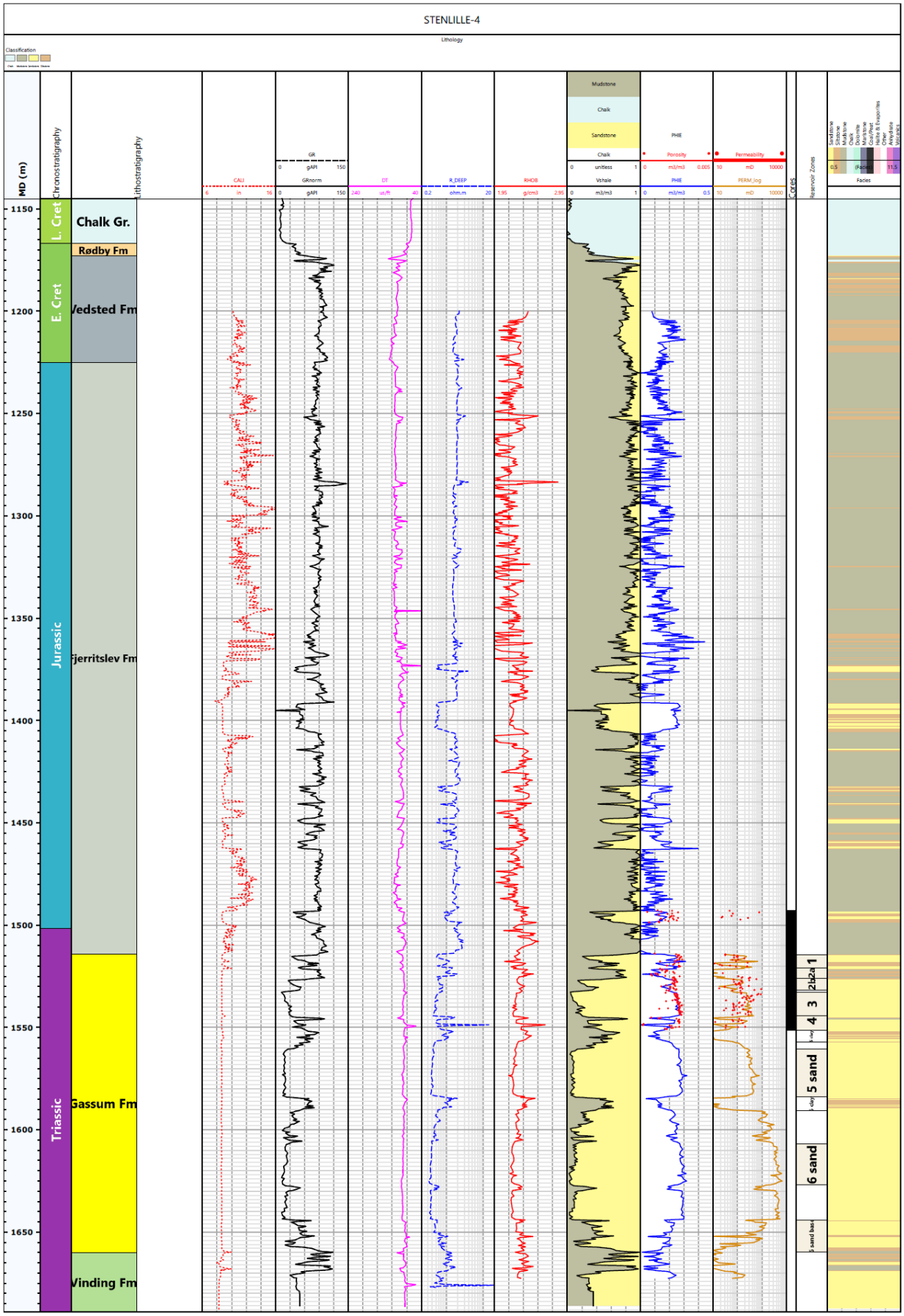
STENLILLE-4
Lithology
Classification
MD (m)
Chronostratigraphy
Lithostratigraphy
L. Cret
E. Cret
Jurassic
Triassic
Chalk Gr.
Rødby Fm
Vedsted Fm
Fjerritslev Fm
Gassum Fm
Vinding Fm
1150
1200
1250
1300
1350
1400
1450
1500
1550
1600
1650
CALI
GR
GRnorm
DT
R_DEEP
RHOB
Mudstone
Chalk
Sandstone
Vshale
PHIE
Porosity
Permeability
PERM_log
Cores
Reservoir Zones
2b2a 1
3
4
5 sand
6 sand
Facies

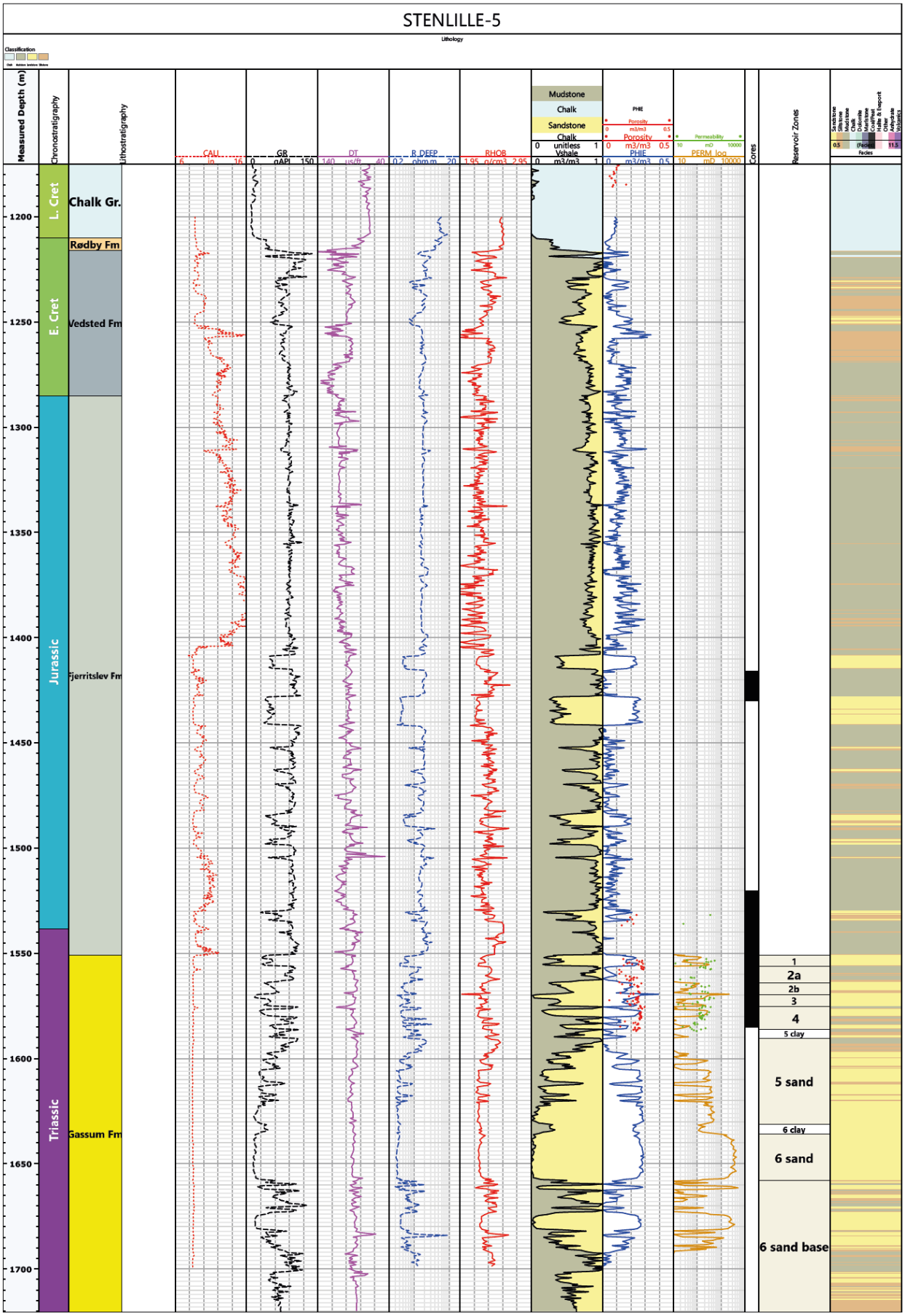
STENLILLE-5
Lithology
Classification
Measured Depth (m)
Chronostratigraphy
Lithostratigraphy
CALI
GR
DT
R_DEEP
RHOB
Mudstone
Chalk
Sandstone
Chalk
PHIE
Porosity
PHIE
Permeability
PERM_log
Cores
Reservoir Zones
Facies
L. Cret
E. Cret
Jurassic
Triassic
Chalk Gr.
Rødby Fm
Vedsted Fm
Fjerritslev Fm
Gassum Fm
1200
1250
1300
1350
1400
1450
1500
1550
1600
1650
1700
1
2a
2b
3
4
5 clay
5 sand
6 clay
6 sand
6 sand base

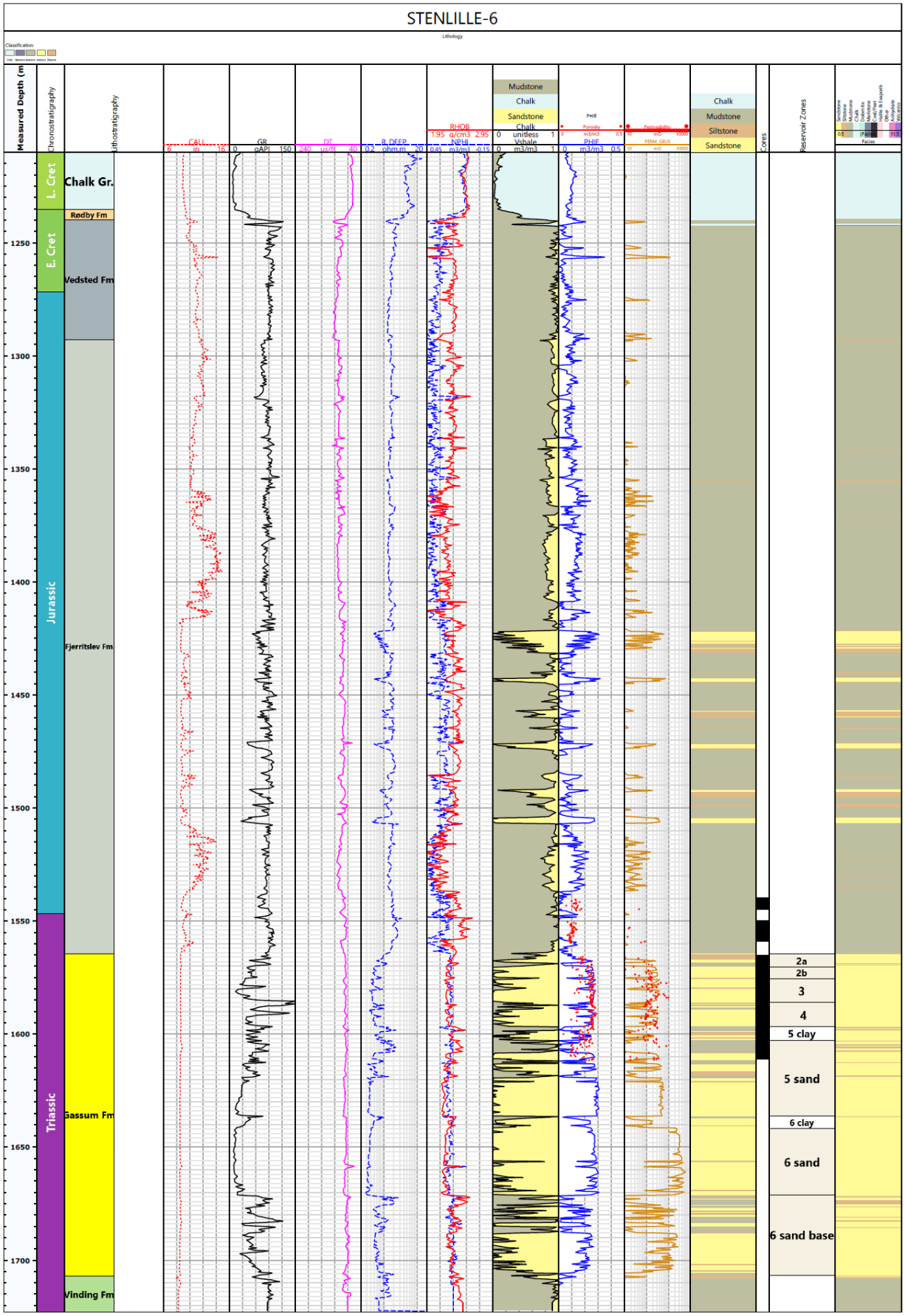
STENLILLE-6
Lithology
Measured Depth (m)
Chronostratigraphy
Lithostratigraphy
CALI
GR
DT
R_DEEP
RHOB
NPHI
Mudstone
Chalk
Sandstone
Chalk
PHIE
Permeability
Chalk
Mudstone
Siltstone
Sandstone
Cores
Reservoir Zones
Facies
L. Cret
E. Cret
Jurassic
Triassic
Chalk Gr.
Rødby Fm
Vedsted Fm
Fjerritslev Fm
Gassum Fm
Vinding Fm
1250
1300
1350
1400
1450
1500
1550
1600
1650
1700
2a
2b
3
4
5 clay
5 sand
6 clay
6 sand
6 sand base

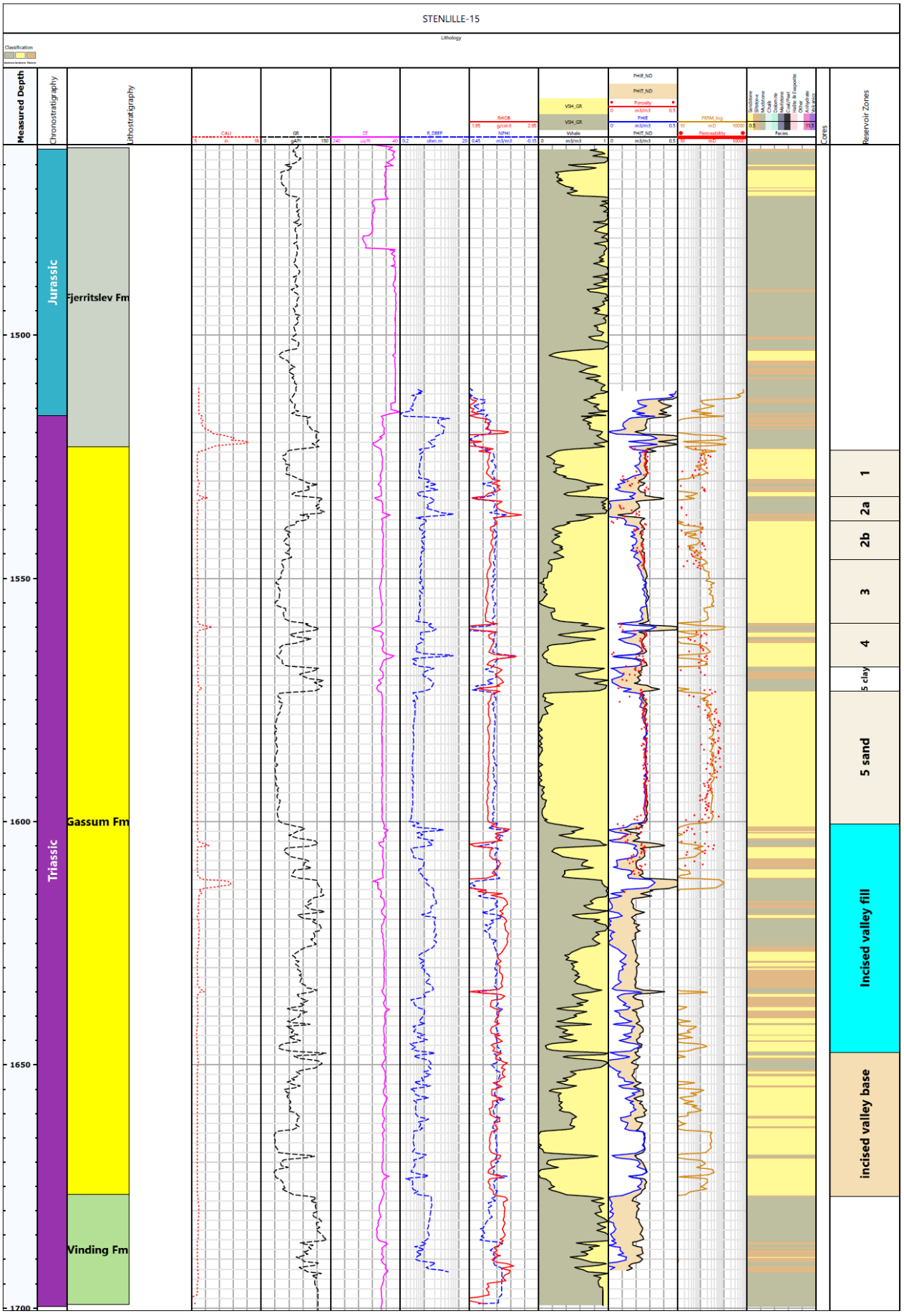
STENLILLE-15
Lithology
Measured Depth
Chronostratigraphy
Lithostratigraphy
Jurassic
Triassic
Fjerritslev Fm
Gassum Fm
Vinding Fm
1500
1550
1600
1650
1700
Cores
Reservoir Zones
1
2a
2b
3
4
5 clay
5 sand
Incised valley fill
incised valley base

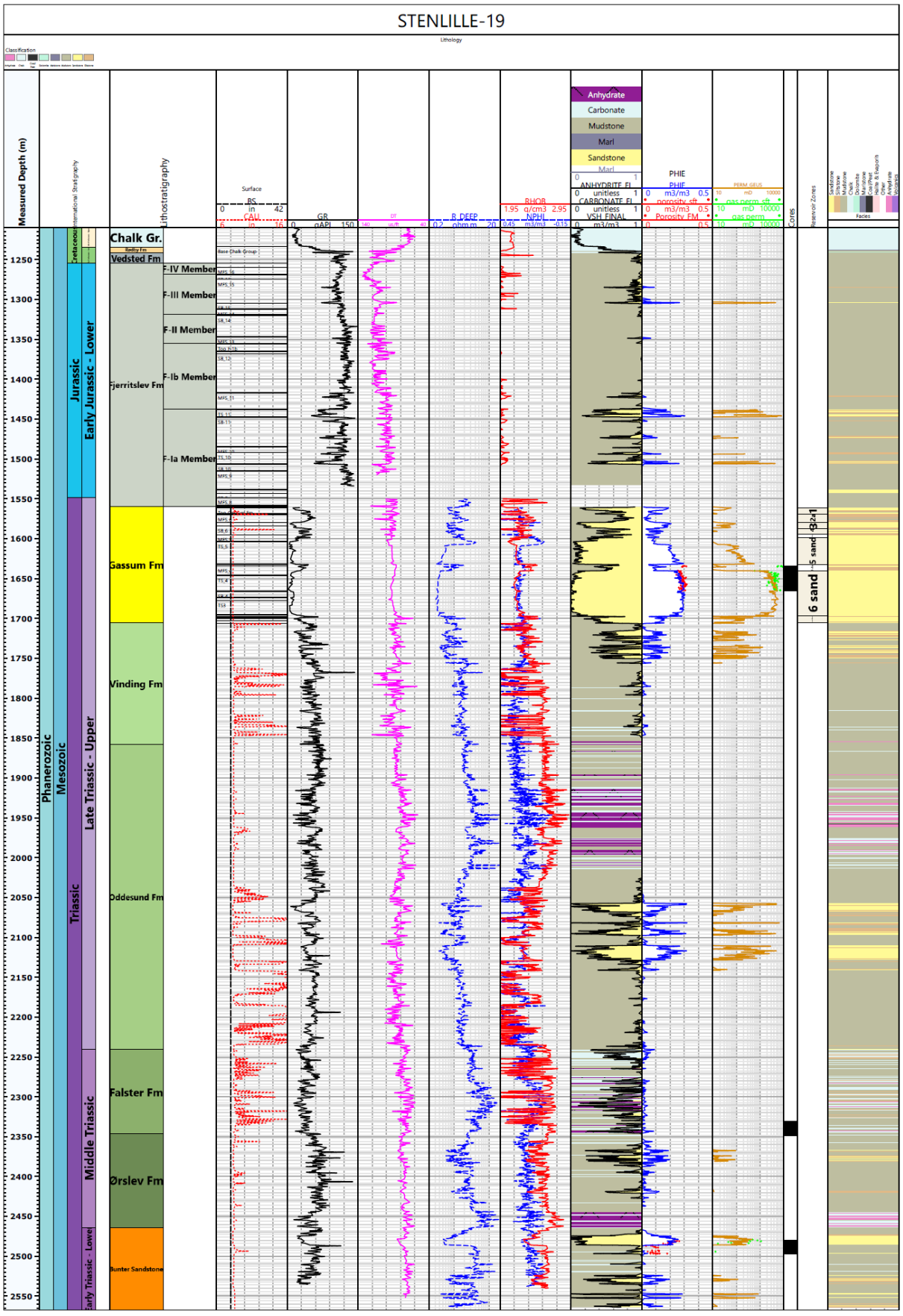
STENLILLE-19
Lithology
Measured Depth (m)
Chronostratigraphy
International Stratigraphy
Lithostratigraphy
Surface
BS
CALI
GR
RHOB
NPHI
Anhydrate
Carbonate
Mudstone
Marl
Sandstone
PHIE
PERM.GEUS
Cores
Reservoir Zones
Facies
Chalk Gr.
Vedsted Fm
F-IV Member
F-III Member
F-II Member
F-Ib Member
F-Ia Member
Fjerritslev Fm
Gassum Fm
Vinding Fm
Oddesund Fm
Falster Fm
Ørslev Fm
Bunter Sandstone
Phanerozoic
Mesozoic
Cretaceous
Jurassic
Triassic
Early Jurassic - Lower
Late Triassic - Upper
Middle Triassic
Early Triassic - Lower
6 sand
5 sand

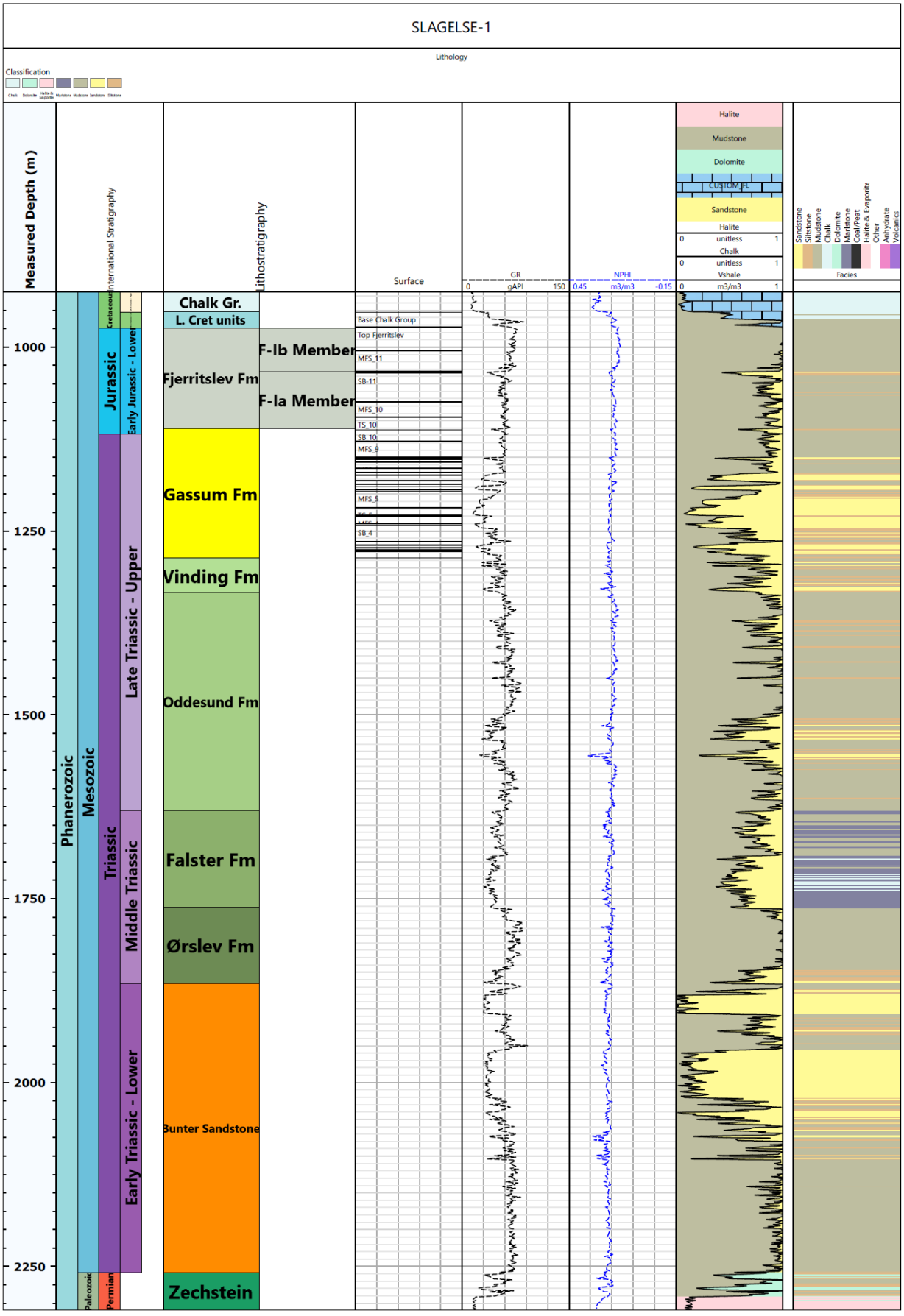
SLAGELSE-1
Lithology
Classification
Measured Depth (m)
International Stratigraphy
Lithostratigraphy
Surface
GR
gAPI
NPHI
m3/m3
Vshale
Facies
Halite
Mudstone
Dolomite
CUSTOM_FL
Sandstone
Chalk
unitless
Sandstone
Siltstone
Mudstone
Chalk
Dolomite
Marlstone
Coal/Peat
Halite & Evaporite
Chert
Anhydrate
Volcanics
Phanerozoic
Mesozoic
Paleozoic
Cretaceous
Jurassic
Triassic
Permian
Early Jurassic - Lower
Late Triassic - Upper
Middle Triassic
Early Triassic - Lower
Chalk Gr.
L. Cret units
Fjerritslev Fm
F-Ib Member
F-Ia Member
Gassum Fm
Vinding Fm
Oddesund Fm
Falster Fm
Ørslev Fm
Bunter Sandstone
Zechstein
Base Chalk Group
Top Fjerritslev
MFS_11
SB-11
MFS_10
TS_10
SB_10
MFS_9
MFS_5
SB_4
1000
1250
1500
1750
2000
2250

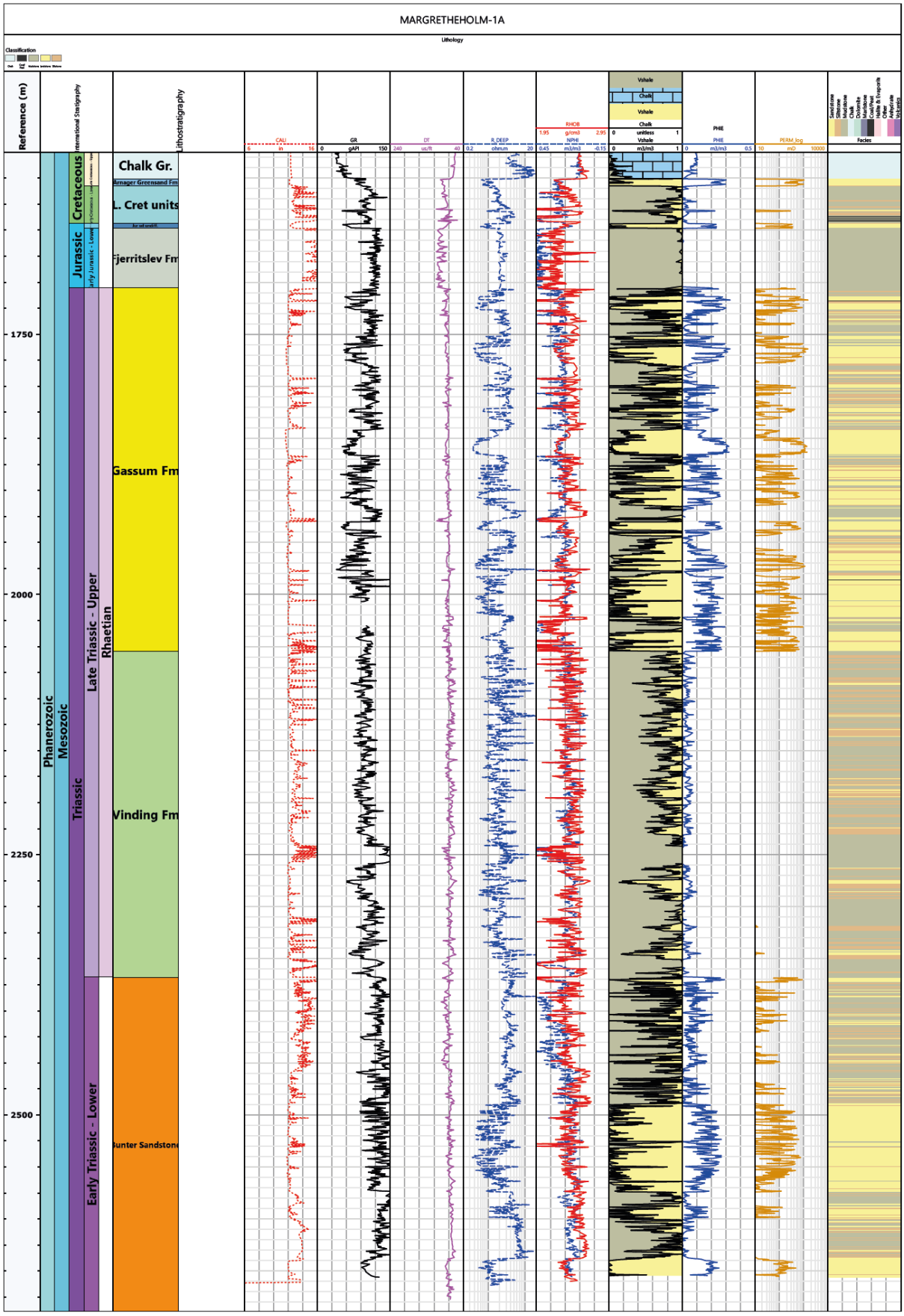
MARGRETHEHOLM-1A
Lithology
Classification
Reference (m)
International Stratigraphy
Lithostratigraphy
Phanerozoic
Mesozoic
Cretaceous
Jurassic
Triassic
Early Triassic - Lower
Late Triassic - Upper
Rhaetian
Chalk Gr.
Arnager Greensand Fm
L. Cret units
Fjerritslev Fm
Gassum Fm
Vinding Fm
Hunter Sandstone
1750
2000
2250
2500
CALI
GR
DT
R_DEEP
RHOB
PHIE
PERM_log
Facies

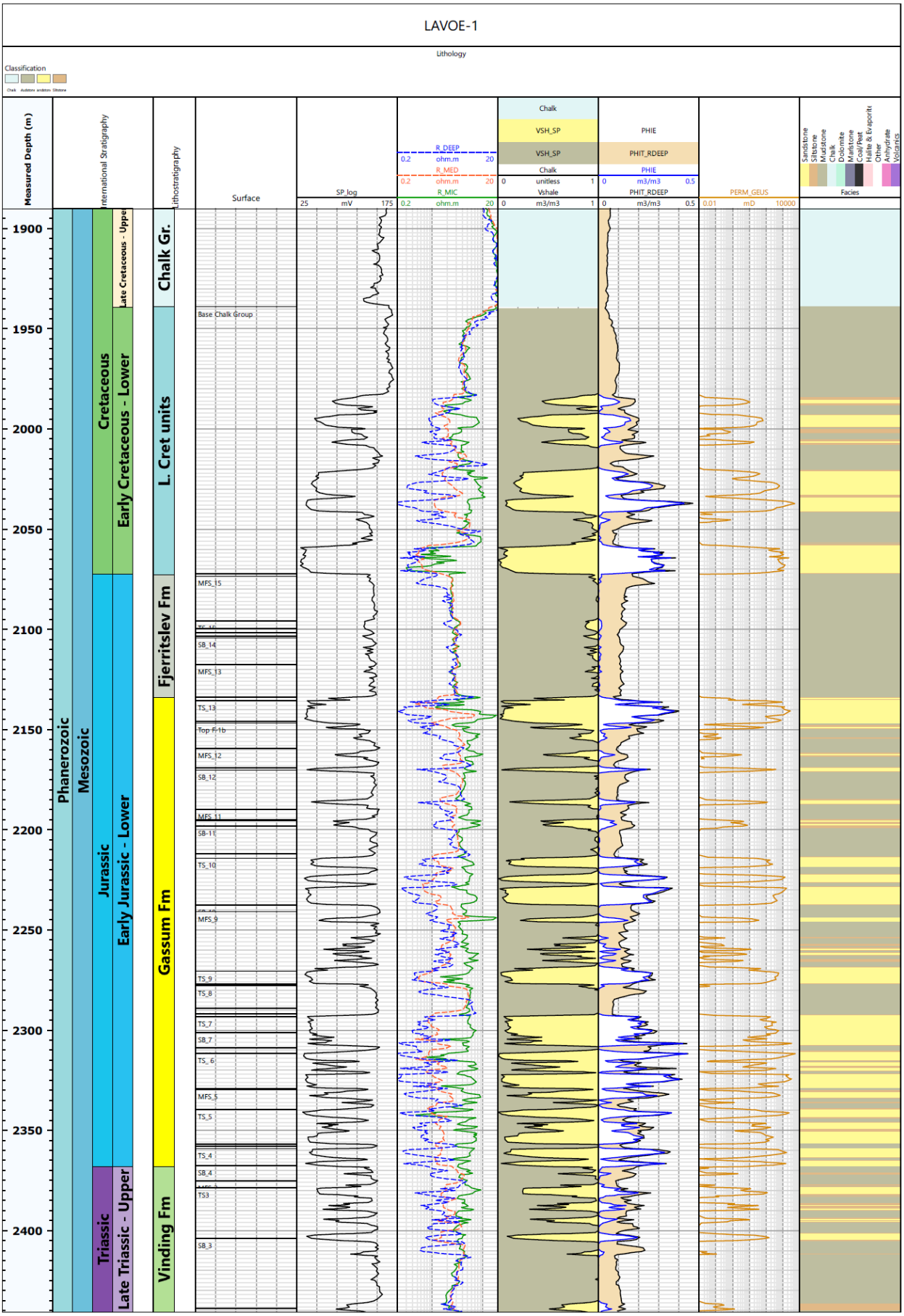
LAVOE-1
Lithology
Classification
Measured Depth (m)
International Stratigraphy
Lithostratigraphy
Surface
SP_log
25 mV 175
R_DEEP
R_MED
R_MIC
0.2 ohm.m 20
Chalk
VSH_SP
Chalk
0 unitless 1
Vshale
0 m3/m3 1
PHIE
PHIT_RDEEP
PHIE
0 m3/m3 0.5
PHIT_RDEEP
0 m3/m3 0.5
PERM_GEUS
0.01 mD 10000
Facies
Sandstone
Siltstone
Mudstone
Chalk
Dolomite
Marlstone
Coal/Peat
Halite & Evaporite
Other
Anhydrite
Volcanics
Phanerozoic
Mesozoic
Cretaceous
Late Cretaceous - Upper
Early Cretaceous - Lower
Jurassic
Early Jurassic - Lower
Triassic
Late Triassic - Upper
Chalk Gr.
L. Cret units
Fjerritslev Fm
Gassum Fm
Vinding Fm
1900
1950
2000
2050
2100
2150
2200
2250
2300
2350
2400
Base Chalk Group
MFS_15
SB_14
MFS_13
TS_13
Top F-1b
MFS_12
SB_12
MFS_11
SB-11
TS_10
MFS_9
TS_9
TS_8
TS_7
SB_7
TS_6
MFS_5
TS_5
TS_4
SB_4
TS3
SB_3

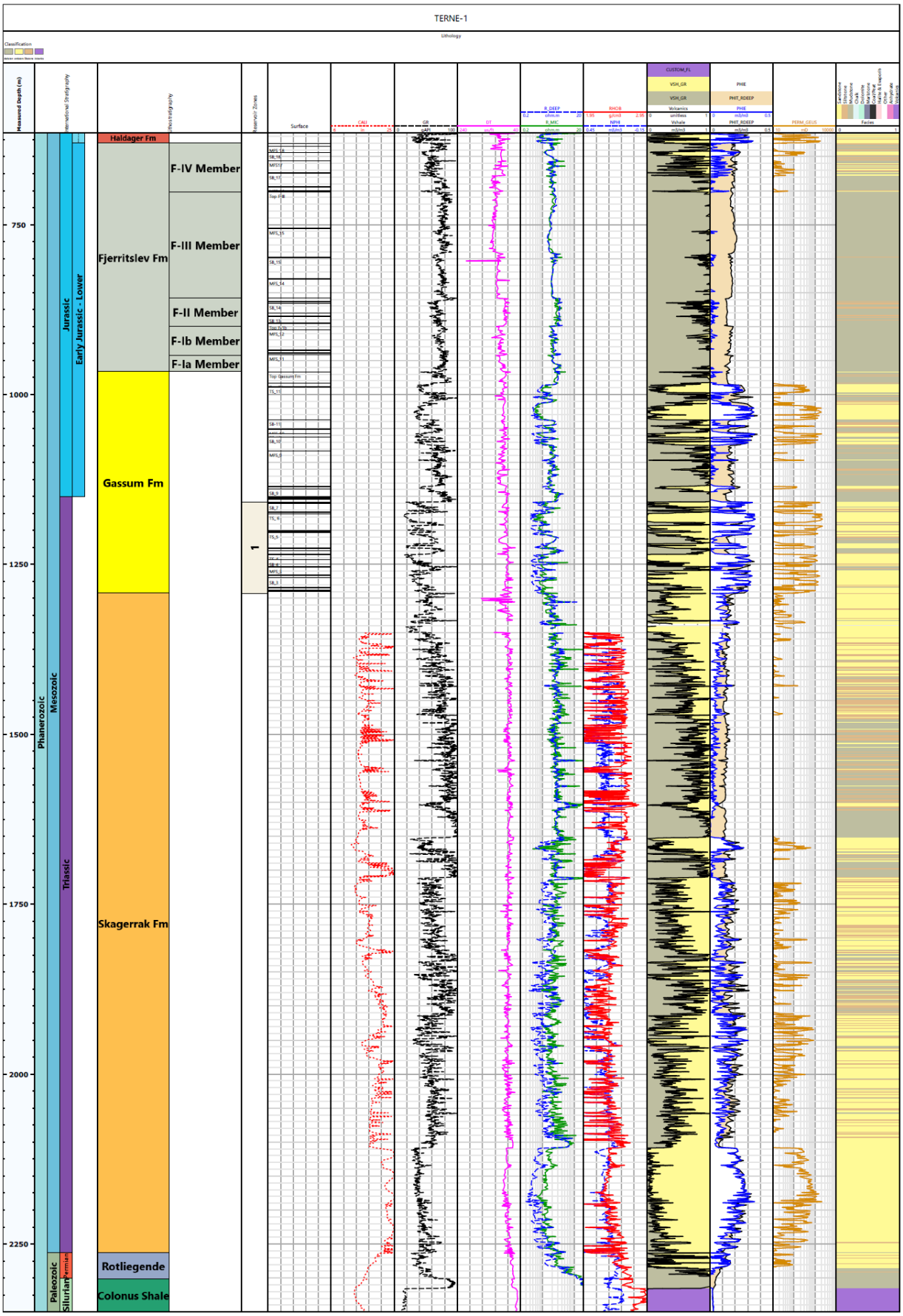
TERNE-1
Lithology
Measured Depth (m)
International Stratigraphy
Local Stratigraphy
Reservoir Zones
Surface
CALI
GR
DT
R_DEEP
R_MIC
RHOB
NPHI
CUSTOM_FL
VSH_GR
PHIE
PHIT_RDEEP
PERM_GEUS
Facies
Haldager Fm
F-IV Member
F-III Member
F-II Member
F-Ib Member
F-Ia Member
Fjerritslev Fm
Gassum Fm
Skagerrak Fm
Rotliegende
Colonus Shale
Jurassic
Early Jurassic - Lower
Phanerozoic
Mesozoic
Triassic
Paleozoic
Permian
Silurian
750
1000
1250
1500
1750
2000
2250

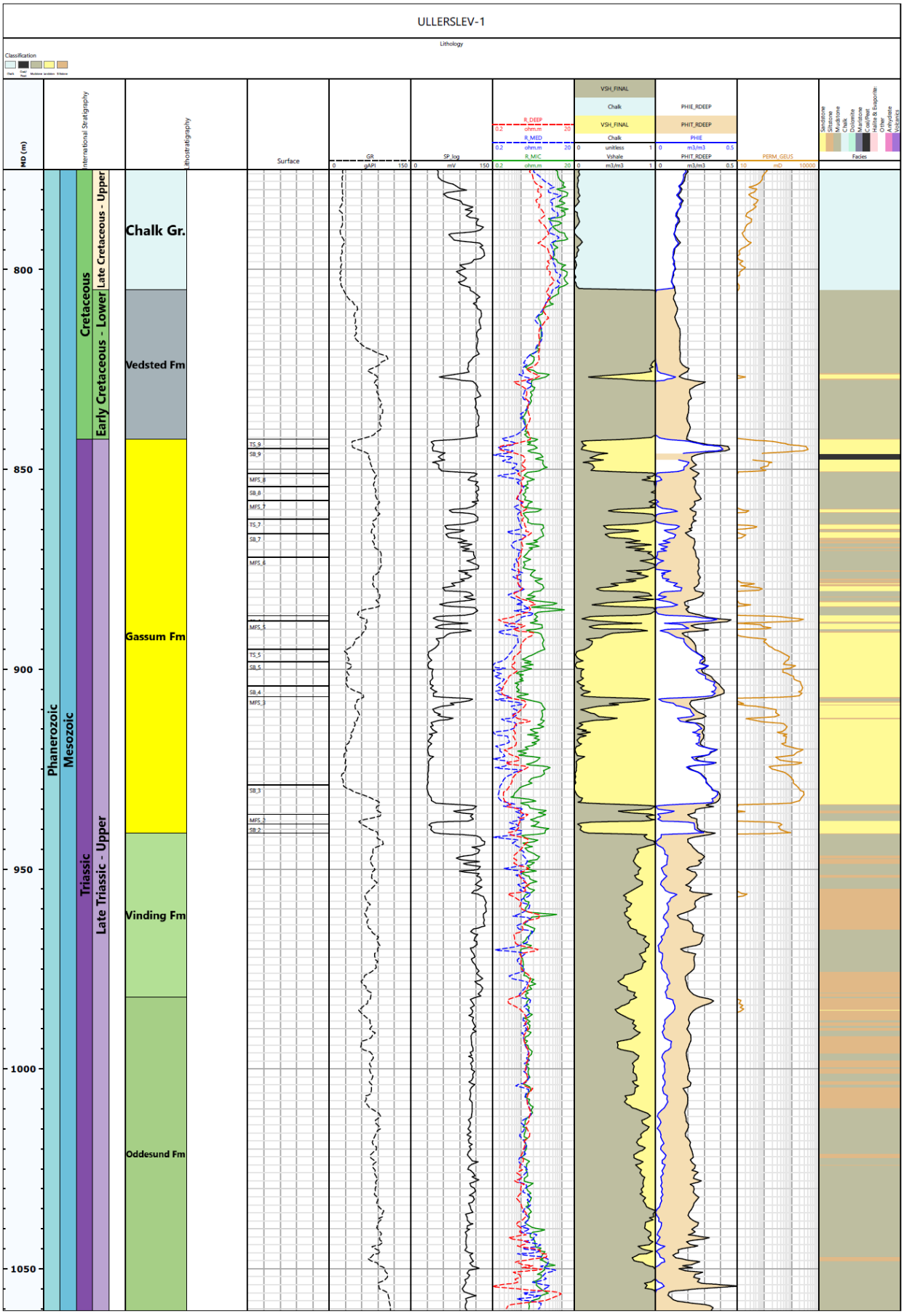
ULLERSLEV-1
Lithology
Classification
MD (m)
International Stratigraphy
Lithostratigraphy
Surface
GR
gAPI
SP_log
mV
R_DEEP
R_MED
R_MIC
ohm.m
VSH_FINAL
Chalk
Vshale
unitless
PHIE_RDEEP
PHIT_RDEEP
PHIE
m3/m3
PERM_GEUS
mD
Facies
Sandstone
Siltstone
Mudstone
Chalk
Dolomite
Marlstone
Limestone
Halite & Evaporite
Other
Anhydrite
Volcanics
Phanerozoic
Mesozoic
Cretaceous
Late Cretaceous - Upper
Early Cretaceous - Lower
Triassic
Late Triassic - Upper
Chalk Gr.
Vedsted Fm
Gassum Fm
Vinding Fm
Oddesund Fm
800
850
900
950
1000
1050

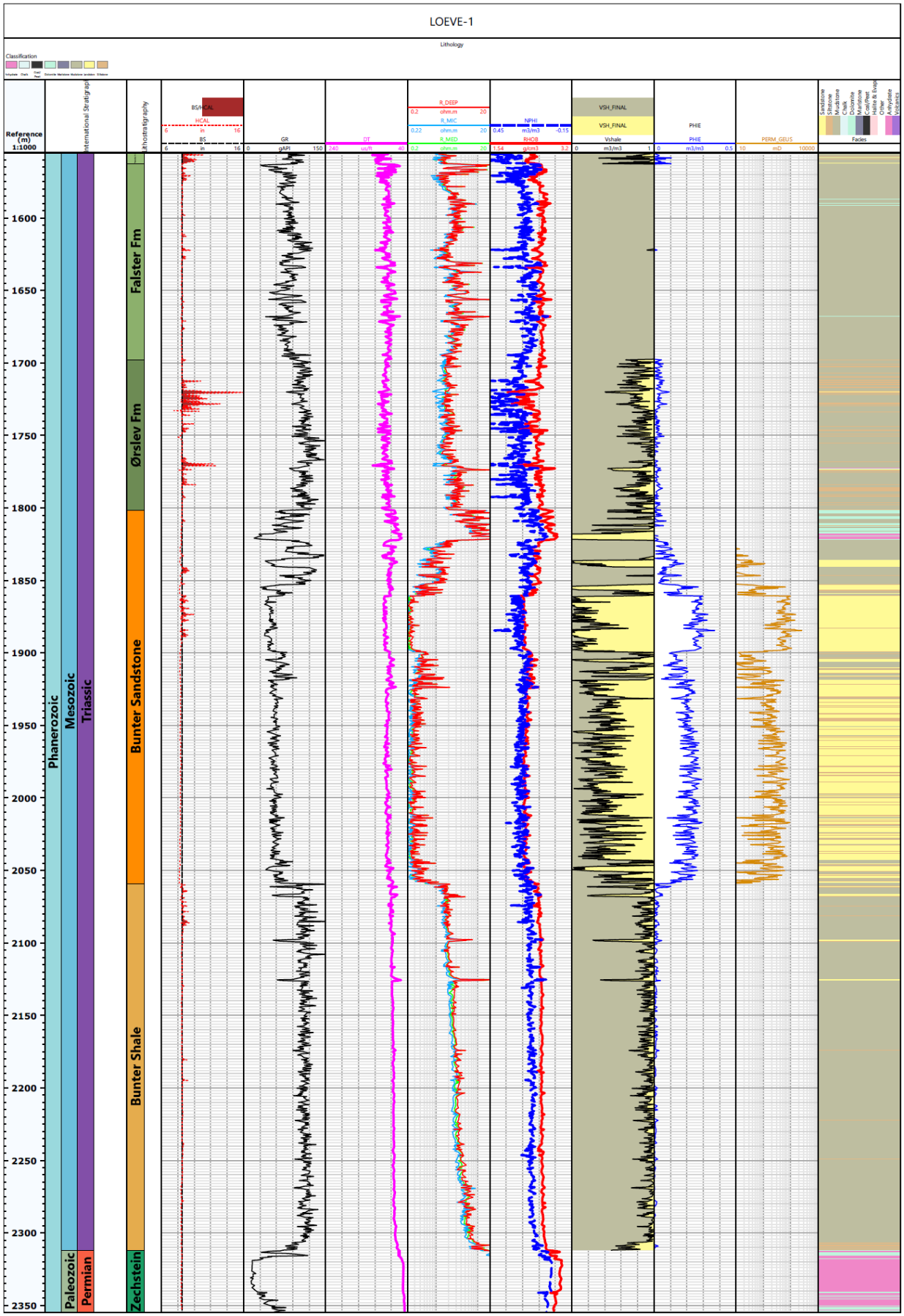
LOEVE-1
Lithology
Classification
Reference (m) 1:1000
International Stratigraphy
Lithostratigraphy
BS/HCAL
HCAL
BS
GR
gAPI
DT
us/ft
R_DEEP
R_MIC
R_MED
ohm.m
NPHI
m3/m3
RHOB
g/cm3
VSH_FINAL
Vshale
PHIE
PERM_GEUS
mD
Facies
Sandstone
Siltstone
Mudstone
Chalk
Dolomite
Marlstone
Carbonate
Halite & Evap
Other
Anhydrite
Volcanics
Phanerozoic
Mesozoic
Triassic
Paleozoic
Permian
Falster Fm
Ørslev Fm
Bunter Sandstone
Bunter Shale
Zechstein
1600
1650
1700
1750
1800
1850
1900
1950
2000
2050
2100
2150
2200
2250
2300
2350

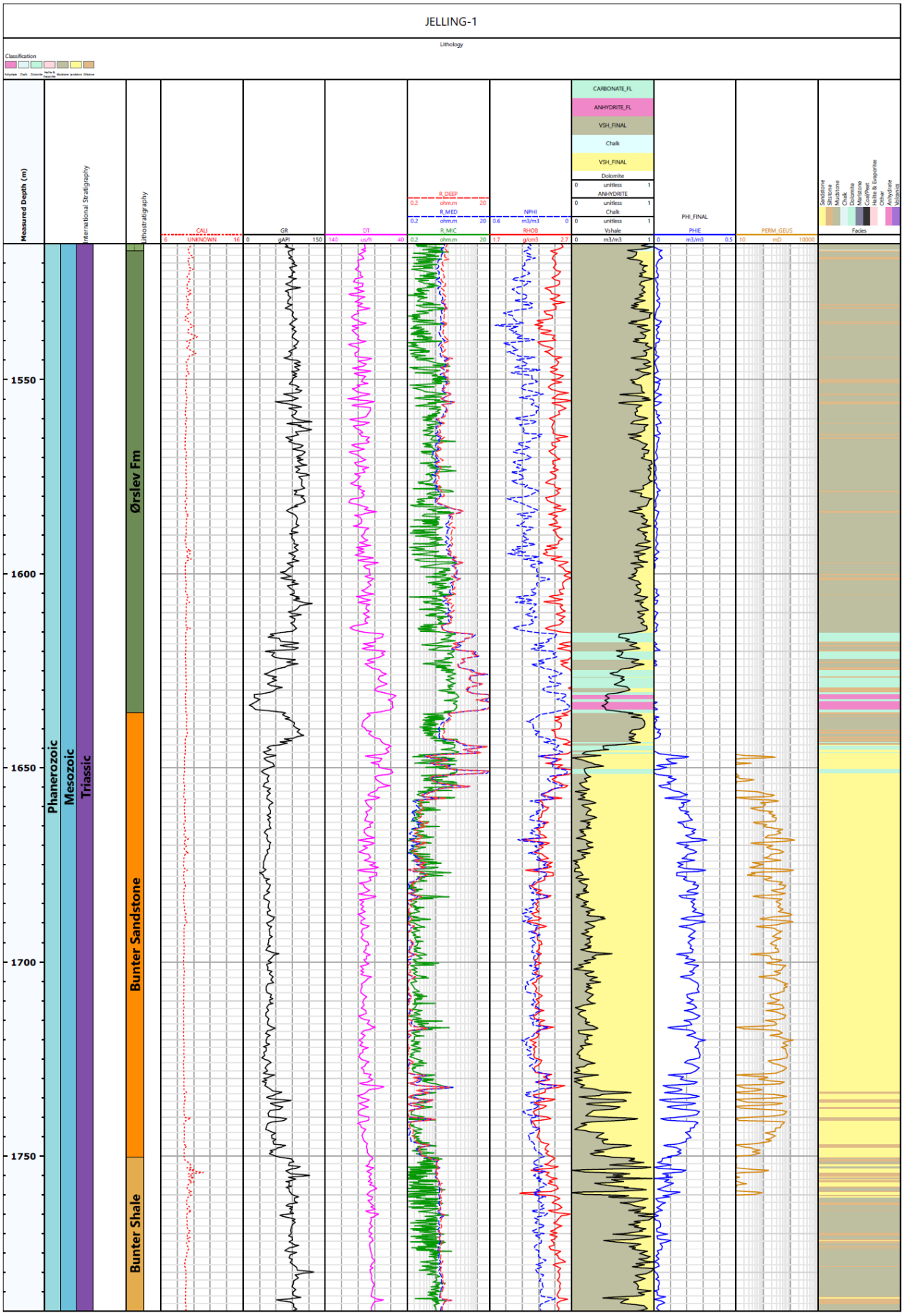
JELLING-1
Lithology
Classification
Measured Depth (m)
International Stratigraphy
Lithostratigraphy
CALI
UNKNOWN
GR
gAPI
DT
us/ft
R_DEEP
R_MED
R_MIC
ohm.m
NPHI
m3/m3
RHOB
g/cm3
CARBONATE_FL
ANHYDRITE_FL
VSH_FINAL
Chalk
VSH_FINAL
Dolomite
ANHYDRITE
Chalk
Vshale
PHI_FINAL
PHIE
PERM_GEUS
mD
Facies
Sandstone
Siltstone
Mudstone
Chalk
Dolomite
Marlstone
Coal/Peat
Halite & Evaporite
Other
Anhydrite
Volcanics
Phanerozoic
Mesozoic
Triassic
Ørslev Fm
Bunter Sandstone
Bunter Shale
1550
1600
1650
1700
1750

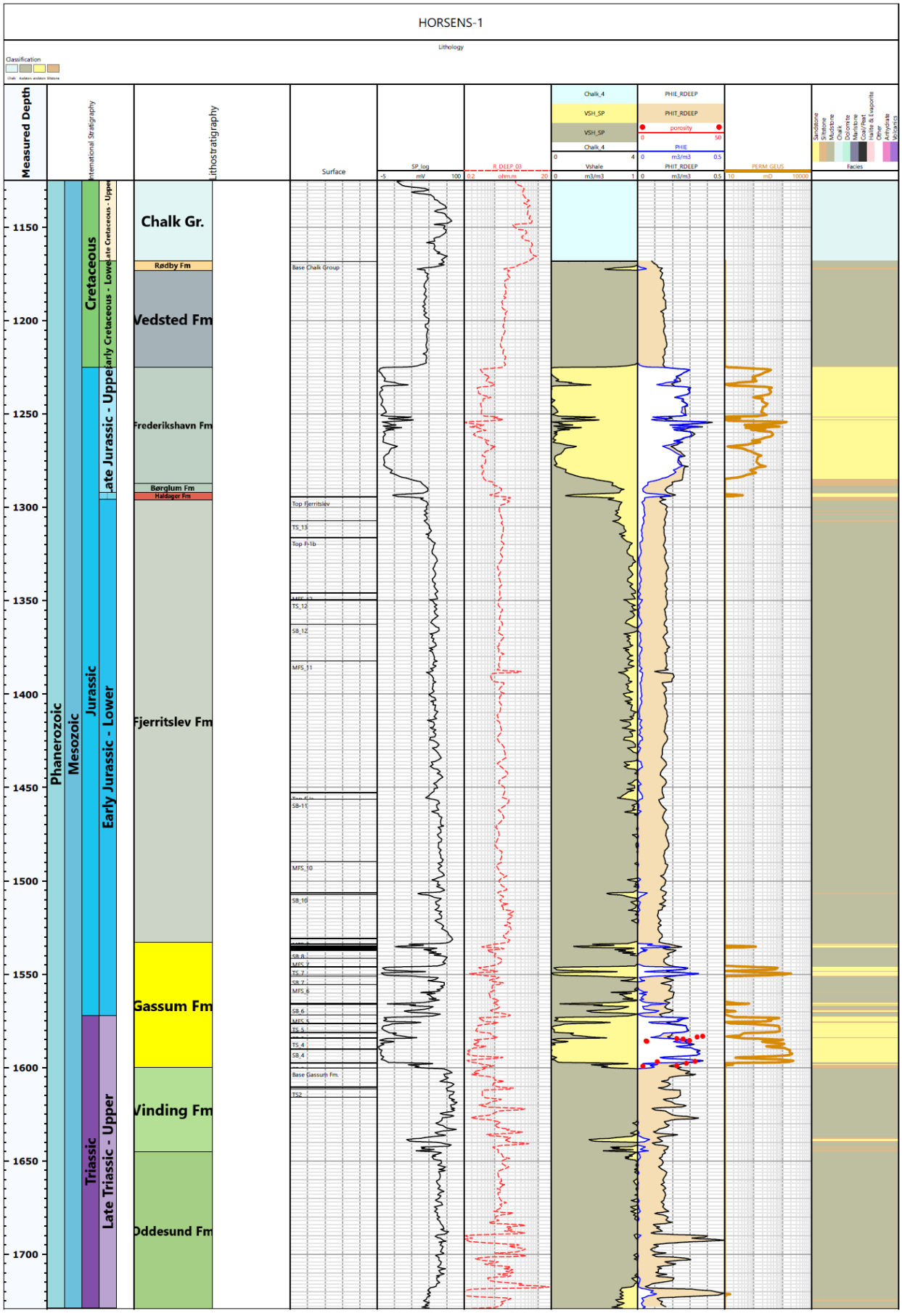
HORSENS-1
Lithology
Classification
Measured Depth
International Stratigraphy
Lithostratigraphy
Surface
SP_log
R_DEEP_03
Chalk_4
VSH_SP
VSH_SP
Chalk_4
Vshale
PHIE_RDEEP
PHIT_RDEEP
porosity
PHIE
PHIT_RDEEP
PERM_GEUS
Facies
Sandstone
Siltstone
Mudstone
Chalk
Dolomite
Marlstone
Coal/Peat
Halite & Evaporite
Other
Anhydrite
Volcanics
Phanerozoic
Mesozoic
Cretaceous
Late Cretaceous - Upper
Early Cretaceous - Lower
Jurassic
Late Jurassic - Upper
Early Jurassic - Lower
Triassic
Late Triassic - Upper
Chalk Gr.
Rødby Fm
Vedsted Fm
Frederikshavn Fm
Børglum Fm
Haldager Fm
Fjerritslev Fm
Gassum Fm
Vinding Fm
Oddesund Fm
Base Chalk Group
Top Fjerritslev
TS_13
Top F-1b
TS_12
SB_12
MFS_11
SB-11
MFS_10
SB_10
SB_8
MFS_7
TS_7
SB_7
MFS_6
SB_6
MFS_5
TS_5
TS_4
SB_4
Base Gassum Fm.
TS2
1150
1200
1250
1300
1350
1400
1450
1500
1550
1600
1650
1700

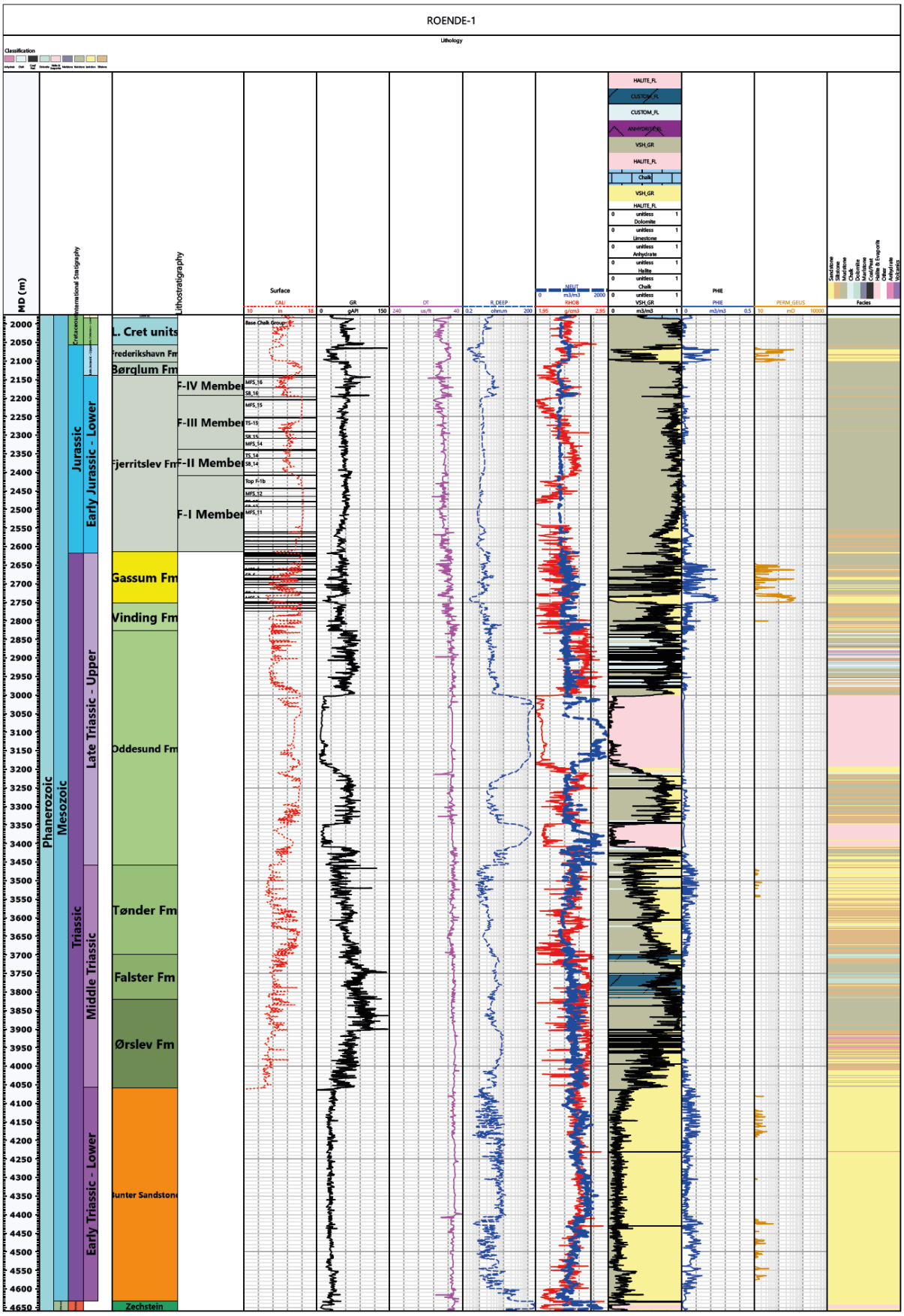
ROENDE-1
Lithology
Classification
MD (m)
International Stratigraphy
Lithostratigraphy
Surface
CALI
GR
DT
R_DEEP
NEUT
RHOB
PHIE
PERM_GEUS
Facies
Phanerozoic
Mesozoic
Jurassic
Early Jurassic - Lower
Triassic
Late Triassic - Upper
Middle Triassic
Early Triassic - Lower
L. Cret units
Frederikshavn Fm
Børglum Fm
F-IV Member
F-III Member
F-II Member
F-I Member
Fjerritslev Fm
Gassum Fm
Vinding Fm
Oddesund Fm
Tønder Fm
Falster Fm
Ørslev Fm
Hunter Sandstone
Zechstein
Base Chalk Group
Top F-1b

Appendix C – Biostratigraphy (See Chapter 7)

(Of the Gassum and Fjerritslev Formations and the overlying Jurassic formations in selected wells surrounding the Havnsø structure).

Introduction

No wells penetrate the Havnsø structure, and the biostratigraphic framework for the Gassum and Fjerritslev Formations is therefore based on data from a series of offset wells surrounding the structure including Terne-1, Lavø-1, Rønde-1, Horsens-1, Ullerslev-1, Slagelse-1, and Stenlille-1 and -19.

The biostratigraphic database varies considerably from well to well. From some wells a solid biostratigraphic framework exists while hardly any data exists from others.

The biostratigraphy has been used to guide the sequence stratigraphic framework for each well and for the correlations between the wells.

For each well a link is given to a digital stratigraphic summary chart as these contain to many details to be seen in a printed version (only available via the pdf version of the report). The charts combine the chronostratigraphy, lithostratigraphy, biostratigraphy and sequence stratigraphy and further include the bio-events and biozonations. The charts represent the interval from base Gassum Formation to base Lower Cretaceous.

Direct links to the Biostratigraphic Summary Charts:

- *Horsens-1, Summary chart and palaeoenvironment*
- *Lavø-1, Summary chart*
- *Rønde-1, Summary chart*
- *Slagelse-1, Summary chart*
- *Stenlille-1, Summary chart and palaeoenvironment*
- *Stenlille-19, Summary chart and palaeoenvironment*
- *Terne-1, Summary chart and palaeoenvironment*
- *Ullerslev-1, Summary chart*

Zonations

The zonations used include the ostracod zonation of Michelsen (1975), the dinocyst zonation of Poulsen & Riding (2003) and a combination of the spore-pollen zonations of Dybkjær (1991), Koppelhus & Nielsen (1994) and Lindström et al. (2023).

Biostratigraphic summary for each of the key-wells

The biostratigraphy summarised here for each well is based on data from reports and publications combined with new data from some of the wells.

Terne-1

As there are no cores and no sidewall cores from the relevant interval, the biostratigraphy is based on data from ditch cuttings samples. The data comprise analysis of spores, pollen and dinoflagellate cysts and consist of a combination of information from a report produced by Paleoservices (1985) and from new analysis made for the present study (Link to stratigraphic summary chart: *Terne-1, Summary chart and palaeoenvironment*).

The biostratigraphic data generally support the lithostratigraphic subdivision for the Terne-1 well presented in Nielsen & Japsen (1991), indicating the presence of a thick Gassum Formation overlain by a thick and complete Fjerritslev Formation. The Fjerritslev Formation is overlain by Middle Jurassic deposits referred to the Haldager Sand Formation and Upper

Jurassic deposits referred to the Flyvbjerg, Børglum and Frederikshavn formations. No major unconformities seem to be present.

The highest occurrence of *Dapcodinium priscum* in the DCS at 980 m, in the uppermost part of the Gassum Formation, strongly indicates that the top of the Gassum Formation is found in the mid-Sinemurian in this well.

The dating of the boundary between the Haldager Sand and the Flyvbjerg formations in Terne-1 are discussable. The biostratigraphic data suggest that the boundary is located in an interval of Bathonian – Callovian age, while the boundary between these two formations according to Michelsen et al. (2003, Fig. 2) is located in the early Oxfordian (see also discussion in Michelsen and Nielsen 1991).

Lavø-1

The majority of samples analysed for biostratigraphy are ditch cuttings samples. However, a few cores exist from the studied interval, and data from these cores turned out to be very important for establishing the stratigraphy in this well. The biostratigraphic data comprise analysis of spores, pollen and dinoflagellate cysts. Poulsen (1996) studied the dinocysts in the interval from 2430-2027 m and suggested a zonation (see stratigraphic summary chart: *Lavø-1, Summary chart*). Lindström, in Vosgerau et al. (2016) studied the spores, pollen and dinocysts in the interval 2395-2077 m. Michelsen (1975) studied the ostracods but found a very sparse assemblage and could therefore not present a stratigraphic subdivision.
The interpretations by Poulsen and Lindström differs with respect to the lower parts of succession referred to the Vinding, Gassum and lower Fjerritslev formations. While Poulsen interpreted the presence of the *Dapcodinium priscum* and possibly the *Liasidium variabile* zones in the interval from 2428-2243 m and thus referred this interval to the Sinemurian, the finding of *Lunnomidinium scaniense* in the sample at 2310 m by Lindström refers this sample to the *Rhaetipollis-Limbosporites*/*Rhaetigonyaulax rhaetica* Zones of Rhaetian age. Both Poulsen (1986) and Lindström (in Vosgerau 2016) indicate the presence of Toarcian in the uppermost part of the Fjerritslev Formation based on the presence of *Mancodinium semitatulatum*, *Manumia delcourtii* and frequent *Halosphaeropsis liassicus*. The possible misinterpretations by Poulsen (1996) for the lower part of the succession is probably due to caving.
Nielsen & Japsen (1991) suggested to locate the top of the Gassum Formation at 2133 m, and further indicated that only the F-I member is present in this well. Vosgerau et al. (2016) suggested to locate the top Gassum Formation at 2269 m and further that the Fjerritslev Formation in this well comprises the F-II member and the lower part of the F-III member as also supported by the biostratigraphy.
Here vi have located the top of the Gassum Formation at 2133 m, following Nielsen & Japsen (1991), but we follow Vosgerau et al. (2016) in suggesting that both the F-II member and the lower part of F-III member of the Fjerritslev Formation is also present. Defining the top of the Gassum Formation within the Pliensbachian identified by the biostratigraphic data is in contrast to previous publications and reports in which this boundary has not been placed above Lower Sinemurian strata (see Nielsen 2003 for discussion). However, in a coming revision of the Lower Jurassic lithostratigraphy, the top of the Gassum Formation will probably be placed at a lower level in the Lavø-1 well, and a new sandstone-dominated lithostratigraphic unit will then be defined on top of the Gassum Formation.

Rønde-1

As there are no cores and no sidewall cores from the relevant interval, the biostratigraphy is based on data from ditch cuttings samples. The data consists of ostracod analysis (Michelsen 1967; 1975) and are presented in the stratigraphic summary chart: *Rønde-1, Summary chart*.

The ostracod data covers the interval from the Hettangian to the Pliensbachian and indicate that the top of the Gassum Formation in this well is located in the lower part of the Hettangian.

According to the lithostratigraphy, there is an inconformity between the top of the Fjerritslev Formation (F-IV member) and the overlying Børglum Formation as the Flyvbjerg Formation seems to be missing (Nielsen and Japsen 1991), but no biostratigraphic data exists from the relevant interval to confirm that.

Horsens-1

Poulsen (1996) analysed a core sample from the lower part of the Fjerritslev Formation and referred it to the *Dapcodinium priscum* dinocyst zone, subzone b. This result refers the sample 1449 m to the Lower Sinemurian.

Michelsen (1975) studied the ostracods in the interval from 1572m–1318 m. He subdivided the interval into

3 ostracod zones and 1 subzone and dated the interval to Hettangian – Upper Pliensbachian.

There is an inconsistency in the location of the top of the Gassum Formation from Nielsen & Japsen (1991) and the present study. Nielsen & Japsen suggested that the top of the formation should be located at 1506 m, while the top in the present study is located at 1533.7 m. The biostratigraphy cannot solve this issue, as both formation tops are located within the Hettangian.

The top of the Fjerritslev Formation is Upper Pliensbachian in age indicating that the youngest part of the formation has been removed by erosion. It is unconformably overlain by Middle and Upper Jurassic deposits referred to the Haldager-, Børglum- and Frederikshavn formations. See further the stratigraphic summary chart: *Horsens-1, Summary chart and palaeoenvironment*.

Ullerslev-1

Biostratigraphic information from this well is restricted to preliminary data included in the completion report (DAPCO/DGU 1951). According to the “Drilling summary” all of the Jurassic, including the Fjerritslev Formation, is missing and there is a major unconformity at 2668´ between the Rhaetian (Upper Triassic) and the Upper Cretaceous. However, the report includes analysis from several different persons and some of the results indicate the presence of Lower Cretaceous as well.

Nielsen & Japsen (1991) also indicates that the Jurassic (including the Fjerritslev Formation) is missing and suggest that the Gassum Formation (from 3088´to 2763´) is unconformably overlain by a Lower Cretaceous succession spanning from 2763´ to 2640´ and Upper Cretaceous chalk from 2640´. See further the stratigraphic summary chart: *Ullerslev-1, Summary chart*.

Slagelse-1

As there are no cores and no sidewall cores from the relevant interval, the biostratigraphy is based on data from ditch cuttings samples. The data consist of ostracod analysis made by Michelsen (1975) and are presented in the stratigraphic summary chart: xxxxx. According to Nielsen & Japsen (1991) the top of the Gassum Formation should be located at 1150 m, which is followed here. Michelsen (1975) found the presence of the *O. aspinata* Zone in the interval 1142–1152 m indicating a Hettangian – Early Sinemurian age. The presence of the *C. betzi-C. crassireticulata* Zone and the *O. danica* Zone in the interval from 1042–987 m indicates a Sinemurian age for that interval. Both Nielsen & Japsen (1991) and the present study indicate the presence of an unconformity from the Sinemurian to the Lower Cretaceous, comprising large parts of the Fjerritslev Formation and the Middle and Upper Jurassic. No biostratigraphic data exists to confirm that. See further the stratigraphic summary chart: *Slagelse-1, Summary chart*.

Stenlille-1

Many palynological data, both spore-pollen data and dinocyst data, are available from the Rhaetian (uppermost Triassic) to the Hauterivian (Lower Cretaceous) interval, from cores, sidewall cores as well as ditch cuttings samples from the Stenlille-1 well (e.g. Dybkjær 1998; Lindström et al. 2012; 2015; 2017; 2019; 2023; Vosgerau et al. 2016; Lindström 2016; 2020; 2021; Gregersen et al. 2023). The majority of the data comes from the transition zone between the Gassum and Fjerritslev formations and the lowermost Jurassic interval. The Stenlille-1 well was one of the key-wells in establishing the spore-pollen zonation for the Stenlille-area published by Lindström et al. (2023). These data show that the top of the Gassum Formation (1507 m) is located closely below the Triassic–Jurassic boundary (1494 m).

According to Nielsen & Japsen (1991) an unconformity is present between the Fjerritslev and Vedsted formations and this unconformity should be located at 1247 m. According to their interpretation the F-III and F-IV members of the Fjerritslev Formation are missing in the Stenlille-1 well. However, new palynological and nannofossils analysis were made in connection with the study of Gregersen et al. (2023), in the interval from 1241–1203.95 m. These data strongly indicate that the location of the unconformity between the Fjerritslev and Vedsted formations should be moved upwards to 1220.5 m and further that both the F-III member and the lower part of the F-IV member are present.

The Fjerritslev Formation is unconformably overlain by Lower Cretaceous deposits referred to the Vedsted and Rødby formations. See further the stratigraphic summary chart: Stenlille-1, Summary chart and palaeoenvironment.

Stenlille-19

Only a few palynological data exists from the Stenlille-19 well and these are from core 3, from the middle part of the Gassum Formation (Lindström 2020; Lindström et al. 2023). The spore-pollen data and the dinocyst data indicate a mid-Rhaetian age for the core. See further the stratigraphic summary chart: *Stenlille-19, Summary chart and palaeoenvironment*.

References

DAPCO/DGU 1951. Completion report Ullerslev-1 DAPCO well [Compiled by DGU, August 1993], 143 p. + 2 Enclosures.

Dybkjær, K. 1991. Palynological zonation and palynofacies investigation of the Fjerritslev Formation (Lower Jurassic – basal Middle Jurassic) in the Danish Subbasin. Danmarks Geologiske Undersøgelse Serie A 30, 1–150.

Dybkjær, K. 1998. Datering og palynofacies-anlyse af 6 udvalgte prøver fra Stenlille – boringerne. Danmarks og Grønlands Geologiske Undersøgelse Rapport 1998/75.

Gregersen, U., Hjelm, L., Vosgerau, H., Smit, F.W.H., Nielsen, C.M., Rasmussen, R., Bredesen, K., Lorentzen, M., Mørk, F., Lauridsen, B.W., Pedersen, G.K., Nielsen, L.H., Mathiesen, A., Laghari, S., Kristensen, L., Sheldon, E., Dahl-Jensen, T., Dybkjær, K., Hidalgo, C.A. and Rasmussen, L.M. 2023. CCS2022-2024 WP1: The Stenlille structure - Seismic data and interpretation to mature potential geological storage of CO2. Danmarks og Grønlands Geologiske Undersøgelse Rapport 2022/26. GEUS. 164 pp. DOI: https://doi.org/10.22008/gpub/34661

Koppelhus, E.B. and Nielsen, L.H. 1994. Palynostratigraphy and palaeoenvironments of the Lower to Middle Jurassic Bagå Formation of Bornholm, Denmark. Palynology 18(1), 139–194.

Lindström S. 2016. Palynofloral patterns of terrestrial ecosystem change during the end-Triassic event – a review. Geological Magazine 153(2), 223–251.

Lindström, S. 2020. Capture, Storage and Use of CO2 (CCUS). Palynology of the Gassum and lowermost Fjerritslev formations in the Stenlille area: biostratigraphic and palaeonenvironmental implications (Part of Work packages 5 in the CCUS project). Danmarks og Grønlands Geologiske Undersøgelse Rapport 2020/36.

Lindström, S. 2021. Two-phased mass rarity and extinction in land plants during the End-Triassic climate crisis. Frontiers in Earth Science 9: 780343.

Lindström, S., van de Schootbrugge, B., Dybkjær, K., Pedersen, G.K., Fiebig, J., Nielsen, L.H. and Richoz, S. 2012. No causal link between terrestrial ecosystem change and methane release during the end-Triassic mass extinction. Geology 40(6), 531–534.

Lindström, S., Pedersen, G.K., van de Schootbrugge, B., Hansen, K.H., Kuhlmann, N., Thein, J., Johansson, L., Petersen, H.I., Alwmark, C., Dybkjær, K., Weibel, R., Erlström, M., Nielsen, L.H., Oschmann, W. and Tegner, C. 2015. Intense and widespread seismicity during the end-Triassic mass extinction due to emplacement of a large igneous province. Geology 43(5), 387–390.

Lindström, S., van de Schootbrugge, B., Hansen, K.H., Pedersen, G.K., Alsen, P., Thibault, N., Dybkjær, K., Bjerrum, C.J. and Nielsen, L.H. 2017. A new correlation of Triassic–Jurassic boundary successions in NW Europe, Nevada and Peru, and the Central Atlantic Magmatic Province: a time-line for the end-Triassic mass extinction. Palaeogeography Palaeoclimatology Palaeoecology 478, 80–102.

Lindström, S., Sanei, H., van de Schootbrugge, B., Pedersen, G.K., Lesher, C.E., Tegner, C., Heunisch, C., Dybkjær, K. and Outridge, P.M. 2019. Volcanic mercury and mutagenesis in land plants during the end-Triassic mass extinction. Science Advances 5(10): eaaw4018.

Lindström, S., Pedersen, G.K., Vosgerau, H., Hovikoski, J., Dybkjær, K. and Nielsen, L.H. 2023: Palynology of the Triassic–Jurassic transition of the Danish Basin (Denmark): a palynostratigraphic zonation of the Gassum–lower Fjerritslev formations. Palynology, DOI: 10.1080/01916122.2023.2241068

Michelsen, O. 1967. Lias, räht og keuper. En biostratigrafisk vurdering baseret på ostracoder [Rønde-1].

Michelsen, O. 1975. Lower Jurassic ostracods of the Danish Embayment. Danmarks Geologiske Undersøgelse, II Række, nr. 104. 287pp.

Michelsen, O. and Nielsen, L.H. 1991. Well records on the Phanerozoic stratigraphy in the Fennoscandian Border Zone, Denmark – Hans-1, Sæby-1, and Terne-1 wells. DGU serie A 29.

Michelsen, O., Nielsen, L.H., Johannessen, P.N., Andsbjerg, J. and Surlyk, F. 2003. Jurassic lithostratigraphy and stratigraphic development onshore and offshore Denmark. In: Ineson, J.R. and Surlyk, F. (eds): The Jurassic of Denmark and Greenland. Geological Survey of Denmark and Greenland Bulletin 1, p. 145–216. https://doi.org/10.34194/geusb.v1.4651

Nielsen, L.H. 2003. Late Triassic – Jurassic development of the Danish Basin and the Fennoscandian Border Zone, southern Scandinavia. In: Ineson, J.R. and Surlyk, F. (eds): The Jurassic of Denmark and Greenland. Geological Survey of Denmark and Greenland Bulletin 1, p. 459–526. https://doi.org/10.34194/geusb.v1.4681

Nielsen, L.H. and Japsen, P. 1991. Deep wells in Denmark 1935-1990. Lithostratigraphic subdivision. Danmarks Geologiske Undersøgelse, DGU Serie A, No. 31, 177 pp.

Paleoservices Ltd./Forbes, G.A., Rasul, S., Smout, R., King, A.D., Jacovides, J. and Canham, A. 1985. Stratigraphical paleontological final report (and sidetrack). Well: Terne-1. Depth interval: 120m–3361m. Licence 4/84.

Poulsen, N.E. 1996. Dinoflagellate cysts from marine Jurassic deposits of Denmark and Poland. AASP contribution series 31, 227pp.

Poulsen, N.E. and Riding, J.B. 2003. The Jurassic dinoflagellate cyst zonation of Subboreal Northwest Europe. Geological Survey of Denmark and Greenland Bulletin 1, 115–144.

Vosgerau, H., Gregersen, U., Hjuler, M.L., Holmslykke, H.D., Kristensen, L., Lindström, S., Mathiesen, A., Nielsen, C.M., Olivarius, M., Pedersen, G.K. and Nielsen, L.H. 2016. Reservoir prognosis of the Gassum Formation and the Karlebo Member within two areas of interest in northern Copenhagen. The EUDP project “Geothermal pilot well, phase 1b”. GEUS Rapport 2016/56. 138 pp + app 1–5. https://doi.org/10.22008/gpub/32477

Danish Ministry of Climate,
Energy and Utilities

Geological survey of
Denmark and Greenland (GEUS)

Øster Voldgade 10
DK-1350 Copenhagen K
Denmark

GEUS is a research and advisory
institution in the Danish Ministry
of Climate, Energy and Utilities